Self-assembly of Small Molecules and Peptides: Relevant Applications

A Dissertation Submitted to the
Indian Institute of Technology Guwahati
As Partial Fulfillment for the Degree of

Doctor of Philosophy in Chemistry

Submitted by

Gobinda Dolai

Roll No. 166122002

Department of Chemistry
Indian Institute of Technology Guwahati
Guwahati-781039, Assam, India

Dedicated

To

My family

INDIAN INSTITUTE OF TECHNOLOGY GUWAHATI

Department of Chemistry

STATEMENT

I do hereby declare that the matter embodied in this thesis entitled "**Self-assembly of Small Molecules and Peptides: Relevant Applications**" is the result of experiments carried out by me in the Department of Chemistry, Indian Institute of Technology Guwahati, India, under the supervision of Prof. Bhubaneswar Mandal.

In keeping with the general practice of reporting scientific observations, due acknowledgements have been made wherever the work described is based on the findings of other investigators.

Date: June, 2022
Place: IIT Guwahati **Gobinda Dolai**

Indian Institute of Technology Guwahati
Department of Chemistry
North Guwahati, Guwahati-781039, India
Phone: +91 (361) 258 2319 (O); Fax: +91 (361) 258 2349
e-mail: **bmandal@iitg.ac.in**

CERTIFICATE

This is to certify that **Mr. Gobinda Dolai** (Roll No. 166122002) has been working under my supervision since July 2016 as a regular registered Ph.D. student. I am forwarding his thesis entitled "**Self-assembly of Small Molecules and Peptides: Relevant Applications**" to be submitted for the Ph.D. (Science) Degree of this Institute. I certify that he has fulfilled all the requirements according to the rules of this institute regarding the investigations embodied in his thesis and this work has not been submitted elsewhere for a degree.

Date: June, 2022
Place: IIT Guwahati

Prof. Bhubaneswar Mandal
Thesis Supervisor
Department of Chemistry

Acknowledgements

The journey of the Ph.D. is not always a smooth one. However, along the way, I have encountered persons who helped to make this journey a pleasurable. I would like to express sincere gratitude to them who directly or indirectly helped me throughout the Ph.D. journey and motivated me on the path to success.

First and foremost, I would like to express my sincere gratitude and thanks to my thesis supervisor Prof. Bhubaneswar Mandal for his invaluable guidance, encouragement, and inspiration throughout my Ph.D. program, which helped me to enhance my knowledge and inspired me to take right decisions at crucial moments. I am also thankful to him for giving me the freedom to pursue my interests in his lab, and I find myself privileged to have worked under his kind guidance.

I would like to acknowledge my sincere gratitude to all my doctoral committee members, Prof. Anil Kumar Saikia, Prof. Lal Mohan Kundu, and Dr. Dipankar Srimani for their valuable suggestions and pieces of advice during my doctoral studies.

I am grateful to the Ministry of Human Resource and Development (MHRD), India, for financial support and IIT Guwahati for all the facilities that were made available to me. I want to thank the department of chemistry and the Central Instrument Facility (CIF) and North East Centre for Biological Sciences and Healthcare Engineering (NECBH), IIT Guwahati for providing the instrumental facilities.

Further, I would like to thank all my past and present group members for their friendship and assistance. I especially want to thank Dr. Rajat Subhra Giri for his assistance and for always being willing to discuss problems and ideas with me. I also especially thank my jonior, for their help during the Ph.D. tenure. I thank the other labmates, Dr. Dharam Dev, Dr. Srinivasa Rao Manne, Dr. Tanmay Mondal, Dr. Sourav Kalita, Dr. Tapasi Kalita, Dr. Sujan Kalita, Sandip, Sayanta, Rinku, Altaf, Sukesh and Avisek for their co-operation in my research work, without which it would not be easy to complete the Ph.D. thesis. I also want to thank my M.sc juniors Srijit and Ariyan for their co-operation in my research work. It was great to work and spend time with these

lovely human beings, and I will always carry the memories of their jokes, laughter, and humor throughout my life. I am lucky to get such type of research environment and labmates.

I thank all of my Ph.D. batchmates (July 2016), the other research scholars in the chemistry department, and all my IITG friends who have shared their thoughts and views with me. I also specially thank to asesh and mihir for their significant help in Ph.D thesis work and metal support. I also thank my all M.Sc. and Ph.D. friends at IIT Guwahati with whom I spent good time and shared many joyful moments during festivals, picnics and sports .

I would like to express my special thanks of gratitude to my school and college teachers, who give light in my educational journey. I would also like to thank to all my friend from childhood to now to give such a wonderful memory.

Finally, I want to thank all of my family members. Without their love, care, support, and encouragement, it would not have been possible. They have been nothing short of incredible. I wish to express my sincere gratitude to my parents, brothers, sisters, late uncle, aunt, and my little nephew for their endless moral support and motivation, especially at difficult times. My Ph.D. endeavors would not have been completed without their blessings. They are the main soul and inspiration for every step that I achieve in my life.

Gobinda Dolai

List of abbreviations

Aβ	Amyloid beta
AD	Alzheimer's disease
AFM	Atomic force microscopy
AU	Arbitrary unit
Aib	2-aminoisobutyric acid
Ant	Anthranilic acid
BDMP	5-(1H-benzotriazol-1-yloxy)-3,4-dihydro- 1-methyl 2H-pyrrolium hexachloroantimonate
BET	Brunauer–Emmett–Teller
Boc	*tert*-Butyloxycarbonyl
BOMI	benzotriazol-1-yloxy-N,N-dimethyl-methaniminium hexachloroantimonate
BOP	Benzotriazol-1-yloxy-tris(dimethylamino) phosphoniumhexafluorophosphate
BPMP	1-(1H-benzotriazol-1-yloxy)phenyl-methylene pyrrolidinium hexachloroantimonate
CD	Circular dichroism
DBU	1,8-Diazabicyclo[5.4.0]undec-7-ene
DCC	N, N′-Dicyclohexylcarbodiimide
DCM	Dichloromethane
DIPEA	*N,N*-Diisopropylethyl amine
DCU	N,N -Dicyclohexylurea
deg	degree

3D	Three dimensional
DLS	Dynamic Light Scattering
DMF	*N*,*N*-Dimethylformamide
ESI-MS	Electrospray Ionization Mass Spectrometry
EtOAc	Ethyl Acetate
Et	Ethyl
Equiv	Equivalent
Fmoc	9-Fluorenylmethoxycarbonyl
FT-IR	Fourier Transformation Infra-red Spectroscopy
FESEM	Field Emission Scanning Electron Microscopy
FETEM	Field Emission Transmission Electron Microscopy
KBr	Potassium bromide
HATU	O-(7-azabenzotriazol-1-yl)-1,1,3,3-tetramethyluronium hexafluorophosphate
HBTU	O-(benzotriazol-1-yl)-1,1,3,3-tetramethyluronium hexafluorophosphate
HBMDU Or BOI	O-(benzotriazol-1-yl)-1,3-dimethyl-1,3-dimethyleneuronium hexafluorophosphate
HBPyU	O-(benzotriazol-1-yl)oxybis-(pyrrolidino)- uranium hexafluorophosphate
HOBt	1-hydroxybenzotriazole
HPLC	High performance Liquid Chromatography
MeOH	Methanol
MeCN	Acetonitrile
Me	Methyl

mL	Milli Liter
mM	milli mol
µM	micro mol
m-ABA	*meta* amino benzoic acid
MS	Mass spectra
2-NBs	1H-benzo[d][1,2,3]triazol-1-yl 2-nitrobenzenesulfonate
nm	Nanometre
NMI	*N*-Methyl imidazole
NMR	Nuclear Magnetic Resonance
o-ABA	*ortho* amino benzoic acid
ORTEP	Oak Ridge Thermal Ellipsoid Plot
o-NosylOXY	Ethyl 2-cyano-2-(2-nitrophenylsulfonyloxyimino)
Oxyma	Ethyl 2-cyano-2-(hydroxyimino)acetate
o-NBS	*Othro*-nitrobenzene sulfonyl
PBS	Phosphate buffer solution
Phg	Phenylglycine
p-NBS	*para*-nitrobenzene sulfonyl
PyBOP	benzotriazol-1-yloxytri(pyrrolidino)- phosphonium hexafluorophosphate
RB	Round bottom flask
RP	Reverse Phase
SC-XRD	Single Crystal X-Ray Diffraction
tBu	*tert*-Butyl
TCBOXY	(E)-ethyl-2-cyano-2-(((2,4,6-

	trichlorobenzoyl)oxy)imino)acetate
TCB-Cl	2,4,6-trichlorobenzoyl chloride
TCB-DMAP	2,4,6-trichlorobenzoyl chloride-4- dimethylaminopyridine
TGA	Thermogravimetric analysis
TEM	Transmission electron microscopy
TFA	Trifluoroacetic Acid
ThT	Thioflavin T
THF	Tetrahydrofuran
TLC	Thin-layer chromatography
R_t	Retention time
UV	Ultraviolet

Abbreviations for intensities of ^{1}H-NMR signals

s	singlet	q	quartet
d	doublet	m	multiplate
dd	doublet of doublet	Hz	Hertz
t	triplet	MHz	Mega-Hertz

The list of 22 coded amino acids				
	R group		Amino acids	Abbreviation Three & One letter code
Non-polar	Aliphatic		Glycine	Gly, G
			Alanine	Ala, A
			Proline	Pro, P
			Valine	Val, V
			Leucine	Leu, L
			Isoleucine	Ile, I
			Methionine	Met, M
	Aromatic		Phenylalanine	Phe, F
			Tryptophan	Trp, W
Polar	Aromatic		Tyrosine	Tyr, Y
	Neutral	Nucleophilic	Serine	Ser, S
			Selenocysteine	Sec, U
			Threonine	Thr, T
			Cysteine	Cys, C
		Amide	Asparagine	Asn, N
			Glutamine	Gln, Q
	Positively charged	Basic	Lysine	Lys, K
			Arginine	Arg, R
			Histidine	His, H
			Pyrrolysine	Pyl, O
	Negatively charged	Acidic	Aspartic acid	Asp, D
			Glutamic acid	Glu, E

Abstract

The contents of the thesis entitled, **"Self-assembly of Small Molecules and Peptides: Relevant Applications,"** are divided into six chapters based on the results of the experimental work performed during the complete course of the doctoral studies.

Chapter 1: This chapter provides a basic introduction to the supramolecular self-assembly of small organic molecules and peptides.

Chapter 2: In this chapter, we narrate the self-assembly of 1-(2,4,6-trichlorobenzoyloxy)benzotriazole (TCB-OBt) reagent and its application in amidation reaction.

Chapter 3: In this chapter, we demonstrate the effect of the N-terminal protecting group on the self-assembly of Ant-Aib dipeptides.

Chapter 4: In this chapter, we describe the differences in the self-assembly pattern of enantiomeric and reverse sequences of Ant and Phg containing dipeptide analogs.

Chapter 5: In this chapter, we discuss the crystallographic insights on differences in the supramolecular structure formation of dipeptides by replacing Phe with Trp.

Chapter 6: This chapter describes the supramolecular insights of hetero-chiral tripeptides ($A\beta_{18-20}$) in solid and solution states.

The chapter-wise summaries of the mentioned research works are described below.

Chapter 1: Introduction:

Self-assembly of small peptides has significant contributions to biological, chemical, and material science. The self-assembled structures acquire stability through weak non-covalent interactions such as electrostatic interactions, Van der Waals interactions, water-mediated hydrogen bonds, hydrophobic and hydrophilic interactions, π-π (aromatic) stacking interactions, and hydrogen bonding interactions. Meanwhile, other secondary bonding interactions (SBIs) i.e., chalcogen-chalcogen interaction, also participate in the self-assembly process. Although these interactions are weak, their combined forces produce structurally and chemically stable structures. Several important functional nanostructures, e.g., nanotubes, nanofibres, nanoribbons, nanospheres, nanotapes, and nanorods, have been developed by self-assembly of small peptides.

Amide functionality is available in polymers, active pharmaceutical compounds, natural products, and other biologically significant molecules. 1-Hydroxybenzotriazole (HOBt) based several coupling reagents have been developed for a solution and solid-phase peptide synthesis. Furthermore, modified Yamaguchi reagent plays as an efficient condensation reagent in several essential reactions.

Chapter 2: Self-assembly of 1-(2,4,6-trichlorobenzoyloxy)benzotriazole (TCB-OBt) reagent and its application in amidation reaction:

Purely organic molecules-based creation of supramolecular solid-state architecture has essential applications in crystal engineering and supramolecular chemistry. Moreover, an uncommon O···O interaction is rare. In this context, a small approach has been developed. HOBt based several coupling reagents have been explored for the effective formation of the peptide bond. Moreover, Yamaguchi Reagent (TCB-Cl) and Modified Yamaguchi Reagents have been developed for esterification and amidation reactions.

To explore the advantages of HOBt based Modified Yamaguchi Reagent, we have designed and synthesized the new reagent, **TCB-OBt**. The solid-state analysis suggested that the molecule stabilized via uncommon chalcogen-chalcogen (O···O) interaction, π-π stacking interaction, and aromatic C-H···O interaction. The presence of unusual O···O interaction was verified by Hirshfeld surface analysis. Moreover, molecule constructed self-assembled layer structure and the helical architecture in solid-state. TCB-OBt crystallized in the O-substituted desmotropic form.

Interestingly, the DFT calculation revealed that the O-substituted form is more stable than the N-substituted form (TCB-(N)-OBt). Morphology analysis by various microscopic experiments suggested the creation of continuous block-shaped morphology. Furthermore, this reagent acts as an effective activating reagent for amidation reaction under mild conditions.

Chapter 3: Effect of the N-terminal protecting group on the self-assembly of Ant-Aib dipeptides:

Incorporating nonnatural amino acids into the peptide chains keeps a favorable impression on various branches of biochemistry and other research fields. Especially, two unnatural amino acids, i.e., anthranilic acid and 2-aminoisobutyric acid, positively impact self-assembly due to their conformational rigidity. Moreover, formed nanostructures have significant proteolytic and thermal stability. Furthermore, terminal protecting groups also provide a remarkable contribution to various nanostructure formation by selectivity in the self-assembly process.

To check the role of N-terminal protecting groups on self-assembly, we have designed and synthesized four dipeptides containing two rigid, unnatural amino acids, Ant and Aib (X-Ant-Aib-OMe; Ant: Anthranilic acid, Aib: 2-aminoisobutyric acid, X = Boc (peptide **3A**), Fmoc (peptide **3B**), *o*-NBS (peptide **3C**), and *p*-NBS (peptide **3D**); NBS = nitrobenzyl sulfonyl group). Morphology analysis by FESEM, FETEM, and AFM experiments indicated that while **3A** and **3D** displayed distinct rod-like fiber structures, **3B** and **3C** exhibited vesicular structures in acetonitrile: water (1: 1). Moreover, FESEM and TGA experiments indicated that formed nanostructures possess significant thermal stability in dry conditions. Furthermore, **3B** and **3D** displayed a type-III N_2 gas adsorption isotherm. Nevertheless, the fluorescence experiment suggested that **3B** and **3C** have drug entrapment and salt-triggered releasing ability of curcumin, rhodamine B, and carboxyfluorescein.

Chapter 4: The differences in the self-assembly pattern of enantiomeric and reverse sequences of Ant and Phg containing dipeptide analogs

In addition to several utilities of nonnatural amino acids (Ant and Aib) and D-amino acid, the incorporation of Phenyl-glycine (Phg) in peptide backbone affects the reactivity, physical, structural properties of peptide due to its steric and electronic environment. However, mostly positional isomeric peptides, obtained by reversing the peptide sequences, provide similar morphology under similar environmental conditions. Only a few reports on the diversity in morphology and supramolecular packing of isomeric peptides are available. So, exploration of isomeric peptide-based morphological variety and studies of self-assembly mechanisms is fascinating and challenging.

To study the influence of enantiomeric and reversal of sequences on self-assembly, we have designed and synthesized Boc-Ant-L-Phg-OMe (**4A**), Boc-Ant-D-Phg-OMe (**4B**), and reversal peptide sequences of those peptides Boc-L-Phg-Ant-OMe (**4C**) and Boc-D-Phg-Ant-OMe (**4D**), respectively. Conformational analysis by FT-IR mentioned the existence of conformational heterogeneity of the alternation peptide sequences. Moreover, in the crystalline state, SC-XRD revealed that **4A** and **4B** adopt the helical and β-sheet-like layer structure. On the contrary, **4C** and **4D** displayed altered helical conformation, sheet-like layer structure, and molecular channel in higher-order supramolecular packing. Furthermore, morphology analysis by FESEM, FETEM, and AFM images exposed that **4A** and **4B** formed self-assembled vesicular morphology and alternative sequences, i.e., **4C** and **4D,** exhibited well-formed rod-like fiber structure in methanol. Nevertheless, TGA results suggested that the formed self-assembled nanostructure contains adequate thermal stability.

Chapter 5: Significant change in morphology through replacement of Phe by Trp: molecular-level insights

The hydrophobic region $A\beta_{18-20}$ (VFF) is the most crucial peptide sequence responsible for Alzheimer's disease (AD), forming insoluble amyloid fibril. In this regard, terminally protected $A\beta_{18-19}$ and $A\beta_{19-20}$ sequences based formation of fibrilar morphology and solid-state molecular insights has been established. Interestingly, tyrosine-modified diphenylalanine (FF) perturbs fibril formation, and its structural properties have been explored. Moreover, the tryptophan zipper (Trp-Zipper), a tertiary structural motif, plays a vital role in the biological process due to its conformational selectivity. However, short peptide-based Trp-Zipper is not explored enough.

To investigate the outcome of the incorporation of Tryptophan on amyloidogenic di-peptide sequences, we have designed and synthesized four dipeptides Boc-xxx-Trp-OMe (xxx: Val, Leu, Ile, and Phe) Boc-Val-Trp-OMe (VW), Boc-Leu-Trp-OMe (LW), Boc-Ile-Trp-OMe (IW), and Boc-Phe-Trp-OMe (FW). Morphology analysis by FESEM and AFM suggested the formation of spherical morphology. Moreover, structural insights by SC-XRD revealed that VW and IW displayed parallel β-sheet structure, cross-β-structure (the separation between antiparallel layers), sheet-like layer structure, and helical arrangement. In contrast, peptide FW exhibited inverse γ-turn conformation (familiar with open turn due to lack of intramolecular hydrogen bond), antiparallel β-sheet structure, columnar structure, supramolecular nanozipper structure, sheet-like layer arrangement, and helical architecture in the crystalline state. This may be the first example of dipeptide (FW) based open turn conformation and nanozipper structure. Furthermore, TGA analysis confirmed that formed spherical structures have exceptional thermal stability.

Chapter 6: Supramolecular insights of hetero-chiral tripeptides ($A\beta_{18-20}$) in solid and solution state

Alzheimer's disease (AD) is a progressive neurodegenerative disease that primarily causes dementia. The cause of AD is not entirely understood now. Literature reports revealed that AD mainly involves the accumulation of Amyloid-beta (Aβ) fibrils and neurofibrillary tangles of tau protein in the human brain. The structural features of the full length of Aβ peptide are not appropriately understood. However, the NMR, XRD, and cryoEM experiments demonstrated that Aβ aggregated to form a cross-β-sheet structure. Some crystal structures of Aβ fragments have been developed. Although changing chirality of amino acid residue of VFF ($A\beta_{18-20}$) and their effect on peptide gelation properties are explored, their structural features and morphology analysis remain undiscovered.

We have designed and synthesized eight stereoisomers of Boc-Val-Phe-Phe-OMe (Aβ18-20) and investigated their self-assembly to acquire detailed knowledge. The morphology analysis by FE-SEM displayed that protected VFF and vff (D-amino acids are indicated in small letters) exhibited a ribbon-like fibrous network, other peptides vFF, Vff, VfF, and vFf formed rod-like structures in 50% acetonitrile-water. Moreover, VFf displayed a mixture of two morphologies (rod-like and spherical), vfF exhibited spherical structures. In the crystal state, five of the stereoisomers, i.e., VFf, vfF, Vff, VfF, and vFf displayed a parallel β-sheet arrangement. Moreover, in higher-order molecular packing Vff, VfF, and vFf formed supramolecular sheet-like arrangement, whereas VFf and vfF enantiomeric pair exhibited helical sheet-like architecture. So, all corresponding opposite pairs exhibited similar morphology but opposite conformation. Furthermore, all designed self-aggregated tri-peptides displayed binding properties with thioflavin T, an amyloid binding dye.

Table of contents

Chapter 1

Introduction and Objectives

1.1. Introduction

Critical scientific developments related to the supramolecular self-assembly of small organic molecules and peptides are introduced in this chapter. Also, some basic information about coupling reagents is incorporated. Moreover, we describe small peptides (di- and tri-peptide) based self-assembly, secondary conformation, and morphology.

1.2. Supramolecular assemblies

'Supramolecular chemistry' is defined as 'chemistry beyond the molecule,' i.e., molecules self-assembled via various noncovalent interactions and formed well-organized functional structures. On the other hand, traditional or molecular chemistry mainly deals with covalent bond formation. (Figure 1.1)

The self-assembled supramolecular structures stabilize through the following major noncovalent interactions.[1,2]

- Electrostatic interactions
- Van der Waals interactions
- Hydrophobic interactions
- π-π stacking interactions
- Hydrogen bonding interactions

Although these interactions are weak, their combined force stabilizes the supramolecular structures effectively.

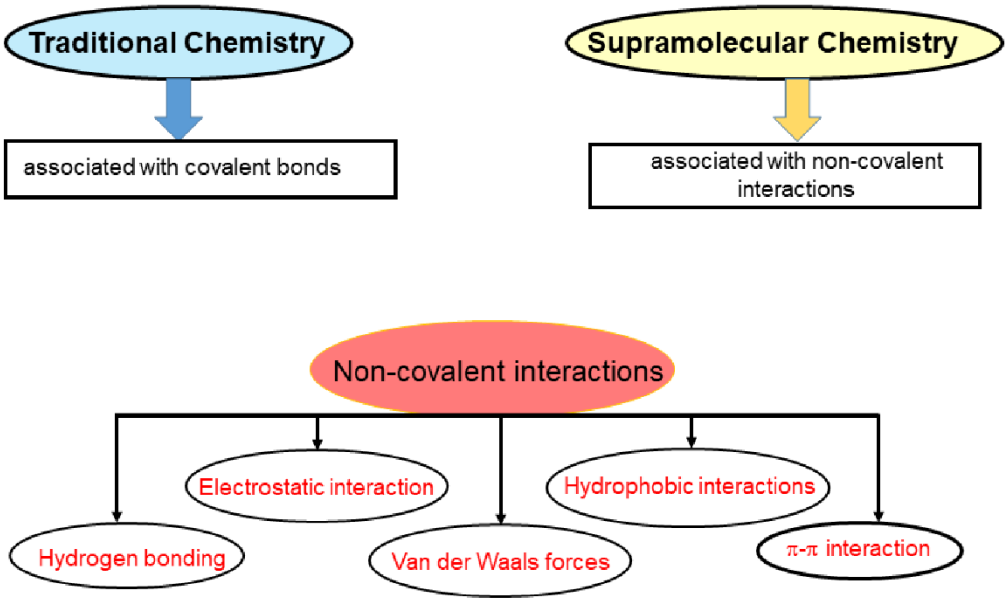

Figure 1.1. *Various kinds of noncovalent interactions in supramolecular chemistry*

1.3. Importance of amides

The amide bond is an essential functional moiety that presents a variety of biologically significant natural products, polymers, and pharmaceutical molecules.[3] For example, Carnosine[4], a dipeptide of β-alanine and histidine, functions as an antioxidant and antiglycation agent. It helps proper cell functioning in the body by inhibiting carbonylation and glycation. Atorvastatin[5] (trade name Lipitor) is used for reducing blood cholesterol. It helps counteract stroke via anti-inflammatory activity. Valsartan[6] is an angiotensin II receptor. It is used for decreasing blood pressure and preventing Alzheimer's disease. (Figure 1.2)

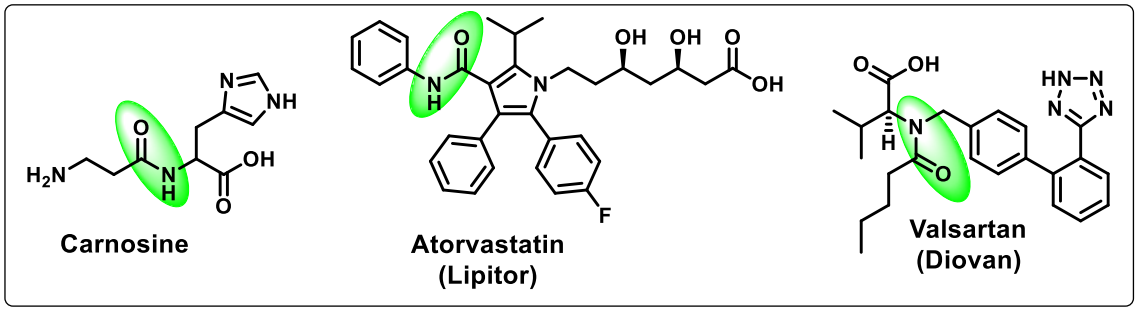

Figure 1.2. *Biologically active amides*

1.3.1. Existing methods for amidation

Forming an amide bond between carboxylic acids and amines can be achieved by various methods. For example, (a) Condensation method: reaction proceeds through higher temperature. This method is unsuitable often because various protecting groups can be deprotected at higher temperatures, or some other by-product can be formed. (b) Acyl halide-based method: some acyl halides, such as thionyl chloride[7] ($SOCl_2$), oxalyl chloride[8] ($COCl_2$), phosphorus trichloride[9] (PCl_3), and phosphorus pentachloride[10] (PCl_5), activated the carboxylic acid via the formation of acyl halide. As it goes via a highly reactive intermediate, this strategy is incompatible with the various cases due to side reactions. (c) Coupling reagent-based method, where reaction proceeds through the formation of activated intermediate (esters or salts) of carboxylic acid. Nucleophiles (amines) react with activated intermediate-formed amide bonds. (Scheme 1.1)

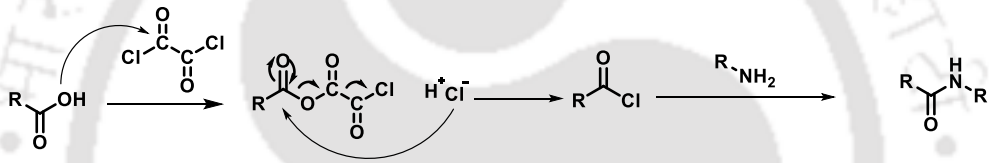

Scheme 1.1. *Acyl halide-based coupling reaction*

The most acceptable and suitable method for forming an amide bond is using coupling reagents. The coupling reagent-based amide bond synthesis was first introduced in 1955 with the enrollment of dicyclohexylcarbodiimide[11] (DCC). Afterward, various additives such as HOBt[12], HOAt[13], and 6-Cl-HOBt[14] were introduced to increase the efficiency of the coupling reaction and suppress the racemization. After that, various practical developments were done, and researchers found many new coupling reagents. (Scheme 1.2)

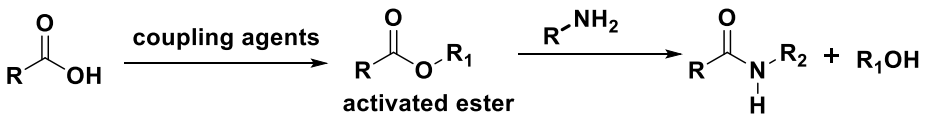

Scheme 1.2. *General pathway for coupling reagents based reaction*

Several excellent HOBt-bearing phosphonium and uranium salt-based coupling reagents, i.e., BOP[15], PyBOP[16], HBTU[17], HBMDU, or BOI[18], HBPyU[19], BOMI[20], BDMP[21], and

BPMP[21] were manifested to enhance the reactivity and reduce racemization in peptide chemistry. (Figure 1.3)

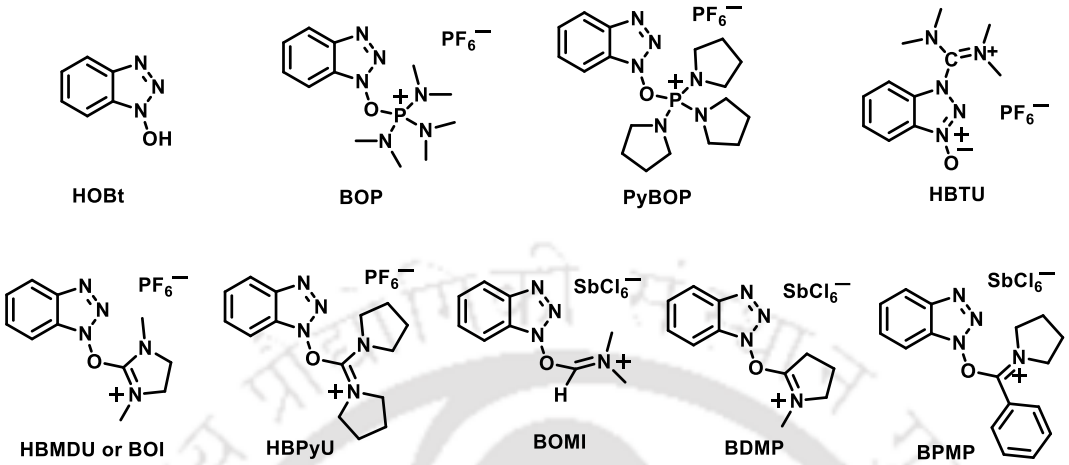

Figure 1.3. *HOBt-based coupling reagents*

Besides HOBt-containing phosphonium and uranium salt-based coupling reagents, various HOBt-bearing sulfonyl and carbonyl ester-based reagents were developed. These reagents also contribute to the synthesis of amides, esters, and peptides.

Topuzyan *et al.* synthesized 1-(o-nitrophenylsulfonyloxy)benzotriazole[22] (2-NBs), which is helpful for carboxylic amide synthesis and peptide synthesis under mild conditions. Moreover, they also discussed the molecular studies of this reagent. Molecule attains stabilization through stacking interaction between electron-deficient benzotriazole ring and electron-rich benzene ring of a neighboring molecule. (Scheme 1.3)

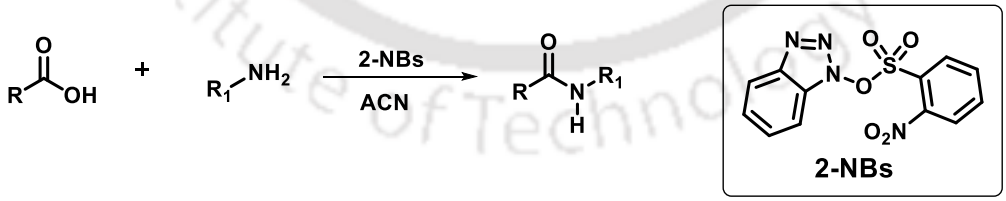

Scheme 1.3. *Amidation reaction using 2-NBs reagent*

Bowen *et al.* used 9-Fluorenylmethyl-1-benzotriazolyl carbonate[23] (Fmoc-OBt) to protect various amines and amino acids, which provided a good yield under mild reaction conditions. (Figure 1.4)

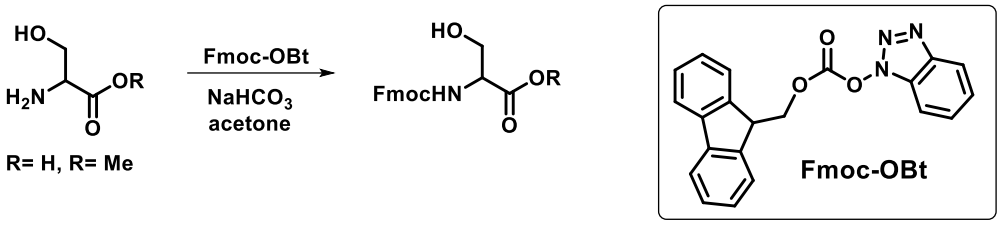

Scheme 1.4. *Fmoc-OBt based protection of amino-acid*

Molecular studies of HOBt-based reagents suggest that reagents stabilized either in O-substituted or N-substituted or both (N- and C-) form due to their desmotropic form (Figure 1.4). Lis and coworkers disclosed that BOP stabilized in O-substituted form.[15] Kates *et al.* reported HBTU crystallized in N-substituted form.[24] Xu *et al.* reported that BOMI and BDMP existed in N-substituted form in the crystalline state.[25] Topuzyan and his group found that 2-NBs remain in O-substituted form in solid-state.[22] Albericio and coworkers reported that Fmoc-OBt crystallized in N-substituted form in the solid-state.[26] Barlos *et al.* established that HOBt and protected amino acid-bearing esters exist in three isomeric forms (one ester and two amides), and all forms have different reactivity.[27]

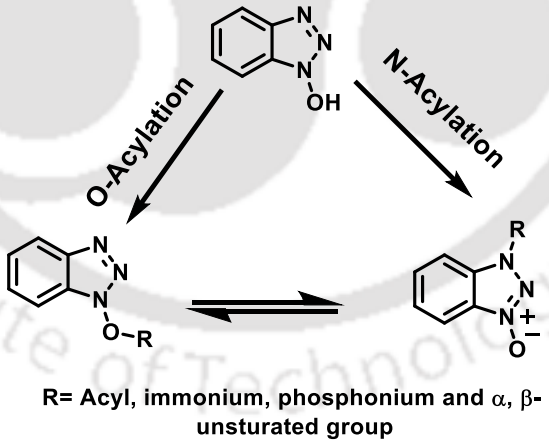

Figure 1.4. *General representation of different substitution pathways of HOBt*

1.4. Yamaguchi reagent and its modification

In 1979, Yamaguchi *et al.* manifested Yamaguchi reagent TCB-Cl (2,4,6-trichlorobenzoyl chloride)[28]. It is used for the formation of various esters and macrocyclic

lactones. The esterification reaction proceeds through the creation of a mixed-anhydride intermediate. Moreover, this reagent is also applicable for synthesizing thiols and esters. (Scheme 1.5)

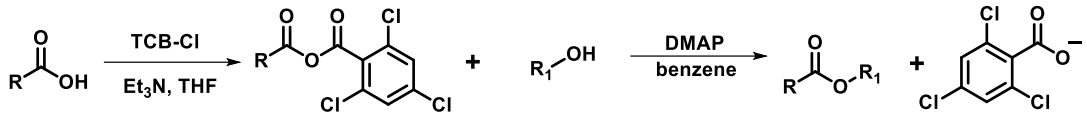

Scheme 1.5. *Yamaguchi reagent (TCB-Cl) mediated esterification reaction*

Furthermore, several modified Yamaguchi reagents were developed to increase the efficiency of the Yamaguchi reagent.

Takeda and his group explored 2,4,6-trichlorobenzoyl chloride-4-dimethylaminopyridine (TCB-DMAP)[29], a modified Yamaguchi reagent that plays a promising role in the formation of esters with enough yields under suitable reaction condition and this method restrained the use of most intractable acid chlorides (Scheme 1.6).

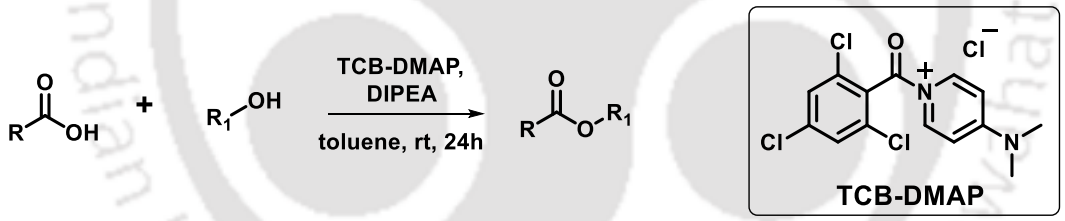

Scheme 1.6. *TCB-DMAP reagent-based esters synthesis*

Matsubara *et al.* explored several fluorous Yamaguchi (FY)[30] reagents, which serve as a critical coupling reagent for esterification under suitable reaction conditions. The reactivity of FY reagent is almost identical to the traditional Yamaguchi (TY) reagent. (Scheme 1.7)

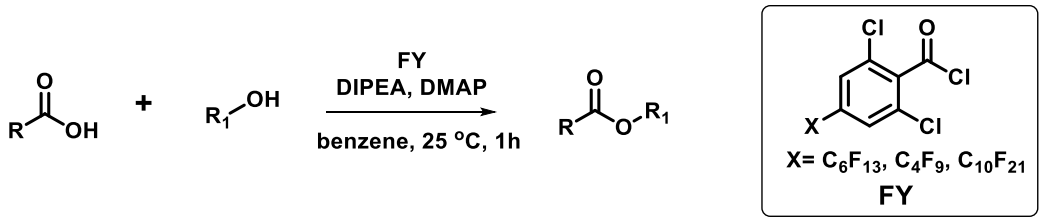

Scheme 1.7. *Synthesis of esters by using Fluorous Yamaguchi (FY) reagents*

Our group developed a newly Oxyma containing modified Yamaguchi reagent, (E)-ethyl-2-cyano-2-(((2,4,6-trichlorobenzoyl)oxy)imino)acetate (TCBOXY)[31], which is used for the effective formation esters, thioesters, amides, and peptides. The critical point of this method is racemization suppression ability and recyclability. (Scheme 1.8)

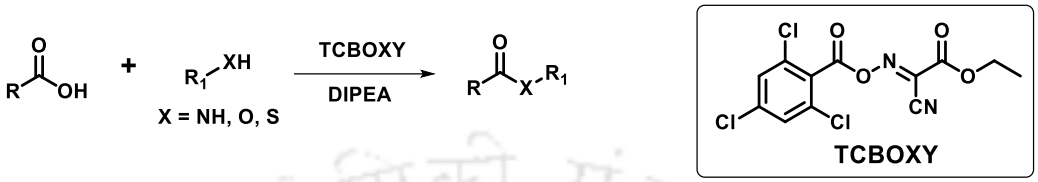

Scheme 1.8. *Synthesis of amides, esters, and thioesters by using TCBOXY reagent*

1.5. Amino acids

Amino acids are an elementary unit of peptides as well as proteins. Naturally occurring α-amino acid contains one amino group (-NH_2) and a side chain (-R) in the 2- or α-position of the carboxylic acid (-COOH) group. In nature, 22 α-amino acids are available for protein formation. Between the two optically active forms (L/D) of amino acids, only L-amino acids exist in the protein structure. These L-amino acids are called coded or proteinogenic amino acids. D-amino acids are present only in a few protein sequences, but these are not common. Depending on the side chain (R -group), amino acids are classified into various classes such as neutral, acidic, and basic. The physical and chemical features of amino acids depend on the side chain. At biological pH (7.4), all amino acids exist as dipolar ions, i.e., NH_3^+ ($–NH_2^+$ for proline) and CO_2^-; this dipolar ion is known as zwitterions. (Figure 1.5)

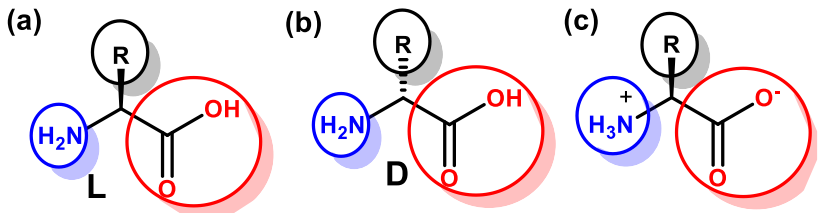

Figure 1.5. *(a) The general structure of L-α-amino acid and (b) D-α-amino acid, respectively, and (c) Zwitterionic structure of amino acid*

Aside from 22 coded amino acids, some unnatural or non-proteinogenic amino acids such as 2-aminoisobutyric acid (Aib), Phenylglycine (Phg), β-alanine, ornithine, and D-amino acids are present in a biological system. These amino acids enhance the proteolytic stability of a peptide. Non-proteinogenic amino acids are created through metabolic pathways or post-translational modification.

1.6. Peptides and proteins

In living systems, proteins (an essential class of large biomolecules) play a vital role in performing various biological functions. Proteins are polypeptide chains usually containing more than 50 amino acid residues, and their molecular mass varies from 10 kDa to 100 kDa. They serve as enzymes, receptors, hormones, cytokines, neurotransmitters, and growth factors.[32] A schematic representation is drawn to understand the amino acid to protein formation (Figure 1.6) and the basic structure of peptides (Figure 1.7).

Figure 1.6. *The pathway of amino acid to protein formation*

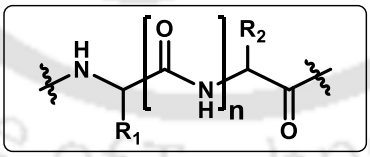

Figure 1.7. *The basic structure of peptides*

Peptides generally link amino acids through peptide bonds (amide bonds, Figure 1.7). It forms via a condensation reaction between the carboxylic acid (-COOH) group and amine ($-NH_2$) group of two amino acids with the removal of a water molecule. Depending on the number of peptide bonds, peptides are classified as di-, tri-, tetra-peptide, etc. Peptide chains have the potential for hydrogen bonding due to the availability of a suitable H-bond acceptor (-C=O) and donor (-NH) group. Usually, the Hydrogen bond (-C=O···HN-)

between polypeptide chains stabilizes the proteins. Peptide bond (C-N) cannot rotate freely because of its planarity. It attains resonance stabilize partials double bond character due to delocalization of lone pair electron of nitrogen (Figure 1.8a). Peptide bonds exist in two isomeric geometrical forms because of their double bond nature (Figure 1.8b).

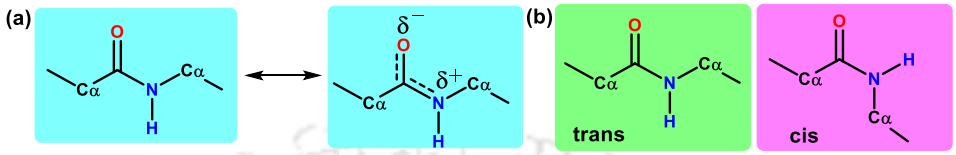

Figure 1.8. *(a) Resonance structure of the peptide and (b) cis-trans isomers of peptide bond*

1.6.1. Torsion angles

The peptide conformations are determined by three dihedral angles, also called torsion angles, denoted as phi (φ), psi (ψ), and omega (ω). Although planarity and partial double character restrict the rotation of peptide bond (C-N), the other two single bonds C_α-C and N-C_α in a peptide, can be rotated.[33] These two bonds provide the flexibility of the peptide backbone. The angle of rotation around N-C_α is called phi (φ) angle, and the rotation around C_α-C bond is considered as psi (ψ) angle (Figure 1.9). Its value may alter in the -180° to +180° region. The omega (ω) angle remains close to 180° due to its double bond nature.

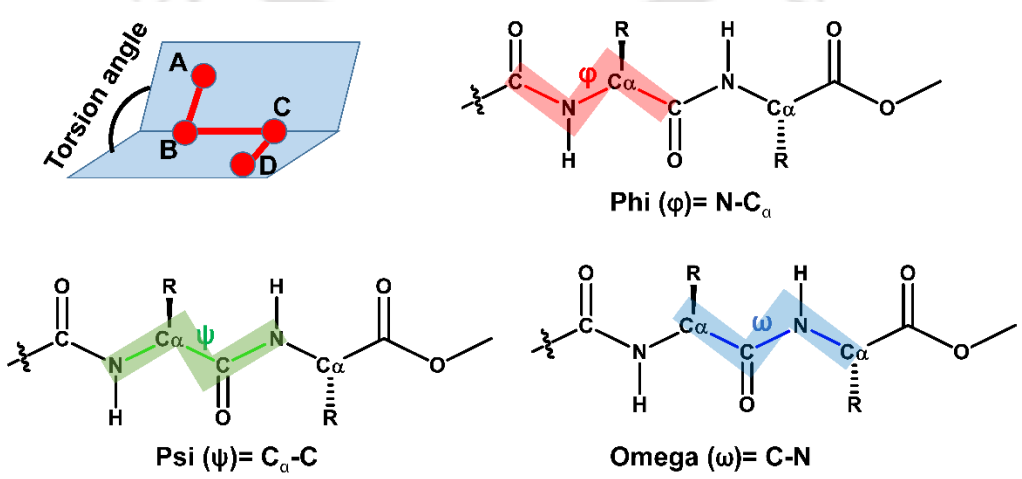

Figure 1.9. *A graphical presentation of various torsion angles of terminally protected dipeptide*

1.6.2. Structure of proteins

Usually, proteins molecule contains specific 3D Structure to perform crucial biological functions. Proteins structure is described in four stages such as primary, secondary, tertiary, and quaternary.

Primary structure

The linear arrangement of amino acids in a polypeptide chain is defined as the primary structure of proteins.

Secondary structure

Short-range 3D Structure of protein or peptide chain conformation, predominantly interconnected through H-bonding interaction between NH and C=O group of the peptide chain, is called a secondary Structure of proteins. In general, it contains three kinds of conformation, i.e., α-helix, β-sheet, and β-turn.[34]

α-helix

First, in 1951, Linus Pauling and Robert Corey discovered α-helix structure. This is a coil-like secondary conformation of peptide backbone which runs longitudinally through an imaginary axis, where side-chain groups are directed toward the outside from a helical strand. It earned stability via intramolecular H-bonding between CO group of i^{th} residue and NH group of $(i+4)^{th}$ residue. (Figure 1.10) The separation between helical turns is 5.4 Å (also known as pitch), and each turn contains 3.6 amino acid residues. For α-helix, the torsion angle lies between φ =-57° and ψ =-47°. All essential proteins contain right-handed α-helixes.

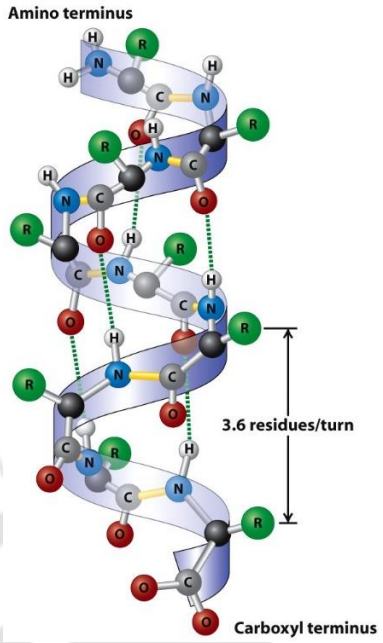

Figure 1.10. *Graphical representation of α-helix Structure (Courtesy: picture collected from Molecular Cell Biology, Sixth Edition © 2008 W. H. Freeman and Company).*

β-sheet

This is another secondary conformation where peptide backbones are fully extended. The stability of the β-sheet structure is governed by intermolecular hydrogen bonding interaction between the C=O group of one peptide chain and the NH group of another peptide chain.[35] The separation between two amino acids residue in the β-sheet strand is 3.5 Å. Depending on the direction of the adjacent peptide chain, two kinds of β-sheet are present in protein, such as parallel β-sheet and anti-parallel β-sheet. When two adjacent peptide chains run in the same direction, a β-sheet is called a parallel β-sheet, and if two adjacent peptide chains run in the opposite direction, a β-sheet is called an anti-parallel β-sheet (Figure 1.11). The stability of the anti-parallel β-sheet is higher than the parallel β-sheet because of the difference in the hydrogen-bonding pattern.

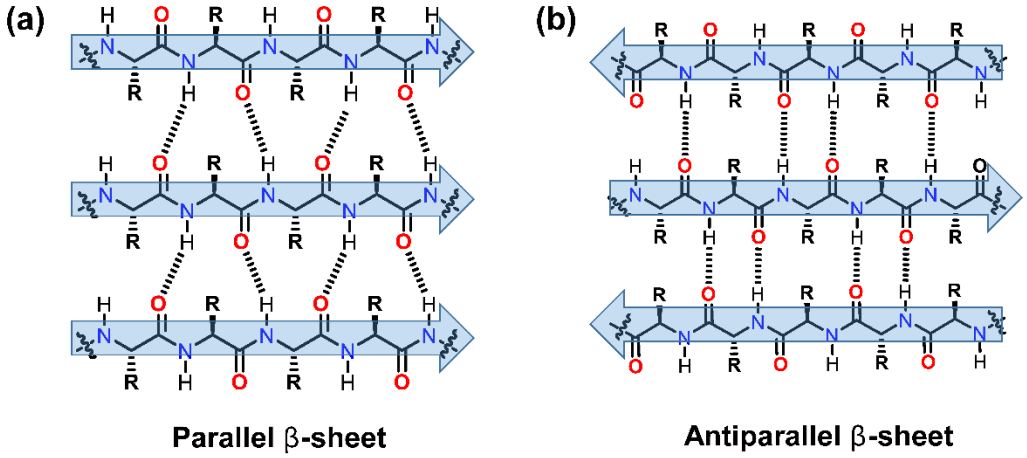

Figure 1.11. *(a) Represents a parallel β-sheet structure and (b) represents an anti-parallel β-sheet structure.*

β-turn

In this secondary structure, the polypeptide chain goes reverse direction and forms a turn or bent structure. The stability is established by intramolecular H-bonding between the CO group of the i^{th} residue and the NH group of $(i+3)^{th}$ residue. Inside the turn, the other two residues do not participate in any interaction but make a loop (Figure 1.12).

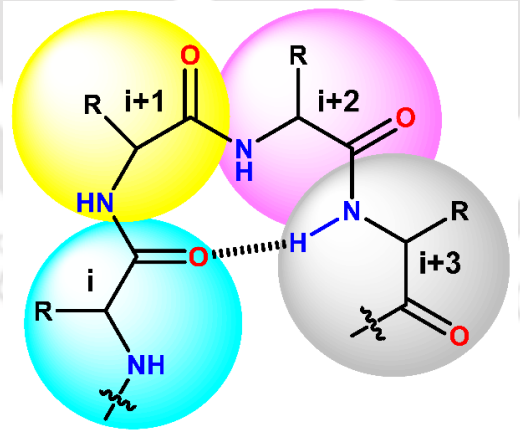

Figure 1.12*. General representation of β-turn structure*

Tertiary Structure

The entire 3D shape is obtained by various supramolecular noncovalent interactions called the tertiary structure of proteins.

Quaternary Structure

The various tertiary domain of proteins or several protein molecules interacts through noncovalent interaction and form a larger aggregate 3D complex called quaternary structure.

1.7. Alzheimer's disease

Alzheimer's disease is a growing neurodegenerative disorder. It is the reason for approximately 60-70% cause of dementia. The primary symptoms associated with this disease are memory loss, problems with language, depression, mood swings, and loss of thinking ability.[36] The proper reason for Alzheimer's disease is still unknown. Scientists consider that two kinds of protein aggregation are the leading cause of this disease.

1. Tau proteins intracellularly self-aggregate and change shape to form neurofibrillary tangles (NFTs). These tangles disrupt normal neuronal functioning and connectivity.

2. Amyloid β (Aβ) proteins extracellularly accumulate as amyloid plaques, which play a toxic role on neurons and affect cell-cell communication.[37] Both Aβ plaques and NFTs are biomarkers of Alzheimer's disease.

1.7.1. Amyloid β (Aβ) peptide

Aβ peptide is a peptide chain containing 36-43 amino acids. This is the primary unit of amyloid plaques. The enzymatic (beta-secretase and gamma-secretase) cleavage of amyloid precursor protein (APP) generated Aβ peptide.[38] The peptide sequence of $A\beta_{1\text{-}42}$ is displayed in Figure 1.13.

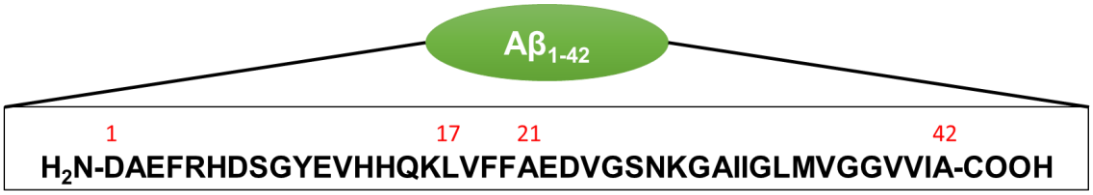

Figure 1.13. *The peptide sequence of $A\beta_{1\text{-}42}$*

1.7.2. The structural characteristics of Aβ peptide

The aggregation of Aβ peptide to create a cross-β-sheet structure was observed in XRD, NMR, and cryoEM experiments.[39-41] Lansbury group established the anti-parallel β-sheet arrangement of $A\beta_{34-42}$ peptides through ssNMR studies.[42-43] Tycko *et al.* demonstrated an anti-parallel β-sheet conformation of a model $A\beta_{16–22}$ peptides by ssNMR experiment.[44] It is predicted that the central hydrophobic core region ($A\beta_{17-21}$, LVFFA) is a crucial fragment for fibril formation of Aβ peptide than that of the *C*-terminal hydrophobic region ($A\beta_{29-42}$).[45-47] The fibril formation pathway of Aβ peptide is not clear yet. Researchers are trying to develop the actual structure of the full length of Aβ peptide or several small fragments of this by SCXRD study. Banerjee and coworkers developed that $A\beta_{40-42}$ formed an anti-parallel β-sheet arrangement in solid-state and displayed amyloidogenic properties.[48] Further, they demonstrated that $A\beta_{9–11}$ peptides formed β-sheet structures and exhibited amyloidogenic nature.[49] Haldar and his group demonstrated that terminally capped Boc-VF-OMe ($A\beta_{18-19}$) peptides are organized in a cross-β-sheet arrangement in solid-state.[50] They also reported Boc-FF-OMe ($A\beta_{19-20}$) formed an inverse γ-turn structure and anti-parallel β-sheet arrangement.[51] Terminally protected Boc-VV-OMe ($A\beta_{39-40}$) and Boc-IA-OMe ($A\beta_{41-42}$) displayed parallel β-sheet architecture.[52-53]

1.8. Small peptide-based nanostructure

The speciality of the self-assembly process is the fabrication of various novel supramolecular structures. The concept of advancement of structural architecture comes from nature, as it produces various complex structures from amino acids, lipids, and nucleic acids in the biological system. Peptide nanostructures are essential due to their self-association efficiency, chemical variety, biocompatibility, capability for specific molecular recognition, and biodegradability.[54-57] The fabrication of various vital nanostructures such as nanorods, nanobelts, nanofibrils, nanotapes, nanotubes, nanospheres, nano-ribbons, and gel has been developed by diverse self-assembled Structure, i.e., aromatic or aliphatic dipeptides[58-59], cyclic peptides[60], amphiphile peptides[61], and surfactant-like peptides[62]. These nanostructures have essential applications in biotechnology and medicinal chemistry like ion channels[63], drug delivery[64], nano-

electronics[65], nano-sensors[66], tissue engineering[67], and glucose transporters[68]. (Figure 1.14)

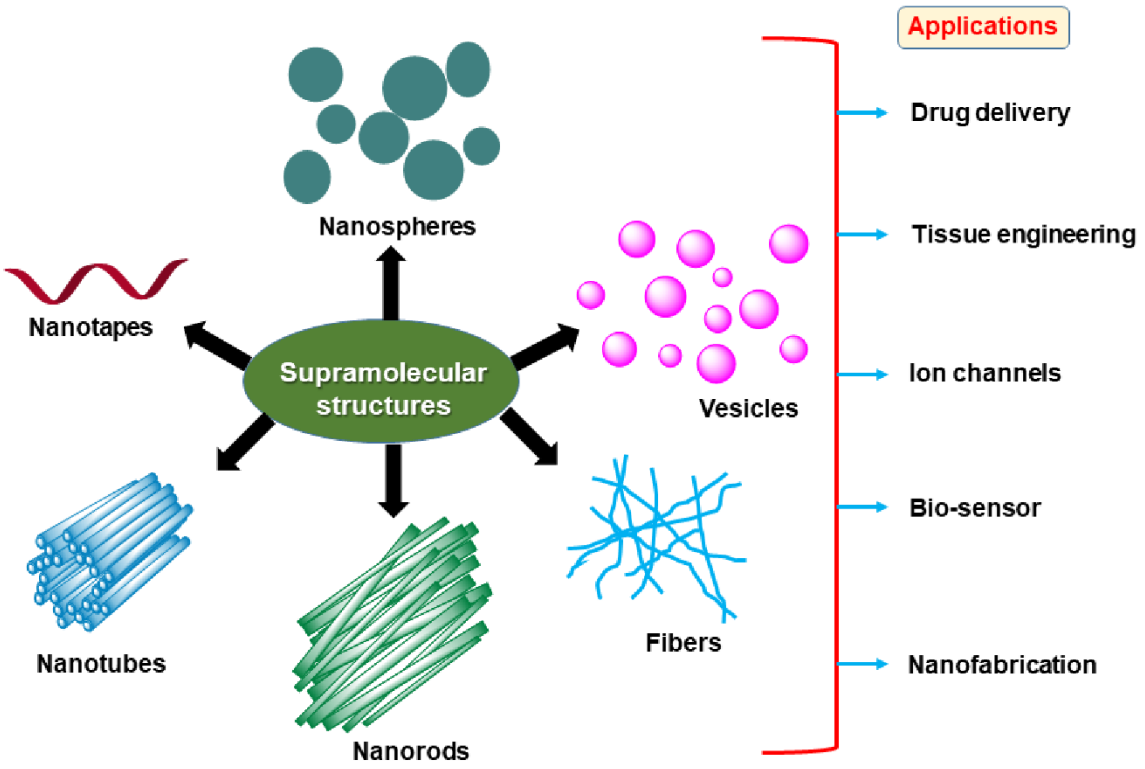

Figure 1.14. *Various kinds of supramolecular strucrures and their applications*

1.8.1. Di-peptides based self-assembly

Reches and Gazit reported that dipeptide Phe-Phe (FF), a central hydrophobic region of $A\beta_{42}$, formed self-assembled peptide nanotubes. This nanotube has versatile applications in casting silver nanowire[59], low molecular-mass organogel, electrochemical biosensing[69], nanoforests[70], and template for magnetic nanoparticles.[71] Görbitz studied the structural insights of a series of unprotected hydrophobic di-peptides crystal, including FF peptides, which explain the mechanism of the formation of nanotubes.[72] Zelenovskiy *et al.* reported that right and left-handed helix created by L-Phe-L-Phe and D-Phe-D-Phe peptides, respectively, and both formed nano-tubes structures.[73]

Yang and his group developed the formation of the twisted nano-ribbons structure by eight dipeptides containing L/D amino acid Phe and Phg.[74] The handedness of nano-ribbons structure is governed by chirality and steric factor of Phe and Phg, respectively.

Ponnuswamy *et al.* discussed the crystalline properties of dipeptide Boc-VF-OMe ($A\beta_{18-19}$).[75] Haldar *et al.* reported that this peptide formed amyloid-like fibrillar aggregates, and in solid-state, its exhibited supramolecular β-sheet and cross-β-sheet structure.[50]

They also reported that tyrosine-modified peptides (terminally protected FY, YF, YY) of Boc-FF-OMe ($A\beta_{19-20}$) peptide-based inhibition of fibrils formation.[51] Modified peptides formed microspheres structure compared to the fibrillar structure of protected FF. SCXRD suggested that protected FF adopts an inverse γ-turn structure, whereas modified peptides formed a parallel β-sheet conformation.

Furthermore, they reported inhibition of fibril formation of modified peptide sequence of Boc-FL-OMe (AS_{6-7}) by increasing peptide chain length and replacing aromatic-H with -OMe group.[76] Different kinds of supramolecular arrangements were created by peptides sequence.

Görbitz et al. investigated the structural features of Boc-VV-OMe ($A\beta_{39-40}$), which displayed a parallel β-sheet conformation.[52] Our group reported crystallographic architecture of Boc-VV-OMe and Boc-IA-OMe ($A\beta_{41-42}$); both formed parallel β-sheet structures in the solid-state but generated different morphology.[53]

Lorenzi et al. published the solid-state molecular packing of both side protected (Boc- for N-terminal, -OMe for C-terminal) dipeptides, containing L and D amino acids of Leu, Ile, allo-Ile.[77]

Later our group manifested diversity in nanostructure formation by terminally blocked (Boc- for N-terminal, -OMe for C-terminal) dipeptides bearing various combinations of L and D amino acids of Val and Ile.[78] SC-XRD analysis suggested that peptides create different helix-like structure and hollow hexagonal tube-like architectures.

Moreover, our group discussed the diversity in conformation, morphology, and supramolecular packing of four terminally protected hydrophobic di-peptides bearing Ile, L/D Phe, and Phg, depending on chirality and side-chain of the amino acids.[79]

Pramanik et al. demonstrated the ω-amino acid bearing di-peptides such as Boc-β-Ala-*m*-ABA-OMe and Boc-γ-Abu-*m*-ABA-OMe (γ-Abu: γ -aminobutyric acid) self-assembled to β-sheet structure in solid-state.[80] Both peptides formed amyloid-like fibrils structure, which has Congo red binding affinity.

Koley and Pramanik reported the formation of various nanostructures such as nanotubes, nanorods, nanovesicles, and nanofibrils by one hydrophobic amino acids (Phe, Tyr Trp, and Leu) and unnatural (*o*/*m*/*p*)-aminobenzoic acids bearing protected (Boc- for N-terminal, -OMe for C-terminal) di-peptides.[81] Morphological variety depends on protecting group parameters and solvent polarity. Structural studies also discussed explaining the self-assembly mechanism.

Halder *et al.* reported that N-terminal protected three isomeric di-peptides of Boc-Phe-*o/m/p*-ABA-OH exhibited different morphology and N_2-gas adsorption tendency.[82] In the crystalline state, all formed a different kind of helical architecture.

Tai and his groups discussed the nano-structural diversity, i.e., nano-vesicles, nano-ribbons/fibrils, and nanotubes of Boc-m-ABA-Aib-OMe peptide in the presence of several physical and chemical stimuli.[83] In a crystalline state, peptides form β-sheet layer-like structures, which explain the self-assembly mechanism for nano-vesicles formation. Later, they studied the self-assembly of its reverse peptide sequence, i.e., Boc-Aib-m-ABA-OMe.[84] Interestingly, the two peptides displayed distinctly different morphology and cell viability. Different kinds of molecular packing of those peptides explain the morphological heterogeneity.

1.8.2. Tri-peptides based self-assembly

Banerjee *et al.* developed the amyloid-like fibrils structure of VIA ($A\beta_{39-40}$) peptide, and in solid-state, it formed an anti-parallel β-sheet arrangement.[48] They also published GYE ($A\beta_{9-11}$) hydrophilic tripeptide-based formation of amyloid-like fibrils and β-sheet structure.[49]

Adhikari *et al.* developed the chirality-dependent gelation behavior of conjugated ferrocene tripeptide FFA ($A\beta_{19-21}$) and displayed various nanostructures such as nanorods and nanofibers.[85]

Haldar *et al.* developed organogel with sonication of nanofibers of Boc-VFF-OMe ($A\beta_{18-20}$) tripeptide.[86] Marchesan *et al.* studied the unprotected VFF peptide and heterochiral isomers (D and L amino acid-containing peptides) based formation of hydrogel and various fibrous networks, where amino acids chirality plays the central role in the self-

assembly process.[87,88] They also reported chirality-controlled hydrogel formation properties and fibrous network creation of unprotected FFV peptides and their isomers.[89]

Our group discussed the conformation, morphology, and supramolecular architecture of tri-peptide Boc-GFF-OMe and its analogous peptides by altering chirality and by incorporating unnatural amino acid, Phg.[90]

1.9. Knowledge gap

Although various HOBt-based coupling reagents have been explored, due to their desmotropic nature, its reactivity pathway (either N-substituted or O-substituted or both forms) toward acylation reaction is not clear to date. Therefore, further development is needed to understand the proper pathway.

Furthermore, protecting group-mediated self-assembly of small peptides has not been well explored yet.

Although conformational analyses, self-assembly, and morphology studies of many short peptides have been reported, most of these works are based on homo-chirality (L-predominantly) and natural L-amino acid-containing peptides. Enantiomeric peptide, the introduction of D-amino acid in the peptide chain, alternating D/L-amino acids, and reverse peptide sequences are not well explored.

Moreover, morphology and conformational studies of rigid, unnatural amino acid-containing peptide sequences are not explored enough. However, alternating D/L amino acid and unnatural amino acid in a peptide sequence increases the proteolytic stability of the formed nanostructure.

In addition, conformation and morphology diversity by incorporating tryptophan residue in a small amyloidogenic peptide sequence is not explored enough till now. Therefore, some more exploration is required to address these problems.

1.10. Objectives of the thesis

The following objectives are proposed in my Ph. D. thesis work to address the above-mentioned problems.

1. Development of HOBt-based modified Yamaguchi reagent, TCB-OBt, investigation of its self-assembly impacts, and the efficiency as a coupling reagent.
2. Exploration of the role of various N-terminus protecting groups of unnatural and rigid amino acid containing di-peptides (Ant-Aib) on the supramolecular assembly.
3. Investigation of supramolecular self-assembly, conformation, and morphology of terminally protected Ant and Phg containing di-peptides and their reverse peptide sequences.
4. To examine the contribution of incorporation of the tryptophan residue in amyloidogenic dipeptide sequences on the self-assembly process.
5. Investigation of the effect of chirality on the self-assembly properties of Boc-Val-Phe-Phe-OMe, having sequence similarity with Alzheimer's amyloid-β ($A\beta_{18-20}$) in solution state and the solid-state.

1.11. References

1. Rehm, T. H.; Schmuck, C. Ion-pair induced self-assembly in aqueous solvents. *Chem. Soc. Rev.* **2010**, *39*, 3597-3611.
2. Whitesides, G. M.; Grzybowski, B. Self-Assembly at All Scales. *Science* **2002**, *295*, 2418-2421.
3. Humphrey, J. M.; Chamberlin, A. R. Chemical Synthesis of Natural Product Peptides: Coupling Methods for the Incorporation of Noncoded Amino Acids into Peptides. *Chem. Rev.* **1997**, *97*, 2243-2266.
4. Janssen, B.; Hohenadel, D.; Brinkkoetter, P.; Peters, V.; Rind, N.; Fischer, C.; Rychlik, I.; Cerna, M. Carnosine as a protective factor in diabetic nephropathy: association with a leucine repeat of the carnosinase gene CNDP1. *Diabetes*. **2005**, *54*, 2320-2327.
5. Graul, A.; Castaner, J. Atorvastatin calcium hypolipidemic, HMG-CoA reductase inhibitor. *Drugs Future.* **1997**, *22*, 956-968.
6. De Gasparo, M.; Whitebread, S. Binding of valsartan to mammalian angiotensin AT1 receptors. *Regul. Pept.* **1995**, *59*, 303-311.
7. Roush, A. J.; Eds, W. R. Handbook of reagents for organic synthesis: Activating agents and protecting groups Pearson. *Wiley: New York.* **1999**, 370-373.
8. Knapp, S.; Gibson, F. S. In Organic Syntheses. *Wiley: New York.* **1998**, *9*, 516-521.
9. Pearson, A. J.; Roush. W. R. Handbook of reagents for organic synthesis: activating agents and protecting groups. *Wiley: New York*. **1999**, 333.
10. Antell, M. F.; Patai, S. Ed. In the chemistry of acyl Halides. *Interscience: London.* **1972**, 40-44.
11. Sheehan, J. C.; Hess, G. P. A new method of forming peptide bonds. *J. Am. Chem. Soc*. **1955**, *77*, 1067-1068.
12. King, W.; Geiger, R. A new method for the synthesis of peptides: activation of the carboxyl group with dicyclohexylcarbodiimide with addition of 1-hydroxybenzotriazoles. *Chem. Ber*. **1970**, *103*, 788-799.
13. Carpino, L. A. 1-Hydroxy-7-azabenzotriazole. An efficient peptide coupling additive. *J. Am. Chem. Soc.* **1993**, *115*, 4397-4398.
14. Fenza, A. D.; Rovero, P. Assessment of new 6-Cl-HOBt based coupling reagents for peptide synthesis. Part 2: Racemization studies. *Letters in Peptide Science*, **2002**, *9*, 125-129.
15. Sierosl⁄awski, K.; Picur, B.; Lis, T. Structure of benzotriazole-1-yl-oxy-tris-(dimethylamino)-phosphonium hexafluorophosphate (BOP). *Journal of Molecular Structure* **2003**, *657*, 93-99.
16. Coste, J.; Le-Nguyen, D.; Castro, B. PyBOP®: A new peptide coupling reagent devoid of toxic by-product. *Tetrahedron Lett.* **1990**, *31*, 205-208.
17. Dourtoglou, V.; Ziegler, J. C.; Gross, B. O-Benzotriazolyl-N, N-tetramethyluronium hexafluorophosphate: a new and effective reagent for peptide coupling. *Tetrahedron Lett.* **1978**, *19*, 1269-1272.
18. Kiso, Y.; Fujiwara, Y.; Kimura, T.; Nishitani, A.; Akaji, K. Efficient solid phase peptide synthesis: Use of methanesulfonic acid α-amino deprotecting procedure and new coupling reagent, 2-

(benzotriazol-1-yl)oxy-1,3-dimethylimidazolidinium hexafluorophosphate (BOI). *Int. J. Pept. Protein Res*. **1992**, *40*, 308-314.

19. Chen, S.; Xu, J. A new coupling reagent for peptide synthesis. Benzotriazolvyloxy-bis (pyrroltdino) -carbonium hexaflouorophosphate (BBC). *Tetrahedron Lett*. **1992**, *33*, 647-650.
20. Li, P.; Xu, J. C. BOMI-A Novel Peptide Coupling Reagent. *Tetrahedron Letters* **1999**, *40*, 3605-3608.
21. Li, P.; Xu, J. C. HOBt and HOAt-derived immonium salts: new and highly efficient coupling reagents for peptide synthesis. *Tetrahedron Letters* **2000**, *41*, 721-724.
22. Topuzyan, V. O.; Martirosyan, M. S. 1-(o-Nitrophenylsulfonyloxy)benzotriazole-A Reagent for Condensation of Carboxylic Acids with Amines. *ChemInform* **1992**, *23*, https://doi.org/10.1002/chin.199230149.
23. Wardrop, D. J.; Bowen, E. G. 9-Fluorenylmethyl 1-Benzotriazolyl Carbonate (3-Oxy-benzotriazolinium-1- carboxylic Acid 9H-Fluoren-9-ylmethyl Ester). Encyclopedia of Reagents for Organic Synthesis **2003**, https://doi.org/10.1002/047084289X.rn00275.
24. Abdelmoty, I.; Albericio, F.; Carpino, L. A.; Foxman, B. M.; Kates, S. A. Structural studies of reagents for peptide bond formation: Crystal and molecular structures of HBTU and HATU. *Lett. Pept. Sci.* **1994**, *1*, 57-67.
25. Li, P.; Xu, J. C. The X-ray structures of HOBt-based immonium-type coupling reagents and the rearrangement of benzotriazolyl esters of N_{α}-protected amino acids or peptides: *N- vs. O*-substituted forms. *J. Chem. Soc., Perkin Trans.* **2001**, *2*, 113-120.
26. Crisma, M.; Valle, G.; Moretto, V.; Formaggio, F.; Toniolo, C.; Albericio, F. Reactive intermediates in peptide synthesis: Molecular and crystal structures of HOAt and HOOBt, and some ester and amide derivatives of HOBt, HOAt and HOOBt. *Lett. Pept. Sci.* **1998**, *5*, 247-258.
27. Barlos, K.; Papaioannou, D.; Theodoropoulos, D. Preparation and properties of N_{α}-trityl amino acid 1-hydroxybenzotriazole esters**.** *Int. J. Pept. Protein Res.* **1984**, *23*, 300-305.
28. Inanaga, J.; Hirata, K.; Saeki, H.; Katsuki, T.; Yamaguchi, M. A Rapid Esterification by Means of Mixed Anhydride and Its Application to Large-ring Lactonization. *Bull. Chem. Soc. Jpn.* **1979**, *52*, 1989-1993.
29. Okuno, Y.; Isomura, S.; Nishibayashi, A.; Hosoi, A.; Fukuyama, K.; Ohba, M.; Takeda, K. Modified Yamaguchi reagent: convenient and efficient esterification. *Synth. Commun.* **2014**, *44*, 2854-2860.
30. Nishio, Y.; Kawazu, A.; Hirano, S.; Matsubara, H. Preparation of fluorous Yamaguchi reagents and evaluation of their reactivity in esterification. *Tetrahedron* **2016**, *72*, 720-725.
31. Chandra, J.; Manne, S. R.; Mondal, S.; Mandal, B. (E)-Ethyl-2-cyano-2-(((2,4,6-trichlorobenzoyl)oxy)imino)acetate: A Modified Yamaguchi Reagent for Enantioselective Esterification, Thioesterification, Amidation, and Peptide Synthesis. *ACS Omega* **2018**, *3*, 6120-6133.
32. Clamp, M.; Fry, B.; Kamal, M.; Xie, X.; Cuff, J.; Lin, M. F.; Kellis, M.; Lindblad-Toh, K.; Lander, E. S. Distinguishing protein-coding and noncoding genes in the human genome. *Proc. Natl. Acad. Sci. U.S.A.* **2007**, *104*, 19428-19433.

33. Nelson, D. L; Cox, M. M. *Lehninger's Principles of Biochemistry*, 7th ed.; W. H. Freeman and Company: New York, 2017.
34. Pauling, L.; Corey, R. B.; Branson, H. R. The structure of proteins: Two hydrogen-bonded helical configuration of the polypeptide chain. *Proc. Nat. Acad. Sci. U.S.A.* **1951**, *37*, 205-211.
35. Pauling, L.; Corey, R. B. The pleated sheet, A new layer configuration of polypeptide chains. *Proc. Nat. Acad. Sci. U.S.A.* **1951**, *37*, 251-256.
36. Hamley, I. W. The amyloid beta peptide: a chemist's perspective. Role in and Alzheimer's fibrillization. *Chem. Rev*. **2012**, *112*, 5147-5192.
37. Knowles, T. P. J.; Vendruscolo, M.; Dobson, C. M., The amyloid state and its association with protein misfolding diseases. *Nat. Rev. Mol. Cell Biol*. **2014**, *15*, 384-396.
38. Zheng, H.; Koo, E. H. Biology and pathophysiology of the amyloid precursor protein. *Mol. Neurodegener*, **2011**, *6*, 27.
39. Squires, A. M.; Devlin, G. L.; Gras, S. L.; Tickler, A. K.; MacPhee C. E.; Dobson, C. M. X-ray scattering study of the effect of hydration on the cross-β structure of amyloid fibrils. *J. Am. Chem. Soc.* **2006**, *128*, 11738-11739.
40. Zhang, R.; Hu, X.; Khant, H.; Ludtke, S. J.; Chiu, W.; Schmid, M. F.; Frieden C.; Lee, J.-M. Interprotofilament interactions between Alzheimer's Aβ_{1-42} peptides in amyloid fibrils revealed by cryoEM. *Proc. Natl. Acad. Sci. U. S. A.* **2009**, *106*, 4653-4658.
41. Makin, O. S.; Serpell, L. C. Structures for amyloid fibrils. *FEBS Journal*, **2005**, *272*, 5950-5961.
42. Griffiths, J. M.; Ashburn, T. T.; Lansbury, P. T.; Auger, M.; Costa P. R.; Griffin, R. G. Rotational resonance solid-state NMR elucidates a structural model of pancreatic amyloid. *J. Am. Chem. Soc.* **1995**, *117*, 3539-3546.
43. Lansbury, P.; Costa, P. R.; Griffiths, J. M.; Simon, E. J.; Auger, M.; Halverson, K. J.; Kocisko, D. A.; Hendsch, Z. S.; Ashburn, T. T.; Spencer, R. G. S.; Tidor, B.; Griffin, R. G. Structural model for the β-amyloid fibril based on interstrand alignment of an antiparallel-sheet comprising a C-terminal peptide. *Nat. Struct. Biol.* **1995**, *2*, 990-998.
44. Balbach, J. J.; Ishii, Y.; Antzutkin, O. N.; Leapman, R. D.; Rizzo, N. W.; Dyda, F.; Reed J.; Tycko, R. Amyloid fibril formation by Aβ_{16-22}, a seven-residue fragment of the Alzheimer's β-amyloid peptide, and structural characterization by solid state NMR. *Biochemistry*, **2000**, *39*, 13748-13759.
45. Doran, T. M.; Kamens, A. J.; Byrnes, N. K.; Nilsson, B. L. Role of amino acid hydrophobicity, aromaticity, and molecular volume on IAPP (20–29) amyloid self-assembly. *Proteins*, **2012**, *80*, 1053-1065.
46. Tartaglia, G. G.; Cavalli, A.; Pellarin, R.; Caflisch, A. The role of aromaticity, exposed surface, and dipole moment in determining protein aggregation rates. *Protein Science*, **2004**, *13*, 1939-1941.
47. Tjernberg, L. O.; Naslund, J.; Lindqvist, F.; Johansson, J.; Karlstromi, A. R.; Thyberg, J.; Terenius, L.; Nordstedt, C. Arrest of β-amyloid fibril formation by a pentapeptide ligand. *The J. Biol. Chem.* **1996**, *271*, 8545-8548.
48. Ray, S.; Das, A. K.; Drew M. G. B.; Banerjee, A. A short water-soluble self-assembling peptide forms amyloid-like fibrils. *Chem. Commun.* **2006**, 4230-4232.

49. Naskar, J.; Drew, M. G. B.; Deb, I.; Das S.; Banerjee, A. Water-Soluble tripeptide Aβ (9-11) forms amyloid-like fibrils and exhibits neurotoxicity. *Org. Lett.* **2008**, *10*, 2625-2628.
50. Maity, S.; Kumar, P.; Haldar, D. An amyloid-like fibril-forming supramolecular cross-β-structure of a model peptide: a crystallographic insight. *Org. Biomol. Chem.* **2011**, *9*, 3787.
51. Bera, S.; Jana, P.; Maity, S. K.; Haldar, D. Inhibition of Fibril Formation by Tyrosine Modification of Diphenylalanine: Crystallographic Insights. *Cryst. Growth Des.* **2014**, *14*, 1032-1038.
52. Jacobsen, Ø.; Gebreslasie, H. G.; Klaveness, J.; Rongved P.; Görbitz, C. H. N-(tert-Butoxycarbonyl)-L-valyl-L-valine methyl ester: a twisted parallel β-sheet in the crystal structure of a protected dipeptide. *Acta Crystallogr., Sect. C: Cryst. Struct. Commun.*, **2011**, *67*, 278-282.
53. Giri, R. S.; Mandal, B. Boc-Val-Val-OMe ($A\beta_{39-40}$) and Boc-Ile-Ala-OMe ($A\beta_{41-42}$) crystallize in a parallel β-sheet arrangement but generate a different morphology. *CrystEngComm* **2018**, *20*, 4441-4448.
54. Gazit, E. Self-assembled peptide nanostructures: the design of molecular building blocks and their technological utilization. *Chem. Soc. Rev.* **2007**, *36*, 1263-1269.
55. Reches, M.; Gazit, E. Casting Metal Nanowires Within Discrete Self-Assembled Peptide Nanotubes. *Science* **2003**, *300*, 625-627.
56. Yanlian, Y.; Khoe, U.; Wang, X.; Horii, A.; Yokoi, H.; Zhang, S. Designer self-assembling peptide nanomaterials. *Nano Today* **2009**, *4*,193.
57. Du, C.; Falini, G.; Fermani, S.; Abbott, C.; Oldak, J. M. Supramolecular Assembly of Amelogenin Nanospheres into Birefringent Microribbons. *Science* **2005**, *307*, 1450-1454.
58. Görbitz, C. H. Microporous organic materials from hydrophobic dipeptides. *Chem. Eur. J.* **2007**, *13*, 1022-1031.
59. Reches, M.; Gazit, E. Casting metal nanowires within discrete self-assembled peptide nanotubes. *Science* **2003**, *300*, 625-627.
60. Brea, R. J.; Reiriz, C.; Granja, J. R. Towards functional bionanomaterials based on self-assembling cyclic peptide nanotubes. *Chem. Soc. Rev.* **2010**, *39*, 1448-1456.
61. Cavalli, S.; Albericio, F.; Kros, A. Amphiphilic peptides and their cross-disciplinary role as building blocks for nanoscience. *Chem. Soc. Rev.* **2010**, *39*, 241-263.
62. Vauthey, S.; Santoso, S.; Gong, H.; Watson, N.; Zhang, S. Molecular self-assembly of surfactant-like peptides to form nanotubes and nanovesicles. *Proc Natl Acad Sci U. S. A.* **2002**, *99*, 5355-5360.
63. Sanchez-Quesada, J.; Isler, M. P.; Ghadiri, M. R. Modulating ion channel properties of transmembrane peptide nanotubes through heteromeric supramolecular assemblies. *J. Am. Chem. Soc.* **2002,** *124*, 10004-10005.
64. Zhao, F.; Ma, M. L.; Xu, B. Molecular hydrogels of therapeutic agents. *Chem. Soc. Rev.* **2009**, *38*, 883-891.
65. Ashkenasy, N.; Horne, W. S.; Ghadiri, M. R. Design of self-assembling peptide nanotubes with delocalized electronic states. *Small* **2006**, *2*, 99-102.
66. Kiyonaka, S.; Sada, K.; Yoshimura, I.; Shibkai, S.; Kato, N.; Hamachi, I. Semi-wet peptide/protein array using supramolecular hydrogel. *Nat Mater* **2004**, *3*, 58-64.

67. Zhang, S. Designer Self-assembling peptide nanofiber scaffolds for study of 3-D cell biology and beyond. *Adv. Cancer Res.* **2008**, *99*, 335-362.
68. Granja, J. R.; Ghadiri, M. R. Channel-mediated transport of glucose across lipid bilayers. *J. Am. Chem. Soc.* **1994**, *116*, 10785-10786.
69. Carny, O.; Shalev, D. E.; Gazit, E. Fabrication of Coaxial Metal Nanocables Using a Self-Assembled Peptide Nanotube Scaffold. *Nano Lett.* **2006**, *6*, 1594-1597.
70. Reches, M.; Gazit, E. Controlled patterning of aligned self-assembled peptide nanotubes. *Nat. Nanotechnol.* **2006**, *1*, 195-200.
71. Yemini, M.; Reches, M.; Rishpon, J.; Gazit, E. Novel electrochemical biosensing platform using self-assembled peptide nanotubes. *Nano Lett.* **2005**, *5*, 183-186.
72. Görbitz, C. H. Nanotube Formation by Hydrophobic Dipeptides. *Chem.-Eur. J.* **2001**, 7, 5153-5159.
73. Zelenovskiy, P. S.; Nuraeva, A. S.; Kopyl, S.; Arkhipov, S. G.; Vasilev, S. G.; Bystrov, V. S.; Gruzdev, D. A.; Waliczek, M.; Svitlyk, V.; Shur, V. Y.; Mafra, L.; Kholkin, A. L. Chirality-Dependent Growth of Self-Assembled Diphenylalanine Microtubes. *Cryst. Growth Des.* **2019**, *19*, 6414-6421.
74. Lin, S.; Li, Y.; Li, B.; Yang, Y. Control of the Handedness of Self-assemblies of Dipeptides by the Chirality of Phenylalanine and Steric Hindrance of Phenylglycine. *Langmuir* **2016**, *32*, 7420-7426.
75. Nallini, A.; Saraboji, K.; Ponnuswamy, M. N.; Katti, S. B. Structure and conformation of n- (t-butoxycarbonyl)-l-valine-l-phenylalanine-methyl ester (Boc-Val-Phe-OMe). *Cryst. Res. Technol.* **2004**, 39, 179-184.
76. Paikar, A.; Debnath, M.; Podder, D.; Sasmal, S.; Haldar, D. Synthesis and structural investigation of 2-aminomethyl-3-(4-methoxy-phenyl)-propionic acid containing a peptide analogue of the amyloidogenic AS(6–7) sequence: inhibition of fibril formation. *Org. Biomol. Chem.* **2017**, *15*, 4218-4225.
77. Blasio, B. D.; Saviano, M.; Duca, V. D.; Simone, G. D.; Rossi, F.; Pedone, C.; Benedetti, E.; Lorenzi, G. P. Conformational Studies of Heterochiral Peptides with Diastereoisomeric Residues: Crystal and Molecular Structures of Linear Dipeptides Derived from Leucine, Isoleucine, and allo-lsoleucine. *Biopolymers* **1995**, *36*, 401-408.
78. Giri, R. S.; Pal, S.; Roy, S.; Dolai, G.; Manne, S. R.; Paul, S.; Mandal, B. Nanostructures from protected L/L and D/L amino acid containing dipeptides. *Pept. Sci.* **2020**, *113*, e24176.
79. Roy, S.; Giri, R. S.; Dolai, G.; Mandal, B. Role of side-chain and chirality of the amino acids on the supramolecular assemblies of dipeptides. *J. Mol. Str.* **2020**, *1221*, 128877.
80. Dutt, A.; Drew, M. G. B.; Pramanik, A. β-Sheet mediated self-assembly of dipeptides of ω-amino acids and remarkable fibrillation in the solid state. *Org. Biomol. Chem.*, **2005**, *3* ,2250.
81. Koley, P.; Pramanik, A. Nanostructures from Single Amino Acid-Based Molecules: Stability, Fibrillation, Encapsulation, and Fabrication of Silver Nanoparticles. Adv. Funct. Mater. 2011, 21, 4126-4136.

82. Maity, S.; Jana, P.; Maity, S. K.; Kumar, P.; Haldar, D. Conformational Heterogeneity, Self-Assembly, and Gas Adsorption Studies of Isomeric Hybrid Peptides. *Cryst. Growth Des.* **2012**, *12*, 422-428.
83. Kar, S.; Wu, K. W.; Hsu, I. J.; Lee, C. R.; Tai, Y. Study of the nano-morphological versatility by self-assembly of a peptide mimetic molecule in response to physical and chemical stimuli. *Chem. Commun.* **2014**, *50*, 2638-2641.
84. Kar, S.; Tai, Y. Marked difference in self-assembly, morphology, and cell viability of positional isomeric dipeptides generated by reversal of sequence. Soft Matter, 2015, 11, 1345-1351.
85. Adhikari, B.; Singh, C.; Shah, A.; Lough, A. J.; Kraatz, H. B. Amino Acid Chirality and Ferrocene Conformation Guided Self-Assembly and Gelation of Ferrocene–Peptide Conjugates. *Chem.-Eur. J.* **2015**, *21*, 11560-11572.
86. Maity, S.; Kumar, P.; Haldar, D. Sonication-induced instant amyloid-like fibril formation and organogelation by a tripeptide. *Soft Matter* **2011**, *7*, 5239-5245.
87. Marchesan, S.; Styan, K. E.; Easton, C. D.; Waddington, L.; Vargiu, A. V. Higher and lower supramolecular orders for the design of self-assembled heterochiral tripeptide hydrogel biomaterials. *J. Mater. Chem. B* **2015**, *3*, 8123.
88. Marchesan, S.; Easton, C. D.; Kushkaki, F.; Waddington, L.; Hartley, P. G. Tripeptide self-assembled hydrogels: unexpected twists of chirality. *Chem. Commun.* **2012**, *48*, 2195.
89. Marchesan, S.; Easton, C. D.; Styan, K. E.; Waddington, L. J.; Kushkaki, F.; Goodall, L.; McLean, K. M.; Forsythe, J. S.; Hartley, P. G. Chirality effects at each amino acid position on tripeptide self-assembly into hydrogel biomaterials. *Nanoscale* **2014**, *6*, 5172-5180.
90. Giri, R. S.; Mandal, B. Unique crystallographic signatures of Boc-Gly-Phe-Phe-OMe and Boc-Gly-Phg-Phe-OMe and their self-association. *CrystEngComm* **2019**, *21*, 236-243.

Chapter 2

Self-assembly of 1-(2,4,6-trichlorobenzoyloxy)benzotriazole (TCB-OBt) reagent and its application in amidation reaction

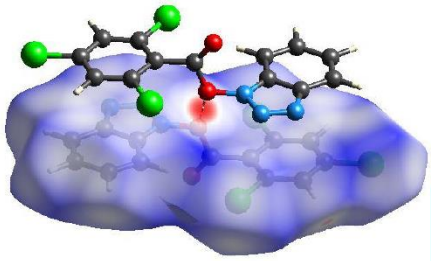

O…O interaction

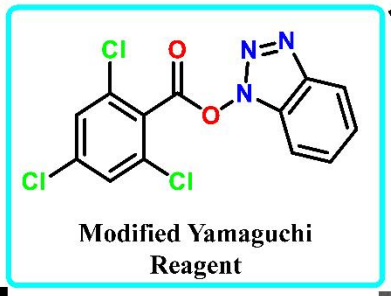

Modified Yamaguchi Reagent

Amidation

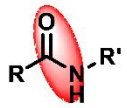

14 examples

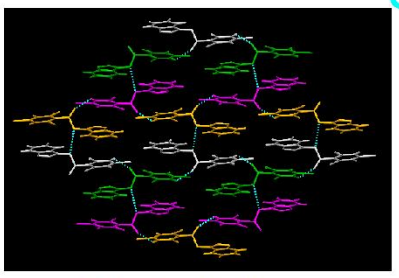

Molecular Packing

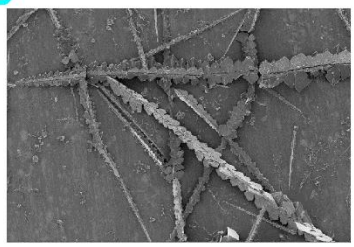

Morphology

2.1. Background

Amide group functionality presents several natural products, peptides, proteins, and other biologically important compounds.[1] Various methodology has been explored to synthesize amide bond-containing compounds, but the reported methods contain some limitations. Although several HOBt (1-Hydroxybenzotriazole) based coupling reagents have been explored, their reaction pathway is not understood well. Moreover, Yamaguchi reagent (TCB-Cl) and several modified Yamaguchi reagents such as TCB-DMAP, fluorous Yamaguchi (FY) reagents, and TCBOXY play a significant role in esterification and amidation. Creating supramolecular solid-state arrangements by organic molecules provides a significant hallmark in crystal engineering and supramolecular chemistry. Furthermore, small organic compound-based self-assembly through various non-covalent interactions, especially uncommon O···O interaction, plays an important effect on supramolecular chemistry and crystal engineering.[2,3] In this chapter, to fulfill the above significant criteria, we have designed and synthesized the HOBt-based coupling reagent TCB-OBt and discussed its self-assembly nature and synthetic role in amidation reaction.

2.2. Synthesis of TCB-OBt reagent

At first, we synthesized 1-(2,4,6-Trichlorobenzoyloxy) Benzotriazole (TCB-OBt) reagent by reacting TCBCl (2,4,6-Trichlorobenzoyl chloride) with HOBt (1-Hydroxybenzotriazole) in EtOAc solvent in the presence of DIPEA base (scheme 2.1). After work-up and recrystallization, a pure white product was obtained. The characterization of the prepared reagent was carried out by NMR spectroscopy, Mass spectrometry, and FT-IR experiment. The reagent remains stable at room temperature (25 °C). To check the stability of the ragent, a time-dependent HPLC experiment was performed and the obtained result indicated TCB-OBt remained unchanged until six months (Figure 2.12 and 2.13, Section 2.13.1).

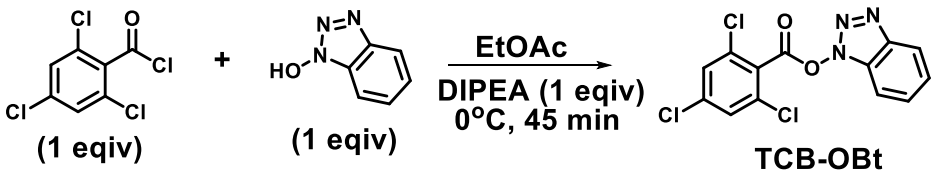

Scheme 2.1. *Synthetic pathway of TCB-OBt reagent.*

2.3. Molecular level insights of TCB-OBt

We examined Single-crystal X-ray Diffraction (SCXRD) to acquire the atomic level understanding of TCB-OBt. A suitable single crystal was grown by slow evaporation of ACN/H_2O solvent. TCB-OBt crystalized in a Monoclinic (*P2(1)/n*) crystal system. It contains single molecule in its asymmetric unit (Figure 2.1a). Two planer aromatic moiety bearing two molecules interlinked through one novel intermolecular oxygen-oxygen (O···O) interaction (2.770 Å) and two similar aromatic antiparallel pi-pi stacking interactions (centroid-centroid distance 3.680 Å) (Figure 2.1b).

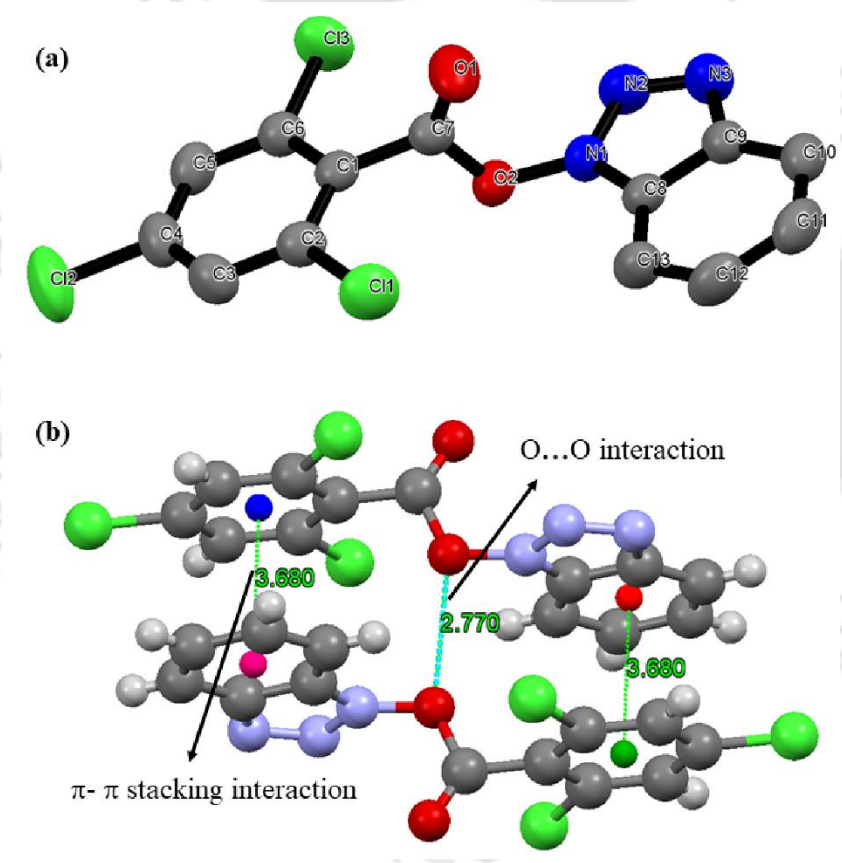

Figure 2.1. *(a) ORTEP image of TCB-OBt containing 30% ellipsoid probability, (b) Antiparallel dimeric structure interlinked via O···O interaction and two π-π stacking interactions.*

Moreover, it generated a well-organized supramolecular layer arrangement via different aromatic pi-pi stacking interactions (centroid-centroid distance 3.702 Å) and aromatic C-H···O interaction (between CH group of 2, 4, 6 trichlorobenzene ring and its

corresponding C=O group, 2.628 Å) including the interactions mentioned above in higher-order supramolecular packing (Figure 2.2).

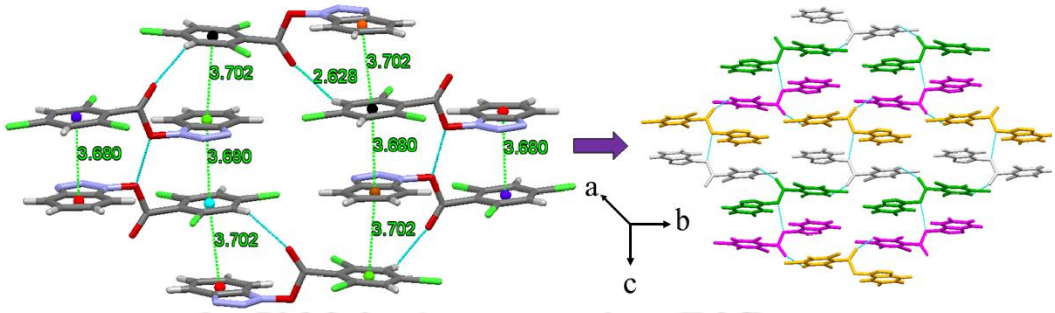

Figure 2.2. *Well-organized supramolecular layer architecture stabilized through π-π stacking interaction, O···O interaction, and aromatic C-H···O interaction.*

Furthermore, higher-order packing created supramolecular helical arrangement via non-covalent π-π stacking interaction, O···O interaction, and aromatic C-H···O interaction, along the crystallographic *b*-axis (Figure 2.3a). The molecule was also self-assembled in a zigzag manner along the *c*-axis (Figure 2.3b). It generated a supramolecular grid-like structure along the *b*-axis through several non-covalent interactions (Figure 2.3c). All crystallographic parameters are listed in Table 2.3.

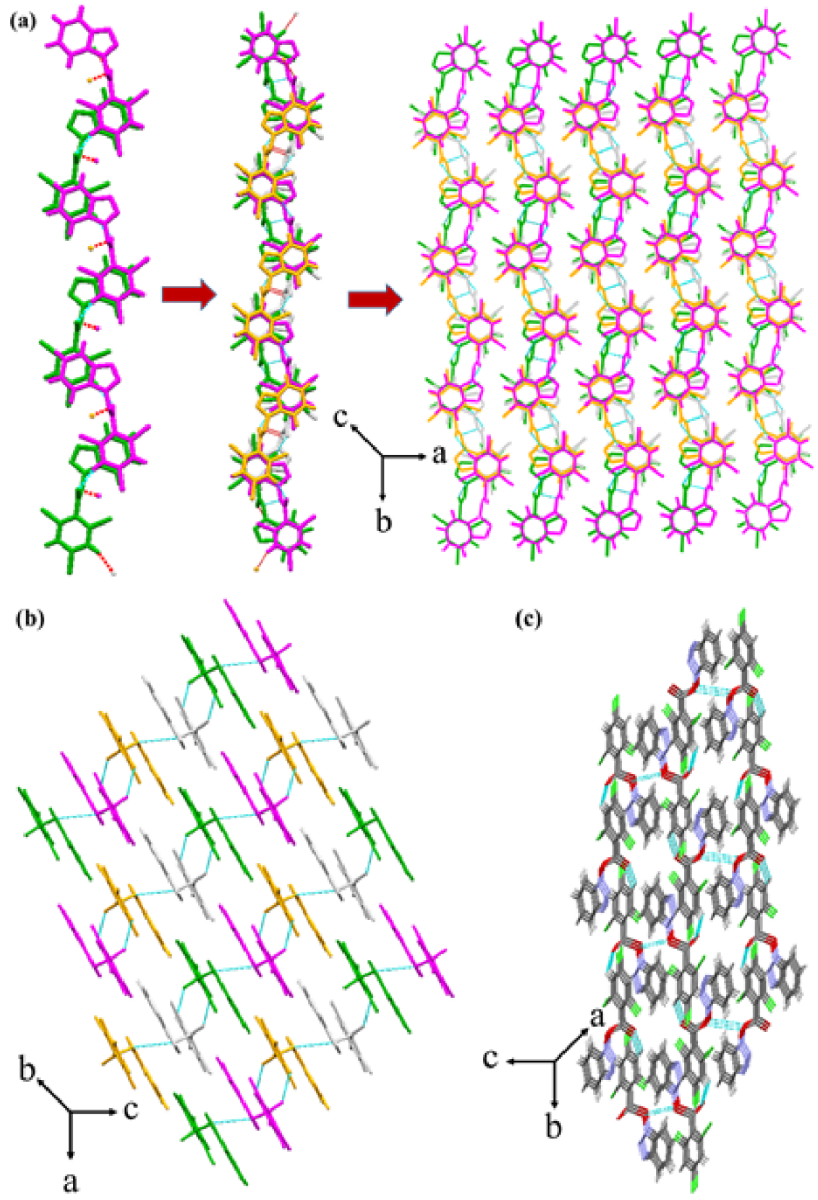

Figure 2.3. *(a) Supramolecular helical arrangement, (b) Supramolecular zigzag packing, (c) Grid-like supramolecular architecture in higher-order self-assembly.*

2.4. DFT study

The lesson on molecular orbitals provides the knowledge of the electronic environment. It is helpful for the analysis of chemical reactions. It indicates the chemical reactivity and kinetic stability of the reagents. Frontier molecular orbital (FMOs) energies, i.e., HOMO and LUMO energies were calculated employing the B3LYP/6-31G (d) method. HOMO and LUMO deal with the potential to donate and accept electrons, respectively. The pictorial representation of the HOMO-LUMO energy gap (Eg) and orbital are displayed

in Figure 2.4. The red and green colors indicated positive and negative phases of molecular orbital, respectively. HOMO is highly situated on benzotriazole moiety, and LUMO is confined around the 2, 4, 6-tricholorobezoyl groups. The energy gap between HOMO and LUMO refers to the stability index. The large energy gap indicates more stability of the reagent and less chemical reactivity.[4] The moderately high calculated energy gap (4.899 eV) reveals the higher stability of the molecule toward chemical reaction.

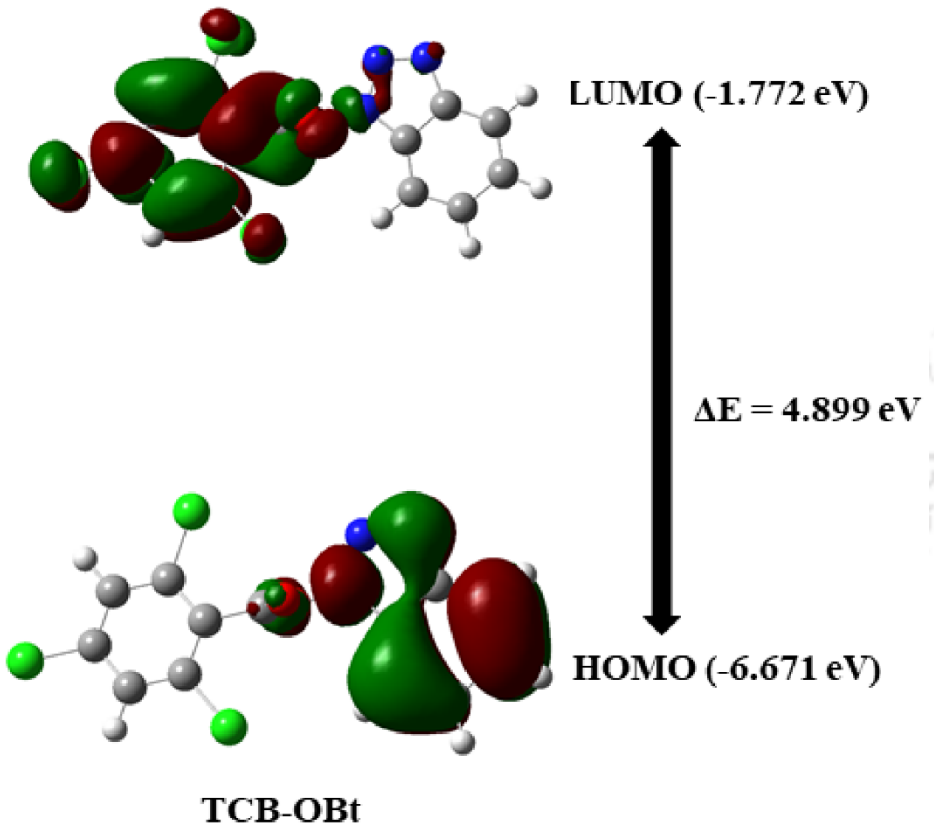

Figure 2.4. *HOMO and LUMO molecular orbitals and energy gap of the molecule TCB-OBt.*

Furthermore, to check the stability of O-substituted and N-substituted forms of TCB-OBt, we have also performed the DFT calculation of the N-substituted form, i.e., TCB-(N)-OBt (Figure 2.5). The optimized structure revealed that TCB-(N)-OBt is not planer. The HOMO-LUMO energy gap (4.184 eV) is less than that of TCB-OBt (the O-substituted form). So, the DFT calculation indicated that the O-substituted form is more stable than

the N-substituted form. Crystallographic structure displayed the formation of the more stable TCB-OBt (O-isomer).

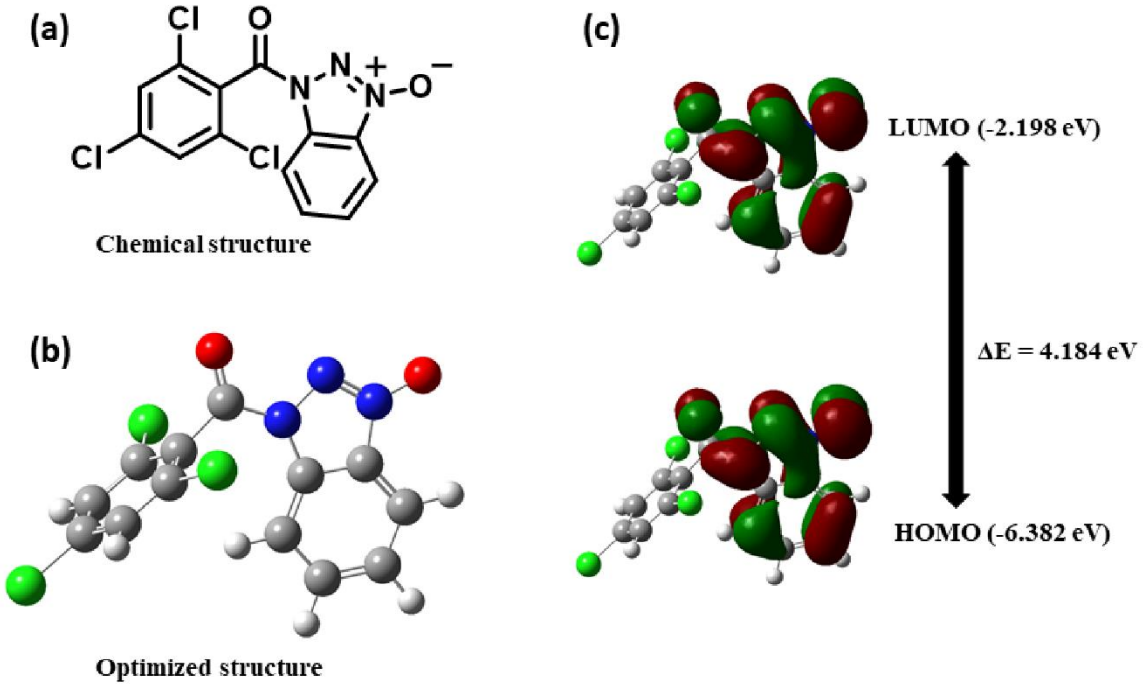

Figure 2.5. *(a) Chemical structure of TCB-(N)-OBt, (b) Optimized structure TCB-(N)-OBt, (c) HOMO and LUMO molecular orbitals and energy gap of the molecule TCB-OBt, respectively.*

2.5. HSs and FPs study

The presence of O···O interaction is not common. To confirm its existence in TCB-OBt, we performed Hirshfeld surface (HSs) and corresponding 2D fingerprint plots (FPs) analysis by using Crystal Explorer software. The presence of an intense red point on the HSs suggested the existence of intermolecular O···O interaction (Figure 2.6a). Moreover, the blue region in 2D FPs indicated the contribution of O···O interaction (1.2 %) in the Self-assembly process (Figure 2.6b).

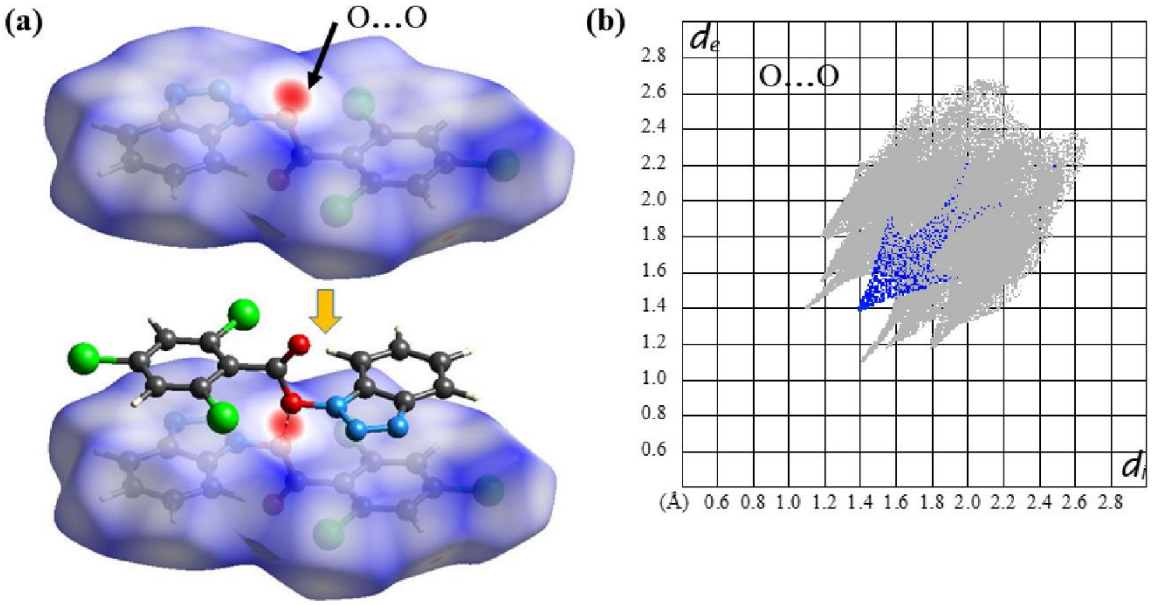

Figure 2.6. *Hirshfeld surface analysis shows (a) the d_{norm} surfaces of TCB-OBt (Highlighted in red color) and (b) 2D fingerprint plots for O···O interaction of this molecule.*

2.6. Morphology analysis

After that, we carried out an optical microscopic and FESEM experiment to check the morphology. Freshly prepared 3 mM TCB-OBt solution in 80% ACN/H_2O was drop-casted on a microscopic slide and aluminum foil containing glass. After drying in a desiccator, it was allowed for optical microscopic imaging and FESEM analysis, respectively. Optical microscopic images displayed a fantastic well organized, continuous block-shaped structure. Corresponding FESEM images also exhibited a similar morphology (Figure 2.7a, 2.7b). Moreover, to find the topographical characteristics of the compound, an atomic force microscopy (AFM) analysis was carried out. The obtained 2D and 3D plots indicate similar kind morphology to the FESEM images (Figure 2.7c, 2.7d).

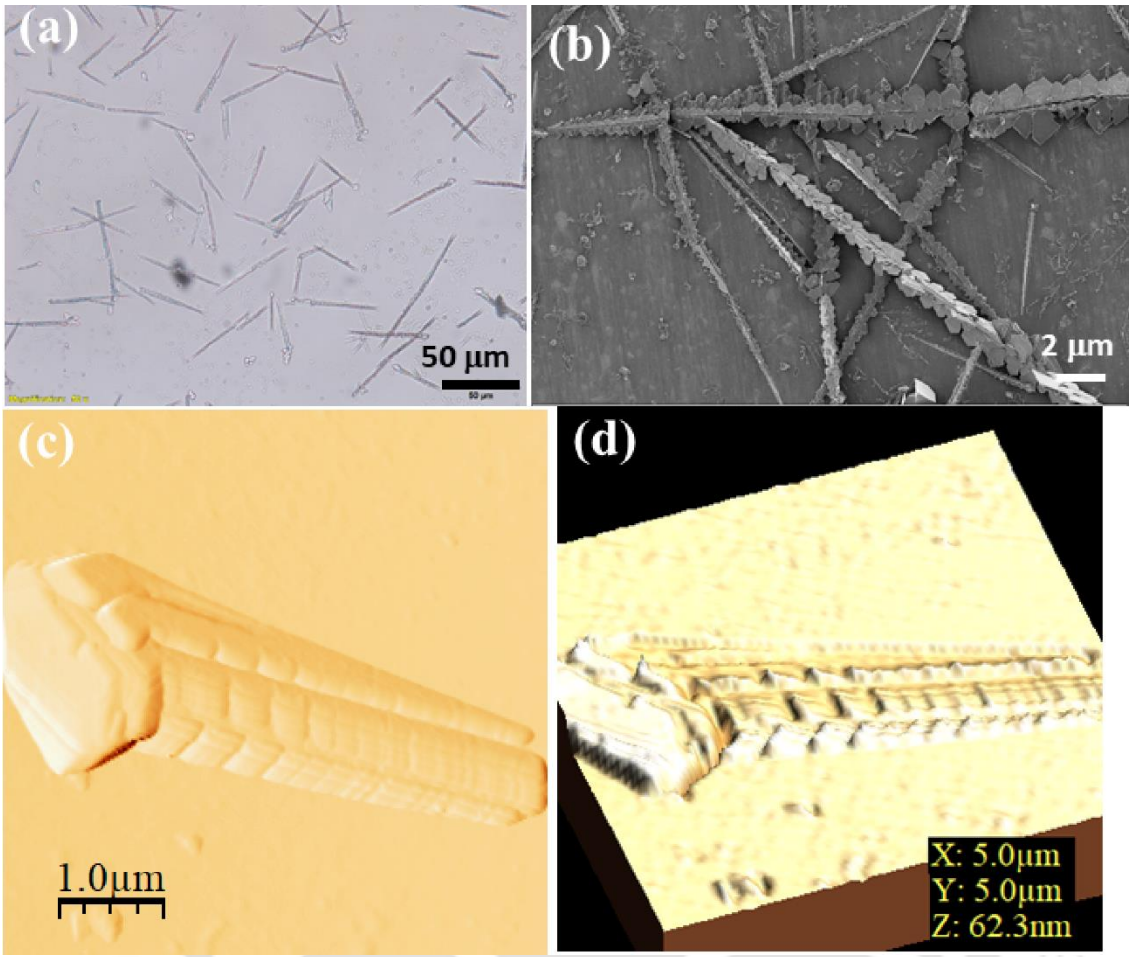

Figure 2.7. *(a) Optical microscopic image, (b) FESEM image, (c, d) 2D and 3D AFM images of TCB-OBt in solution.*

2.7. Efficiency as reagent for amidation reaction

The efficiency of TCB-OBt for amidation was examined by reacting benzoic acid with benzylamine in the presence of DIPEA. Initially, we got a maximum of 55% of the desired N-benzyl benzamide and a significant amount of undesired by-product (N-benzyl-2,4,6-trichlorobenzamide) irrespective of solvents (entry 1-7, Table 2.1). To improve the desired product yield, we added catalytic amount (0.1 equiv) DMAP (which plays a promising role as a selective acyl-transfer reagent)[5] to the reaction mixture in DMF (as we observed maximum product in this solvent). Still, no significant change was noted (entry 8). After that, we used the same amount for another two high-yielding solvents (entry 5 and 6), such as ACN and DCM.

Table 2.1. Optimization of the reaction condition for amidation[a]:

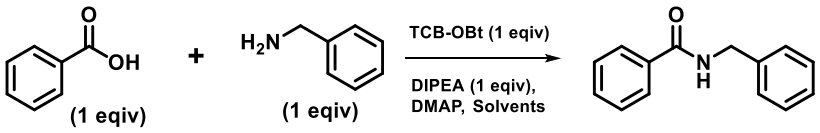

Entry	Solvents	TCB-OBt (equiv)	DMAP (equiv)	Yield[b] (%)
1	EtOAc	1	-	17
2	MeOH	1	-	20
3	$CHCl_3$	1	-	24
4	THF	1	-	26
5	DCM	1	-	39
6	ACN	1	-	50
7	DMF	1	-	55
8	DMF	1	0.1	57
9	ACN	1	0.1	60
10	DCM	1	0.1	85
11	DCM	1	0.2	89
12	DCM	1	0.3	95
13	DCM	0.5	0.3	64
14	DCM	0.3	0.3	24
15	DCM	0.1	0.3	7

[a]Reaction conditions: benzoic acid (100 mg, 0.81 mmol), benzylamine (87 mg, 0.81 mmol), DIPEA (104 mg, 0.81 mmol), DMAP and TCB-OBt under various solvent stirred at room temperature for 3-4h. [b]Isolated yield.

Interestingly we observed a significant improvement of the desired product (85%) in DCM. Further increasing of DMAP amount from 0.1 to 0.3 equivalent, we obtained 95% desired product (**entry 12**). The yield of the desired amide decreased with decreasing TCB-OBt amount (**entry 13-15**). The above observation indicated that the best condition for this reaction was 0.3 equiv DMAP, 1.0 equiv TCB-OBt, and DCM as solvent. The pre-activation step required 45 minutes, and completion required another 2-3h.

Table 2.2. Substrate scope of amidation by using TCB-OBt:

Entry	Carboxylic acid	Amine	Yield (%)	ID
1	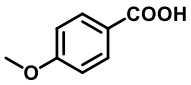	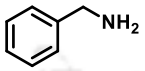	96	2a
2	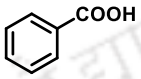	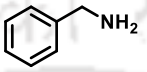	95	2b
3	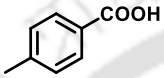	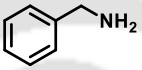	90	2c
4	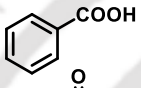	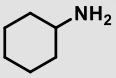	89	2d
5	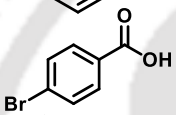	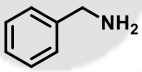	86	2e
6	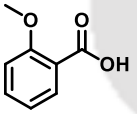		80	2f
7	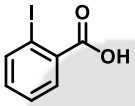		71	2g
8	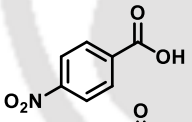	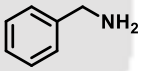	45	2h
9	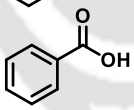	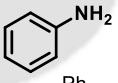	84	2i
10	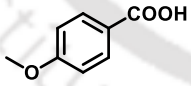	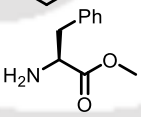	79	2j
11	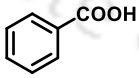	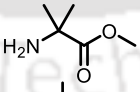	81	2k
12	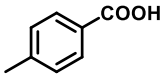	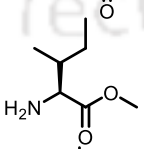	78	2l
13	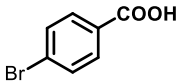	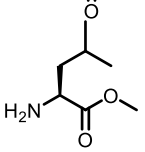	73	2m
14	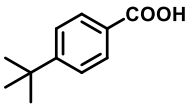	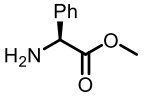	82	2n

Various substituted carboxylic acids and amine (aliphatic and aromatic) reacted well in these optimized reaction conditions. The reaction provided good to high yield under mild reaction conditions (Table 2.2). All products were characterized by using NMR spectroscopy and mass spectrometry.

2.8. Plausible mechanism

A plausible mechanism was drawn in scheme 2.2. In the presence of the base, the carboxylate anion acts as a nucleophile. It attacks the TCB-OBt carbonyl center forming a mixed anhydride, I, through nucleophilic substitution, releasing the resonance stabilized benzotriazole anion. At the same time, carboxylate anion also may react with I from the less hindered site and form anhydride II. The anhydrides (I or II) may react with DMAP and form resonance stabilized intermediate N-acyl pyridinium salt III. After that, the generated benzotriazole anion attacks the carbonyl carbon of III and forms intermediate IV (isolated). Finally, amine reacts with IV to generate the desired amide.

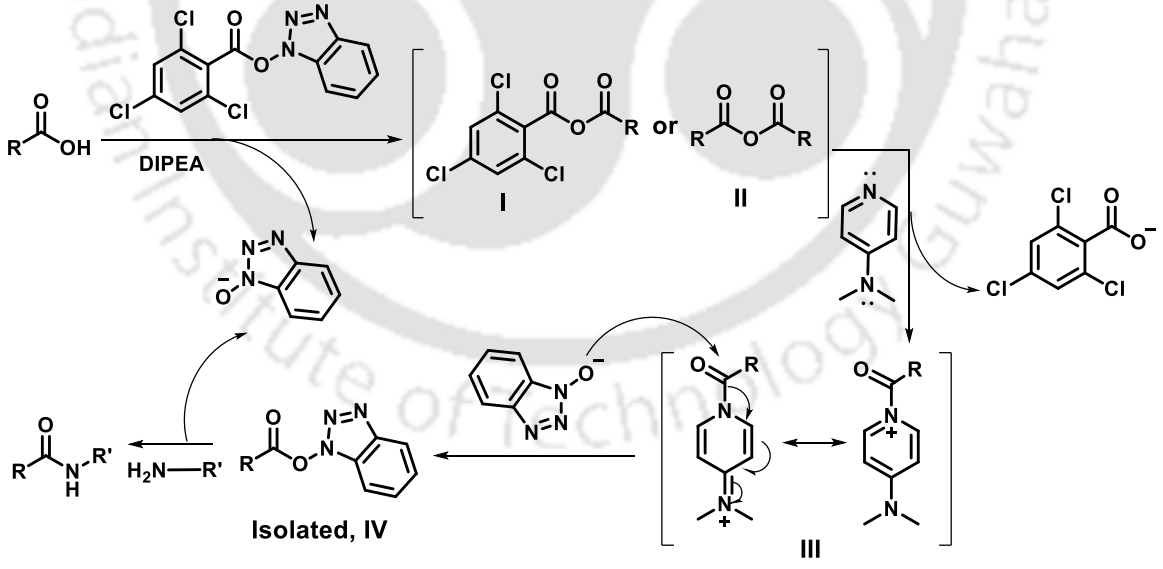

Scheme 2.2. *A plausible mechanism for the synthesis of an amide using TCB-OBt reagent.*

2.9. Conclusion

In summary, we have developed a new modified Yamaguchi Reagent TCB-OBt and investigated its supramolecular assembly. Interestingly, this molecule gets stabilized through a rare intermolecular oxygen-oxygen interaction, π-π stacking interaction, and aromatic C-H···O interaction. By this driving force, it constructed diverse supramolecular layer structures and helical architecture. Crystal structure and DFT calculation suggest the O-substituted (TCB-OBt) form is more stable than the N-substituted form (TCB-(N)-OBt). Morphology analysis by FESEM and AFM images reveals a fantastic, well-organized, continuous block-shaped structure. The newly synthesized compound acted as an efficient condensation reagent for amidation reactions under mild conditions and provided a high yield. This kind of molecular design and morphology study may be helpful for material science research. Furthermore, this reagent may be applicable to other important Functional Group Interconversions (FGI).

2.10. Experimental section

2.10.1. Materials and instrumentation

As described in chapter 7

2.10.2. General procedure for the synthesis of TCB-OBt (1H-benzo[d][1,2,3]triazol-1-yl 2,4,6-trichlorobenzoate)

DIPEA (1.06 gm, 8.2 mmol) was added to the solution of HOBt (1.11 gm, 8.2 mmol) in ethyl acetate at 0 °C. After that, TCBCl (2.0 gm, 8.2) was added slowly, and 45-minute stirring was required to complete the reaction. After solvent removal, crude product dissolves in DCM and work-up with 5% HCl solution. Organic portions were dried over anhydrous $CaCl_2$, and removing the solvent provided the pure desired product. No further purification was required.

2.10.3. Determination of intermediate IV (1H-benzo[1,2,3]triazol-1-yl benzoate)

TCB-OBt (277 mg, 0.81 mmol) added to the solution of Benzoic acid (100 mg, 0.81 mmol), DIPEA (104 mg, 0.81 mmol) and DMAP (29 mg, 0.24 mmol) in DCM. After 45 min pre-activation time (confirmed by TLC), the reaction mixture was washed with 10% citric acid and 10% $NaHCO_3$ solution. The collected organic layer was evaporated. The separation of the desired product was performed by column chromatography.

2.10.4. General procedure for the synthesis of amides

TCB-OBt (1 equiv) added to the solution of carboxylic acid (1 equiv), DIPEA (1 equiv) and DMAP (0.3 equiv) in DCM. It required about 45 min pre-activation of carboxylic acid. After that, amine (1 equiv) was added to the reaction mixture. TLC observation confirmed the completion of the reaction. The reaction mixture was diluted with DCM, washed with 10% citric acid, and 10% $NaHCO_3$ solution. The collected organic layer was evaporated by a rotary evaporator. The purification of the desired product was performed by column chromatography.

2.11. Characterization data

TCB-OBt.

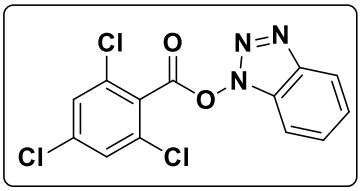

White solid; Yield-2.67 gm, 95%; melting point - 199-202; **^{1}H NMR (400 MHz, $CDCl_3$)** δ 7.79-7.45 (1H, m); 7.53 (2H, s); 7.61-7.60 (2H, m); 8.13-8.10 (1H, d, J = 8.4 Hz);. **^{13}C NMR (100 MHz, $CDCl_3$)** δ 108.4, 120.6, 125.1, 126.9, 128.4, 128.6, 129.2, 133.8, 138.9, 143.4, 160.3. ESI-MS: calculated $[M+H]^+$ 341.9604, obtained m/z 341.9605.

Side product N-benzyl-2,4,6-trichlorobenzamide:

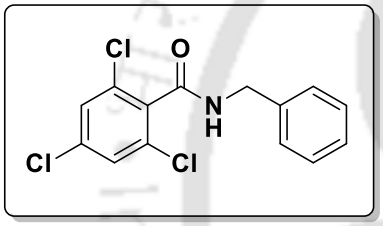

White solid, **^{1}H NMR (400 MHz, $CDCl_3$)** δ 4.56-4.55 (2H, d, J = 5.6 Hz); 6.46 (1H, s); 7.32-7.25 (7H, m);. **^{13}C NMR (100 MHz, $CDCl_3$)** δ 44.1, 127.8, 128.1, 128.2, 128.8, 133.1, 134.6, 135.8, 137.3, 163.7. ESI-MS: calculated $[M+H]^+$ 313.9906, obtained m/z 313.9900.

Intermediate 1H-benzo[1,2,3]triazol-1-yl benzoate (IV):

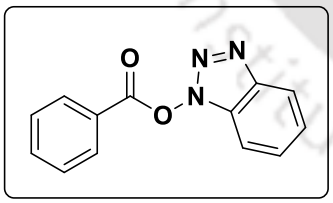

White solid, **^{1}H NMR (400 MHz, $CDCl_3$)** δ 7.48-7.42 (2H, m); 7.62-7.53 (3H, m); 7.79-7.75 (1H, t, J =7.2 Hz); 8.11-8.09 (1H, d, J =8.4 Hz); 8.29-8.27 (2H, d, J =7.2 Hz); **^{13}C NMR (100 MHz, $CDCl_3$)** δ 108.5, 120.7, 125.05, 125.07, 128.9, 129.4, 130.9. 135.6, 143.7, 162.9. ESI-MS: calculated $[M+H]^+$ 240.0773, obtained m/z 240.0772.

N-benzyl-4-methoxybenzamide (2a)

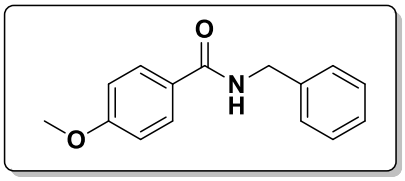

White solid, (152 mg, 96%), **^{1}H NMR (400 MHz, $CDCl_3$)** δ 3.82 (1H, s); 4.60-4.59 (2H, d, J = 6 Hz); 6.52 (1H, s); 6.89-6.87 (2H, d, J = 8.8 Hz); 7.33-7.25 (5H, m); 7.76-7.74 (2H, d, J = 8.8 Hz);. **^{13}C NMR (100 MHz, $CDCl_3$)** δ 44.2, 55.5, 113.9, 126.8, 128.0, 128.8, 128.9, 138.6, 162.3, 167.1. ESI-MS: calculated $[M+H]^+$ 242.1181, obtained m/z 242.1182.

N-benzylbenzamide (2b).

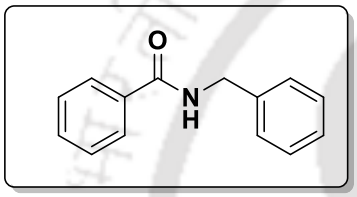

White solid, (164 mg, 95**%), ^{1}H NMR (600 MHz, $CDCl_3$)** δ 4.64-4.63 (2H, d, J = 6 Hz); 6.77 (1H, s); 7.32-7.30 (1H, m); 7.36-7.35 (4H, m); 7.44-7.41 (2H, t, J = 7.8 Hz); 7.52-7.50 (1H, t, J = 7.2 Hz); 7.81-7.80 (2H, d, J = 7.2 Hz);. **^{13}C NMR (150 MHz, $CDCl_3$)** δ 44.2, 127.1, 127.7, 128.0, 128.7, 128.8, 131.6, 134.4, 138.3, 167.6. ESI-MS: calculated $[M+H]^+$ 212.1075, obtained m/z 212.1079.

N-benzyl-4-methylbenzamide (2c).

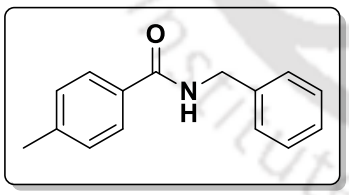

White solid, (149 mg, 90%), **^{1}H NMR (400 MHz, $CDCl_3$)** δ 2.37 (3H, s); 4.60-4.59 (2H, d, J = 5.6 Hz); 6.59 (1H, s); 7.20-7.18 (2H, d, J = 8 Hz); 7.32-7.24 (5H, m); 7.68-7.66 (2H, d, J = 8 Hz);. **^{13}C NMR (100 MHz, $CDCl_3$)** δ 21.5, 44.1, 127.1, 127.6, 12.0, 128.8, 129.3, 131.7, 138.5, 142.0, 167.5. ESI-MS: calculated $[M+H]^+$ 226.1232, obtained m/z 226.1240.

N-cyclohexylbenzamide (2d):

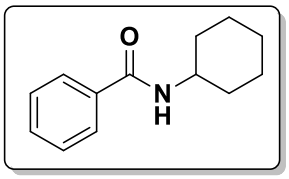

White solid, (148 mg, 89%), **^{1}H NMR (400 MHz, $CDCl_3$)** δ 1.25-1.13 (1H, m); 1.46-1.35 (2H, m); 1.66-1.62 (1H, m); 1.77-1.71 (2H, m); 2.03-1.99 (2H, m); 4.01-3.92 (1H, m); 6.10 (1H, s); 7.41-7.38 (2H, t, *J* = 7.6 Hz); 7.48-7.45 (1H, t, *J* = 7.2 Hz); 7.76-7.74 (2H, d, *J* = 7.6 Hz);. **^{13}C NMR (100 MHz, $CDCl_3$)** δ 25.0, 25.7, 33.3, 48.8, 127.0, 128.6, 131.3, 135.2, 166.8. ESI-MS: calculated $[M+H]^+$ 204.1388, obtained m/z 204.1387.

N-benzyl-4-bromobenzamide (2e):

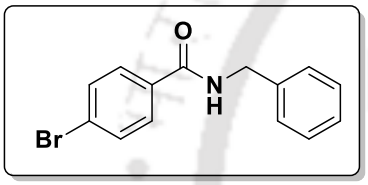

White solid, (124 mg, 86%), **^{1}H NMR (400 MHz, $CDCl_3$)** δ 4.60-4.59 (2H, d, *J* = 5.6 Hz); 6.53 (1H, s); 7.36-7.25 (5H, m); 7.54-7.52 (2H, d, *J* = 8.4 Hz); 7.65-7.63 (2H, d, *J* = 8 Hz);. **^{13}C NMR (100 MHz, $CDCl_3$)** δ 44.4, 126.4, 127.9, 128.1, 128.8, 129.0, 132.0, 133.3, 138.1, 166.6. ESI-MS: calculated $[M+H]^+$ 290.0181, obtained m/z 290.0188.

N-(tert-butyl)-2-methoxybenzamide (2f):

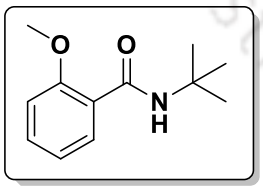

White solid, (108 mg, 80%), **^{1}H NMR (400 MHz, $CDCl_3$)** δ 1.45 (9H, s); 3.93 (3H, s); 6.95-6.92 (1H, d, *J* = 8.4 Hz); 7.07-7.03 (1H, t, *J* = 7.6 Hz); 7.43-7.38 (1H, m); 7.83 (1H, s); 8.18-8.16 (1H, d, *J* = 7.6 Hz);. **^{13}C NMR (100 MHz, $CDCl_3$)** δ 29.0, 51.1, 56.0, 111.4, 121.4, 122.9, 132.0, 132.4, 157.3, 164.2. ESI-MS: calculated $[M+H]^+$ 208.1338, obtained m/z 208.1352.

N-cyclopropyl-2-iodobenzamide (2g):

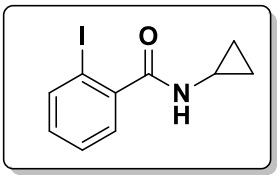

White solid, (82 mg, 71%), **^{1}H NMR (400 MHz, $CDCl_3$)** δ 0.70-0.66 (2H, t, *J* = 6.8 Hz); 0.89-0.84 (2H, q, *J* = 6.4 Hz); 2.91-2.86 (1H, m); 5.95 (1H, s); 7.09-7.05 (1H, m); 7.35-7.34 (2H, m); 7.83-7.81 (1H, d, *J* = 8 Hz);. **^{13}C NMR (100 MHz, $CDCl_3$)** δ 6.8, 23.2, 92.6, 128.3, 128.4, 131.2, 139.9, 142.2, 170.8. ESI-MS: calculated $[M+H]^+$ 287.9885, obtained m/z 287.9880.

N-benzyl-4-nitrobenzamide (2h):

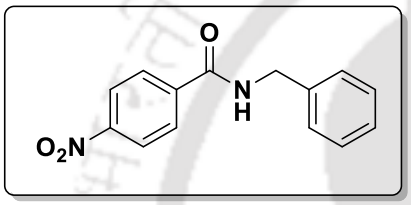

White solid, (69 mg, 45%), **^{1}H NMR (400 MHz, $CDCl_3$)** δ 4.62-4.61 (2H, d, *J* = 6 Hz); 6.84 (1H, s); 7.36-7.29 (5H, m); 7.93-7.91 (2H, d, *J* = 8.4 Hz); 8.23-8.20 (2H, d, *J* = 8.8 Hz);. **^{13}C NMR (100 MHz, $CDCl_3$)** δ 44.5, 123.9, 128.0, 128.4, 129.0, 137.6, 140.0, 149.7, 165.6. ESI-MS: calculated $[M+H]^+$ 257.0926, obtained m/z 257.0929.

N-phenylbenzamide (2i):

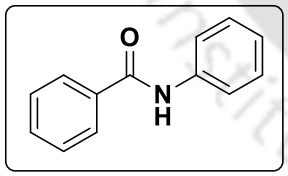

White solid, (135 mg, 84%), **^{1}H NMR (500 MHz, $CDCl_3$)** δ 7.07-7.04 (1H, t, *J* = 7.5 Hz); 7.27-7.24 (2H, t, *J* = 8.0 Hz); 7.37-7.34 (2H, t, *J* = 7.5 Hz); 7.45-7.42 (1H, t, *J* = 7.5 Hz); 7.56-7.54 (2H, d, *J* = 8.0 Hz); 7.77-7.76 (2H, d, *J* = 7.5 Hz); 7.90 (1H, s);. **^{13}C NMR (125 MHz, $CDCl_3$)** δ 120.5, 124.7, 127.2, 128.9, 129.2, 131.9, 135.2, 138.1, 166.0. ESI-MS: calculated $[M+H]^+$ 198.0919, obtained m/z 198.0917.

Methyl (4-methoxybenzoyl)-L-phenylalaninate (2j):

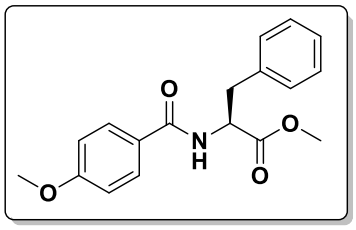

White solid, (162 mg, 79%), **^{1}H NMR (600 MHz, $CDCl_3$)** δ 3.25-3.22 (1H, dd, J = 5.4 Hz); 3.31-3.28 (1H, dd, J = 6.0 Hz); 3.78 (3H, s); 3.86 (3H, s); 5.11-5.08 (1H, q, J = 6.0 Hz); 6.53 (1H, s); 6.93-6.92 (2H, d, J = 9.0 Hz); 7.15-7.14 (2H, d, J = 6.6 Hz); 7.28-7.27 (1H, m); 7.32-7.30 (2H, m); 7.72-7.71 (2H, d, J = 9.0 Hz);. **^{13}C NMR (150 MHz, $CDCl_3$)** δ 38.1, 52.5, 53.6, 55.6, 114.0, 126.3, 127.3, 128.8, 129.0, 129.5, 136.1, 162.6, 166.5, 172.4. ESI-MS: calculated $[M+H]^+$ 314.1392, obtained m/z 314.1388.

Methyl 2-benzamido-2-methylpropanoate (2k):

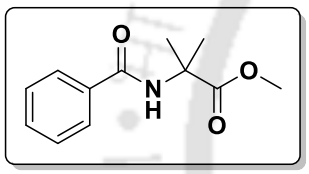

White solid, (148 mg, 81%), **^{1}H NMR (600 MHz, $CDCl_3$)** δ 1.69 (6H, s); 1.69 (6H, s); 3.79 (3H, s); 6.85 (1H, s); 7.45-7.42 (2H, m); 7.52-7.49 (1H, m); 7.80-7.79 (2H, d, J = 7.2 Hz);. **^{13}C NMR (150 MHz, $CDCl_3$)** δ 24.9, 52.9, 57.0, 127.1, 128.7, 131.7, 134.6, 166.8, 175.4. ESI-MS: calculated $[M+H]^+$ 222.1130, obtained m/z 222.1125.

Methyl (4-methylbenzoyl)-L-alloisoleucinate (2l):

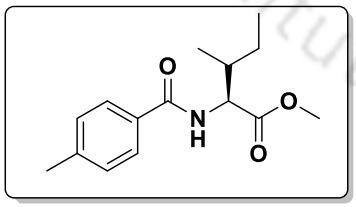

White solid, (151 mg, 78%), **^{1}H NMR (600 MHz, $CDCl_3$)** δ 0.99-0.97 (6H, m); 1.31-1.24 (1H, m); 1.58-1.51 (1H, m); 2.06-1.99 (1H, m); 2.41 (3H, s); 3.78 (3H, s); 4.84-4.82 (1H, m); 6.66-6.64 (1H, d, J = 8.4 Hz); 7.28-7.25 (2H, m); 7.72-7.71 (2H, d, J = 8.4 Hz);. **^{13}C NMR (150 MHz, $CDCl_3$)** δ 11.8, 15.6, 21.6, 25.5, 38.4, 52.3, 56.8, 127.2, 129.4, 131.4, 142.3, 167.2, 172.9. ESI-MS: calculated $[M+H]^+$ 264.1600, obtained m/z 264.1608.

Methyl (4-bromobenzoyl)-L-leucinate (2m):

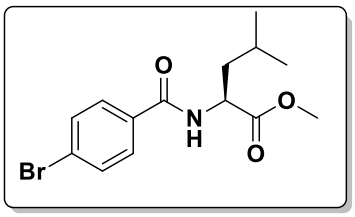

Colourless liquid, (121 mg, 73%), **^{1}H NMR (600 MHz, $CDCl_3$)** δ 0.99-0.96 (6H, m); 1.76-1.70 (3H, m); 3.77 (3H, s); 4.85-4.82 (1H, m); 6.62 (1H, s); 7.57-7.55 (2H, m); 7.66-7.65 (2H, m);. **^{13}C NMR (150 MHz, $CDCl_3$)** δ 22.2, 23.0, 25.1, 41.9, 51.4, 52.6, 126.6, 128.8, 132.0, 132.8, 166.3, 173.9. ESI-MS: calculated $[M+H]^+$ 328.0548, obtained m/z 328.0555.

Methyl (S)-2-(4-(tert-butyl)benzamido)-2-phenylacetate (2n):

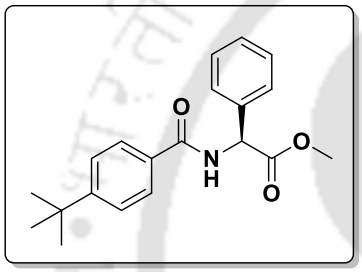

Colourless liquid, (151 mg, 82%), **^{1}H NMR (600 MHz, $CDCl_3$)** δ 1.32 (9H, s); 3.76 (3H, s); 5.78-5.77 (1H, d, J = 7.2 Hz); 7.15 (1H, s); 7.34-7.31 (1H, m); 7.37-7.35 (2H, t, J = 6.6 Hz); 7.45-7.43 (4H, m); 7.76-7.75 (2H, d, J = 8.4 Hz);. **^{13}C NMR (150 MHz, $CDCl_3$)** δ 31.3, 35.1, 53.0, 56.9, 125.7, 127.2, 127.5, 128.7, 129.1, 130.9, 136.8, 155.6, 166.6, 171.7. ESI-MS: calculated $[M+H]^+$ 326.1756, obtained m/z 326.1754.

2.12. References

1. Ghose, A. K.; Viswanadhan, V. N.; Wendoloski, J. J. A Knowledge-Based Approach in Designing Combinatorial or Medicinal Chemistry Libraries for Drug Discovery. 1. A Qualitative and Quantitative Characterization of Known Drug Databases. *J. Comb. Chem.* **1999**, *1*, 55-68.
2. Das, M.; Ghosh, B. N.; Bauza´, A.; Rissanen, K.; Frontera, A.; Chattopadhyay, S. Observation of novel oxygen···oxygen interaction in supramolecular assembly of cobalt(III) Schiff base complexes: a combined experimental and computational study. *RSC Adv.* **2015**, *5*, 73028.
3. Sharma, C.; Singh, A. K.; Joy, J.; Jemmisc, E. D.; Awasthi, S. K. Experimental and theoretical study of intramolecular O-O interaction in structurally rigid β-keto carboxylic esters. *RSC Adv.* **2016**, *6*, 91689.
4. Arjunan, V.; Devi, L.; Subbalakshmi, R.; Rani, T.; Mohan, S. Synthesis, vibrational, NMR, quantum chemical and structure-activity relation studies of 2-hydroxy-4-methoxyacetophenone. *Spectrochimica Acta Part A: Molecular and Biomolecular Spectroscopy* **2014**, *130*, 164.
5. Neises, B.; Steglich, W. Simple Method for the Esterification of Carboxylic Acids. *Angew. Chem., Int. Ed.* **1978**, *17*, 522-524.

2.13. Selected spectra

2.13.1. NMR (^{1}H and ^{13}C), Mass spectra and FT-IR spectra of TCB-OBt:

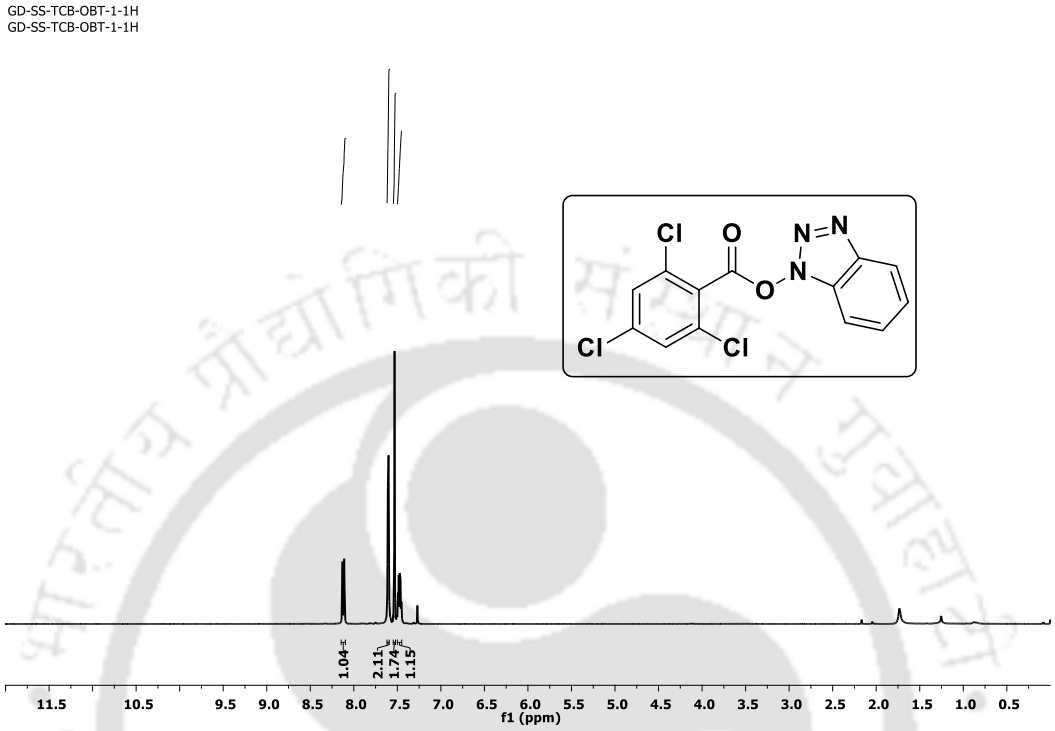

Figure 2.8. *^{1}H NMR spectra of* ***TCB-OBt***

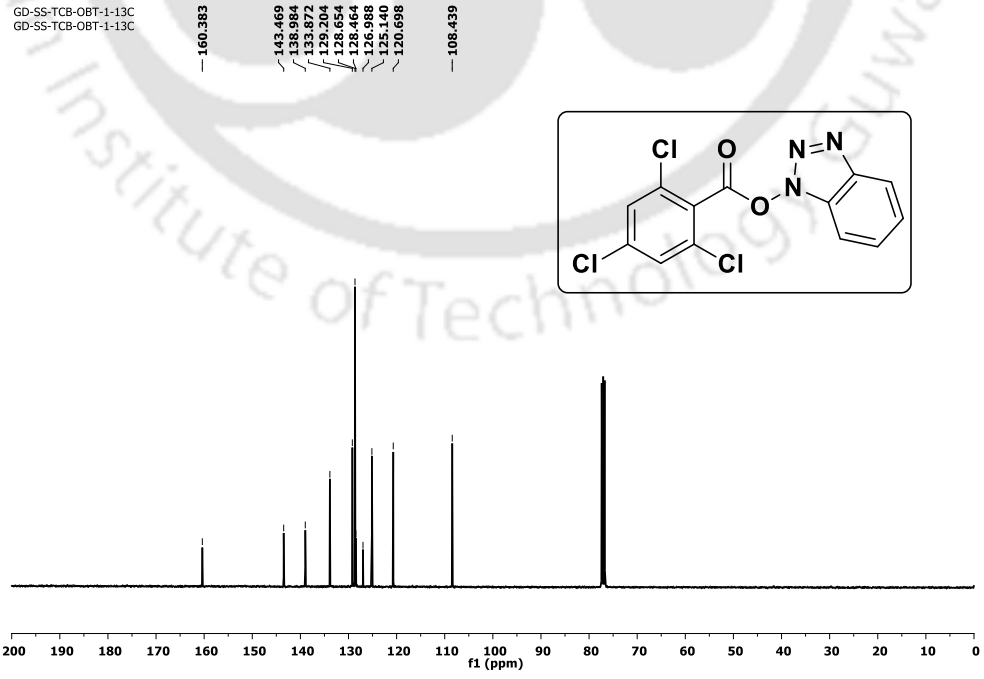

Figure 2.9. *^{13}C NMR spectra of* ***TCB-OBt***

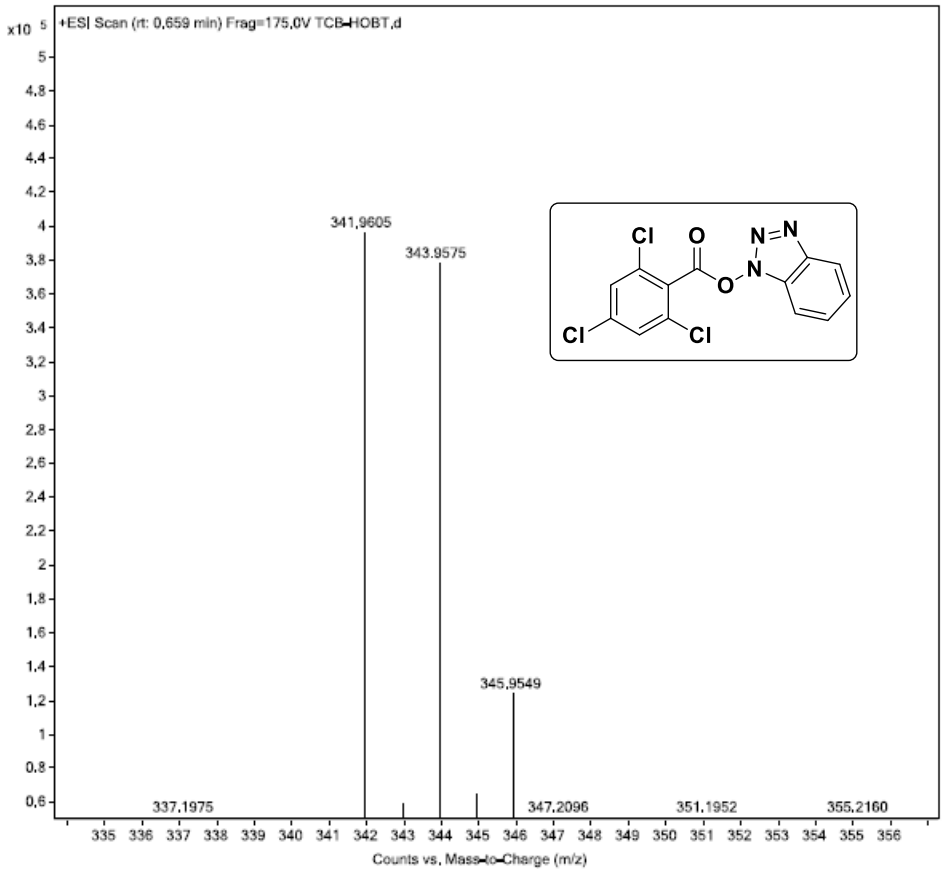

Figure 2.10. *ESI-MASS spectrum of spectra of* ***TCB-OBt***

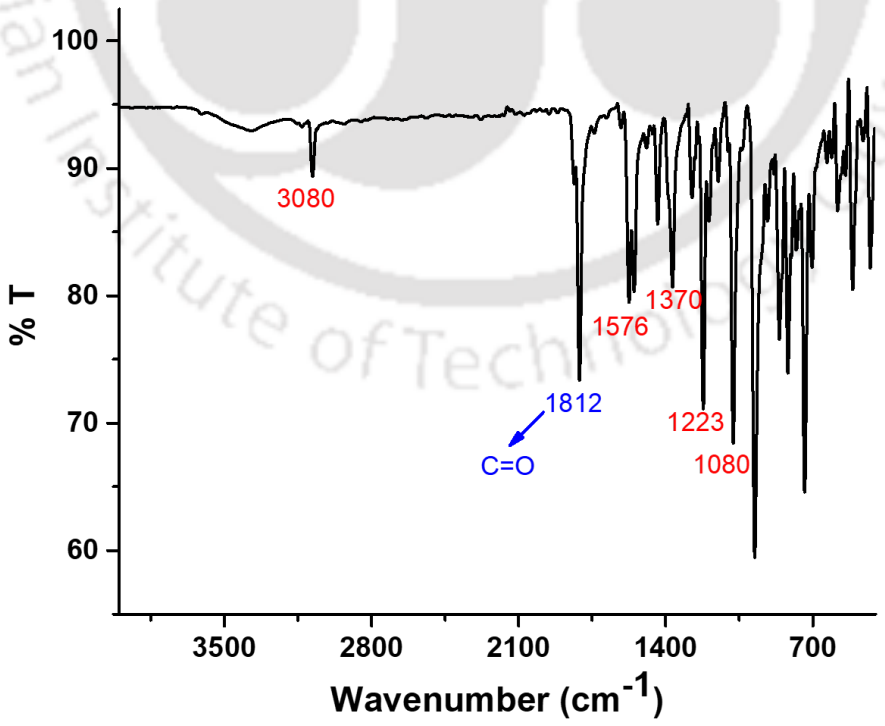

Figure 2.11. *FT-IR spectra of* ***TCB-OBt***

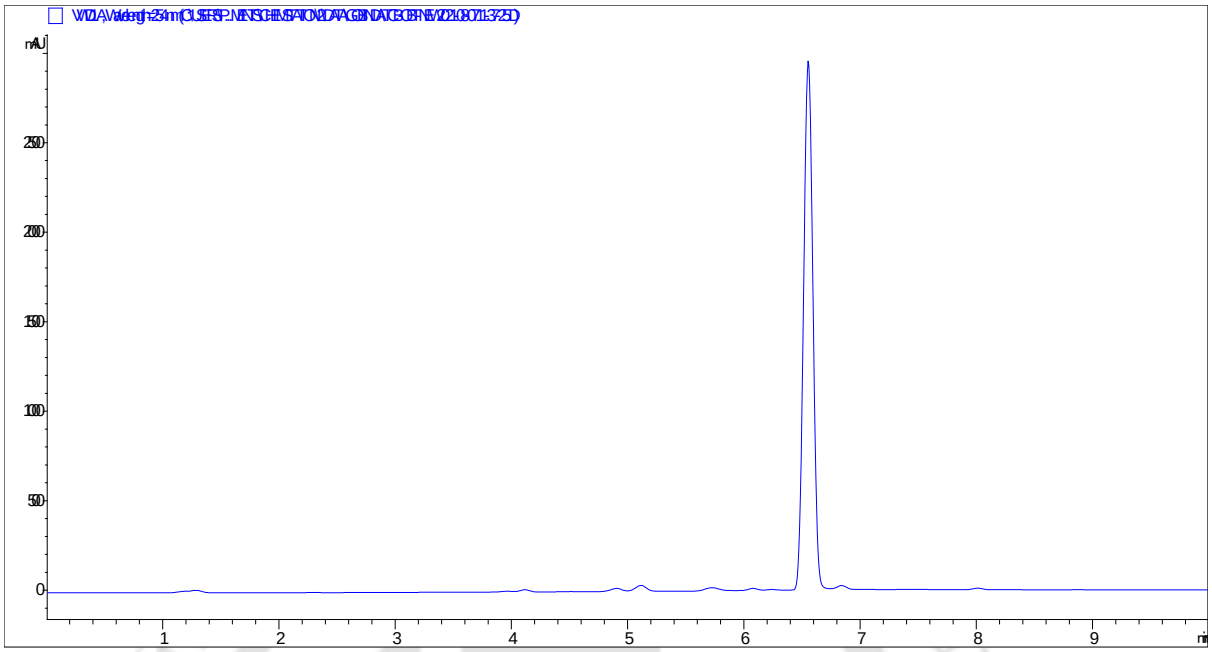

Figure 2.12. *HPLC chromatogram of TCB-OBt, first day of synthesis. (retention time R_t = 6.554 min)*

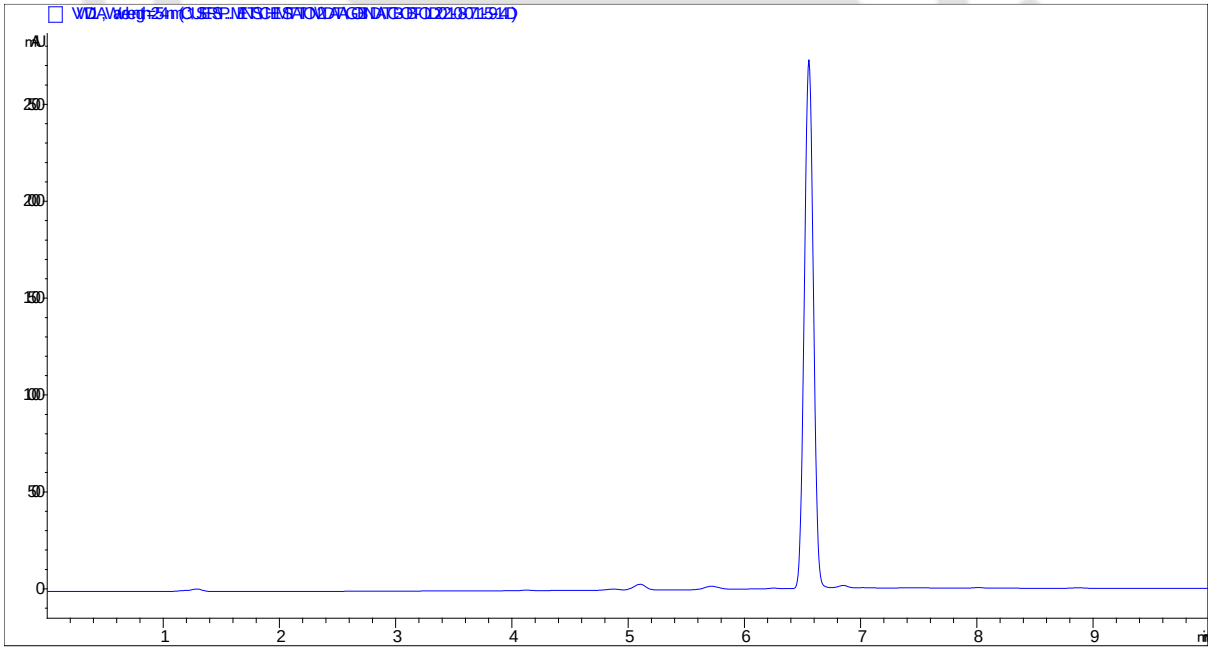

Figure 2.13. *HPLC chromatogram of TCB-OBt, after 6 months of the synthesis. (retention time R_t = 6.555 min)*

2.13.2. NMR (^{1}H and ^{13}C) spectra of side product:

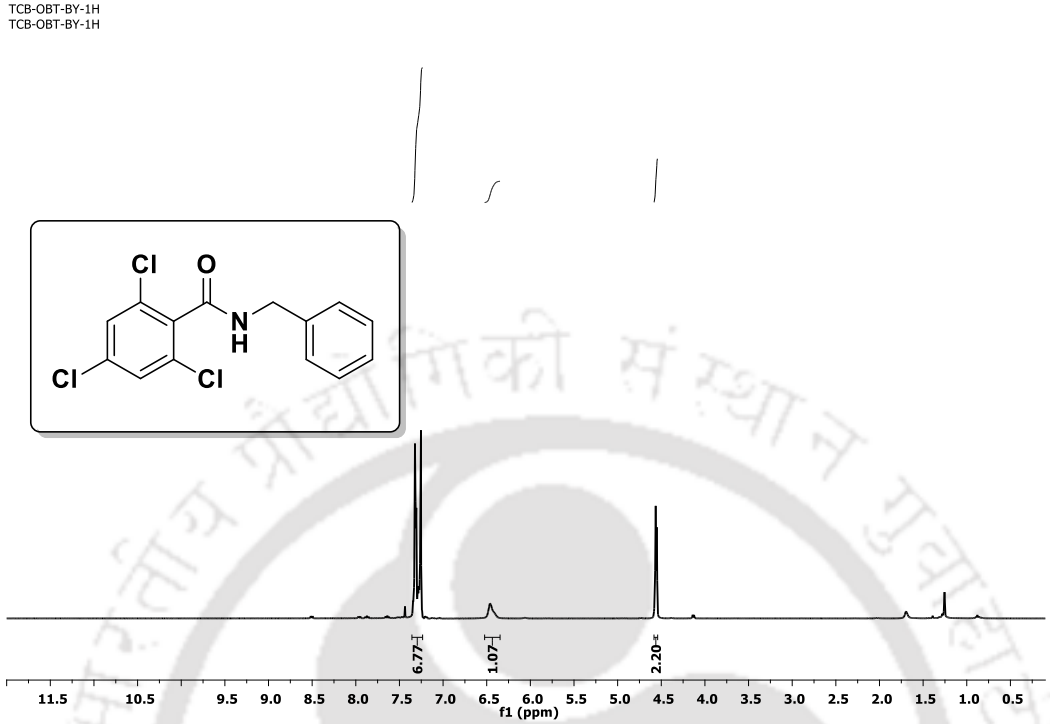

Figure 2.14. *^{1}H NMR spectrum of side product*

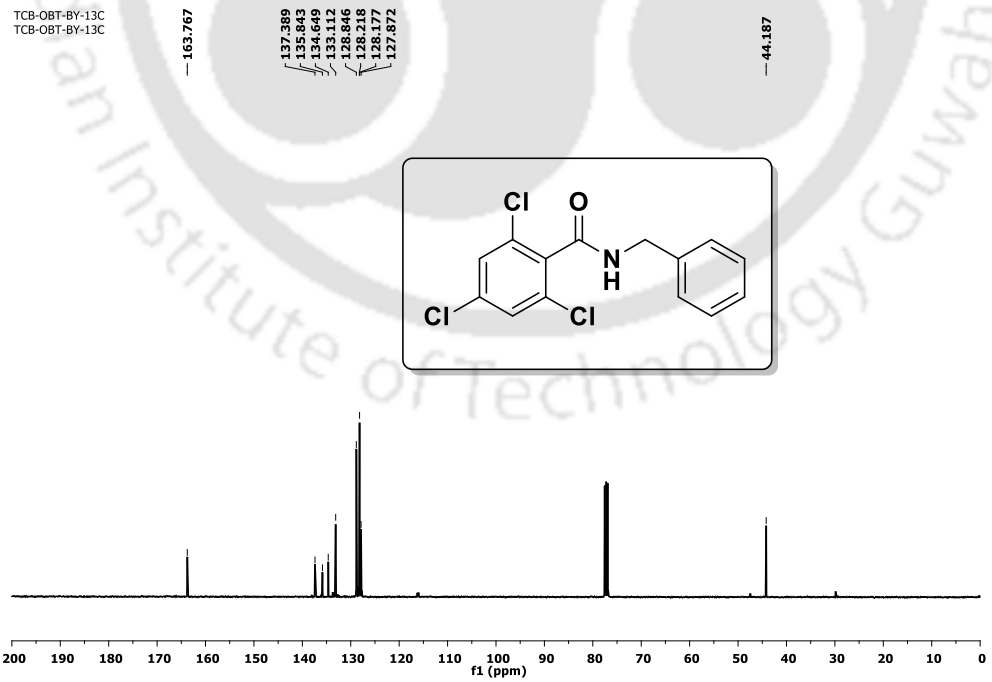

Figure 2.15. *^{13}C NMR spectrum of side product*

2.13.3. NMR (^{1}H and ^{13}C) spectra of isolated intermediate:

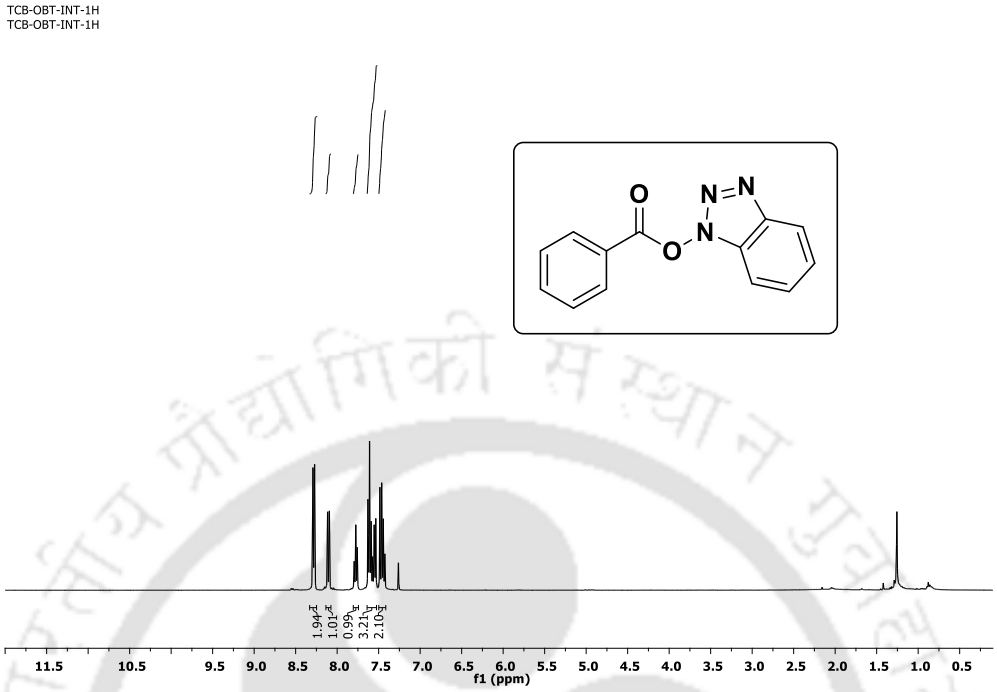

Figure 2.16. *^{1}H NMR spectrum of isolated intermediate*

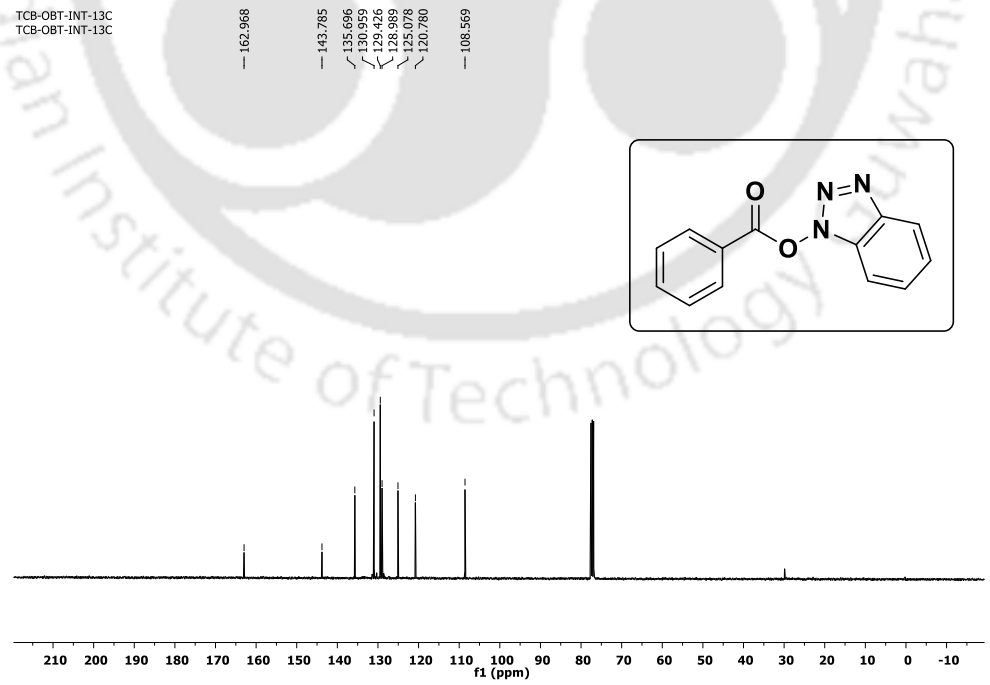

Figure 2.17. *^{13}C NMR spectrum of isolated intermediate*

2.13.4. NMR (^{1}H and ^{13}C) spectra of amides:

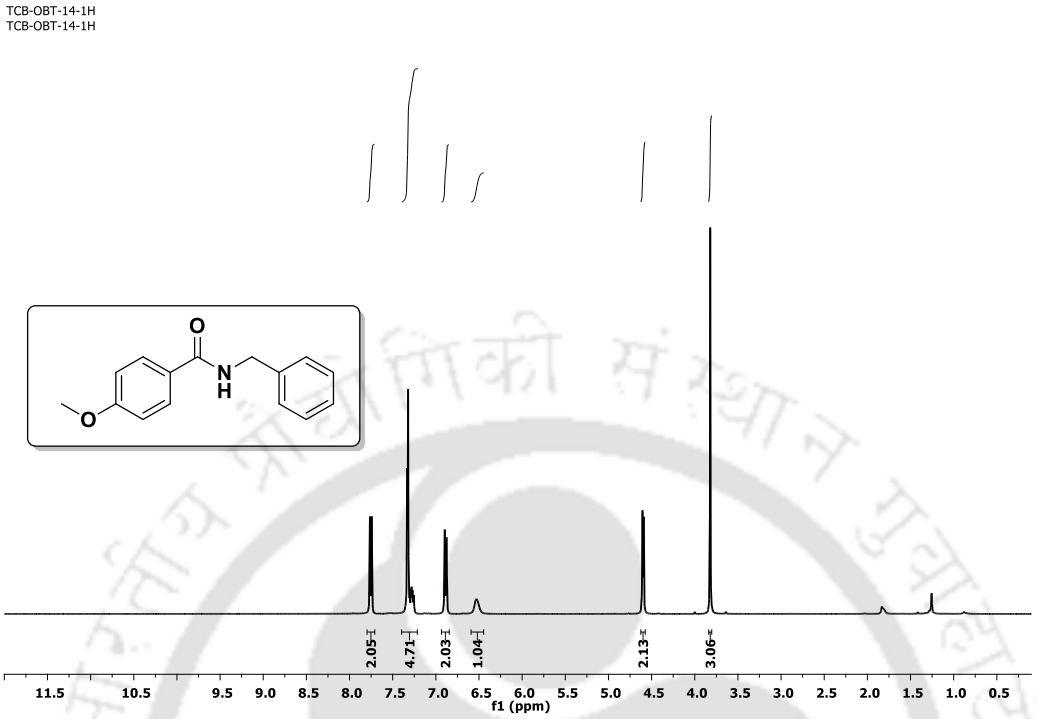

Figure 2.18. *^{1}H NMR spectrum of compound* ***2a***

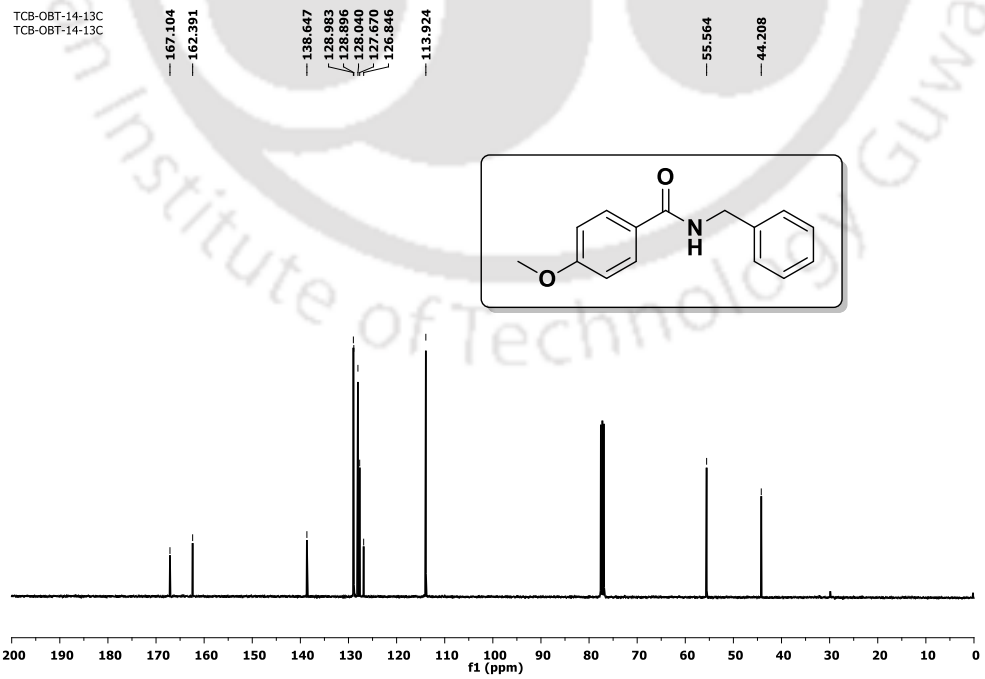

Figure 2.19. *^{13}C NMR spectrum of compound* ***2a***

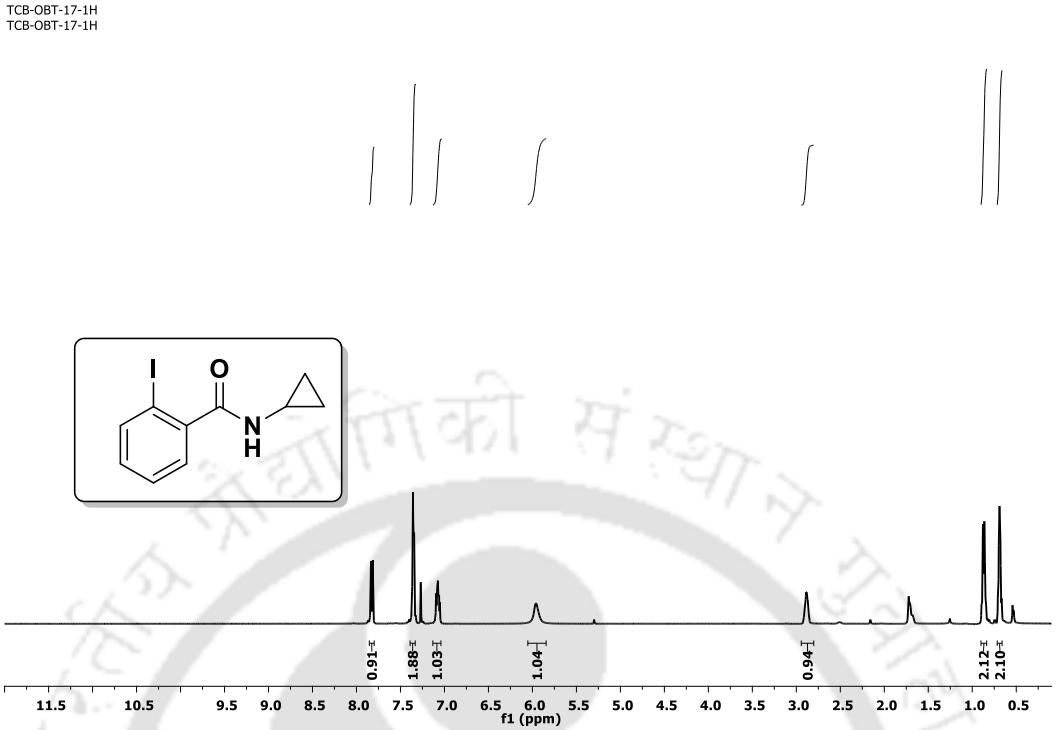

Figure 2.20. *^{1}H NMR spectrum of compound* ***2g***

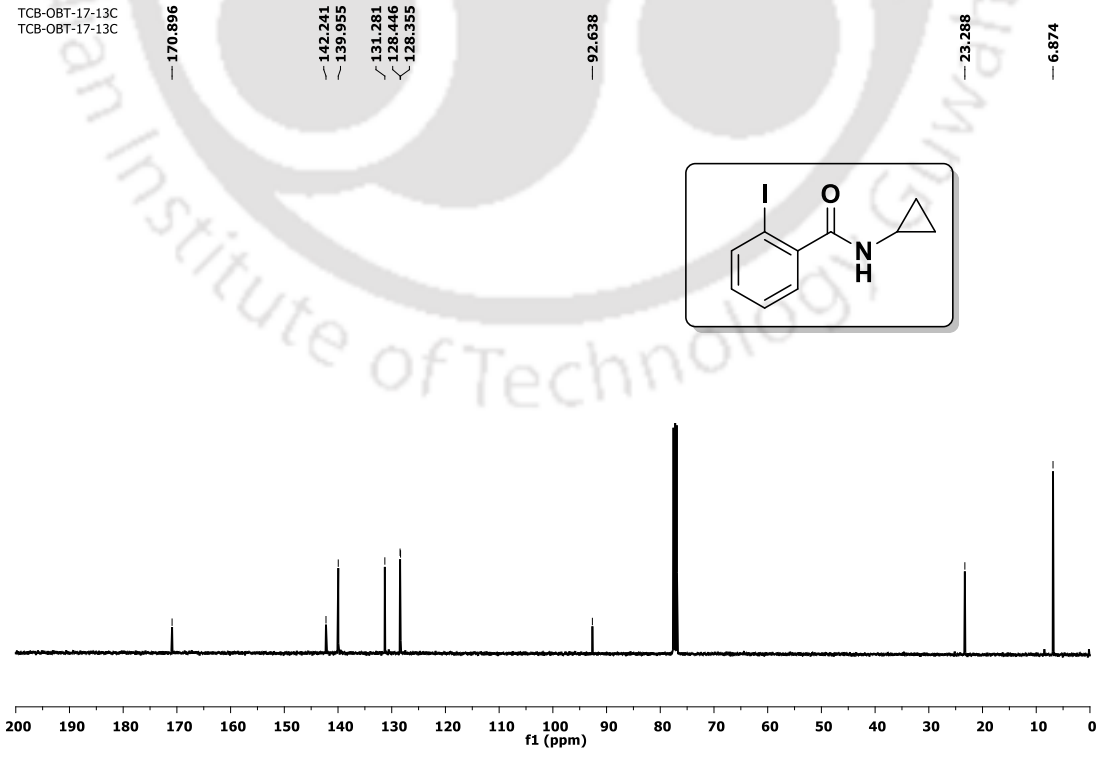

Figure 2.21. *^{13}C NMR spectrum of compound* ***2g***

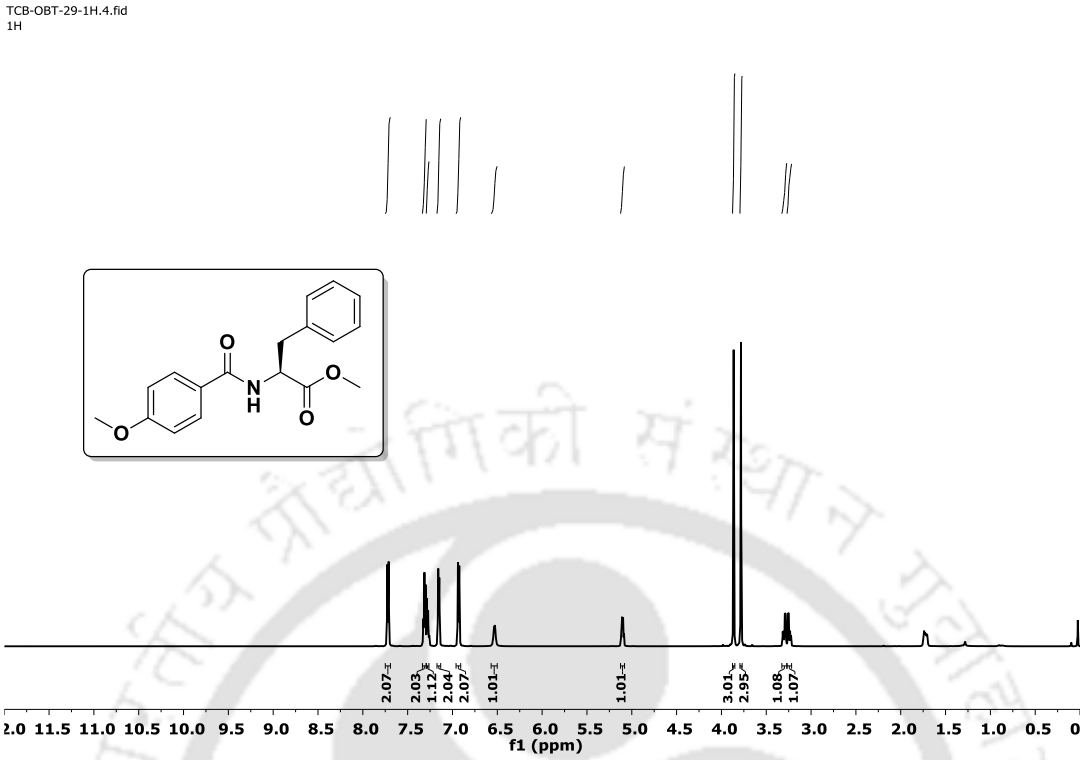

Figure 2.22. *^{1}H NMR spectrum of compound **2j***

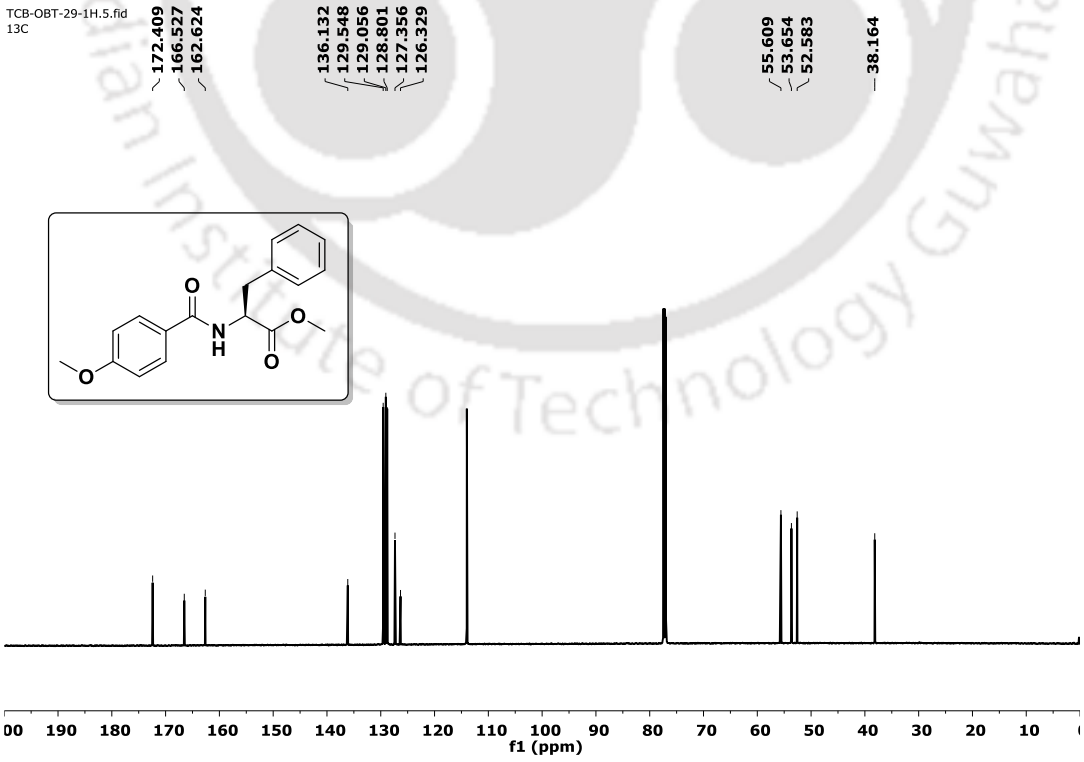

Figure 2.23. *^{13}C NMR spectrum of compound **2j***

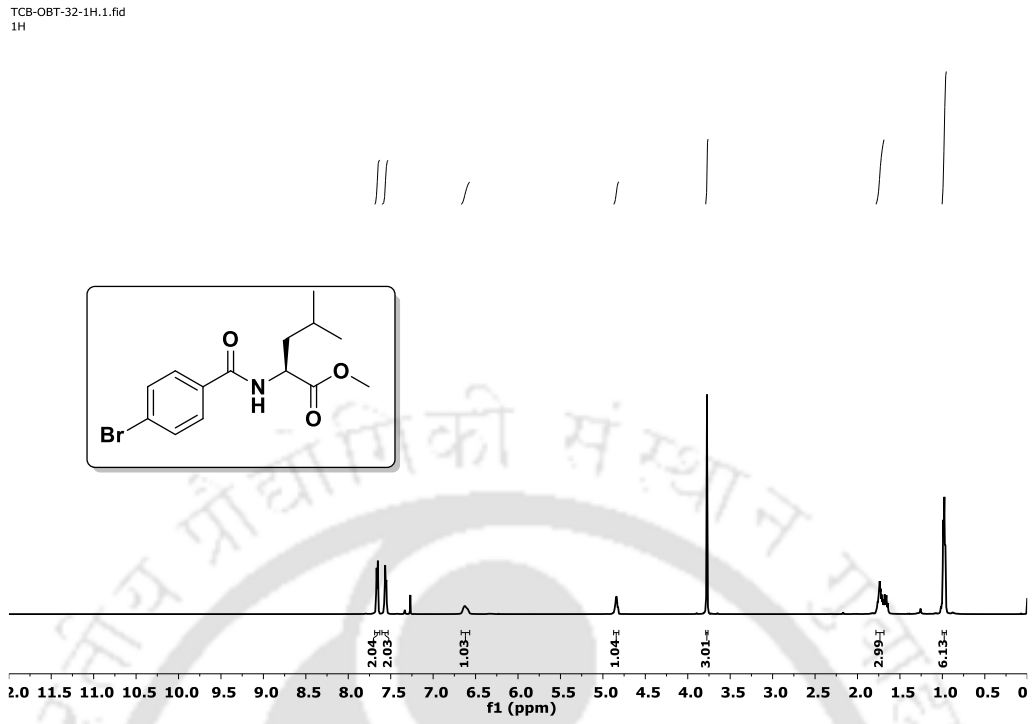

Figure 2.24. *^{1}H NMR spectrum of compound* ***2m***

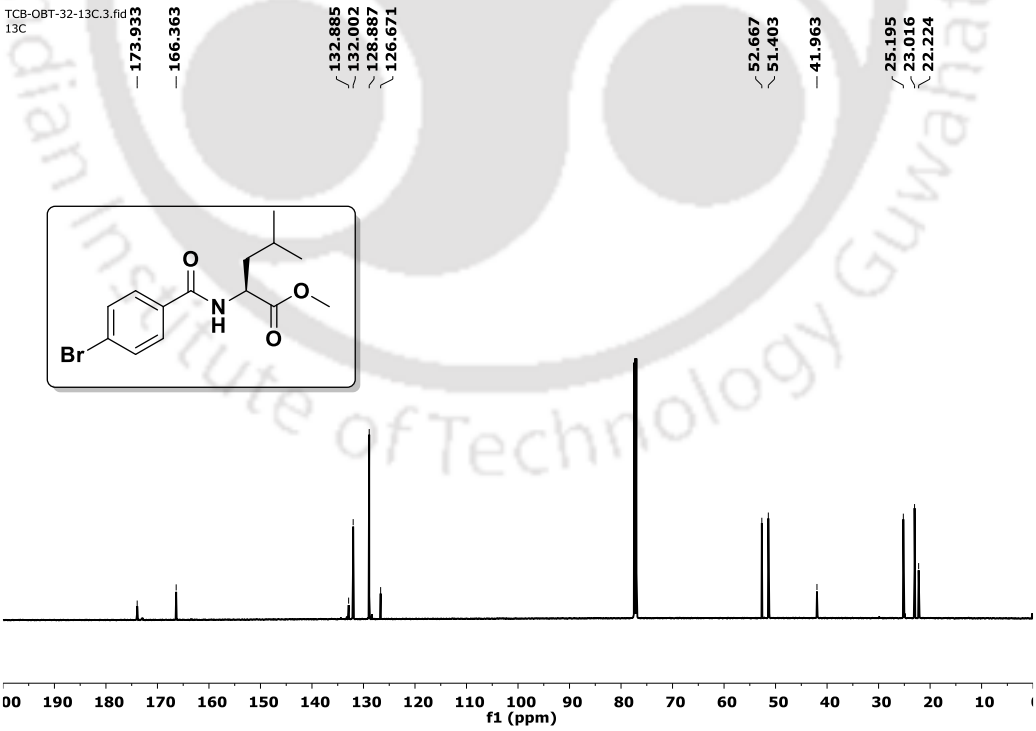

Figure 2.25. *^{13}C NMR spectrum of compound* ***2m***

2.14. Crystallographic data

Table 2.3. Crystallographic refinement details of TCB-OBt

Parameters	TCB-OBt
Formula	C_{13} H_6 Cl_3N_3 O_2
Fw	342.56
Crystal system	Monoclinic
Space group	*P2(1)/n*
a/Å	10.0723(6)
b/Å	13.1809(9)
c/Å	10.5798(8)
α/°	90.00
β/°	90.957(3)
γ/°	90.00
V/Å^3	1404.40(17)
Z	4
D_c/g cm^{-3}	1.620
μ Mo K_α/mm^{-1}	0.658
F000	688
T/K	296(2)
θ max.	25.00
Total no. of reflections	13230
Independent reflections	2452
Observed reflections	2112
Parameters refined	190
R_1, I > 2σ(I)	0.0368
wR_2, I > 2σ(I)	0.1227
GOF (F^2)	0.968
CCDC No.	2102031

Chapter 3

Effect of the N-terminal protecting group on the self-assembly of Ant-Aib dipeptides

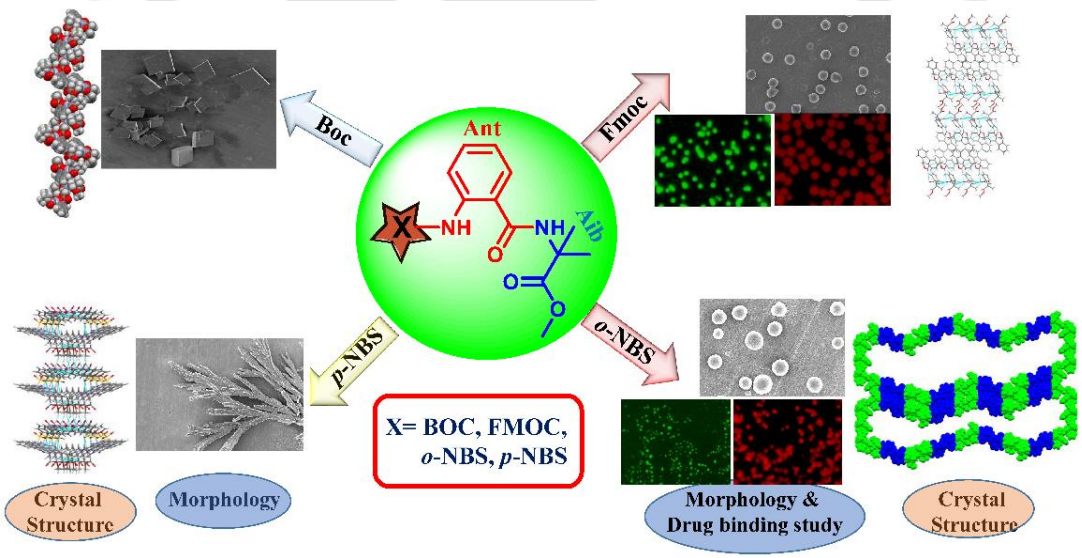

3.1. Background

In chapter 2, we discussed the self-assembly of the small organic compounds. Similarly, small peptide-based self-assembly contributes significantly to nanoscience, bio-organic chemistry, and nanotechnology due to their biocompatibility, easy availability, specific molecular recognition ability, and functional diversity. FF dipeptides formed various nanostructures depending on solvent polarity.[1,2] However, self-assembly diversity governed by protecting groups is not explored sufficiently. Nonnatural rigid amino acids such as aminobenzoic acid and 2-aminoisobutyric acid significantly contribute to the self-assembly process by their conformational rigidity.[3,4] Moreover, incorporating unnatural amino acids increases nanostructures' thermal and proteolytic stability. Inspired by these reports, we designed various N-terminal protecting groups containing di-peptides and studied their self-assembly pattern.

3.2. Design of peptides

To investigate the role of N-terminal protecting groups of conformationally rigid dipeptides on self-assembly, we selected four different protecting groups and two unnatural amino acids. We designed four dipeptides with the general formula X-Ant-Aib-OMe, where X is Boc (peptide **3A)**, Fmoc (peptide **3B)**, *o*-NBS (peptide **3C)**, *p*-NBS (peptide **3D)** and Ant is anthranilic acid or 2-amino benzoic acid, Aib is 2-aminoisobutyric acid, and NBS is nitrobenzyl sulfonyl group (Figure 3.1). The N-terminal Boc protecting group contributes significantly in supramolecular structure creation because of its selectivity in the self-assembly process.[5] Fmoc protecting group also keeps a vital hallmark in nanostructure generation by aromatic π-stacking interactions.[6] Self-assembly properties of *o*-NBS and *p*-NBS protecting groups are not explored much.

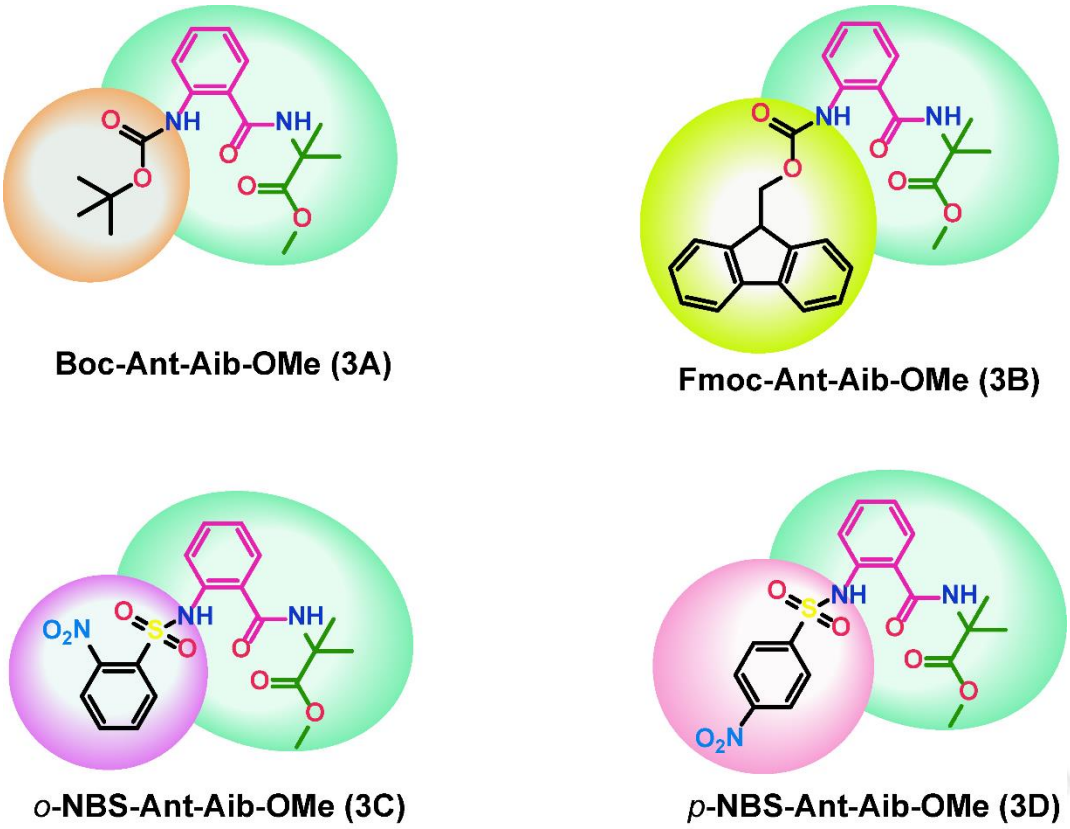

Figure 3.1. *Chemical structures of peptides* ***3A-3D*** *with varying N-terminal protecting groups.*

3.3. Synthesis and characterization of the designed peptides

At first, various N-terminal protecting groups containing dipeptides were synthesized in solution using the conventional peptide coupling method employing DCC/HOBt reagent. The characterization of aimed di-peptides was fulfilled by 1D (^{1}H and ^{13}C) NMR and mass spectrometry. The purity of dipeptides was monitored by the reverse phase analytical HPLC.

3.4. Morphology study

Initially, we checked the morphology of the designed peptides by FESEM, optical microscope, and FETEM. For the morphology study, we have incubated 1.5 mM of each peptide solution in 50% ACN/H_2O at 37 °C for four days. After incubation, a 1.5 mM

peptide solution was placed over aluminum-foil containing glass and microscopic glass and dried for the FESEM and optical microscope experiment. In FESEM and optical microscope, **3A** showed well organized block-shaped structure (Figure 3.2a, 3.2b), peptides **3B** and **3C** displayed highly dense, well-ordered spherical structures, with diameters ranging 1.7 μm to 2.0 μm and 1.1 μm to 2.2 μm, respectively (Figure 3.2d, 3.2e and 3.2g, 3.2h). Moreover, **3D** formed a rod-like fiber structure (Figure 3.2j, 3.2k). To get more detailed structural information FETEM experiment was carried out. For FETEM sample preparation, 1.5 mM peptide solution diluted to 100 μM. FETEM analysis suggested that **3A** and **3D** formed almost similar morphology to the FESEM images (Figure 3.2c, 3.2l). **3B** and **3C** displayed spherical structures, which are nothing but nanovesicles with a diameter range of 275 nm to 430 nm and 500 nm to 580 nm, respectively (Figure 3.2f, 3.2i). The morphology obtained by various microscopic techniques suggests that N-terminal protecting groups play a vital role in the self-assembly process.

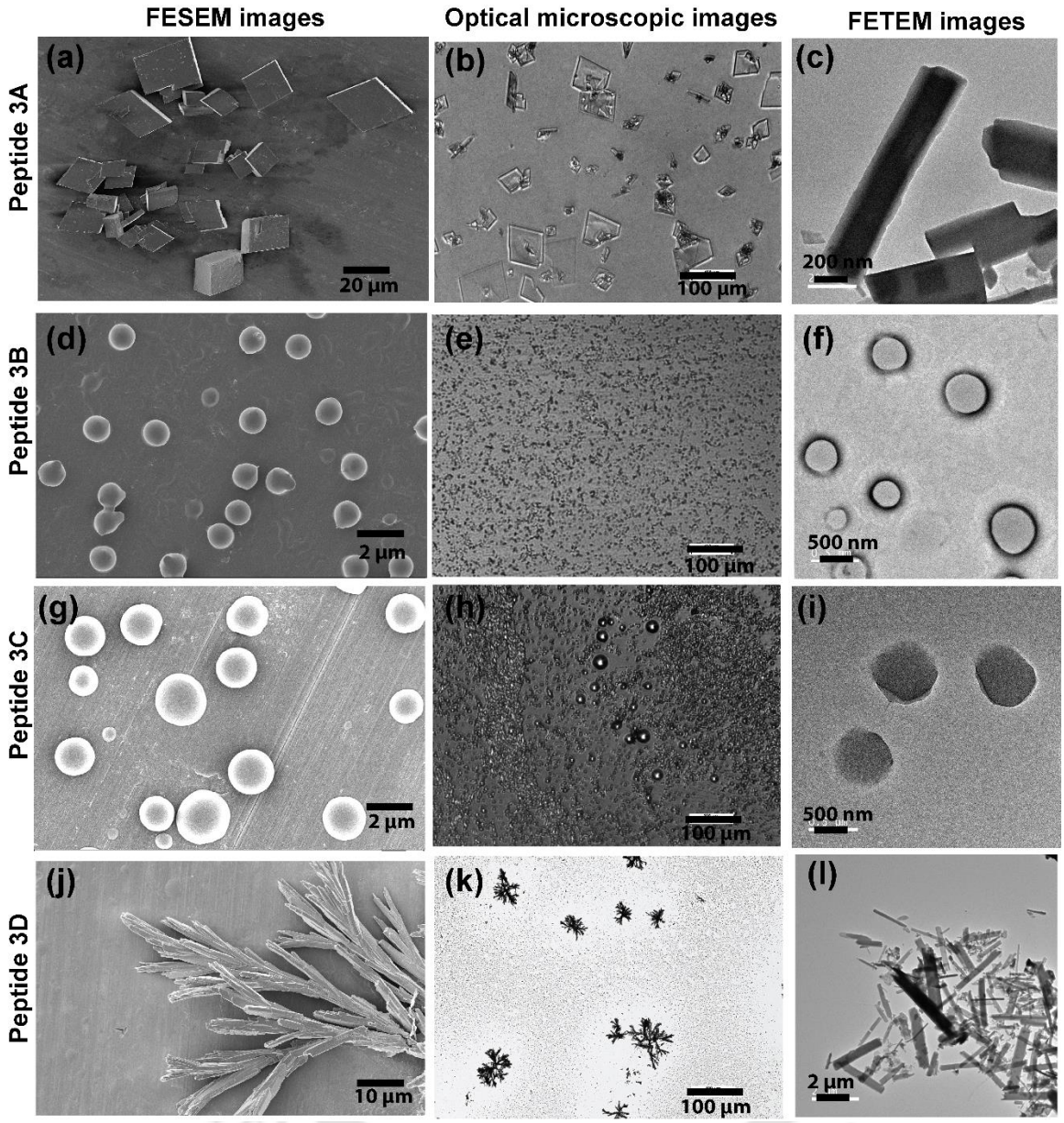

Figure 3.2. *Dipeptide **3A** shows the block-shaped structure (a, b, c), **3B** and **3C** exhibit spherical structures (d, e, f) and (g, h, i), **3D** displays rod-like fiber structure (j, k, l) in FESEM, optical microscope, and FETEM, respectively.*

After that, we calculated the number, intensity, and size (in diameter) of spherical structures by statistical analysis of peptides **3B** and **3C**. (Figure 3.3)

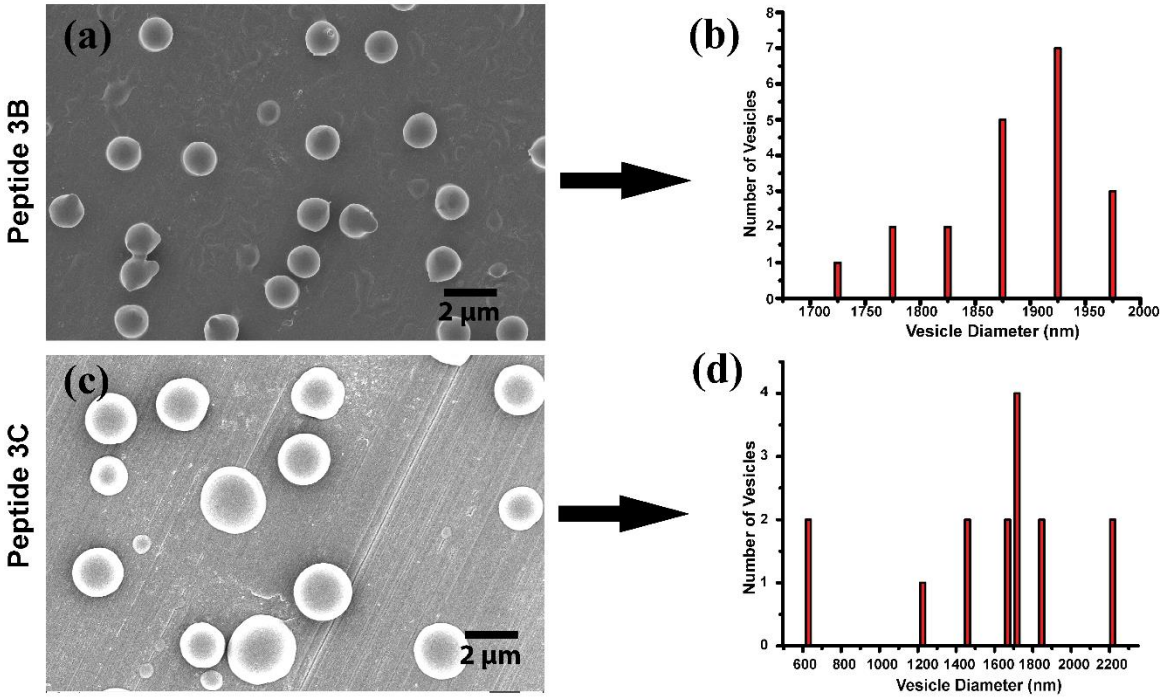

Figure 3.3. *FESEM images, the number density and the diameter of the vesicles formed by 1.5 mM solution of peptide* ***3B (a, b)*** *and peptide* ***3C (c, d)*** *in 50% ACN/H_2O.*

To examine the morphology of freshly prepared peptide solution in 50% ACN/H_2O, FESEM technique was used. Interestingly **3A**, **3B**, and **3C** created almost identical morphologies in comparison to incubated peptide solution, but the self-assembled structures were not completely developed. It may be caused by the period of self-organized structure formation. On the other hand, **3D** formed identical morphology compared to incubated peptide solution (Figure 3.4). It may be because the nanostructure formation was faster for it.

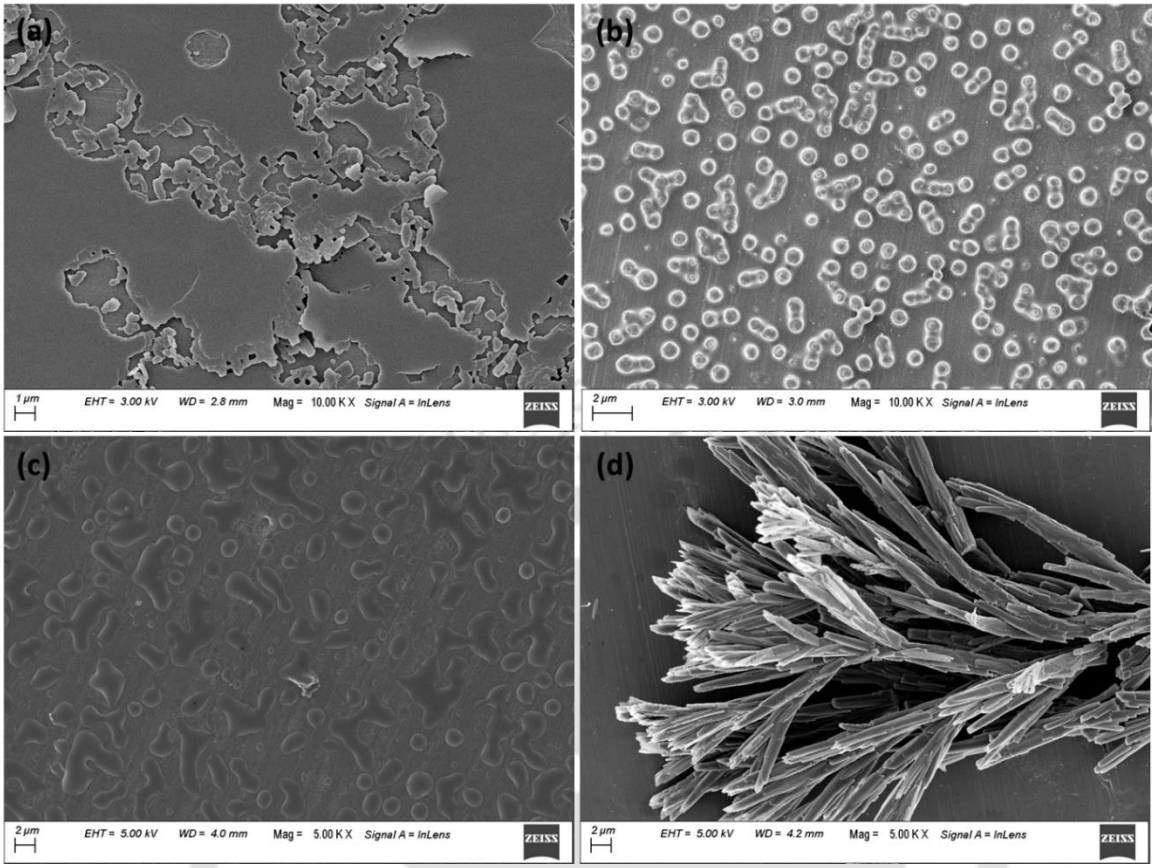

Figure 3.4. *(a, b, c, d) represents FE-SEM images of freshly prepared 1.5 mM peptide samples of* ***3A****,* ***3B****,* ***3C,*** *and* ***3D*** *in 50% ACN/H_2O, respectively.*

Next, to understand the morphology in a different solvent system, such as 50% MeOH/H_2O and 50% Acetone/H_2O rather than 50% ACN/H_2O, FESEM experiment of 4 days of incubated solvent was performed. In both solvent systems, **3A** and **3D** displayed identical morphology. On the other hand, the supramolecular structure obtained by **3B** and **3C** are not similar. This may be due to nanostructure formation for **3B** and **3C** depending on solvent systems (Figure 3.5).

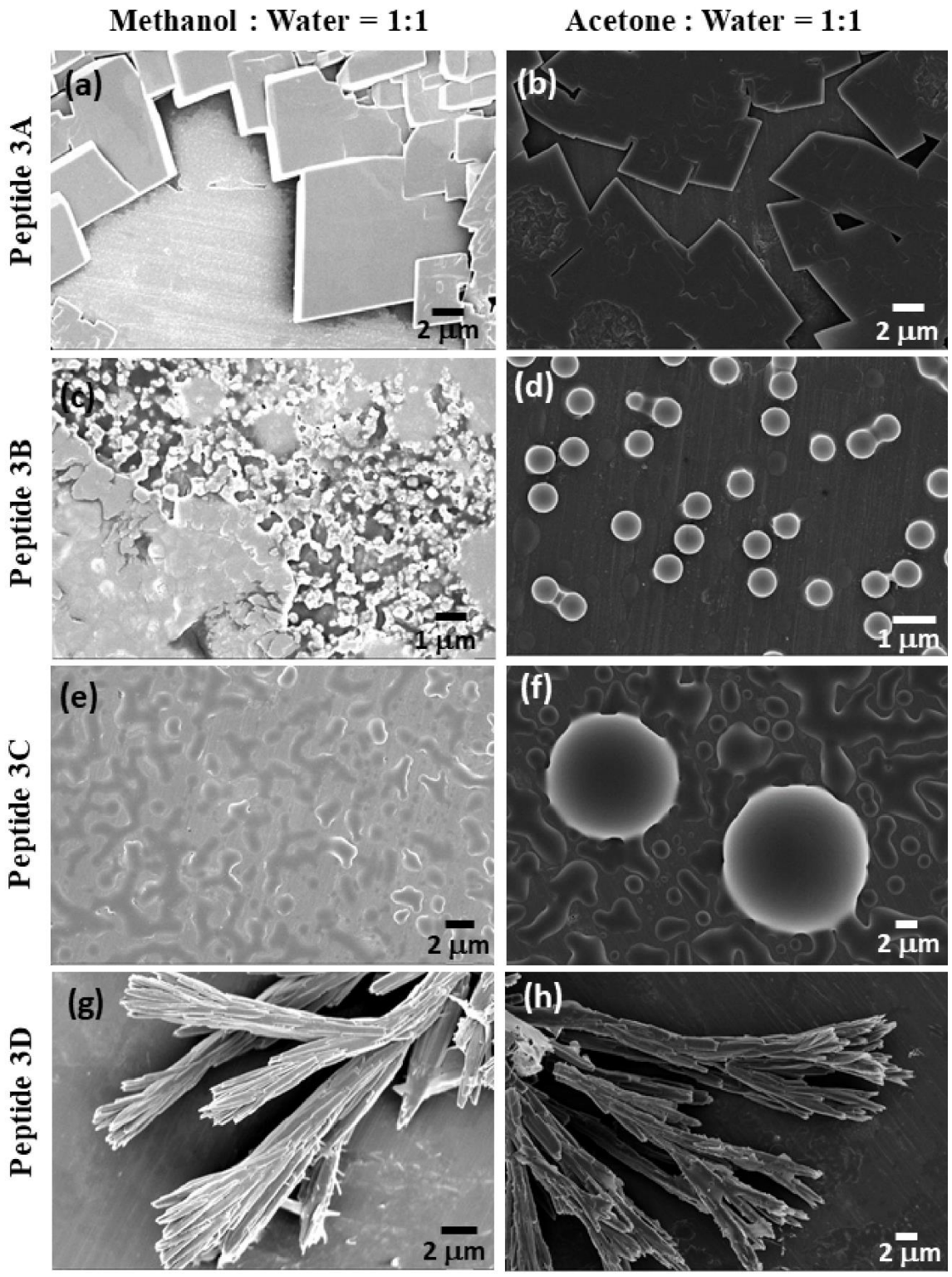

Figure 3.5. *(a, b), (c, d), (e, f) and (g, h) represents FESEM images of 4 days incubated 1.5 mM peptide sample* ***3A***, ***3B***, ***3C*** *and* ***3D*** *in 50% MeOH/H_2O and 50% Acetone/H_2O, respectively.*

Next, we performed atomic force microscopy (AFM) to get the topographical information of the designed peptides. For this experiment, 1.5 mM incubated each peptide solution in 50% ACN/H_2O diluted to 30 μM. AFM images of **3A** displayed a block-shaped structure (an average diameter ~160 nm). Dipeptides **3B** and **3C** exhibited vesicles (average diameter ranging from 700 nm to 1.4 μm). However, peptide **3D** formed rod-like fiber structure (average diameter ~140 nm). The lengths of all the nanostructures were measured from height to distance plot (Figure 3.6). However, the nanostructure sizes measured by various microscopic techniques differed probably due to the concentration difference in the samples.

Therefore, morphology analysis suggests exciting results. The change of protecting group Boc to the more hydrophobic Fmoc group formed a distinctly different supramolecular structure. On the other hand, changing the nitro group's position from *ortho* to *para*, i.e., *o*-NBS to *p*-NBS generated a totally different morphology. Hence, diverse microscopic experiments help to understand that the N-terminal protecting group of a dipeptide impacts the self-assembly process and morphology determination. To the best of our knowledge, the morphological diversity of dipeptides depending on the protecting group was not reported before.

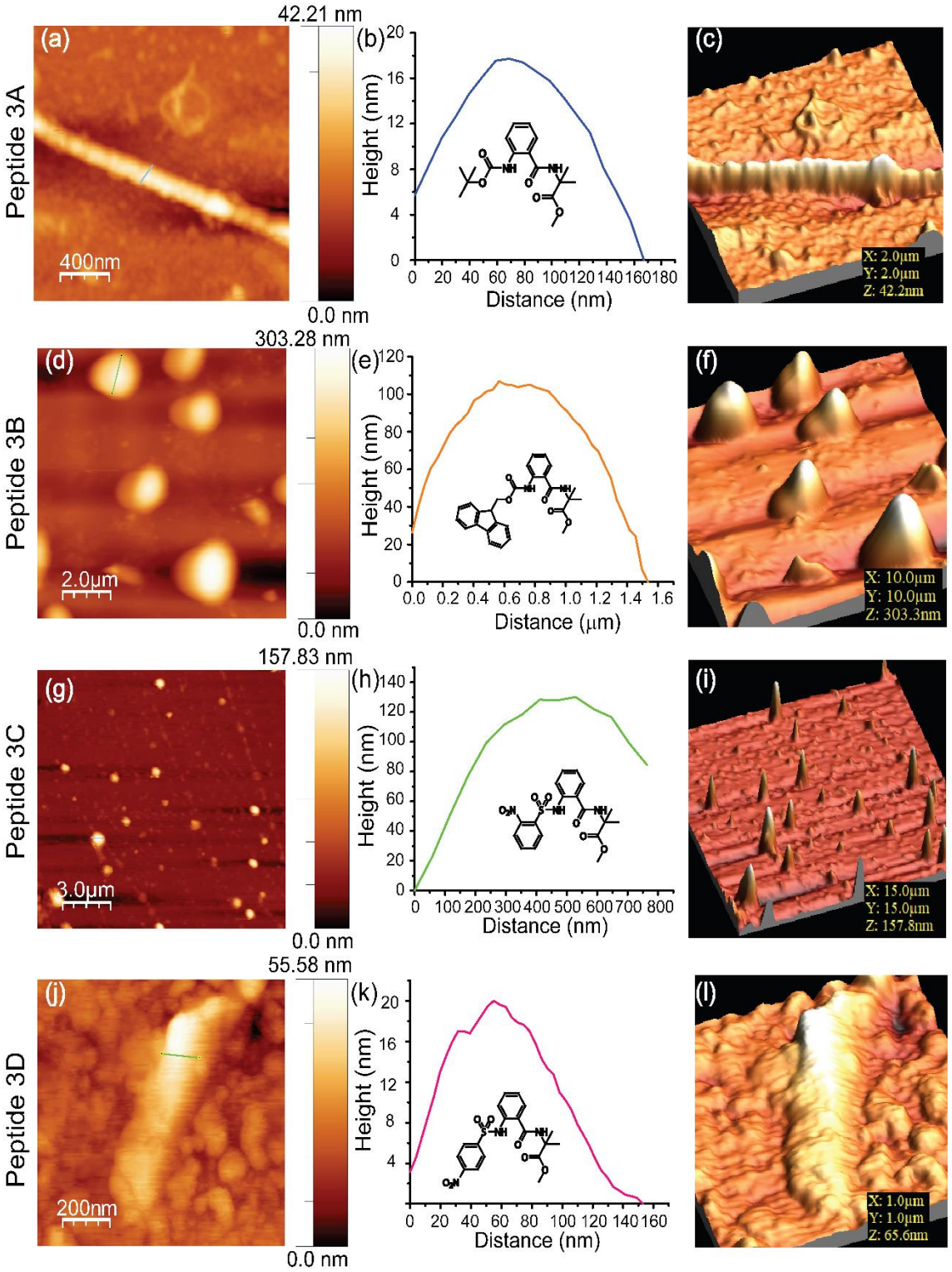

Figure 3.6. *2D AFM images (a, d, g, j), height profile plots (b, e, h, k), and 3D AFM (c, f, i, l) images of dipeptides* ***3A, 3B, 3C,*** *and* ***3D,*** *respectively, 30 µM each in 50% ACN/H_2O.*

3.5. DLS study

Next, to check the size of vesicle formation by 4-days incubated 1.5 mM peptides (**3B** and **3C**) solution in 50% ACN/H_2O, we have performed a dynamic light scattering (DLS) study. The size of nano-vesicles was approximately 406.5 nm and 735.1 nm for **3B** and **3C**, respectively, indicating the creation of a well-equilibrated vesicle structure (Figure 3.7). The created vesicle size in the DLS study was slightly bigger than FETEM. This difference may generate due to the fusion of smaller vesicles to form more giant vesicles and the solvation of vesicles.

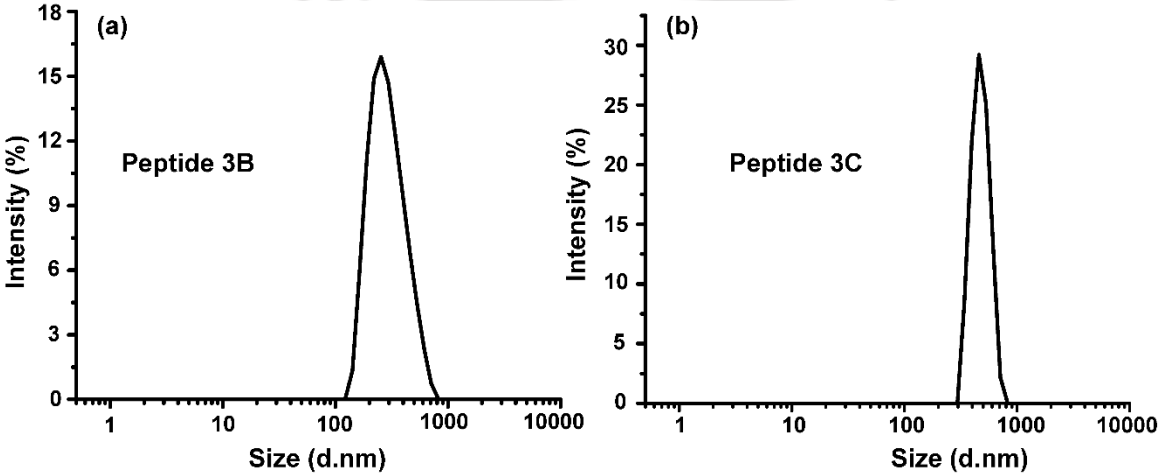

Figure 3.7. *Size distribution plot in DLS experiment. Dipeptides **3B** (a) and **3C** (b) exhibited hydrodynamic diameters, 406.5 nm, 735.1 nm, respectively, and polydispersity index, 0.505 and 0.660, respectively.*

3.6. Responsive nature of nano-vesicles

Next, we studied a salt-triggered experiment to examine the responsive nature of nano-vesicles (generated by **3B** and **3C**) potential as delivery vehicles. The disruption of the vesicular structure happens in the presence of biocompatible metal ions such as K^+ and Ca^{2+}. In our FE-SEM experiment, ruptured vesicular structures were noticed when these dipeptide solutions were treated with 5 mM KCl solution (Figure 3.8). In the presence of several metal salts, nanostructure forming stabilizing forces, weak noncovalent interactions such as hydrogen bonding, aromatic π-π interaction, and hydrophobic interaction were broken.[7] As a result, disruption of these nanostructures happens. This result indicates the salt-responsive nature of the vesicles.

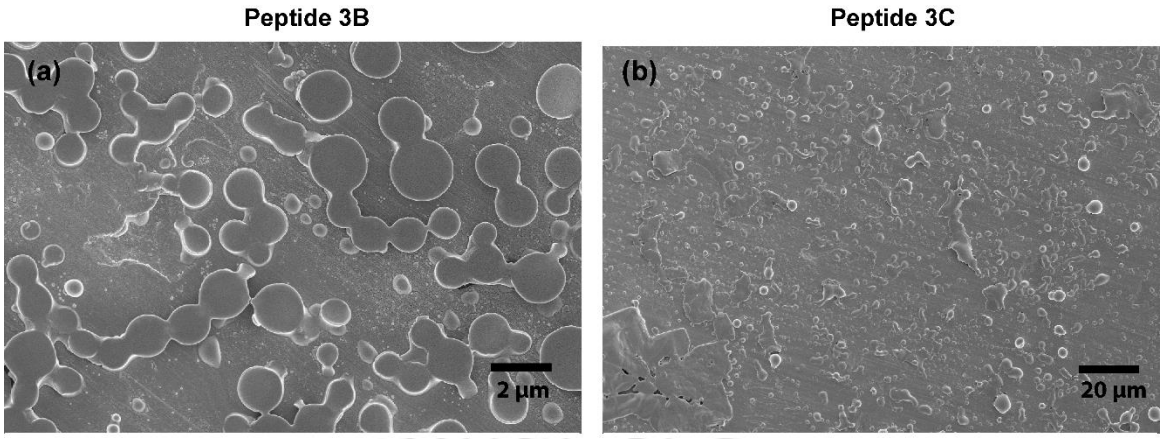

Figure 3.8. *Ruptured nanovesicles of (a)* ***3B*** *and (b)* ***3C****, as observed in the FE-SEM experiment after KCl treatment.*

3.7. Self-assembling mechanism investigation by SC-XRD

Next, we performed Single Crystal X-ray Diffraction (SC-XRD) analyses to get molecular-level information on peptide self-assembly. Excellent quality single crystals were obtained by slow evaporation of acetonitrile/water mixture of the peptides at room temperature. In the crystalline state, peptide **3A** crystallized in (*P 21/n*) space group and contained a single molecule in the asymmetric unit (Figure 3.9a). Each monomeric unit is interlinked through a six-membered cyclic intramolecular H-bonded structure (Figure 3.9b). Dimeric structure formation by intermolecular H-bonding (CO···NH), and various weak hydrophobic interactions along the *c*-direction (Figure 3.9c). Furthermore, **3A** displayed herringbone helical arrangement along the *c*-direction in higher-order molecular packing (Figure 3.9d). This well-organized helical arrangement may provide block-shaped morphology as displayed by various microscopic techniques.

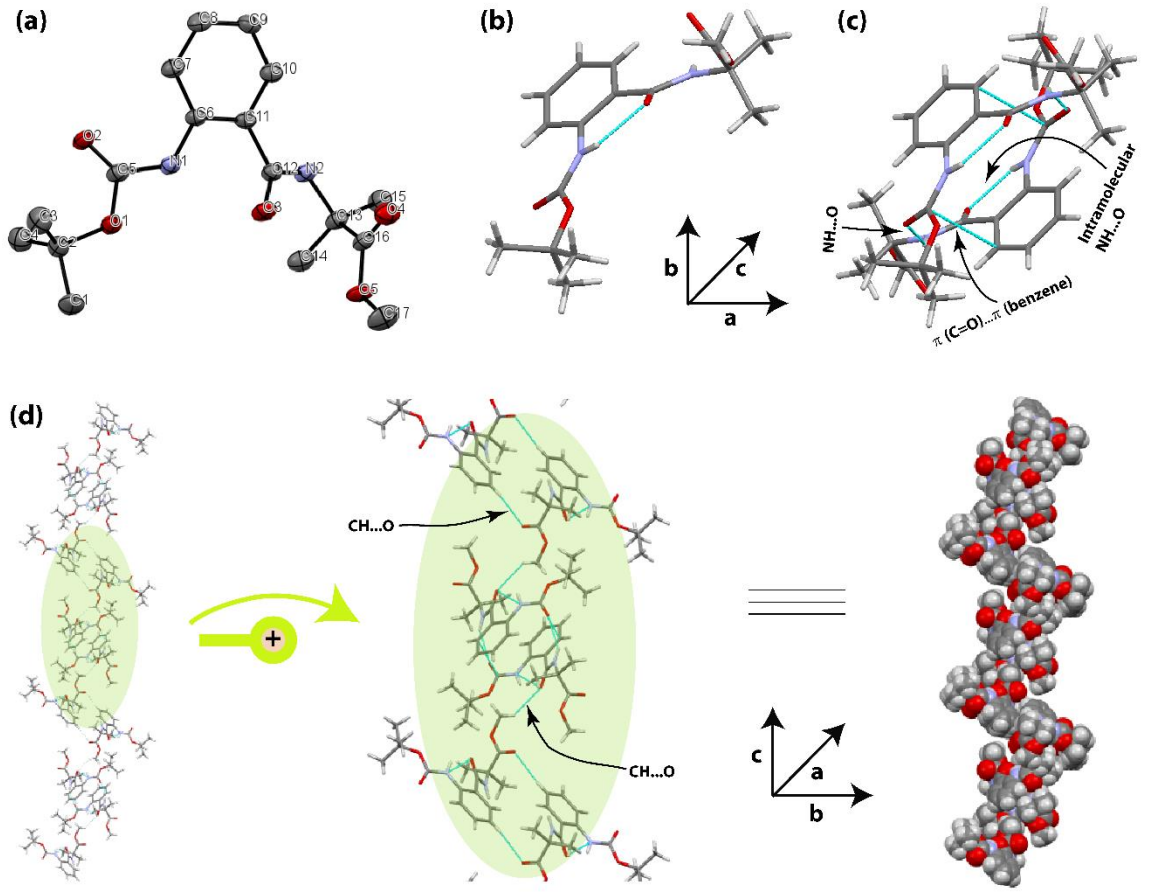

Figure 3.9. *(a) The ORTEP images containing ellipsoid 30% probability, (b) six-membered (C6) hydrogen-bonded cyclic structure, (c) dimeric structure, and (d) herringbone helical structure in the higher-order molecular organization along the c-axis of* ***3A****.*

N-terminal Fmoc protected dipeptide **3B** contained (*P2(1)/c*) space group and exhibited a single molecule in its asymmetric unit (Figure 3.10a). Each molecule was stabilized through a six-membered cyclic intramolecular H-bonding structure (Figure 3.10b), intermolecular H-bonding (CO···NH), and other weak hydrophobic interactions along the *c*-axis (Figure 3.10c). Moreover, **3B** formed a parallel β-sheet-like layer architecture along the *b*-direction (Figure 3.10d) and displayed a diverse sheet-like layered arrangement along the *a*-direction (Figure 3.10e). A closer β-sheet-like layer structure may be responsible for spherical structure formation under suitable conditions.[8]

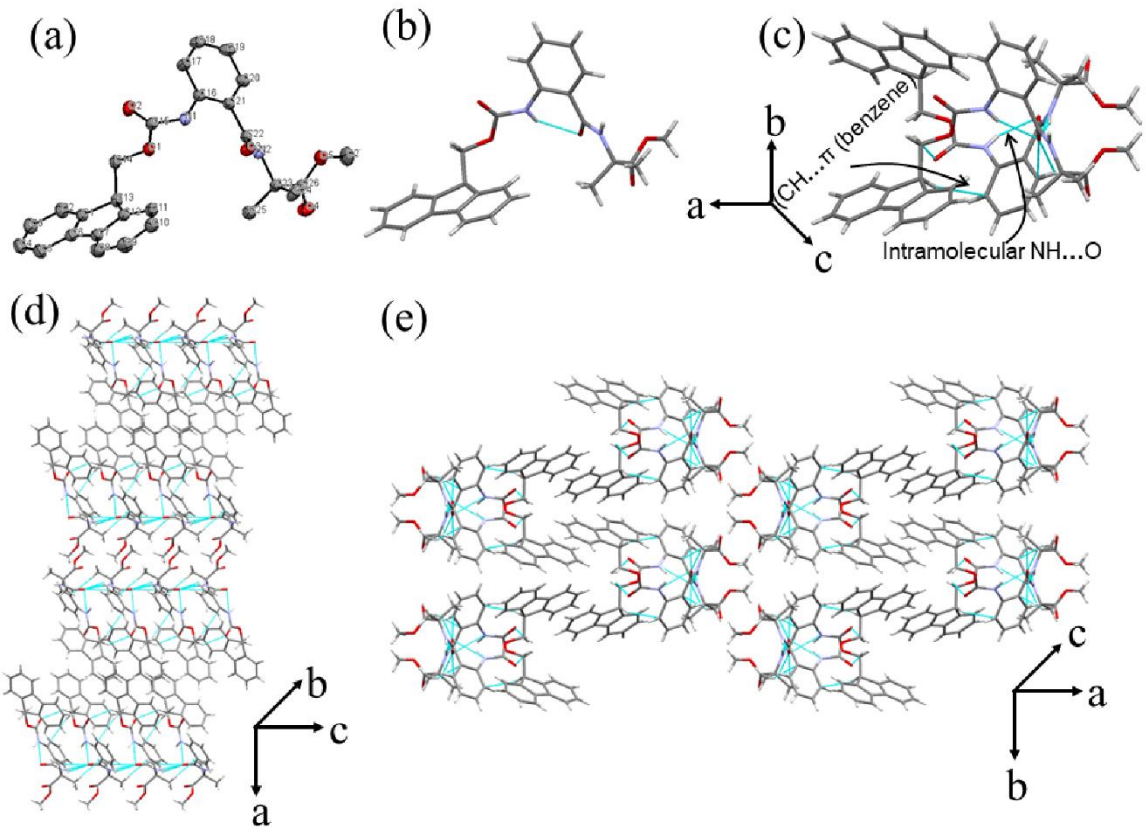

Figure 3.10. *(a) The ORTEP images containing ellipsoid 30% probability, (b) six-membered (C6) hydrogen bonding structure, (c) noncovalent interactions, (d) parallel β-sheet-like layer architecture in the higher-order molecular organization along the b-axis, and (e) complex sheet-like layer self-assembly pattern along the a-axis of* ***3B****.*

Dipeptide **3C** crystalized in (*P 21/n*) space group and showed two molecules in its asymmetric unit (Figure 3.11a). Each molecule was interconnected via a six-membered intramolecular hydrogen-bonded cyclic structure (Figure 3.11b), intermolecular hydrogen bonding (CO···NH), and various other weak hydrophobic interactions, which allowed the formation of a dimer along the *a*-axis (3.11c). In higher-order molecular assembly, **3C** displayed herringbone helical architecture along the *b*-axis (Figure 3.11d) and also shown β-sheet-like layer structure along *c* and *a*-axis (Figure 3.11e). It also exhibited a void-like (garland-like) structure along the *a*-axis (Figure 3.11f). This β-sheet-like layer structure[8] and molecular void may cause spherical structure generation under experimental conditions.

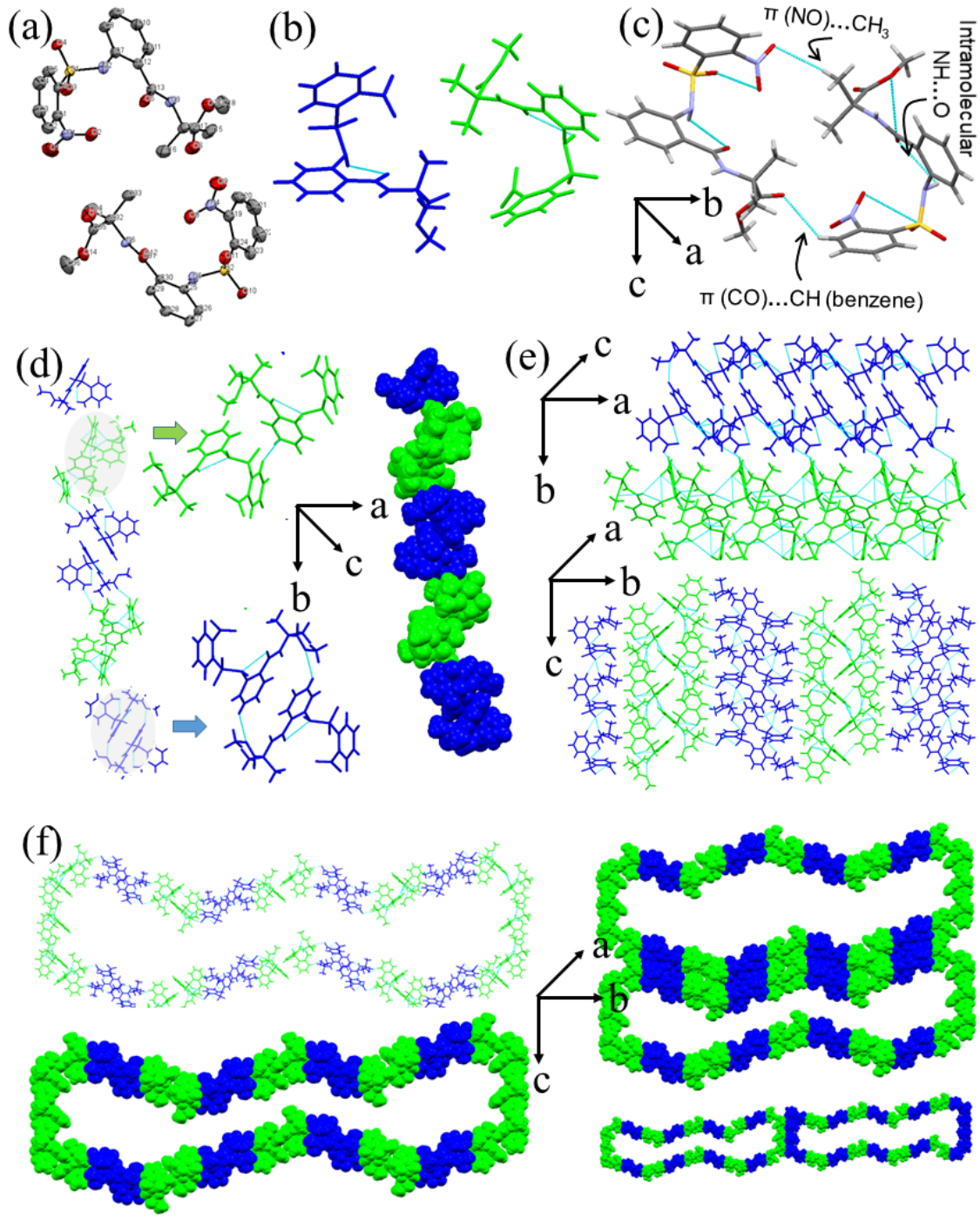

Figure 3.11. *(a) The ORTEP images containing ellipsoid 30% probability, (b) six-membered (C6) hydrogen-bonded cyclic structure, (c) dimer formation via noncovalent interactions, (d) herringbone helical structure along the b-axis, (e) β-sheet-like layer structure along c and a-axis, and (f) void like (garland-like) structure in the higher-order molecular organization along the a-axis of* ***3C****.*

Dipeptide **3D** crystallized in (*P2(1)/c*) space group and exhibited a single molecule in its asymmetric unit (Figure 3.12a). Every subunit was interconnected via six-membered intramolecular hydrogen bonding (Figure 3.12b), intermolecular hydrogen bonding (CO···NH), and other various weak hydrophobic interactions and built dimer along the *c*-axis (3.12c). However, in higher-order molecular assembly, **3D** displayed a distinct sandwich stacking-like structure along the *a*-axis (Figure 3.12d) and a helical wave-like structure along the *b*-axis (Figure 3.12e). The more stable and ordered sandwich stacking and helical wave structure may explain rod-like fiber morphology formation.

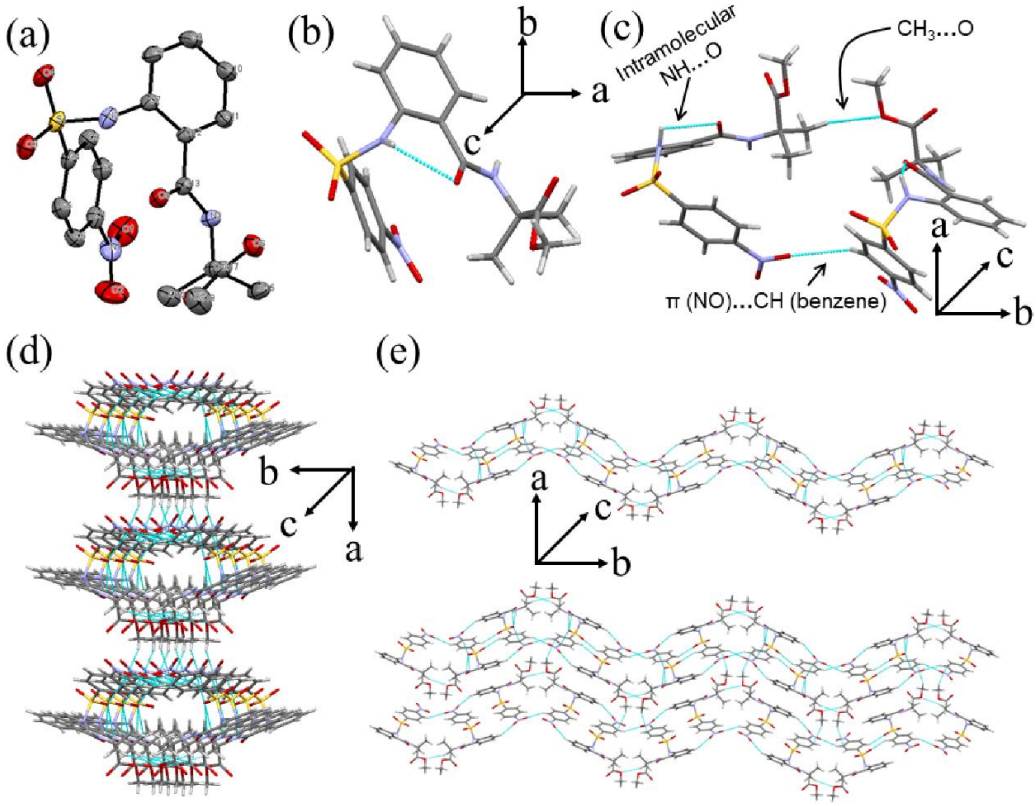

Figure 3.12. *(a) The ORTEP images containing ellipsoid 30% probability, (b) six-membered (C6) hydrogen bonding structure, (c) dimer formation via noncovalent interactions, (d) diverse sandwich stacking like along the a-axis, and (e) helical wave-like architecture in the higher-order assembly along the b-axis of* ***3D****.*

Thus, Ant, Aib, and various protecting groups containing dipeptides created distinct morphologies in solution and different higher-order supramolecular packings in solid-state. Several non-specific week Van der Waals forces and hydrophobic interactions help to stabilize the higher-order supramolecular structures.

3.8. Thermal stability of nanostructures

To check the thermal stability of obtained nanostructures, we have taken FESEM images after constant heating at 60 °C, 100 °C, and 170 °C for 1h in a convection oven. The obtained images indicate that up to 60 °C temperature, **3A** retained its block shape structure, **3B** and **3C** retained their spherical structures, and **3D** displayed rod-like fibrous structures, i.e., all dipeptides retained their original forms. At 100 °C, **3A** started deformation, **3B** exhibited destructed spherical structure and unique rod-like structure, **3C** displayed unsymmetrical spherical structure, and **3D** retained almost its original form. However, at 170 °C temperature, all nanostructures disintegrated and demonstrated unstructured morphology. So, the thermal stability study revealed that **3D** formed a more stable structure than others. The vesicular system obtained from **3C** was comparatively more stable than **3B** (Figure 3.13).

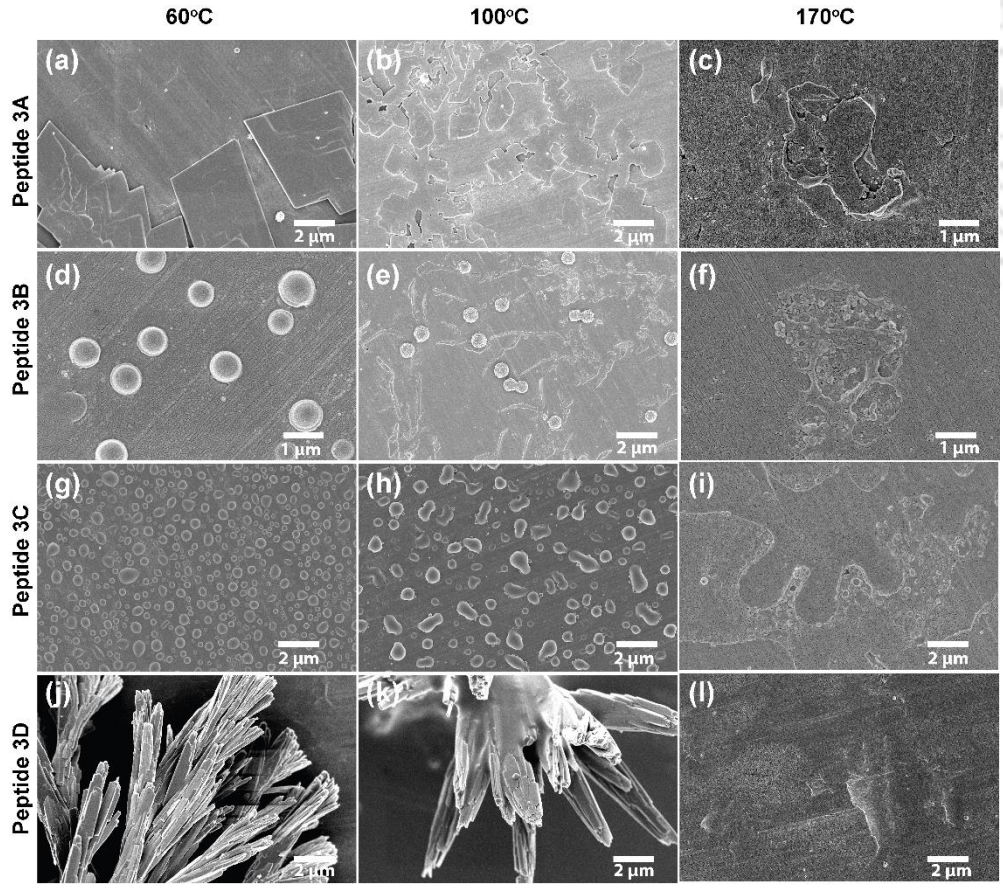

Figure 3.13. *FESEM images of nanostructures of the dipeptides (a, b, c) for* ***3A****, (d, e, f) for* ***3B,*** *(g, h, i) for* ***3C,*** *(j, k, l) for* ***3D*** *after heating at 60 °C, 100 °C, and 170 °C, respectively.*

Moreover, TGA plots indicate that peptide **3A** lost significant weight after 180 °C. The same happened for all other peptides above 180 °C, probably because of the total disintegration of nanostructures. The obtained TGA results are slightly different from FESEM thermal stability results as all nanostructure completely disrupted at ~170 °C there. This difference may be due to the detachment of formed structures from the Al-foil surface during constant heating in a convection oven for FESEM. In the case of TGA, a gradual increase in temperature occurred. The obtained results suggest the significant thermal stability of all these nanostructures (Figure 3.14).

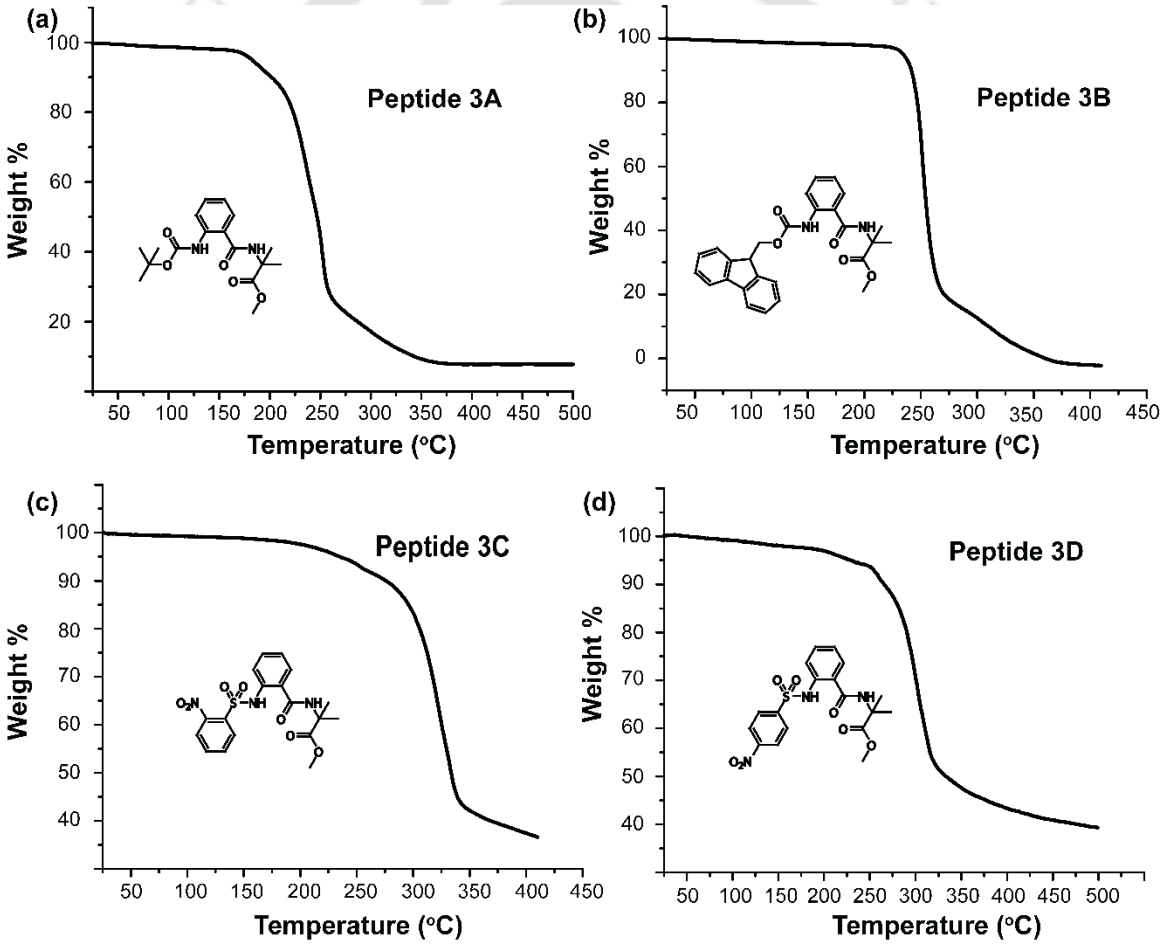

Figure 3.14. *(a, b, c, d) represent TGA profiles of peptides* ***3A****,* ***3B****,* ***3C,*** *and* ***3D****, respectively.*

3.9. N_2 gas adsorption study

To check the porosity of the di-peptides, we have performed gas adsorption studies of all four dipeptides. The N_2 sorption experiment of **3B** and **3D** displays type-III isotherm (Figure 3.15) while **3A** and **3C** remain silent. While the N_2 adsorption capacity of **3B** was 4 cm^3/g, the same of **3D** was 13 cm^3/g. The SC-XRD data revealed that the sheet-like layer supramolecular structure of **3B** (16 Å= 1.60 nm) contained smaller spacings than the helical wave-like structure of **3D** (32 Å = 3.20 nm, Figure 3.35 & 3.36), which may explain their different gas adsorption capacity.

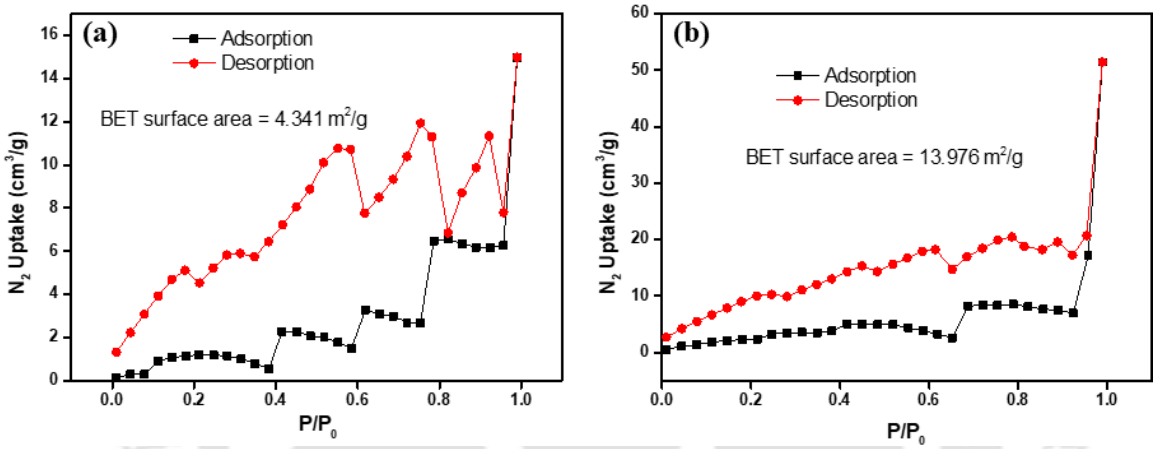

Figure 3.15. *N_2 gas sorption isotherm of a) **3B** and b) **3D**, respectively.*

Next, we wanted to know if such gas adsorption efficiency is due to their supramolecular nanostructure formation. We have performed BET analysis of **3B** and **3D** after incubating for four days in ACN\H_2O mixture, after confirming the same morphology by FESEM and drying. No improvement was observed; instead, a decrease in the surface area was noted. The surface area decreased from 4.341 m^2/g to zero for **3B**, and from 13.976 m^2/g to 5.951 m^2/g for **3D** (Figure 3.16). We have not plotted the graph because the obtained BET surface area was zero for 3B. This decrement may occur due to the formation of a more organized, stable crystalline solid structure than in the powder form, which causes a decrease in surface (as the number of particles is more in powder form). As **3A** and **3C** showed a non-porous nature in previous studies, we have not repeated it for them.

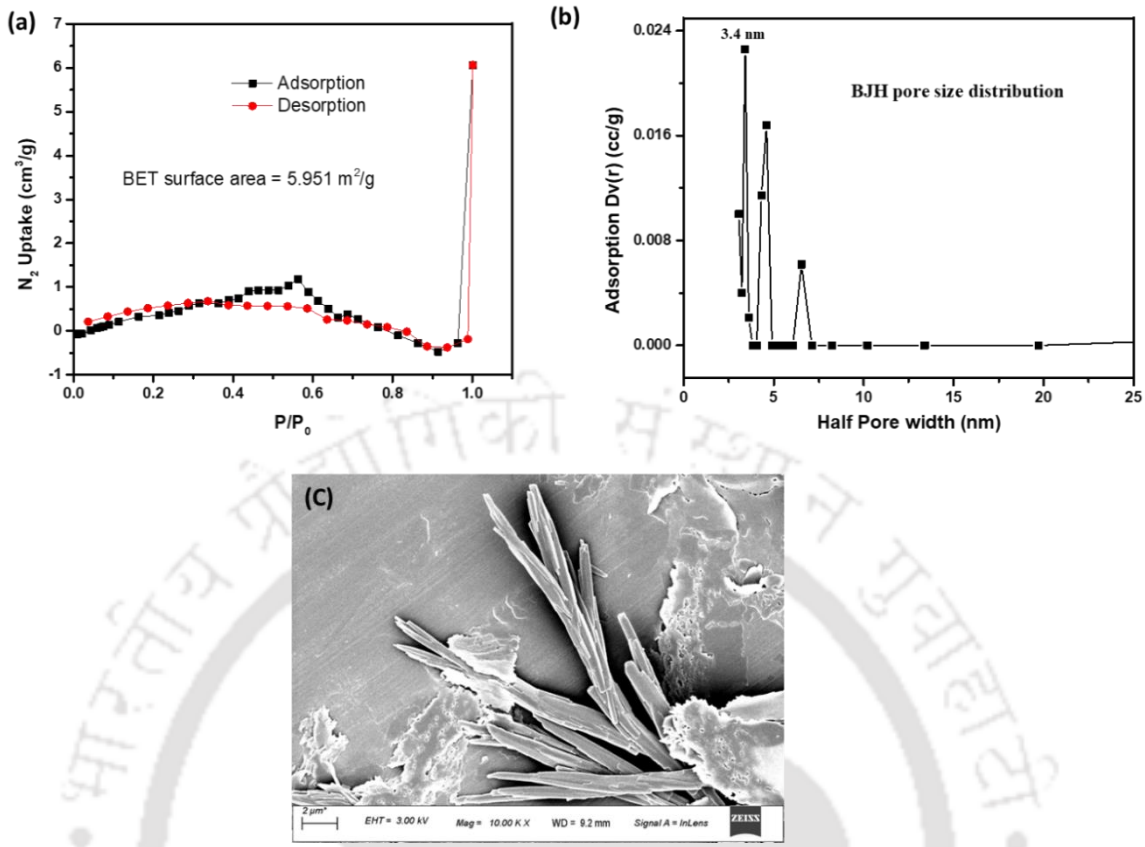

Figure 3.16. *(a) N_2 gas sorption isotherm (b) Density functional theory (DFT) pore size distribution analysis based on the N_2 adsorption data (c) Similar morphology confirmed by FESEM of aggregated mass obtained from peptide* ***3D****.*

3.10. Drug encapsulation capability of dipeptide nanovesicles

Bio-based nanovesicles have been appealing as drug delivery vehicles due to their remarkably high biocompatibility and bioadaptibility. Such nanovesicles encapsulate drugs and other bioactive substances and feasibly deliver them to a target site.[9] Nanovesicles of short peptides have been reported in the literature.[10] However, encapsulating low molecular weight drugs and various biologically active molecules by peptidic materials is rare. We demonstrated that the nano-vesicles formed by **3B** and **3C** can act as a delivery vehicle of Curcumin, a powerful hydrophobic fluorescent drug used for cancer treatment. We also explored the encapsulation properties of Rhodamine B and 6-Carboxyfluorescein dye. To check the encapsulation behavior of these dipeptides, 1 mL

of each dipeptide solution (1.5 mM) in acetonitrile-water (1:1) was incubated with 100 μM Curcumin, Rhodamine B, and Carboxyfluorescein for two days at 37 °C. After that, 10 μL solution was drop-casted over a clean glass slide, dried at room temperature, and observed under a fluorescence microscope. The clear and intense appearance of bright green and red fluorescence from fluorescent spherical structures provides definite evidence for the encapsulation capability of these dyes inside the self-assembled dipeptide nano-vesicles.

Furthermore, we also performed a salt-triggered disruption study. For this purpose, we have added 5 mM KCl solution to the two-day incubated sample and incubated it for a further 24h under identical conditions. The results obtained from fluorescence microscopy indicate the breakage of vesicular structure, i.e., escape of entrapped drug molecules (Figure 3.17 and 3.18). These results corroborated sufficiently with the FESEM experiments.

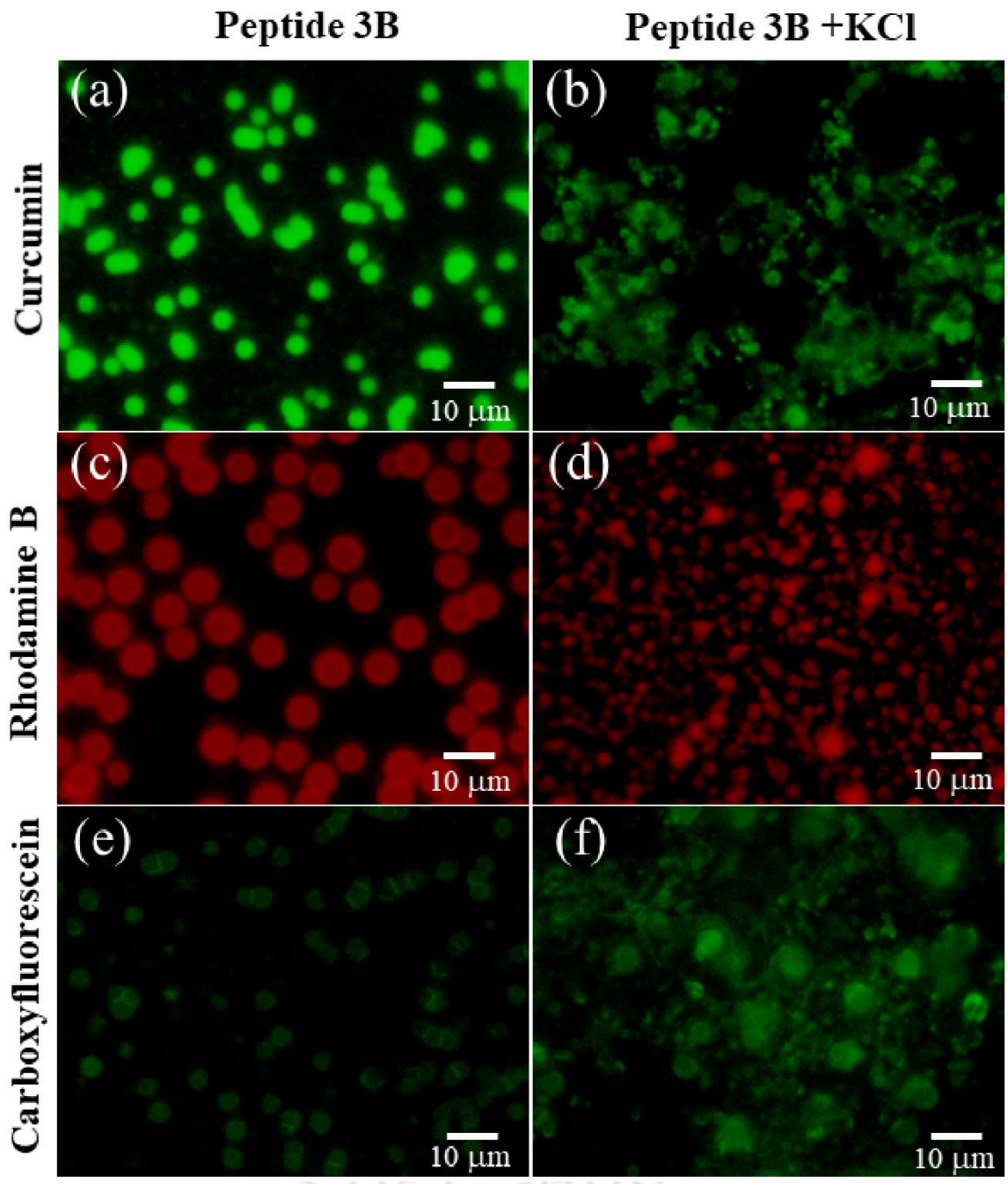

Figure 3.17. *Dipeptide **3B** shows (a, b) bright green fluorescence images of curcumin-loaded nanovesicles and ruptured nanovesicles after the addition of KCl, respectively. (c, d) red fluorescence image of rhodamine B loaded nanovesicles and ruptured nanovesicles after KCl treatment, respectively. (e, f) bright green fluorescence image of Carboxyfluorescein-loaded nanovesicles and ruptured nanovesicles after addition of KCl, respectively.*

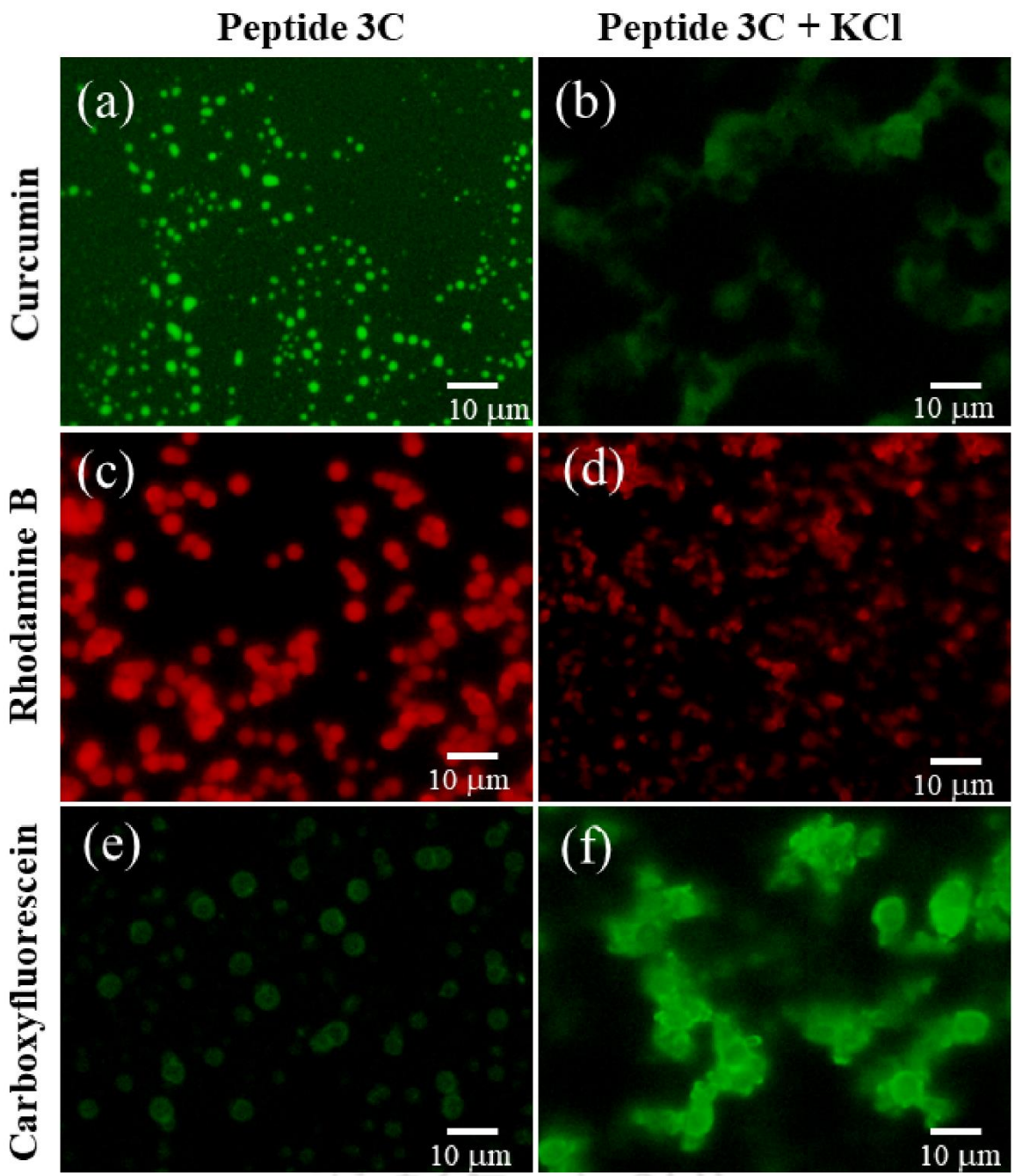

Figure 3.18. *Peptide* ***3C*** *shows (a, b) bright green fluorescence images of curcumin-loaded nanovesicles and ruptured nanovesicles after the addition of KCl, respectively. (c, d) red fluorescence image of rhodamine B loaded nanovesicles and ruptured nanovesicles after KCl treatment. (e, f) bright green fluorescence image of carboxyfluorescein-loaded nanovesicles and ruptured nanovesicles after addition of KCl, respectively.*

Time-dependent fluorescence emission spectra further confirm drug molecules' encapsulation and release properties. In the first few minutes, a slight decrease in intensity and then a gradual decrease up to 24h due to entrapment of drug molecule by **3B** in acetonitrile-water was noted. Moreover, increasing intensity by adding KCl solution indicates the release of entrapped drug molecules (Figure 3.19).

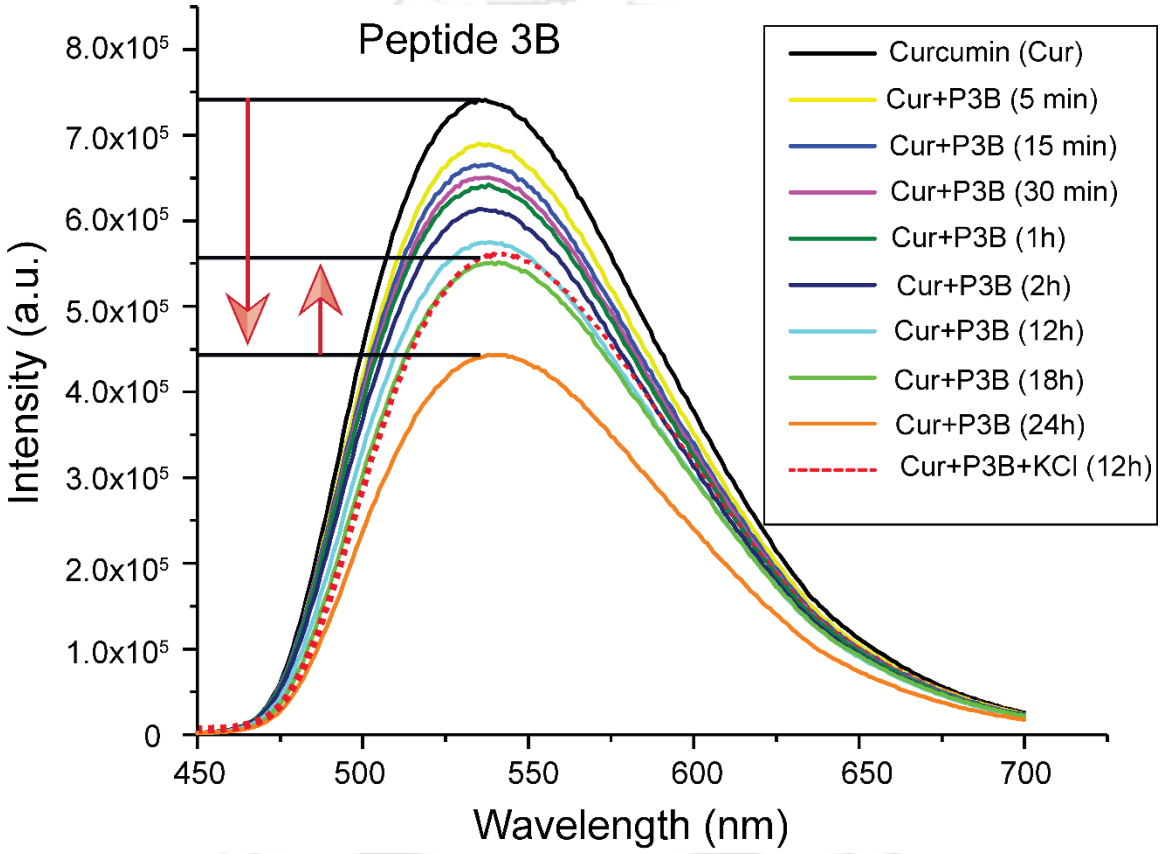

Figure 3.19. *Time-dependent fluorescence emission spectra display the encapsulation properties of Curcumin via the nanovesicle of peptide* ***3B*** *in acetonitrile-water and release of drug molecule upon KCl treatment.*

Table 3.1. Significant results obtained from various experiments

Peptides	FESEM, FETEM, AFM	SC-XRD	N_2-adsorption study	Encapsulation and releasing of dye
3A	block-shaped structure	herringbone helical architecture	-	-
3B	vesicles	sheet-like layer structure	type-III isotherm	display various dye encapsulation and releasing properties
3C	vesicles	β-sheet-like layer structure and void-like (garland-like) architecture	-	Exhibit various dye encapsulation and releasing properties
3D	rod-like fiber structure	sandwich stacking and helical wave-like architecture	type-III isotherm	-

3.11. Conclusion

Herein, we have unveiled the self-assembly of four new dipeptides, which contain two rigid, unnatural amino acids and various N-terminal protecting groups. All freshly synthesized peptides formed different nanostructures in the self-assembly process. The vital features of the structures and functions of the dipeptides are summarized in Table 3.1. Interestingly, the fluorescence and UV experiment results collectively suggest that vesicular nanostructures can encapsulate Curcumin, Rhodamine B, and Carboxyfluorescein. It also displays KCl-mediated salt-triggered disruption of vesicular structures with subsequent release of the drug molecules. Thus such materials may be applied as delivery vehicles for entrapment and transport of these mentioned drug molecules and various essential biological substrates. Some of the dipeptides have gas adsorption properties as well. This work may also contribute significantly to the model study of different peptide-peptide interactions and the design of novel scaffolds for novel functional nanomaterials.

3.12. Experimental section

3.12.1. Materials and instrumentations

As described in chapter 7

3.12.2. General procedure for the synthesis of dipeptides

A conventional peptide synthetic method was applied to synthesize all designed peptides in solution. Boc, Fmoc, *o*-NBS and *p*-NBS protecting groups were used to protect the N-terminal of Anthranilic acid. Methyl ester was used as protecting group for C-terminal of 2-Aminoisobutyric acid. The amino acid coupling reaction was completed by using DCC/HOBt Reagent. Purification of synthesized peptides was executed by column chromatography. For this purpose, silica gel (60-120 mesh) and Ethyl-Acetate/Hexane were employed as stationary phase and mobile phase, respectively. The characterization and purity check of desired peptides were performed by 1D ^{1}H and ^{13}C NMR spectroscopy, mass spectrometry, and Analytical HPLC.

A representative method of preparation of dipeptides:

The dissolved solution of Boc-Ant-OH (400 mg, 1.68 mmol) in 10 mL DCM and 5 mL DMF in 50 mL RB was kept in an ice bath with continuous stirring. Neutralized H_2N-Aib-OMe (294 mg, 2.52 mmol) solution in DMF was immediately added to the reaction mixture after the addition of DCC (519 mg, 2.52 mmol) and HOBt (226, 1.68 mmol) and kept for stirring at room temperature for 24h. The byproduct N, N'-dicyclohexylurea (DCU), was eliminated by filtration. To dilute the organic layer, 50 mL ethyl acetate (EtOAc) was poured into it. Then washed with 10% citric acid and $NaHCO_3$ and brine solution, respectively. Na_2SO_4 was added to the organic part, and the solvent was evaporated by a rotary evaporator. Purification of the peptide by column chromatography provides pure peptide. Other peptides were also prepared similarly.

3.12.3. Sample preparation

1 mL of 1.5 mM peptide solution was prepared in 50% ACN/H_2O and incubated for four days at 37 °C. After, incubation peptide solution was allowed for Optical microscopic image capturing, FESEM experiment, thermal stability study, FETEM, AFM, and DLS experiment.

3.13. Characterization data

Boc-Ant-Aib-OMe (3A)

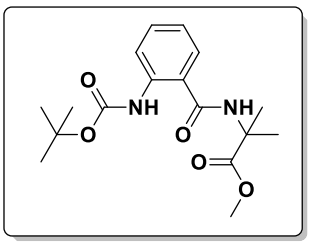

White solid, (391 mg, 69%), **M.P** 171-174°C, (**IR**- 3344, 3265, 2997, 1736, 1693, 1647, 1590, 1519 cm^{-1}) **^{1}H NMR ($CDCl_3$; 600 MHz)** δ in ppm 1.50 (9H, s); 1.66 (6H, s); 3.78 (3H, s); 6.72 (1H, s); 7.00-6.98 (1H, t, *J* = 7.2 Hz); 7.45-7.41 (2H, q, *J* = 7.8 Hz, *J* = 10.2 Hz); 8.34-8.32 (1H, d, *J* = 8.4 Hz); 9.89 (1H, s). **^{13}C NMR ($CDCl_3$; 150 MHz)** δ in ppm 24.9, 28.5, 52.9, 57.1, 80.4, 120.1, 121.6, 126.9, 132.7, 140.3, 153.3, 168.7, 175.1. HRMS (ESI): calculated $[M+H]^+$ =337.1765, observed m/z = 337.1825. HPLC: retention time (t_R) = 5.880 min.

Fmoc-Ant-Aib-OMe (3B)

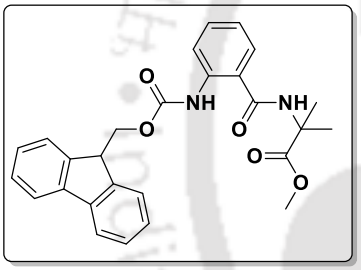

White solid, (372 mg, 73%), **M.P** - 122-125°C (**IR**- 3361, 3224, 3066, 1740, 1623, 1586, 1559, 1510 cm^{-1}), **^{1}H NMR (400 MHz, $CDCl_3$)** δ in ppm 1.70 (6H, s), 3.78 (3H, s), 4.32 – 4.28 (1H, t, *J* = 7.6 Hz), 4.42 – 4.41 (2H, d, *J* = 7.6 Hz), 6.80 (1H, s), 7.05 -7.02 (1H, t, *J* = 7.2 Hz), 7.33 – 7.29 (2H, m), 7.42 -7.38 (2H, t, *J* = 7.6 Hz), 7.51 – 7.44 (2H, m), 7.66 – 7.64 (2H, d, *J* = 7.2 Hz), 7.78 -7.76 (2H, d, *J* = 7.6 Hz), 8.32 -8.30 (1H, d, *J* = 8.4 Hz), 10.43 (1H, s); **^{13}C NMR (100 MHz, $CDCl_3$)** δ in ppm 24.7, 46.9, 52.8, 57.0, 67.2, 120.0, 120.2, 120.3, 122.0, 125.2, 126.7, 127.1, 127.7, 132.6, 139.5, 141.2, 143.8, 153.6, 168.4, 174.9. HRMS (ESI): calculated $[M+H]^+$ = 459.1920, observed m/z = 459.1916. HPLC: retention time (t_R) = 6.552 min.

***o*-NBS-Ant-Aib-OMe (3C)**

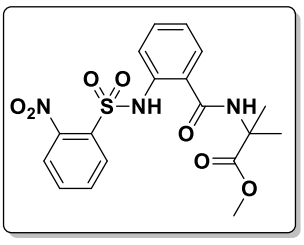

White solid, (360 mg, 68%), mp 130-133°C (IR- 3399, 2943,1742, 1641, 1596, 1529, 1365, 1263, 1159, 765 cm^{-1}), **^{1}H NMR (600 MHz, $CDCl_3$)** δ in ppm 1.66 (6H, s), 3.81 (3H, s), 6.93 (1H, s), 7.12 -7.09 (1H, t, *J* = 7.2 Hz), 7.44 – 7.42 (1H, t, *J*

= 7.8 Hz), 7.51 -7.49 (1H, d, *J* = 7.8 Hz), 7.73 -7.67 (3H, m), 7.81 – 7.79 (1H, d, *J* = 7.8 Hz), 8.10 – 8.09 (1H, d, *J* = 7.8 Hz), 11.21 (1H, s); **^{13}C NMR (150 MHz, CDCl$_3$)** δ in ppm 24.5, 53.2, 57.5, 120.2, 122.0, 123.8, 125.3, 127.5, 131.2, 132.5, 132.8, 133.3, 133.9, 137.9, 148.3, 167.6, 175.2. HRMS (ESI): calculated $[M+H]^+$ = 422.1022, observed m/z = 422.1039. HPLC: retention time (t_R) = 5.259 min.

***p*-NBS-Ant-Aib-OMe (3D)**

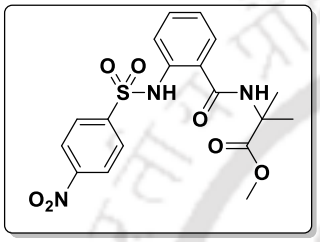

White solid, (366 mg, 70%), **M.P** 151-153ºC(**IR**- 3386, 2926, 1740,1636, 1600, 1528, 1348, 1260, 1158, 775 cm^{-1}) **^{1}H NMR (600 MHz, CDCl$_3$)** δ in ppm 1.62 (6H, s), 3.83 (3H, s), 6.85 (1H, s), 7.14 -7.11 (1H, t, *J* = 7.2 Hz), 7.46 – 7.44 (2H, t, *J* = 7.8 Hz), 7.74 -7.72 (1H, d, *J* = 7.8 Hz), 8.01 – 8.00 (2H, d, *J* = 8.4 Hz), 8.27 – 8.26 (2H, d, *J* = 9.0 Hz), 11.19 (1H, s); **^{13}C NMR (150 MHz, CDCl$_3$)** δ in ppm 24.6, 53.2, 57.4, 121.1, 121.4, 124.4, 124.4, 127.4, 128.7, 133.2, 138.4, 145.4, 150.2, 167.8, 174.9. HRMS (ESI): calculated $[M+H]^+$ = 422.1022, observed m/z = 422.1027. HPLC: retention time (t_R) = 5.489 min.

3.14. References

1. Reches. M.; Gazit. E. Controlled patterning of aligned self-assembled peptide nanotubes. *Nat. Nanotechnol.* **2006**, *1*, 195.
2. Demirel. G.; Malvadkar. N.; Demirel. M. C. Control of Protein Adsorption onto Core-Shell Tubular and Vesicular Structures of Diphenylalanine/Parylene. *Langmuir* **2010**, *26*, 1460-1463.
3. Dutt. A.; Drew. M. G. B.; Pramanik. A. β-Sheet mediated self-assembly of dipeptides of ω-amino acids and remarkable fibrillation in the solid state. *Org. Biomol. Chem.* **2005**, *3*, 2250-2254.
4. Mishra. A.; Panda. J. J.; Basu. A.; Chauhan. V. S. Nanovesicles Based on Self-Assembly of Conformationally Constrained Aromatic Residue Containing Amphiphilic Dipeptides. *Langmuir* **2008**, *24*, 4571-4576.
5. Xu. Y. X.; Wang. G. T.; Zhao. X.; Jiang. X. K.; Li. Z. T. Self-Assembly of Vesicles from Amphiphilic Aromatic Amide-Based Oligomers. *Langmuir* **2009**, *25*, 2684-2688.
6. Fleming, S.; Ulijn, R. V. Design of Nanostructures Based on Aromatic Peptide Amphiphiles. *Chem. Soc. Rev.* **2014**, *43*, 8150-8177.
7. Curtis. R. A.; Prausnitz. J. M.; Blanch. H. W. Protein-Protein and Protein-Salt Interactions in Aqueous Protein Solutions Containing Concentrated Electrolytes. *Biotechnol. Bioeng.* **1998**, *57*, 11-21.
8. Reches. M.; Gazit. E. Formation of Closed-Cage Nanostructures by Self-Assembly of Aromatic Dipeptides. *Nano Lett.* **2004**, *4*, 581-585.
9. Ghosh. S.; Singh. S. K.; Verma. S. Self-assembly and potassium ion triggered disruption of peptide-based soft structures. *Chem. Commun.* **2007**, 2296-2298.
10. Koley. P.; Pramanik. A. Nanostructures from Single Amino Acid-Based Molecules: Stability, Fibrillation, Encapsulation, and Fabrication of Silver Nanoparticles. *Adv. Funct. Mater.* **2011**, *21*, 4126-4136.

3.15. Selected spectra

3.15.1. Characterization spectra of peptide Boc-Ant-Aib-OMe (3A):

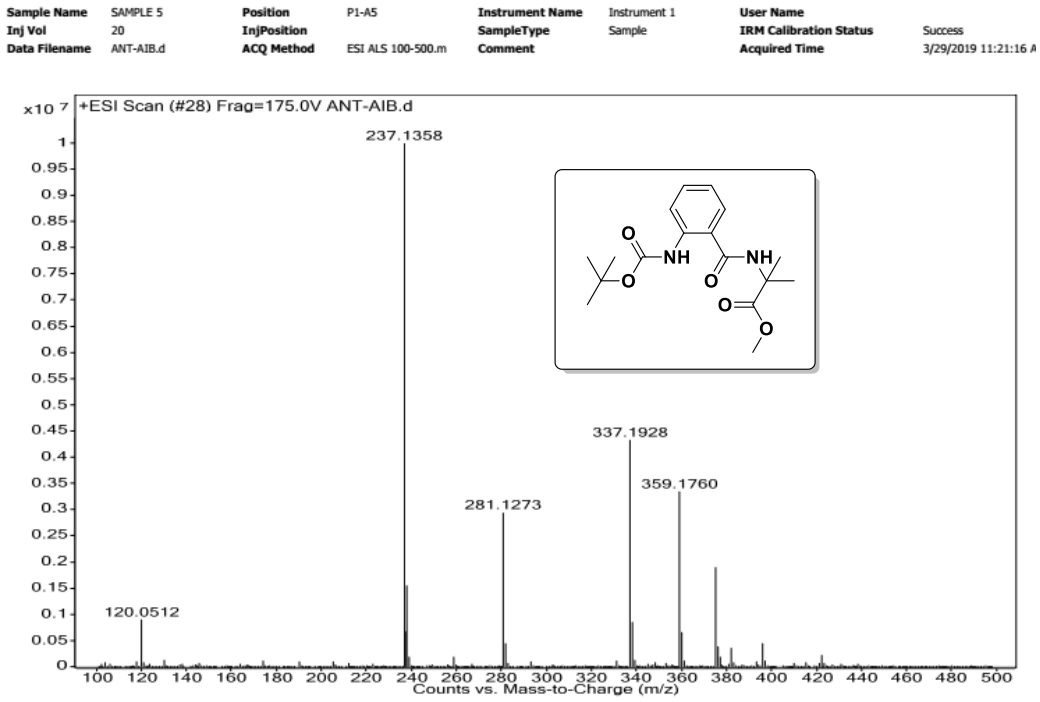

Figure 3.20. *MS spectra of peptide* ***Boc-Ant-Aib-OMe (Peptide 3A)***

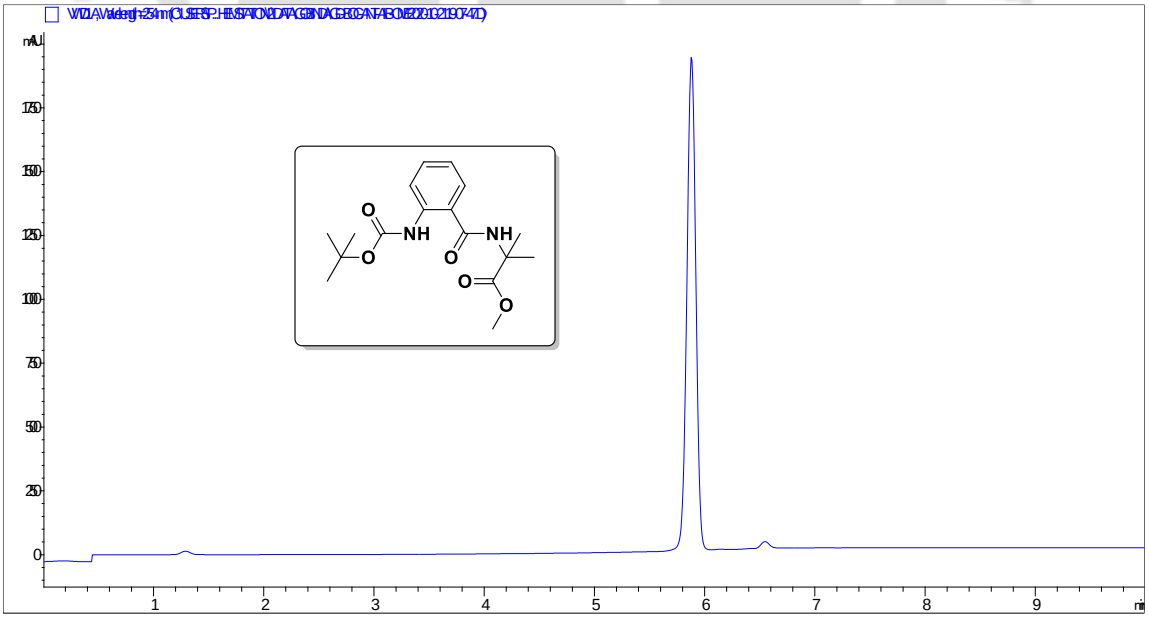

Figure 3.21. *HPLC profile picture of purified peptide* ***Boc-Ant-Aib-OMe (Peptide 3A)***

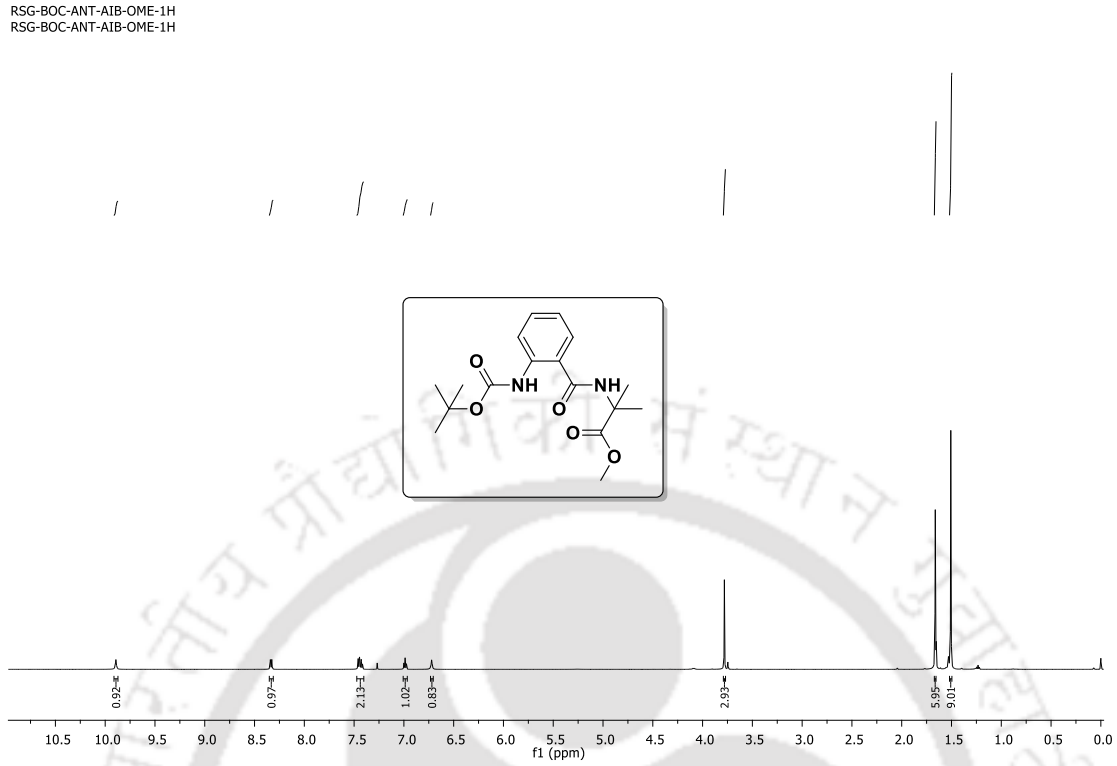

Figure 3.22. *^{1}H NMR spectra of peptide* ***Boc-Ant-Aib-OMe (Peptide 3A)***

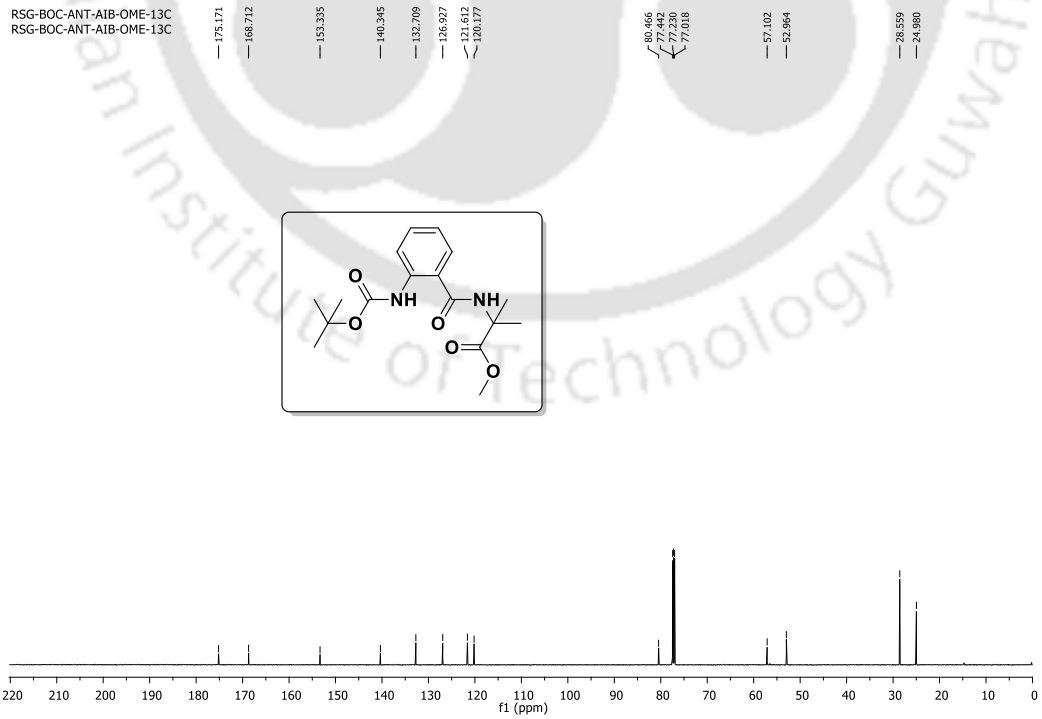

Figure 3.23. *^{13}C NMR spectra of peptide* ***Boc-Ant-Aib-OMe (Peptide 3A)***

3.15.2. Characterization spectra of peptide Fmoc-Ant-Aib-OMe (3B)

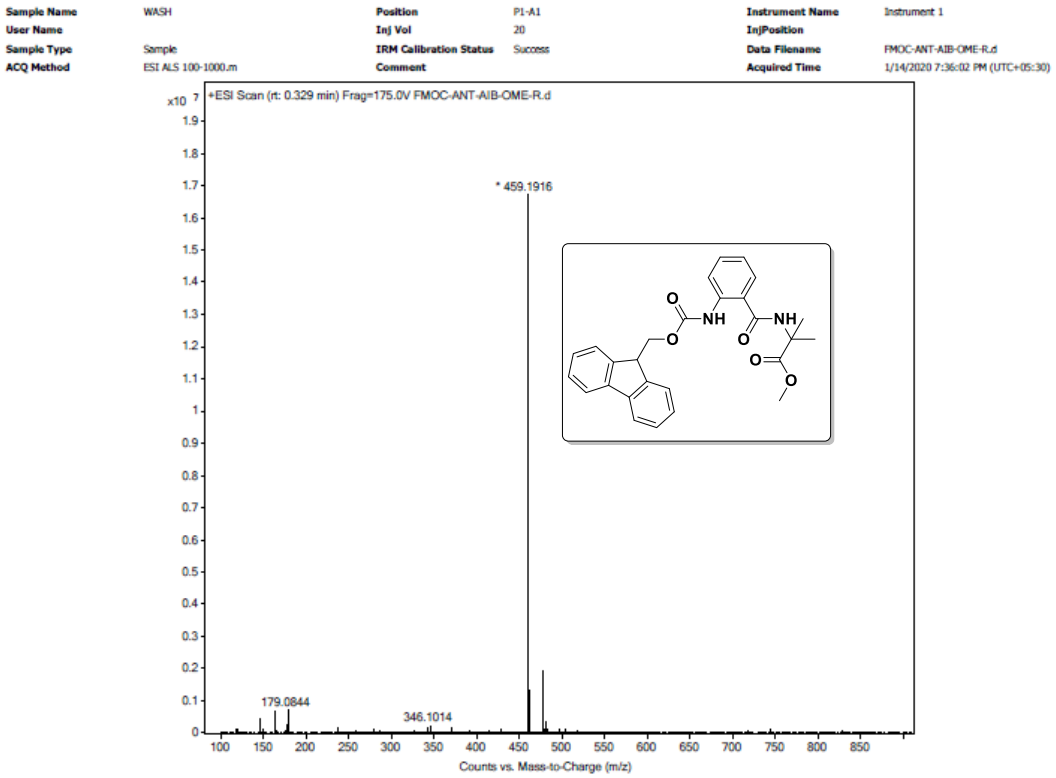

Figure 3.24. *MS spectra of peptide* ***Fmoc-Ant-Aib-OMe (Peptide 3B)***

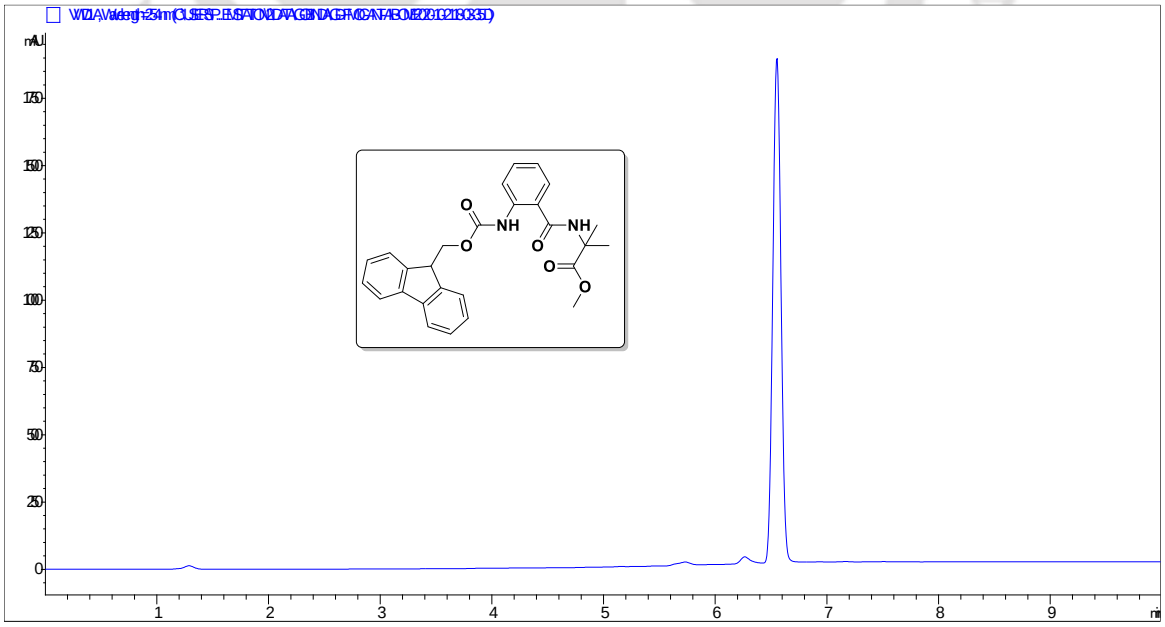

Figure 3.25. *HPLC profile picture of purified peptide* ***Fmoc-Ant-Aib-OMe (Peptide 3B)***

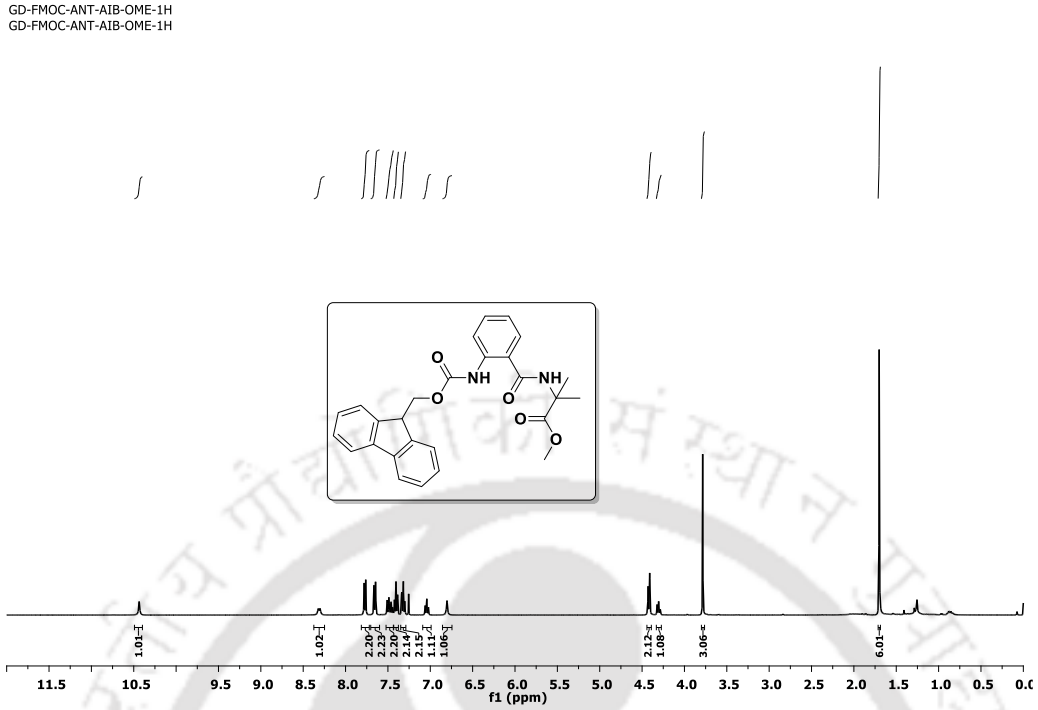

Figure 3.26. *^{1}H NMR spectra of peptide* ***Fmoc-Ant-Aib-OMe (Peptide 3B)***

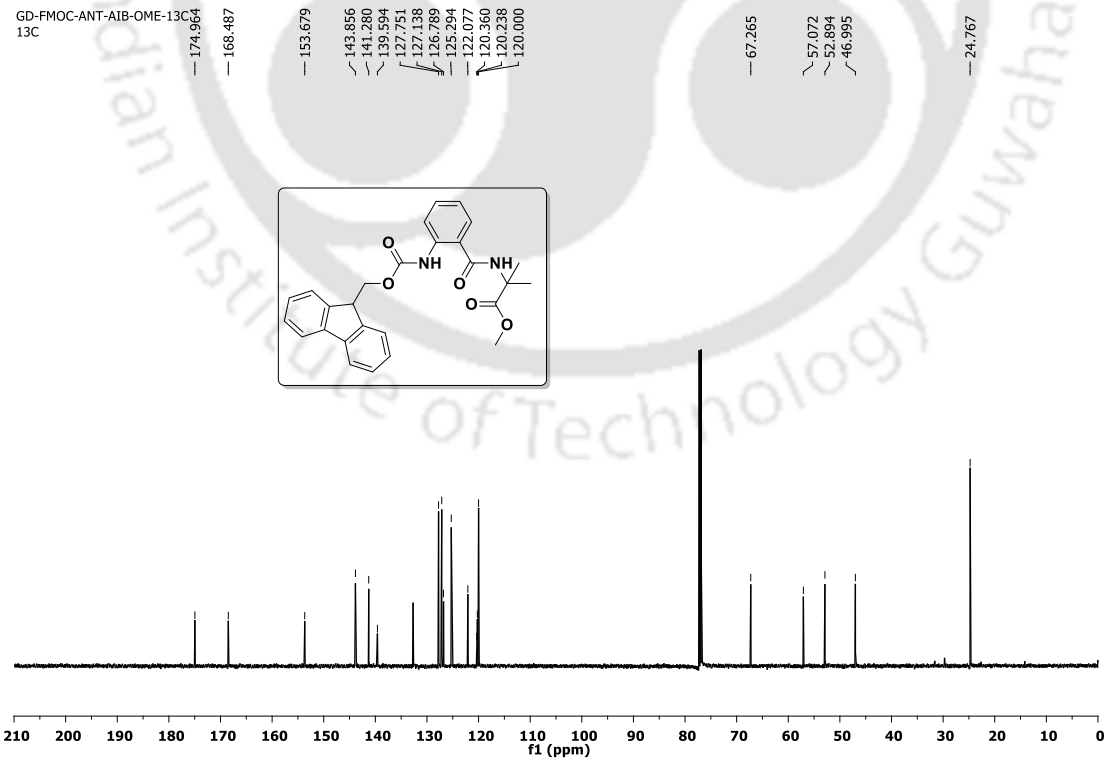

Figure 3.27. *^{13}C NMR spectra of peptide* ***Fmoc-Ant-Aib-OMe (Peptide 3B)***

3.15.3. Characterization spectra of peptide *o*-NBS-Ant-Aib-OMe (3C)

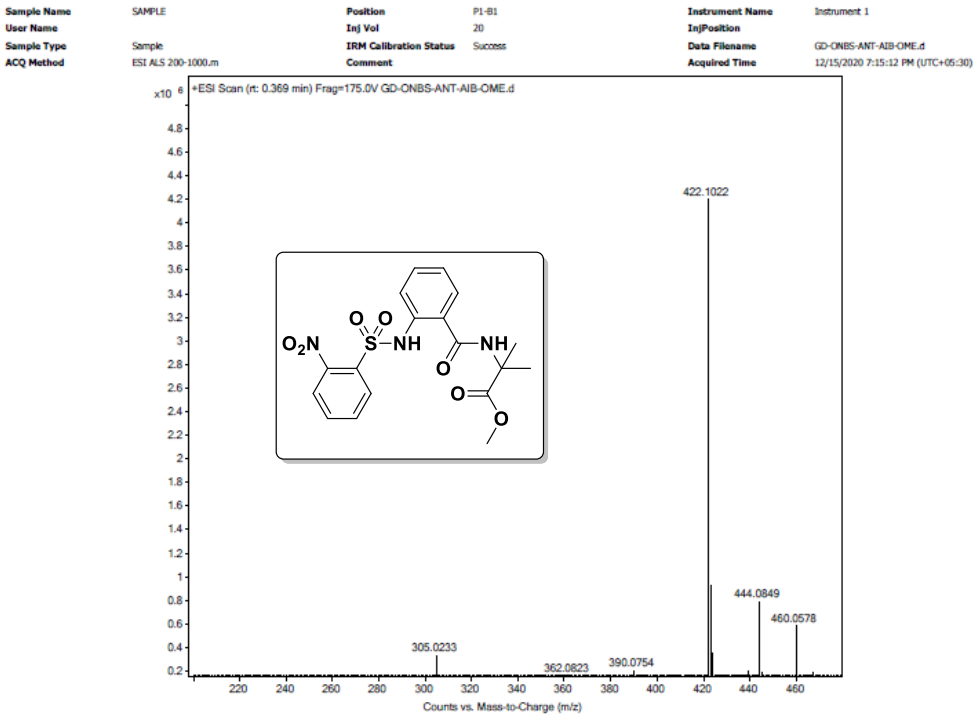

Figure 3.28. *MS spectra of peptide* ***o-NBS-Ant-Aib-OMe (Peptide 3C)***

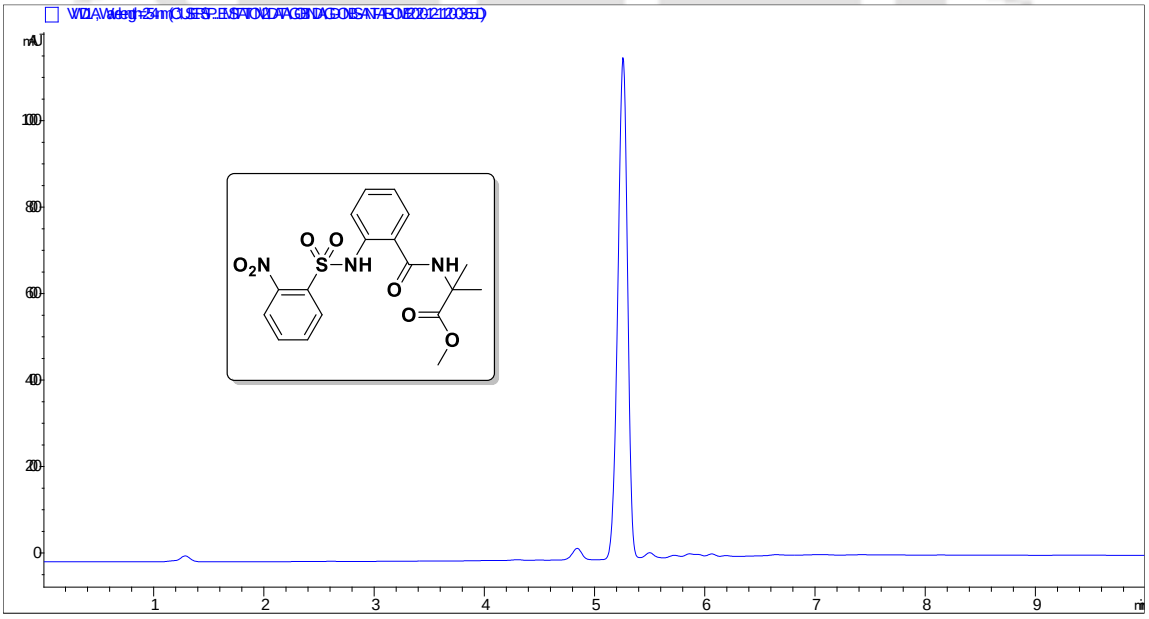

Figure 3.29. *HPLC profile picture of purified peptide* ***o-NBS-Ant-Aib-OMe (Peptide 3C)***

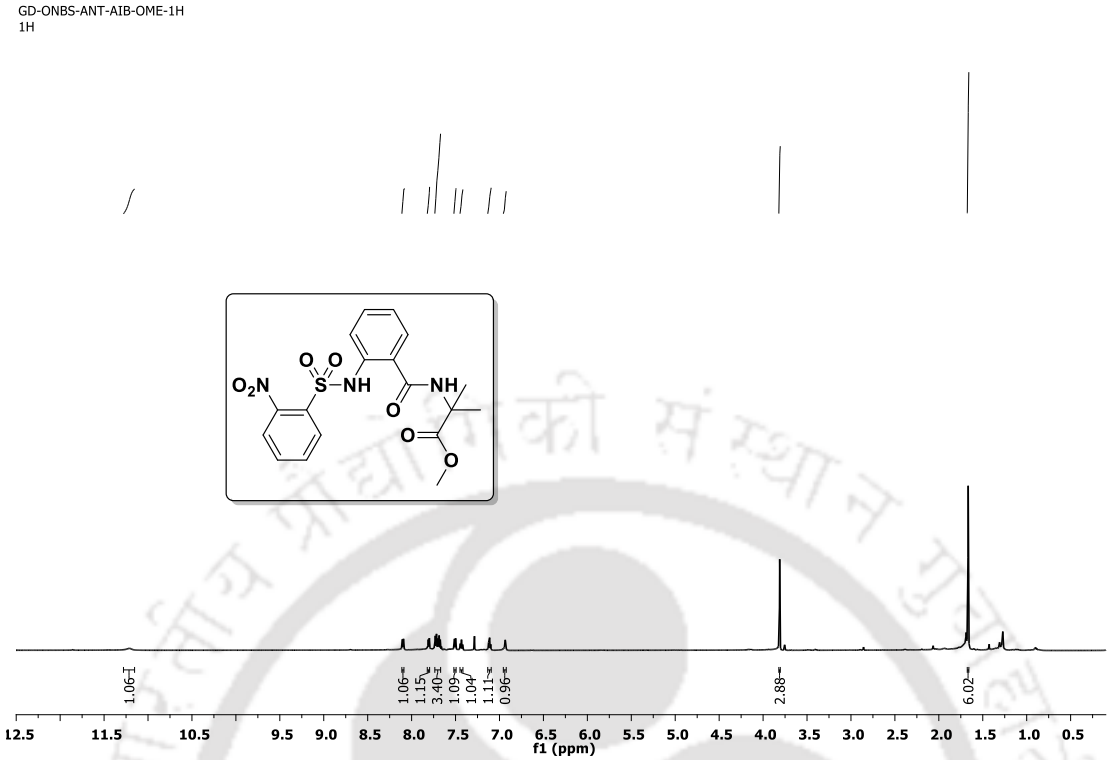

Figure 3.30. *^{1}H NMR spectra of peptide* ***o-NBS-Ant-Aib-OMe (Peptide 3C)***

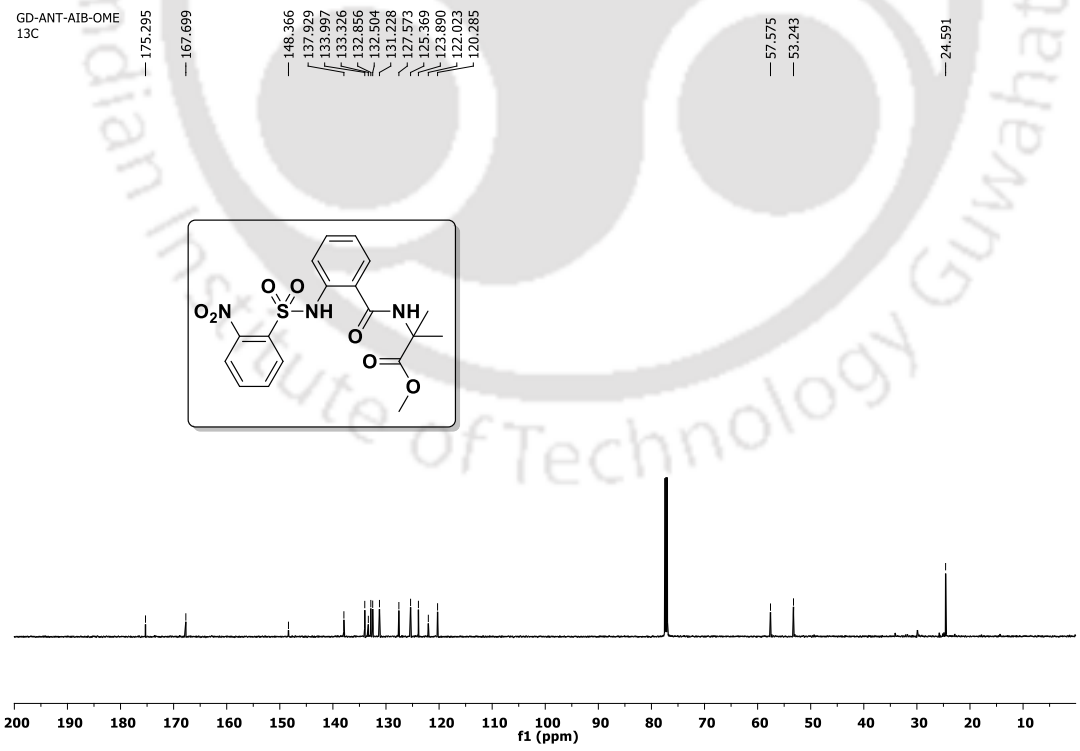

Figure 3.31. *^{13}C NMR spectra of peptide* ***o-NBS-Ant-Aib-OMe (Peptide 3C)***

3.15.4. Characterization spectra of peptide *p*-NBS-Ant-Aib-OMe (3D)

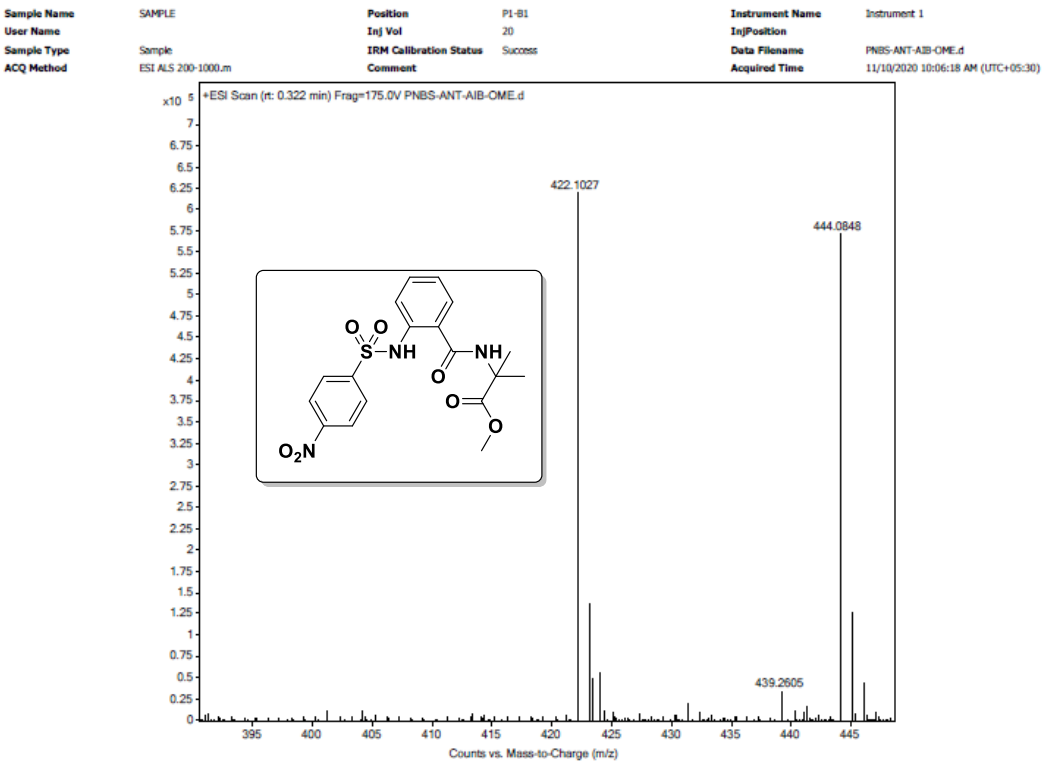

Figure 3.32. *MS spectra of peptide* ***p-NBS-Ant-Aib-OMe (Peptide 3D)***

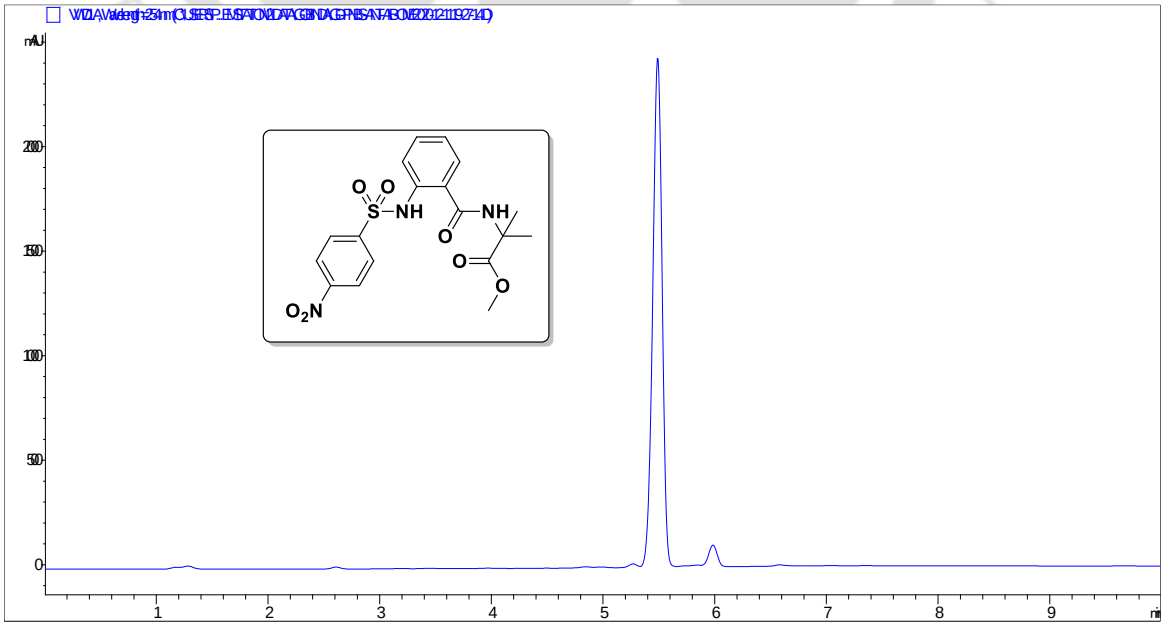

Figure 3.33. *HPLC profile picture of purified peptide* ***p-NBS-Ant-Aib-OMe (Peptide 3D)***

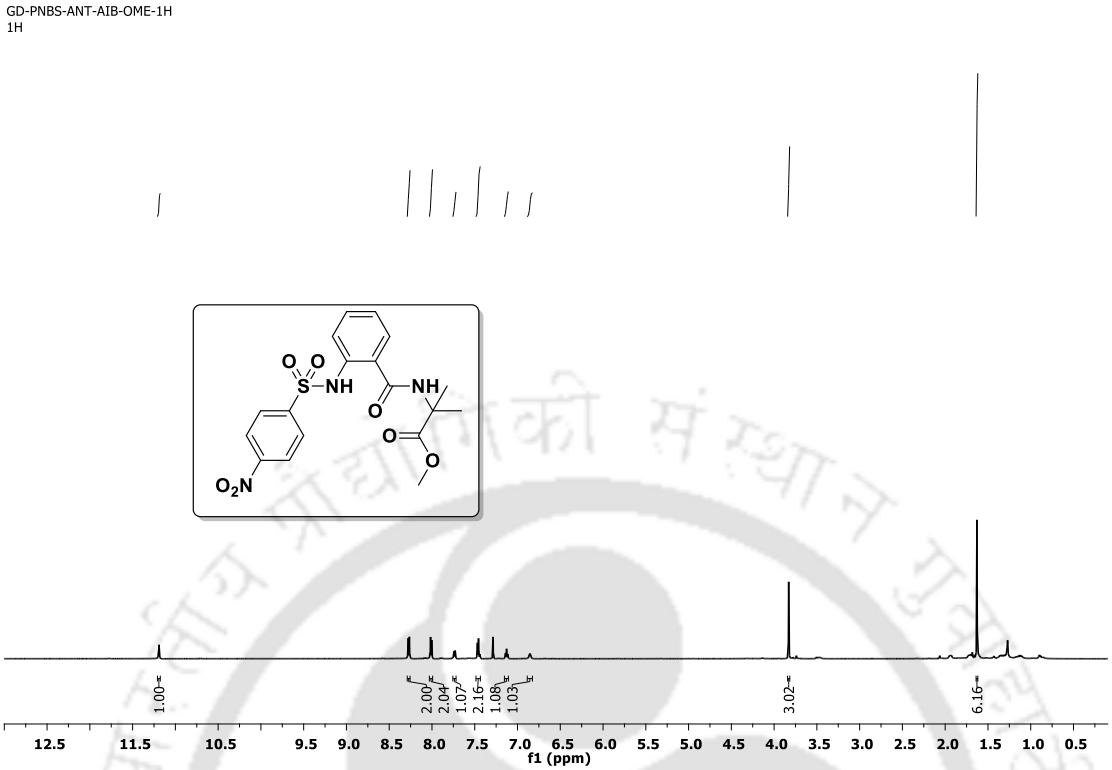

Figure 3.34. *^{1}H NMR spectra of peptide* ***p-NBS-Ant-Aib-OMe (Peptide 3D)***

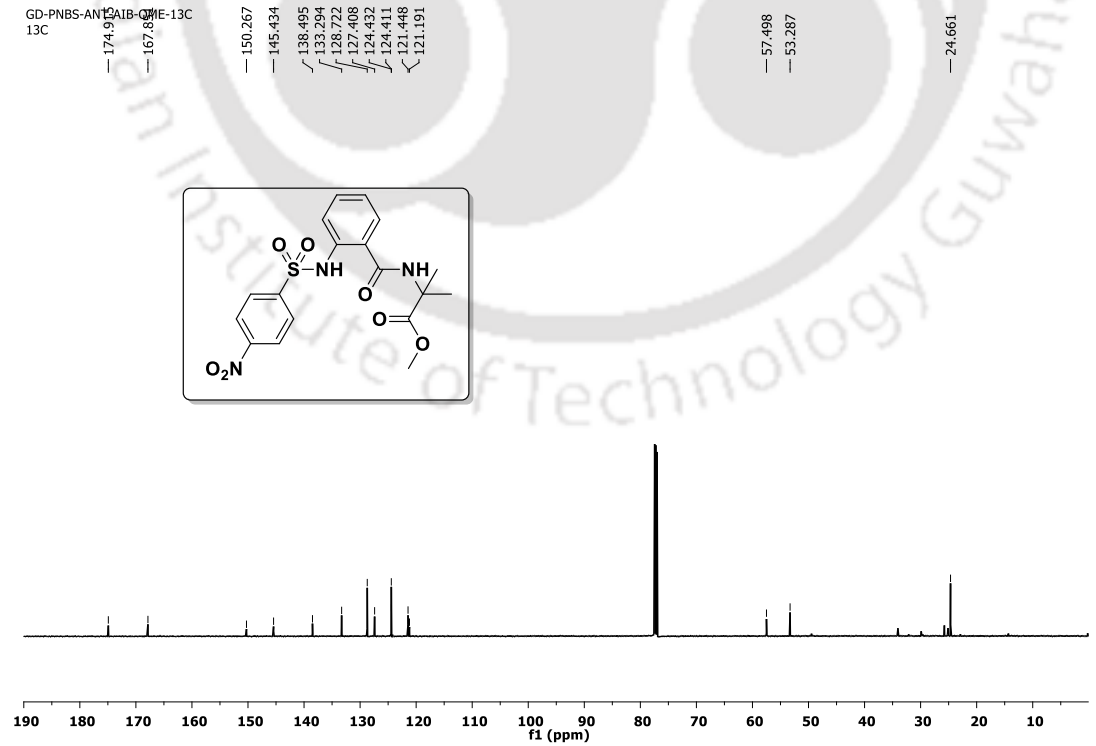

Figure 3.35. *^{13}C NMR spectra of peptide* ***p-NBS-Ant-Aib-OMe (Peptide 3D)***

3.16. Crystallographic data

Table 3.2. Selected back-bone torsion angles (°) of peptide **3A, 3B, 3C** and **3D**

peptide		ω_0	ω_1	ϕ_1	ϕ_2	ψ_1	ψ_2	θ_1
3A	N1-C5-O1-C2 = 178.7(3)	C6-N1-C5-O1 = 178.4(4)	C13-N2-C12-C11 = 177.7(3)	C11-C6-N1-C5 = -160.0(3)	C16-C13-N2-C12 = -49.6(4)	N2-C12-C11-C6 = 152.4(3)	O5-C16-C13-N2 = 136.2(3)	N1-C6-C11-C12 = 0.8(5)
3B	N1-C15-O1-C14 = 172.4(1)	C16-N1-C15-O1 = -175.0(1)	C23-N2-C22-C21 = 176.7(1)	C21-C16-N1-C15 = 145.2(2)	C26-C23-N2-C22 = 51.6(2)	N2-C22-C21-C16 = -141.5(2)	O5-C26-C23-N2 = 42.7(2)	N1-C16-C21-C22 = -0.0(2)
3C	N2-S1-C6-C1 = 87.1(4), N2-S1-C6-C5 = -93.6(3) N5-S2-C24-C29 = 81.9(4), N5-S2-C24-C23 = -101.6(3),	C7-N2-S1-C6 = 59.4 (3) C25-N5-S2-C24 = 60.9 (3)	C14-N3-C13-C12 = -175.6(3) C32-N6-C31-C30 = -177.2(3)	C12-C7-N2-S1 = -136.0(3) C30-C25-N5-S2 = -136.3(3)	C17-C14-N3-C13 = -52.0(5) C35-C32-N6-C31 = -50.4(4)	N3-C13-C12-C7 = 172.8(3) N6-C31-C30-C25 = 155.4(3)	O7-C17-C14-N3 = -44.1(5) O14-C35-C32-N6 = -39.5(4)	N2-C7-C12-C13 = -5.2(5) N5-C25-C30-C31 = -2.1(4)
3D	N2-S1-C4-C3 = -83.1(2)	C7-N2-S1-C4 = 54.9(2)	C14-N3-C13-C12 = 177.1(2)	C12-C7-N2-S1 = -108.0(2)	C17-C14-N3-C13 = -48.5(3)	N3-C13-C12-C7 = 162.0(2)	O7-C17-C14-N3 = 133.0(2)	N2-C7-C12-C13 = -4.2(3)

Table 3.3. Hydrogen bonding parameters of crystals of peptide **3A, 3B, 3C** and **3D**

Type	H…A(Å)	D...A(Å)	D-H...A(°)
Peptide 3A			
N1-H1...O3[a]	2.04	2.7086(6)	135
N2-H2...O2[b]	2.32	3.0750(7)	146
Peptide 3B			
N1-H1...O3[a]	2.17	2.773(3)	126
N2-H2...O3[c]	2.04	2.886(3)	166
Peptide 3C			
N2-H2...O5[a]	2.688	2.586(4)	73.9
N3-H3...O3[d]	2.42	3.2615(4)	167
N5-H5...O12[a]	2.680	2.631(3)	77.4
N6-H6...O11[e]	2.24	3.0744(4)	163
Peptide 3D			
N2-H2...O5[a]	2.468	2.656(3)	93
N2-H2...O3[d]	2.36	2.9745(1)	128

Symmetry elements: [a]x, y, z; [b]1-x, 1-y, 1-z; [c]x, 3/2-y, -1/2+z; [d]x, y,-1+z; [e]1+x, y, z

Table 3.4. Crystallographic refinement details for Peptide **3A**, **3B**, **3C** and **3D**

Parameters	**Boc-Ant-Aib-OMe (3A)**	**Fmoc-Ant-Aib-OMe (3B)**	***o*-NBS-Ant-Aib-OMe (3C)**	***p*-NBS-Ant-Aib-OMe (3D)**
Formula	C_{17} H_{24} N_2 O_5	C_{27} H_{26} N_2 O_5	C_{18} H_{19} N_3 O_7S	C_{18} H_{19} N_3 O_7S
Fw	336.38	458.51	421.42	421.42
Crystal system	Monoclinic	Monoclinic	Monoclinic	Monoclinic
Space group	*P 21/n*	*P2(1)/c*	*P 21/n*	*P2(1)/c*
a/Å	9.2576(7)	25.17(2)	8.4692(9)	10.3327(5)
b/Å	8.9629(6)	10.270(9)	54.328(7)	27.0894(13)
c/Å	21.703(5)	9.635(9)	8.7904(8)	6.9917(3)
α/°	90.00	90.00	90.00	90.00
β/°	93.775(12)	96.43(3)	94.735(3)	94.541(2)
γ/°	90.00	90.00	90.00	90.00
V/Å^3	1796.9(5)	2475(4)	4030.8(8)	1950.88(16)
Z	4	4	8	4
D_c/g cm^{-3}	1.243	1.230	1.389	1.435
μ Mo K_α/mm^{-1}	0.092	0.085	0.206	0.213
F000	720.0	904	1760	736
T/K	293(2)	296(2)	296(2)	296(2)
θ max.	28.853	26.20	25.00	26.16
Total no. of reflections	6837	41851	42276	23150
Independent reflections	3997	4344	4386	2652
Observed reflections	1872	3407	6774	3450
Parameters refined	223	310	529	265
R_1, I > 2σ(I)	0.0946	0.0412	0.0652	0.0450
wR_2, I > 2σ(I)	0.2394	0.1300	0.1521	0.1394
GOF (F^2)	0.988	1.041	1.019	1.060
CCDC No.	2068403	2068307	2068401	2068402

Chapter 4

The differences in the self-assembly pattern of enantiomeric and reverse sequences of Ant and Phg containing dipeptide analogs

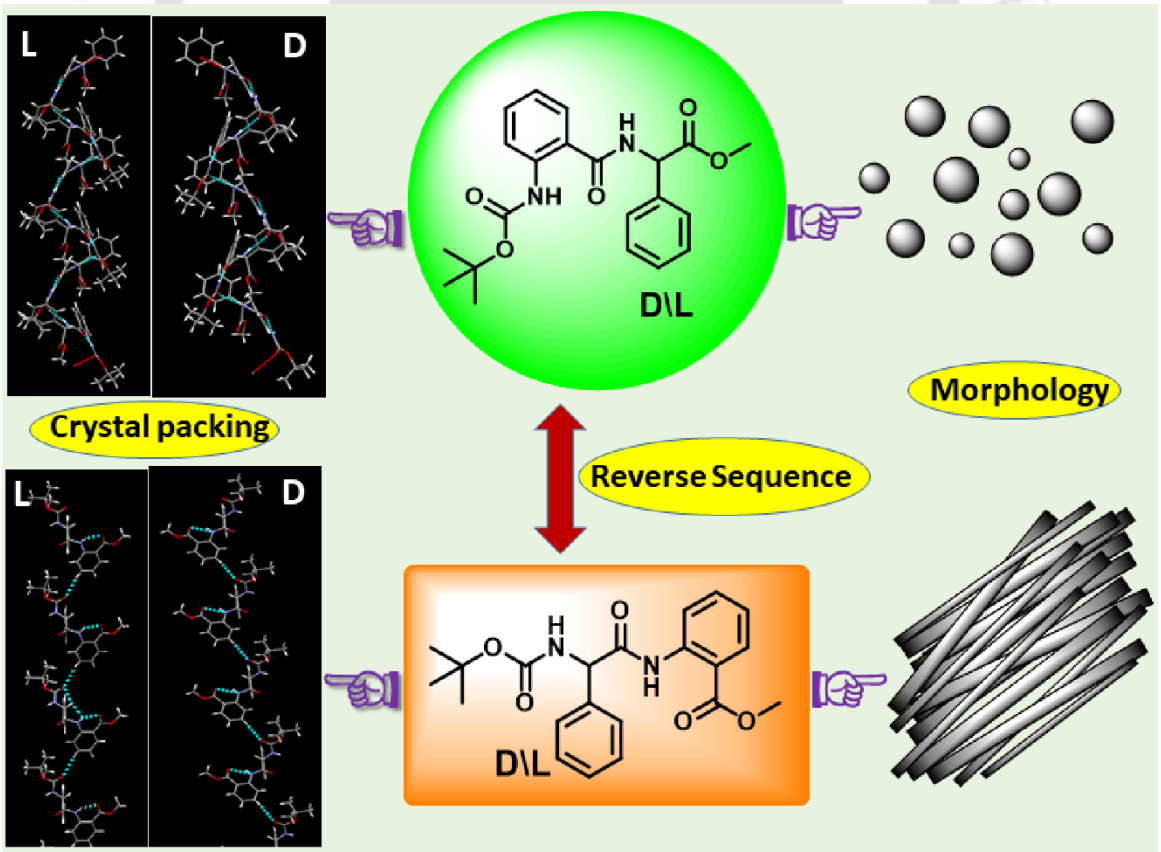

4.1. Background

In chapter 3, we demonstrated the self-assembly and morphological diversity of Ant-Aib peptides depending on various N-terminal protecting groups. Non-proteinogenic amino acid phenyl glycine (Phg) impacts the physical properties, structural diversity, and reactivity of peptides because of the steric and electronic features of the aromatic ring.[1] Moreover, insertion of D-amino acid in the peptide chain increases enzymatic stability, therapeutic effect, and antimicrobial activity.[2] Mostly isomeric peptides, generated by reversing the sequence, form similar morphology.[3,4] In this context, significantly less literature is available on diversity in the morphology of isomeric peptides.[5,6] Herein, we designed enantiomeric and reverse peptides and studied their morphology and conformation in solid and solution states.

4.2. Design of peptides

Conformationally rigid, unnatural amino acids, peptides made up of them, and reverse peptides play an essential role in the self-assembly process by creating various novel nanostructures. By this inspiration, we have designed Ant and (L/D)-Phg containing four N, C- terminal protected dipeptides such as Boc-Ant-L-Phg-OMe (**4A**), Boc-Ant-D-Phg-OMe (**4B**) and their corresponding reverse peptide sequences Boc-L-Phg-Ant-OMe (**4C**) and Boc-D-Phg-Ant-OMe (**4D**), respectively (Figure 4.1).

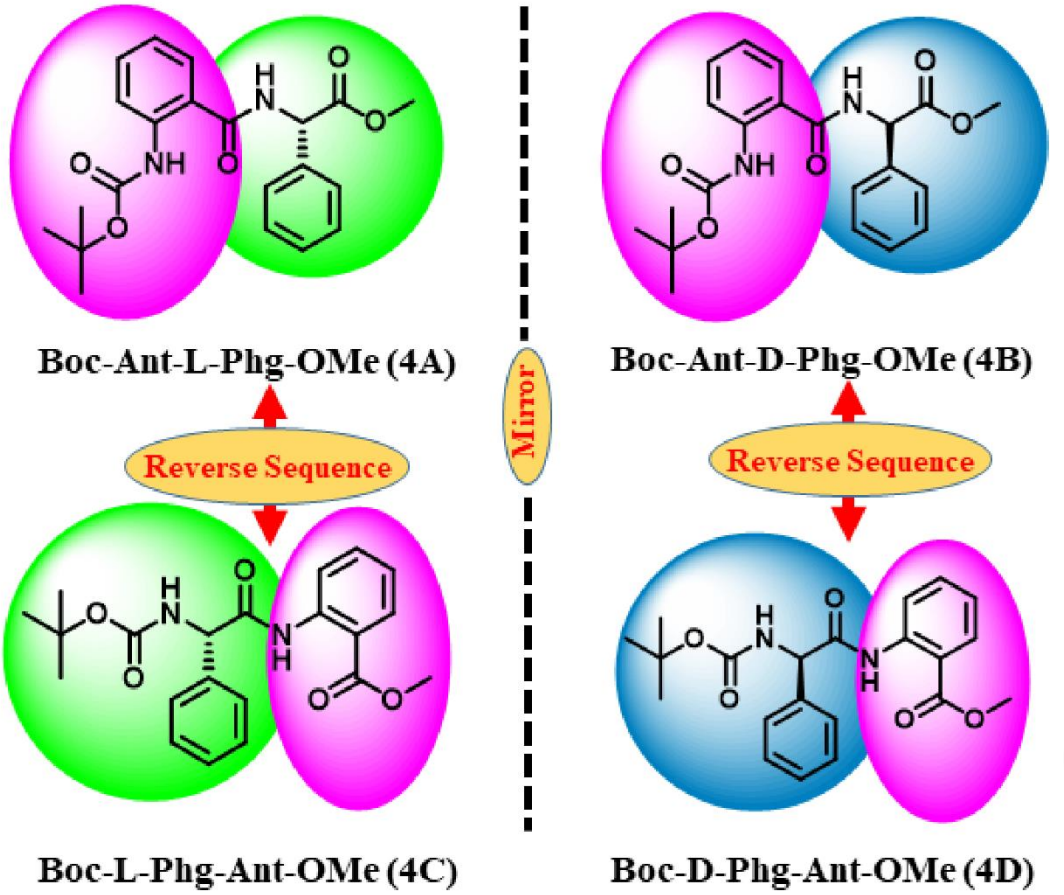

Figure 4.1. *Chemical structures of peptides*

4.3. Synthesis and characterization of the designed peptides

At first, designed N-terminal Boc- and C-terminal methyl ester (OMe) protected di-peptides were synthesized using the standard peptide synthesis method (Scheme 4.1 and 4.2). After synthesis, all peptides were purified by column chromatography. Peptides were characterized by NMR spectroscopy and mass spectrometry. The purity of the peptides were examined by reverse-phase HPLC.

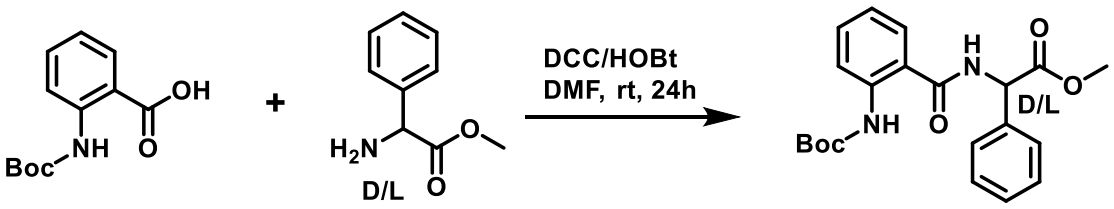

Scheme 4.1. *Schematic presentation of synthesis of di-peptide* ***4A*** *and* ***4B***

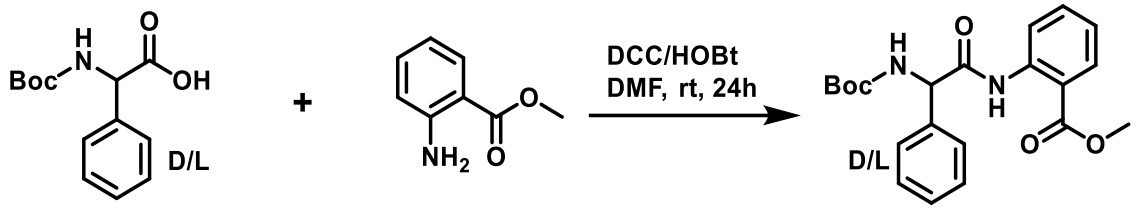

Scheme 4.2. *Schematic presentation of synthesis of di-peptide* ***4C*** *and* ***4D***

4.4. Morphology study

Next, we carried out optical microscopy, FESEM, and FETEM studies to check the morphology of designed di-peptides. For optical microscopy and FESEM study, freshly prepared 1.5 mM methanolic solution of each peptide was drop-casted on clean microscopic glass and Al-foil wrapping glass. After drying of samples, we analyzed the morphology. The obtained morphologies exhibited that **4A** and **4B** created spherical (diameter ~1.6 μm and ~3.0 μm, respectively) structures. On the other hand, **4C** and **4D** generated a well-organized nano rod-like fiber structure, which diameter varies several nm size and various μm long. Moreover, for FETEM study, 1.5 mM of each peptide solution was diluted to 300 μM, and after the sample preparation, images were captured. The acquired data indicated that the sphere-like structure was vesicles (diameter ~240 nm for **4A** and ~300 nm for **4B**). Therefore, the obtained data manifested that the enantiomeric peptides (**4A**, **4B**) and (**4C**, **4D**) display identical morphology, whereas reverse peptides sequence (**4A**, **4C**) and (**4B**, **4D**) exhibit distinguishable dissimilar morphology (Figure 4.2).

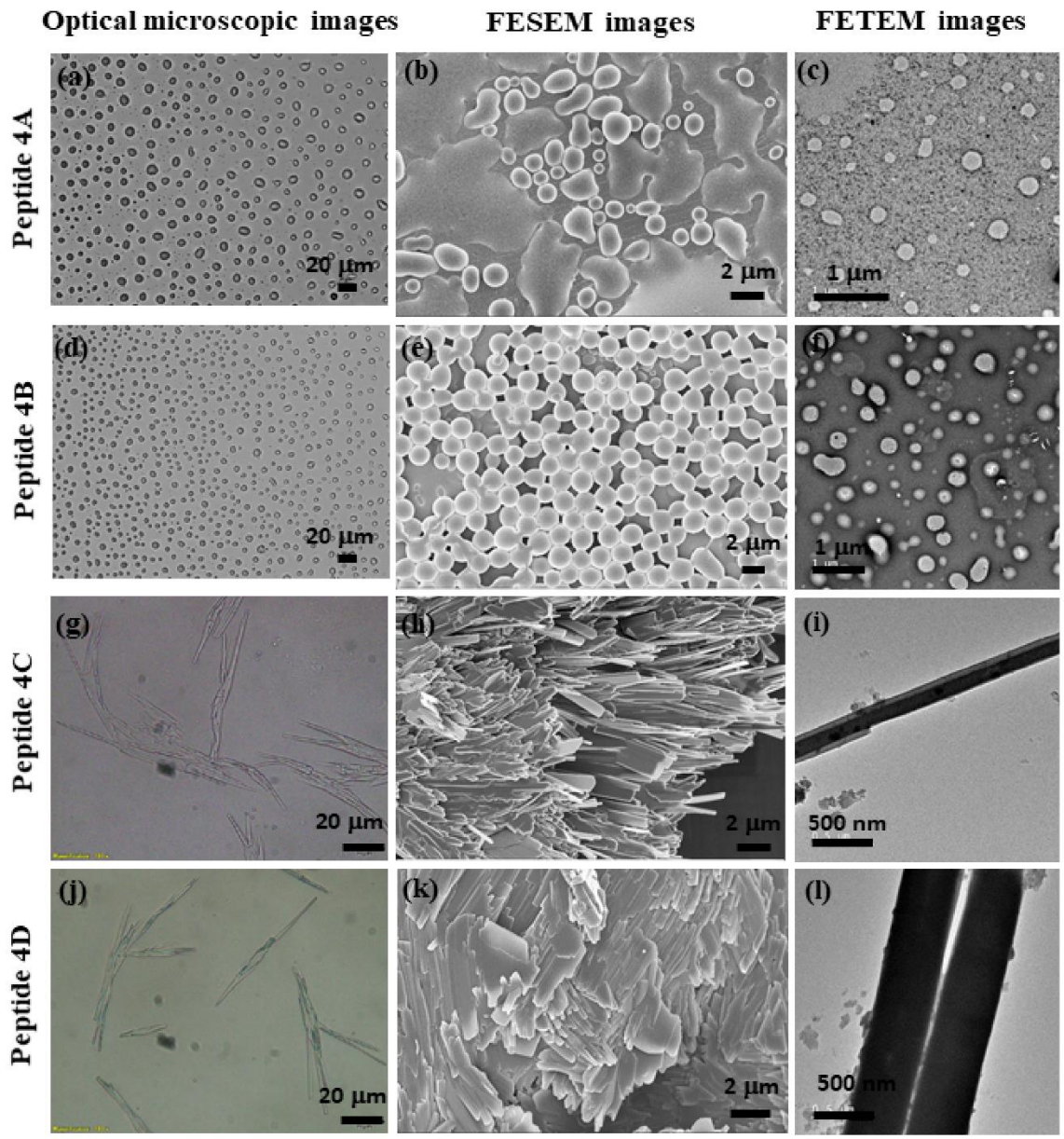

Figure 4.2. *(a, d, g, j) represents optical microscopy image (concentration 1.5 mM), (b, e, h, k) displays FESEM image (concentration 1.5 mM), and (c, f, i, l) exhibits FETEM image (concentration 300 µM), of peptide* ***4A****,* ***4B****,* ***4C*** *and* ***4D*** *respectively, in methanol.*

Next, we performed atomic force microscopy (AFM) to obtain topographical knowledge. For AFM study, 1.5 mM of each peptide solution was diluted to 60 µM, and after sample preparation, images were recorded. The AFM images also mentioned the formation of similar morphology like FESEM and FETEM. **4A** and **4B** created spherical morphology, **4C** and **4D** generated rod-like fiber structures (Fig. 4.3).

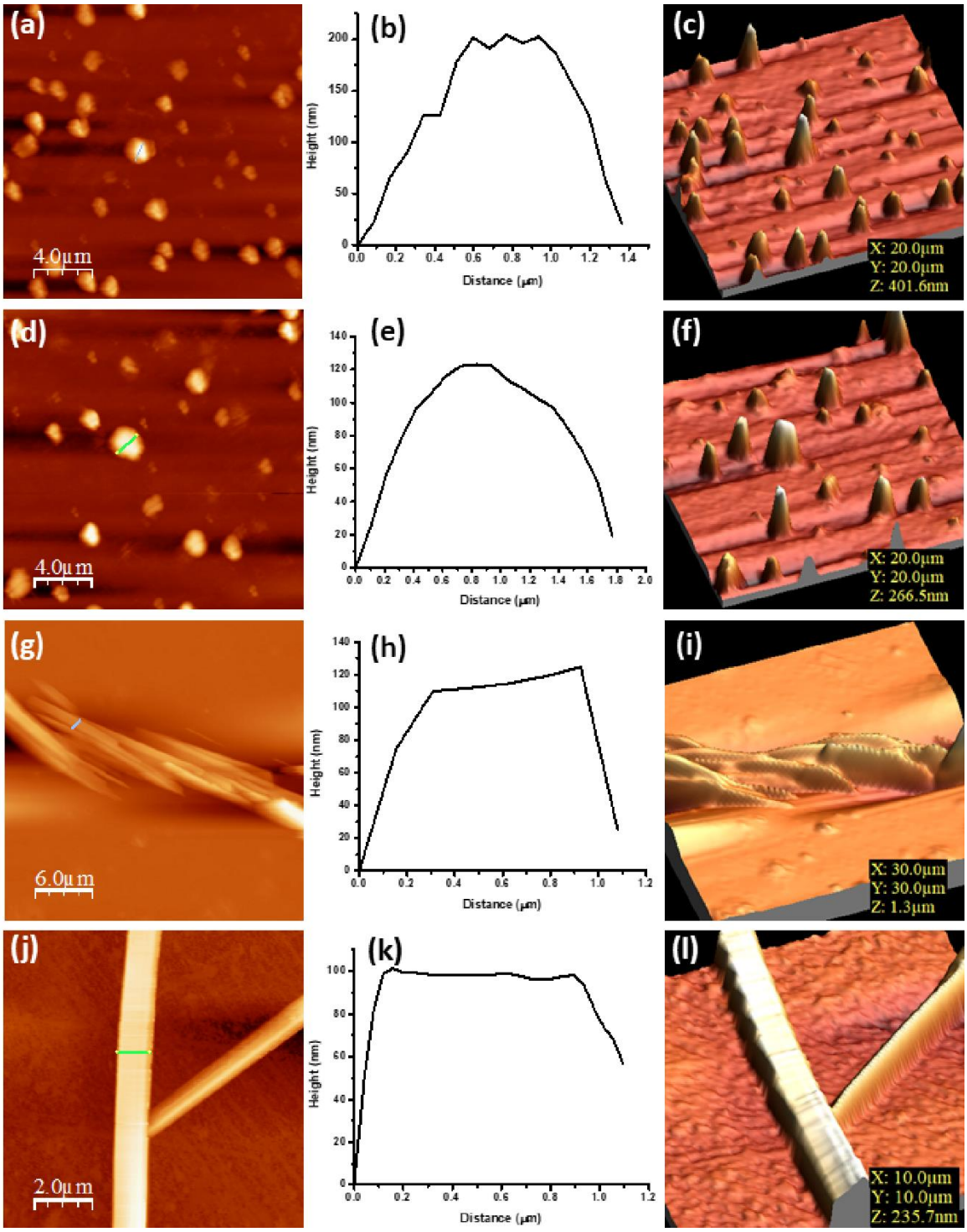

Figure 4.3. *(a, d, g, j) 2D AFM images, (b, e, h, k) height profile plots, and (c, f, i, l) 3D AFM images of dipeptides* ***4A, 4B, 4C,*** *and* ***4D,*** *respectively, with 60 µM each in MeOH.*

4.5. Conformational analysis by FT-IR:

Initially, we studied FT-IR to understand the conformational similarity and dissimilarity of designed peptides in solid-state. The FT-IR stretching frequency for amide I, amide II (bending), and hydrogen-bonded urethane groups varies between 1800-1500 cm^{-1}.[7] Moreover, another significant FT-IR band for N-H bond vibration of a peptide remains 3500-3200 cm^{-1} region.[8] In the present study, peptides **4A**, **4B**, **4C**, and **4D** exhibited intense FT-IR stretching frequency at 3315 cm^{-1}, 3315 cm^{-1}, 3319 cm^{-1}, and 3359 cm^{-1}, respectively, suggesting the presence of strongly H-bonded N-Hs. Therefore, each peptide subunit remains in strongly intermolecular/intramolecular hydrogen bonding in the solid-state. Furthermore, the absence of FT-IR band 3430-3440 cm^{-1} region indicates all -NH groups involved in hydrogen bonding in the peptide. Another, informative FT-IR band (1752 cm^{-1}, 1701 cm^{-1}, 1640 cm^{-1}, 1585 cm^{-1} and 1509 cm^{-1}) for peptide **4A**, (1750 cm^{-1}, 1702 cm^{-1}, 1640 cm^{-1}, 1585 cm^{-1} and 1514 cm^{-1}) for peptide **4B**, (1684 cm^{-1}, 1604 cm^{-1} and 1522 cm^{-1}) for peptide **4C** and (1690 cm^{-1}, 1590 cm^{-1} and 1510 cm^{-1}) for peptide **4D** were noticed for designed peptides. The above results suggest that enantiomeric peptides sequences (**4A**, **4B**) and (**4C**, **4D**) display an almost identical FT-IR band. However, reverse peptide sequences such as (**4A**, **4C**) and (**4B**, **4D**) contain different FT-IR bands. Hence, enantiomeric peptides generated similar conformations, whereas the reverse peptides formed different conformations (Figure 4.4).

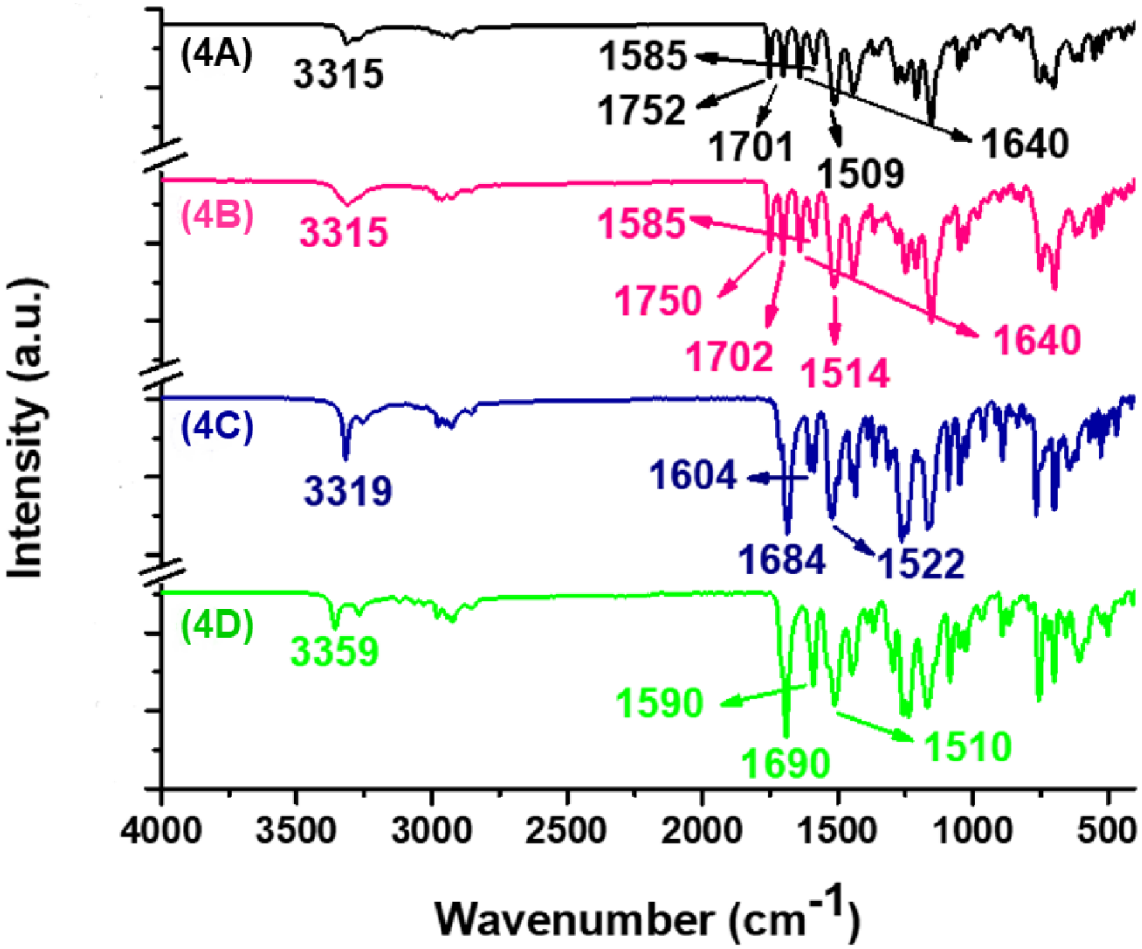

Figure 4.4. *FT-IR spectrum of designed di-peptide* ***4A****,* ***4B****,* ***4C,*** *and* ***4D,*** *respectively, in solid-state.*

4.6. Solid-state molecular arrangement by SC-XRD:

Next, to acquire the atomic-level information, we performed SC-XRD technique. The suitable single crystals of **4A**, **4B**, **4C,** and **4D** were obtained by slow evaporation of methanol-water solvent at room temperature. Each peptide contains a single molecule in a corresponding asymmetric unit.

In a crystalline state, peptides 4A and 4B crystallized in a monoclinic crystal system. Each subunit of **4A** and **4B** was interconnected by intramolecular H-bonding between NH and C=O group of Ant (N1-H1···O3, 2.00 Å, 2.69 Å, 137º) (Figure 4.5b). This intramolecular H-bonding interaction attains the rigid conformation of the di-peptides. The dimeric structure of dipeptides Boc-Ant-L/D-Phg-OMe (**4A** and **4B)** interlinked via

intermolecular H-bonding interaction between NH (Phg) and C=O (urethane) (N2-H2···O2, 2.16 Å, 3.00 Å, 169°) and one another weak H-bonding interaction between C=O (Phg) and CH (aromatic ring of Ant) (C9-H9···O4, 2.53 Å, 3.24 Å, 133°) (Figure 4.5c). Moreover, by using intermolecular H-bonding interaction, these two peptides created a helical arrangement (Figure 4.5d) and anti-parallel β-sheet-like arrangement along the *b*-axis, respectively (Figure 4.5e).

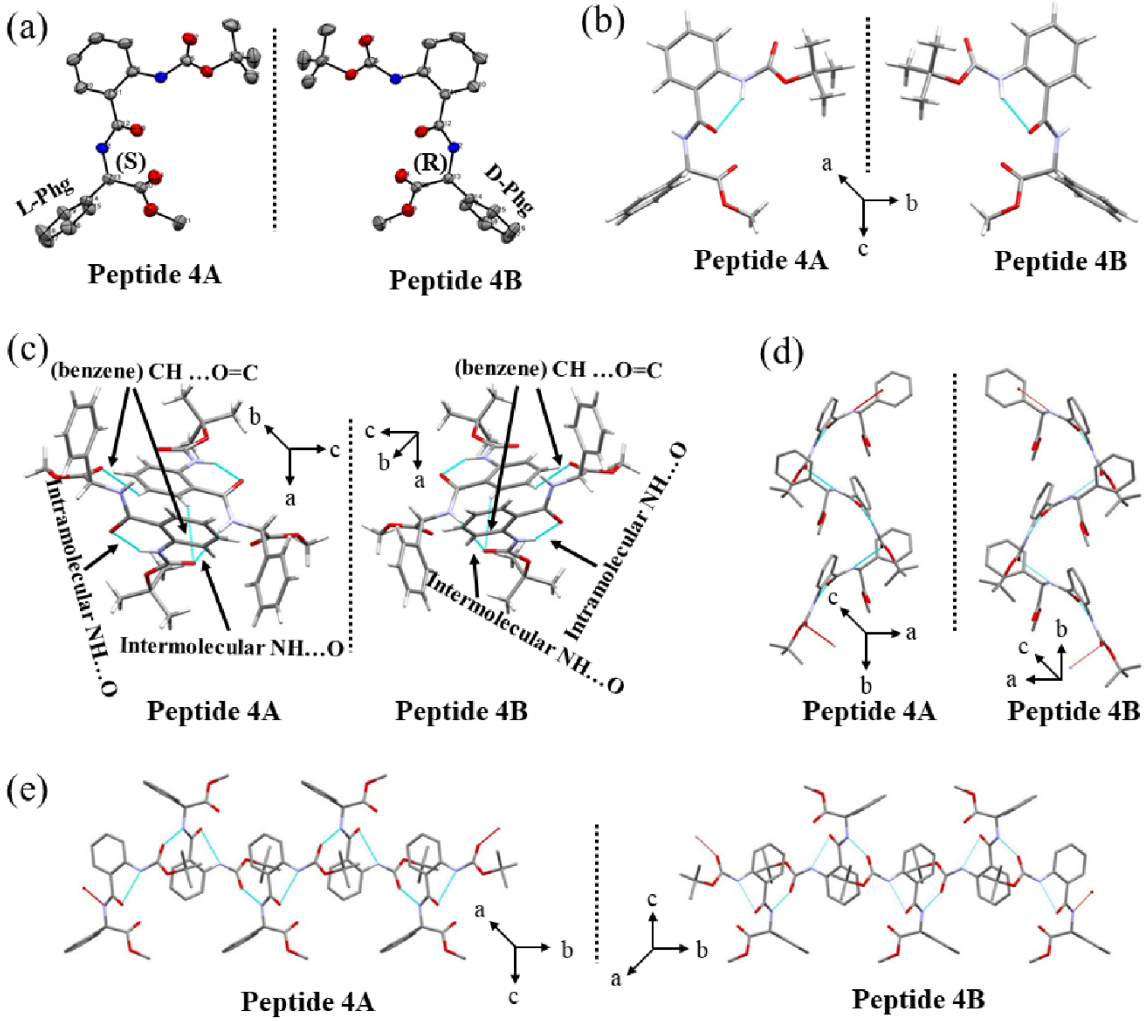

Figure 4.5. *(a) The ORTEP profile (ellipsoid of probability 30%), (b) Intramolecular hydrogen bonding arrangement, (c) peptide dimer by various noncovalent interactions, (d) helical like arrangement, and (e) anti-parallel β-sheet-like structure of two enantiomeric peptides Boc-Ant-L-Phg-OMe (**4A**) and its Boc-Ant-D-Phg-OMe (**4B**), respectively.*

Interestingly, peptides **4A** and **4B** displayed helix-like diverse supramolecular arrangement, which interconnected through H-bonding interaction along the *b*-direction (Figure 4.6a, 4.6b). Furthermore, in higher-order supramolecular packing, both peptides formed β-sheet-like layer structure, which interlinked through H-bonding and non-covalent interaction along *a*-direction (Fig. 4.6c, 4.6d). This kind of supramolecular layer structure may be responsible for generation of vesicular morphology.

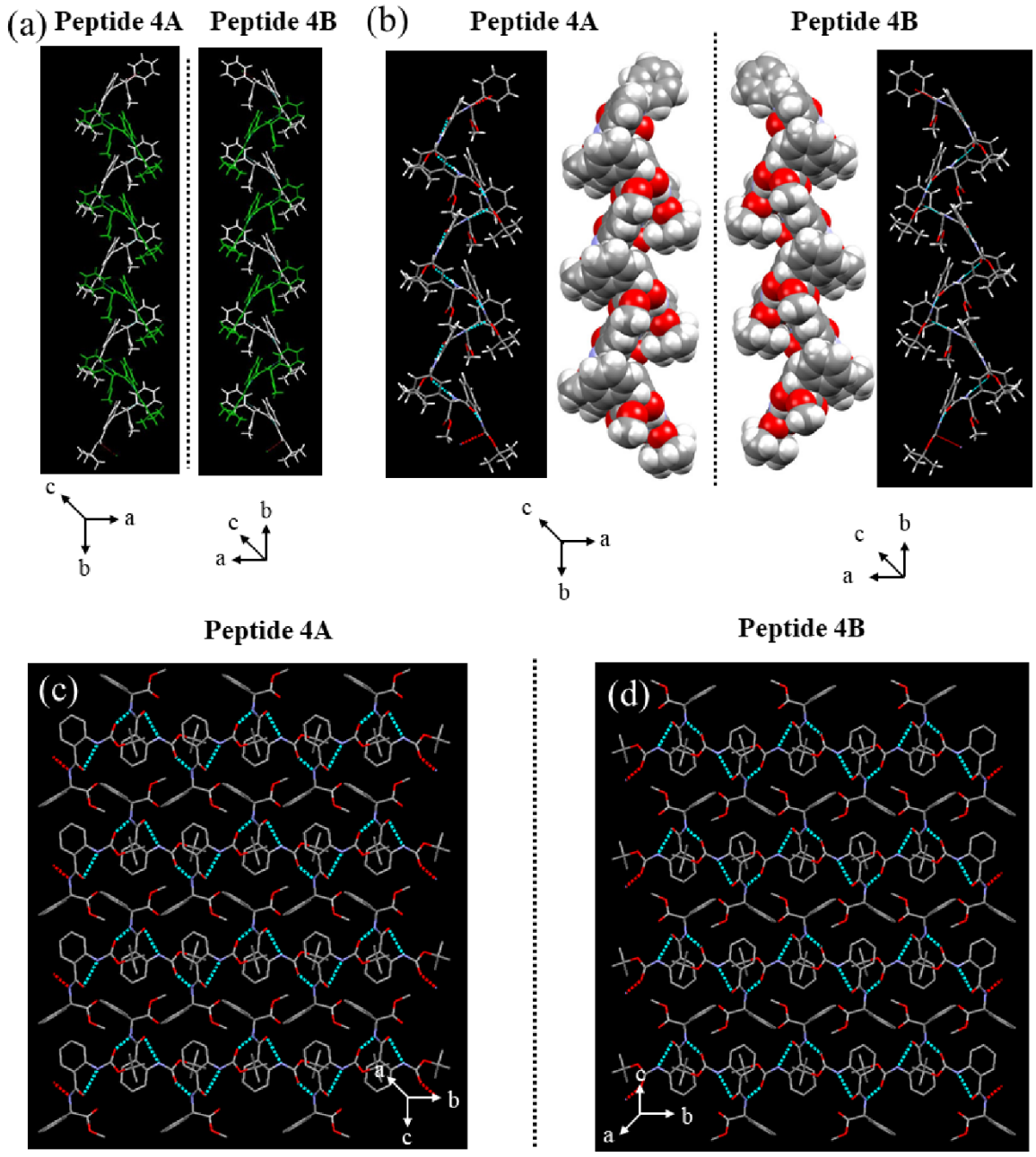

Figure 4.6. *(a, b) represents helix-like architecture, and (c, d) indicates β-sheet-like layer architecture of* ***4A*** *and* ***4B****, respectively.*

The reverse peptides sequence of **4A** and **4B**, such as **4C** and **4D**, their subunit interconnected through six-membered intramolecular H-bonding interaction between Ant NH and C=O group (N2-H2···O4, 1.98 Å, 2.66 Å, 135°) (Figure 4.7b). **4C** and **4D** crystallized in a triclinic crystal system, different from **4A** and **4B**. Both peptides displayed two different dimeric structures. One kind of dimeric structure stabilized via two intermolecular H-bonding interactions between C=O and NH group of Phg of two subunits (N1-H1···O3, 2.03 Å, 2.89 Å, 173°). Another kind of dimeric structure interconnected through π-π stacking interaction of aromatic moiety of Phg (4.31 Å), week H-bonding interaction between CH of the aromatic ring of Phg and C=O of the Ant (C9-H9···O4, 2.46 Å, 3.32 Å, 159°) and intramolecular H-bond (Figure 4.7c and 4.7d). These two dimeric structures stabilized supramolecular staircase-like architecture along the *c*-axis (Figure 4.7e).

Interestingly, a different single helical arrangement was created through C-H···O interaction along the *a*-axis (Figure 4.8a). Moreover, a supramolecular zigzag helical arrangement formation by aromatic π-π stacking, hydrogen bonding, and noncovalent interaction was noticed along *b*-axis (Figure 4.8b). Furthermore, supramolecular sheet-like layer structures (Figure 4.8c) and molecular channels (Figure 4.8d) structure were stabilized using the before-mentioned interactions for peptides **4C** and **4D**. This kind of molecular channel architecture may be responsible for creating rod-like fiber morphology.

The obtained backbone torsion angles (°), hydrogen bonding distance of crystals and crystallographic refinement details of peptide **4A, 4B, 4C,** and **4D** were listed in Table 4.2, 4.3 and 4.4, respectively.

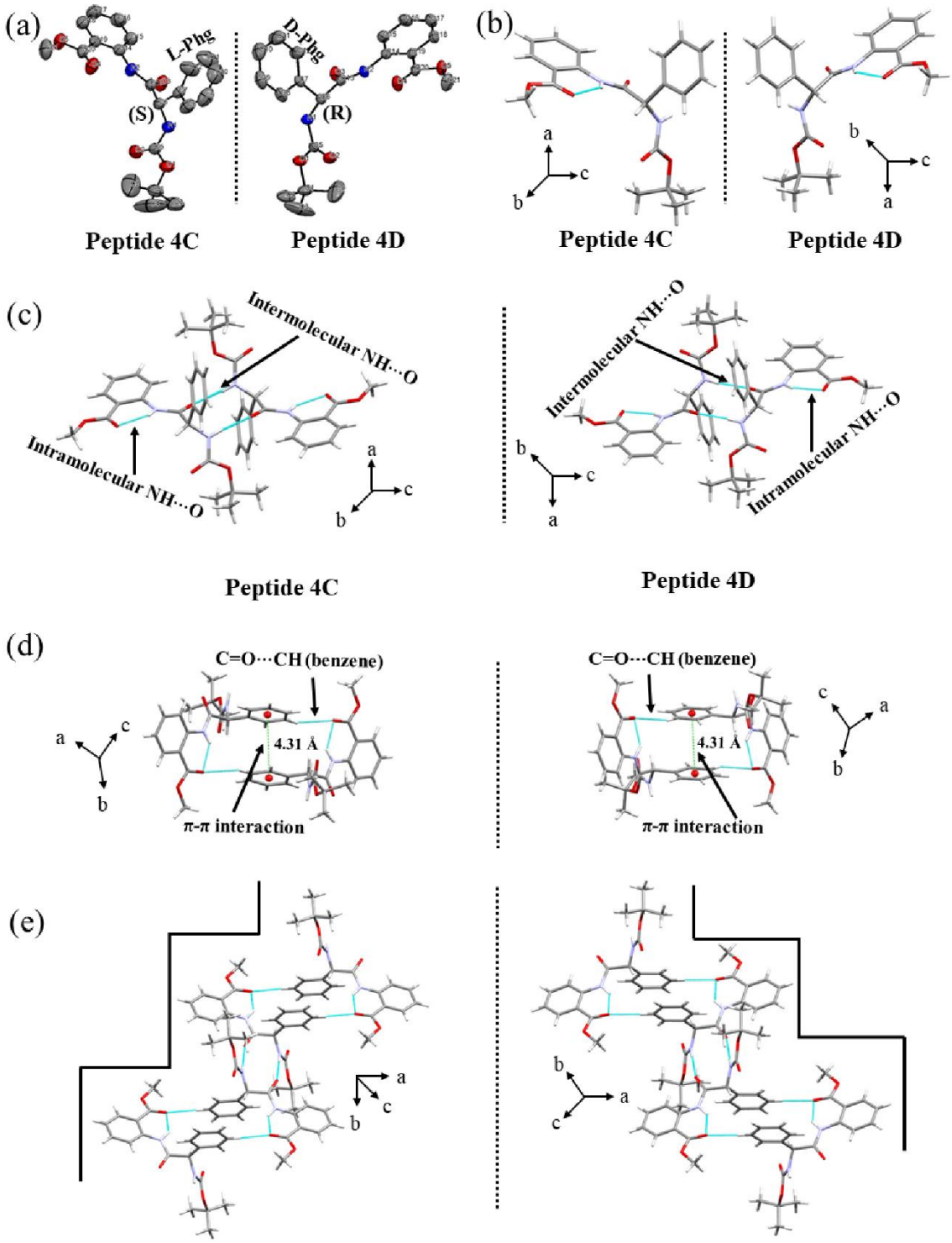

Figure 4.7. *(a) The ORTEP profile (ellipsoid of probability 30%), (b) Intramolecular H-bonding arrangement, (c) peptide dimer formation by intermolecular hydrogen bonding, (d) peptide dimer formation by π-π stacking (e) staircase-like architecture via hydrogen bonding and aromatic π-π stacking interaction of peptide* ***4C*** *and* ***4D*** *respectively.*

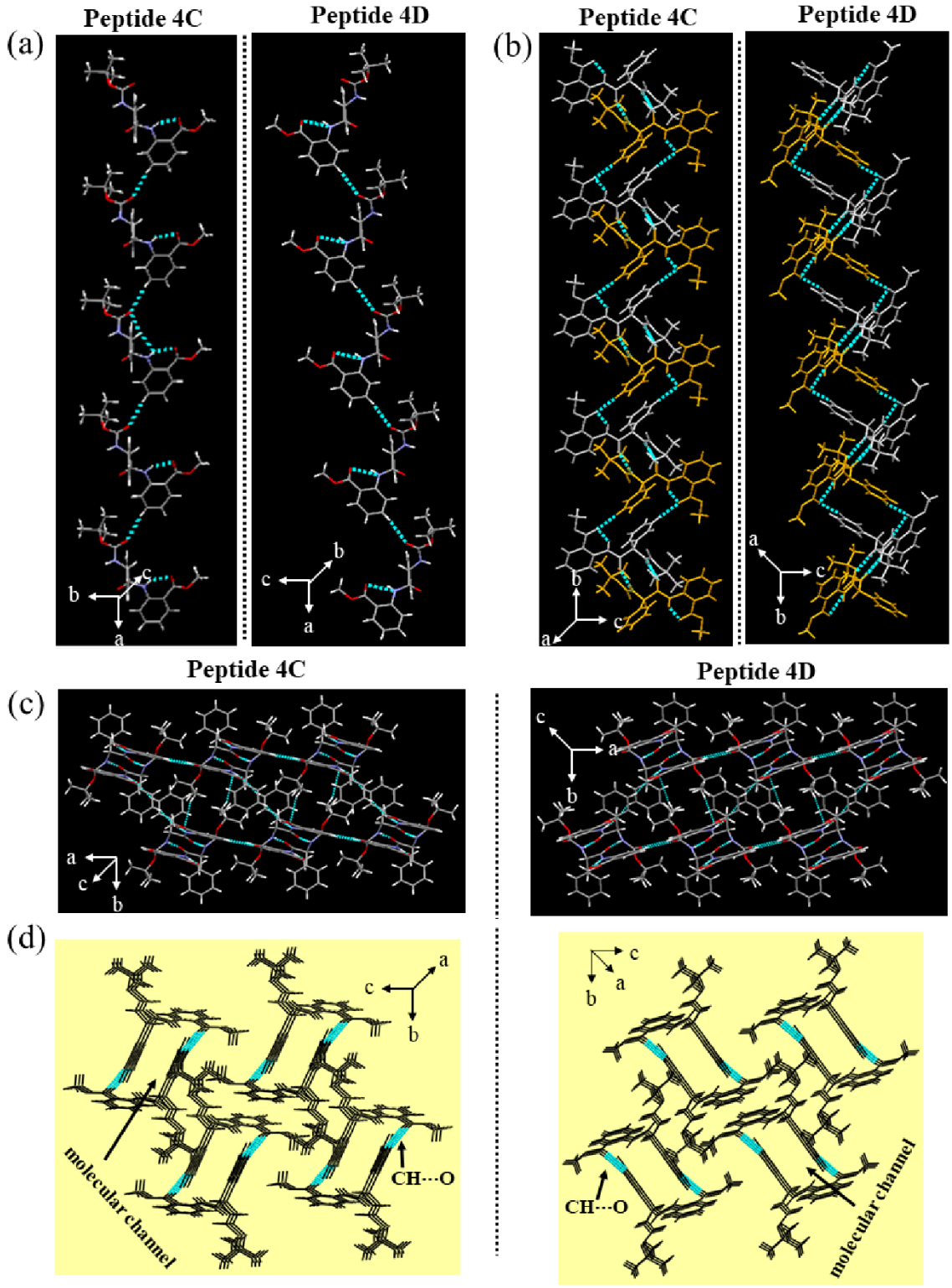

Figure 4.8. *(a) Single helical structure, (b) Zigzag helical arrangement, (c) Sheet-like layer structure, and (d) Molecular channel formation (other molecules and interactions are omitted for clear visualization) by* ***4C*** *and* ***4D,*** *respectively.*

4.7. NMR titration

Non-covalent interaction, especially hydrogen bonding, plays a vital role in peptide secondary conformation and self-assembled supramolecular structure formation. Using solvent ^{1}H-NMR titration study, we can understand different kinds of H-bonding (intramolecular and intermolecular) interaction in the peptide. Solvent ^{1}H-NMR titration was performed by adding d_6-DMSO (a suitable hydrogen bond acceptor) to the peptide solution in $CDCl_3$. In general, the chemical shift of intramolecular H-bonded protons remains unchanged, while intermolecular H-bonded protons displayed characteristic downfield shift with the addition of d_6-DMSO.[9] In the case of all designed peptides, NH of Ant remains unchanged with the increasing volume of d_6-DMSO, indicating these protons are involved in intramolecular H-bonding (Figure 4.9a-b, 4.10a-b Figure 4.29-4.32). The crystal structure of these peptides suggested that NH of Ant involves in intramolecular H-bond formation (Figure 4.5b, 4.7b). Moreover, NH of Phg (peptide **4A** and **4B**) exhibits a significant downfield shift with the addition of d_6-DMSO, indicating these proton involves in intermolecular bonding (Figure 4.9a, 4.10a Figure 4.29-4.30). Crystal structure suggests that this proton involves in intermolecular H-bonding (Figure 4.5c). Interestingly, NH of Phg (peptide **4C** and **4D**) display significantly less downfield shift or remain unchanged with the addition of d_6-DMSO, suggesting these protons take part in intramolecular H-bonding interaction (Figure 4.9b, 4.10b Figure 4.31-4.32). Although, crystal structure indicates these NH are participating in intermolecular H-bonding (Figure 4.7c). This interesting observation for **4C** and **4D** may be due to the formation of a stable ten membered dimeric structure in an antiparallel manner in solid-state (Figure 4.7c), and their H-bonding distance very close to like intramolecular H-bond (Table 4.3). Therefore, enantiomeric peptides, i.e., (**4A**, **4B**) and (**4C**, **4D**) displayed similar proton shifts, but their reverse sequence (**4A**, **4C**) and (**4B**, **4D**) exhibited remarkably different proton shifts in solution (Figure 4.9a-b and 4.10a-b).

Chemical shifts of all hydrogen-bonded protons with the addition d_6-DMSO are listed in Table 4.1.

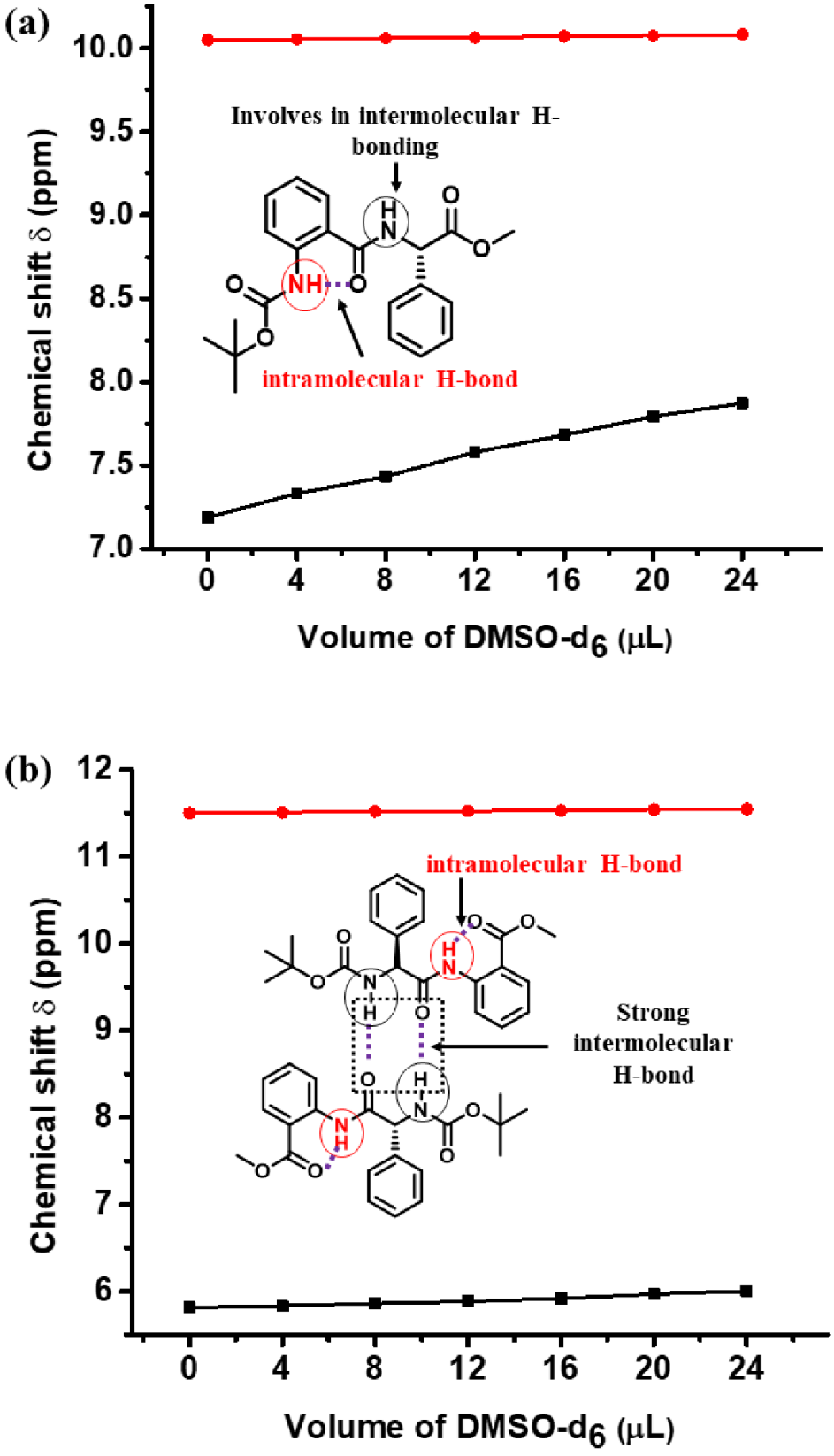

Figure 4.9. *(a, b) Represents solvent-dependent ^{1}H-NMR titration of peptides* ***4A*** *and* ***4C****, respectively.*

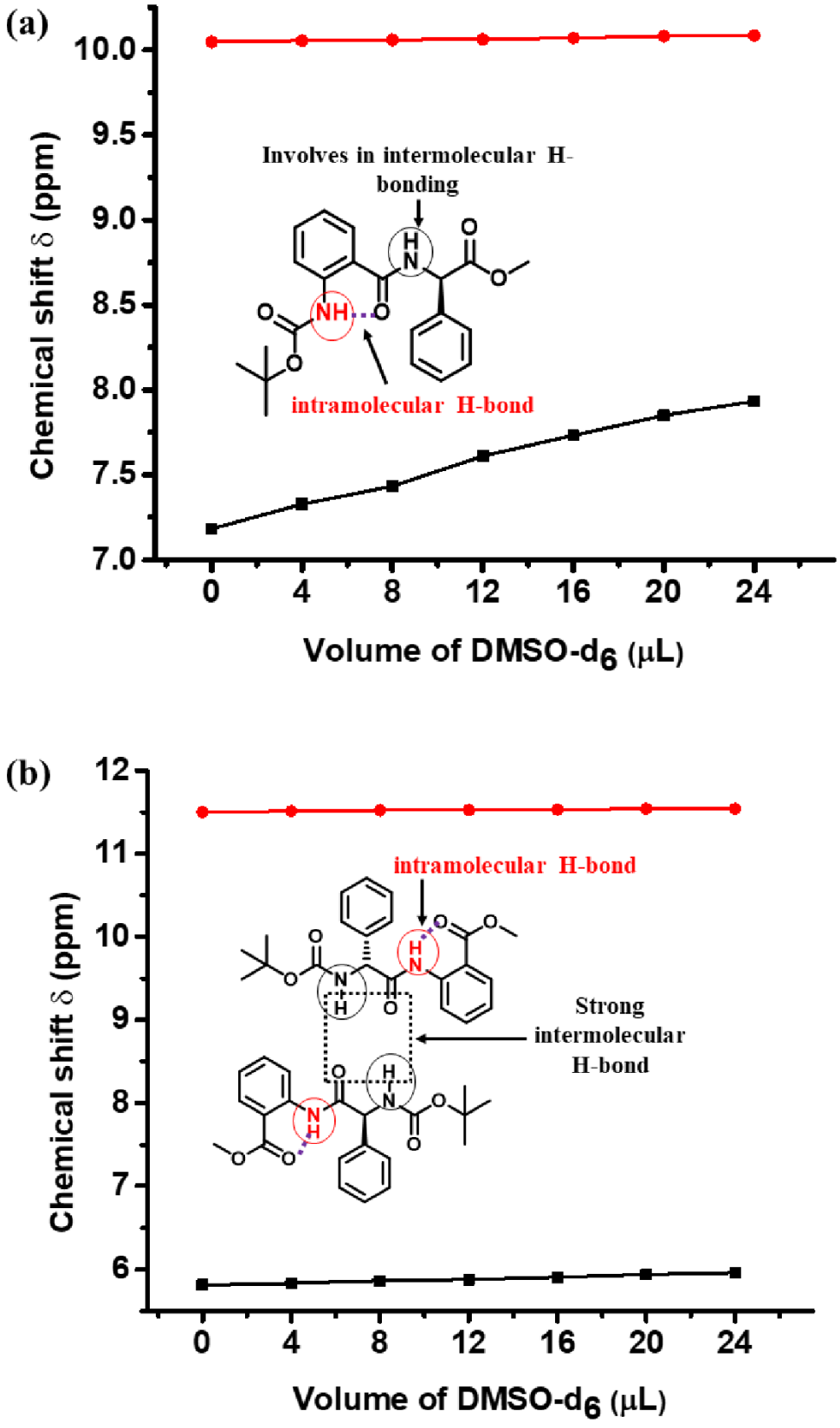

Figure 4.10. *(a, b) Represents solvent-dependent ^{1}H-NMR titration of peptides* ***4B*** *and* ***4D****, respectively.*

4.8. CD experiment

To check the secondary structure conformation in solution, we carried out circular dichroism (CD) experiment. For this experiment, 1.5 mM peptide solution in methanol was diluted to 375 μM to overcome high HT voltage. Peptide **4A** and **4B** displayed non-characteristic one positive band at 222 nm and one negative CD signal at 252 nm. Therefore, both peptides displayed a mixture of secondary conformation in the solution. The reverse peptide sequence, i.e., **4C** and **4D**, displayed a non-characteristic CD signal remaining around baseline (Figure 4.11). Depending on the environment, short peptides have flexible chemical structures which can form several stable conformations. In the case of solid-state peptide crystal, one stable conformation is organized and formed crystal, which is self-associated to build diverse molecular arrangements. Moreover, short peptides can also adopt different stable conformations in the solution.[9] Therefore, a significant change in CD signal was observed for alternation of peptide sequences.

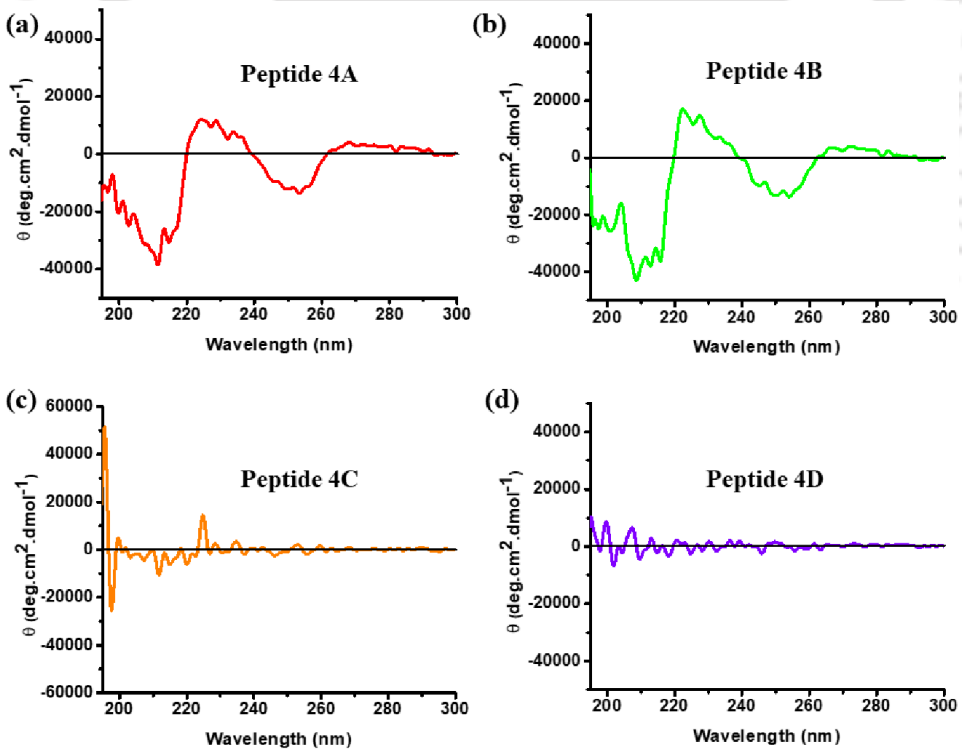

Figure 4.11. *(a, b, c, d) CD spectra of 375 μM peptide solution of* ***4A***, ***4B***, ***4C,*** *and* ***4D****, respectively, in methanol.*

4.9. Thermal stability study

Next, to examine the thermal stability of the self-assembled supramolecular structure, we carried out TGA experiment in solid-state. In the case of peptides, weight loss was observed in two thermal periods, such as (i) absorbed water molecule loosened at temperature range 25-200 °C and (ii) peptide bonds broken at temperature range 200-500 °C.[10] Peptides **4A**, **4B**, **4C**, and **4D** exhibited weight loss at 217 °C, 215 °C, 215 °C, and 215 °C, respectively (higher than their corresponding melting points). It indicates significant thermal stability due to the formation of a self-assembled well-organized structure. Furthermore, no weight loss was observed in the temperature range of 25-200 °C, which suggests the absence of water or solvent in peptides. (Figure 4.12)

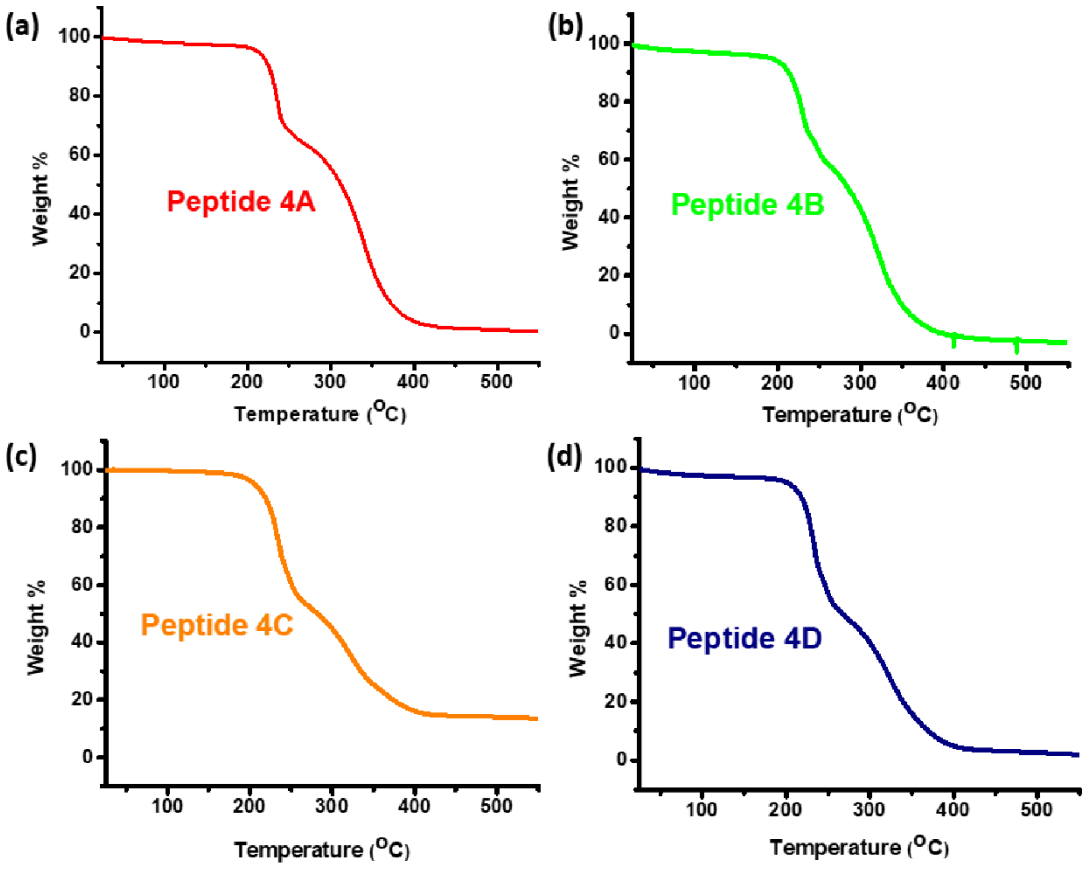

Figure 4.12. *TGA profile of peptides (a)* ***4A****, (b)* ***4B****, (c)* ***4C,*** *and (d)* ***4D****, respectively*

4.10. Conclusion

In conclusion, we demonstrated the conformational, self-assembly, and morphological variation of non-coded amino acids containing dipeptides Boc-Ant-L/D-Phg-OMe and its reverse peptide sequences. FT-IR experiment suggested the conformational homogeneity and heterogeneity of enantiomeric and reverse peptide sequences, respectively, in solid-state. SC-XRD revealed that **4A** and **4B** formed supramolecular helical structure and β-sheet-like layer arrangement in the crystalline state. Reverse peptide sequences **4C** and **4D** created different supramolecular helical structures, sheet-like layer arrangements, and molecular channels in the crystalline state. All self-assembled structures stabilized through H-bonding and several other noncovalent interactions. Morphology analysis by diverse microscopic techniques exhibited that **4A** and **4B** formed vesicular structures, whereas **4C** and **4D** generated rod-like fiber structures.

Moreover, solvent-dependent NMR titration and CD analysis displayed diverse behavior for reverse peptides in solution. Therefore, enantiomeric peptides and their reverse peptides displayed conformational, self-assembly, morphological homogeneity, and heterogeneity, respectively. These exciting results may help design peptide-based novel materials.

4.11. Experimental section

4.11.1. Materials and instrumentations

As described in chapter 7

4.11.2. General procedure for the synthesis of dipeptides

As described in chapter 3, section 3.12.2.

(Each N-terminal protected amino acid was taken 300 mg)

4.11.3. Sample preparation

A freshly prepared 1.5 mM each peptide solution in methanol was allowed for optical microscopic and FESEM experiments. A diluted peptide solution, 300 μM and 60 μM, were used for FETEM and AFM image collection,

4.12. Characterization data

Boc-Ant-L-Phg-OMe (4A)

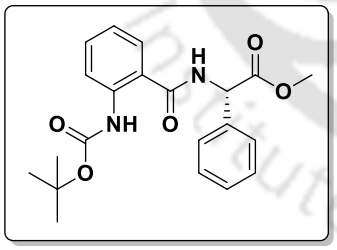

White solid, (350 mg, 72%), M.P 122-125ºC, **^{1}H NMR (CDCl$_3$; 400 MHz)** δ 1.49 (9H, s); 3.77 (3H, s); 5.73-5.71 (1H, d, *J* = 6.8 Hz); 7.03-6.99 (1H, t, *J* = 7.2 Hz); 7.20-7.19 (1H, d, *J* = 6.4 Hz); 7.47-7.35 (6H, m); 7.57-7.56 (1H, d, *J* = 7.6 Hz); 8.38-8.36 (1H, d, *J* = 8.4 Hz); 10.05 (1H, s). **^{13}C NMR (CDCl$_3$; 100 MHz)** δ 28.5, 53.2, 56.9, 80.5, 118.7, 120.0, 121.6, 127.1, 127.4, 128.9, 129.3, 133.2, 136.3, 140.8, 153.2, 168.3, 171.4. HRMS (ESI): calculated $[M+H]^+$ 385.1763, found m/z . 385.1780. HPLC: retention time (t_R) = 6.935 min.

Boc-Ant-D-Phg-OMe (4B):

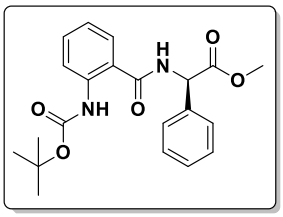

White solid, (360 mg, 74%), **M.P** 121-124°C, **^{1}H NMR (CDCl$_3$; 400 MHz)** δ 1.49 (9H, s); 3.77 (3H, s); 5.73-5.71 (1H, d, *J* = 6.8 Hz); 7.03-6.99 (1H, t, *J* = 7.6 Hz); 7.20-7.19 (1H, d, *J* = 6.4 Hz); 7.47-7.35 (6H, m); 7.58-7.56 (1H, d, *J* = 7.6 Hz); 8.38-8.36 (1H, d, *J* = 8.4 Hz); 10.05 (1H, s). **^{13}C NMR (CDCl$_3$; 100 MHz)** δ 28.5, 53.2, 56.9, 80.5, 118.7, 120.0, 121.6, 127.1, 127.4, 128.9, 129.3, 133.2, 136.3, 140.8, 153.2, 168.3, 171.4. HRMS (ESI): calculated $[M+H]^+$ 385.1763, found m/z . 385.1771. HPLC: retention time (t_R) = 6.936 min.

Boc-L-Phg-Ant-OMe (4C):

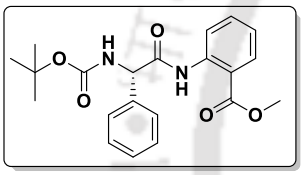

White solid, (295 mg, 64%), **M.P** 105-109°C, **^{1}H NMR (CDCl$_3$; 600 MHz)** δ 1.47 (9H, s); 3.91 (3H, s); 5.35 (1H, s); 5.84 (1H, s); 7.10-7.08 (1H, t, *J* = 7.8 Hz); 7.35-7.32 (1H, t, *J* = 7.8 Hz); 7.40-7.38 (1H, t, *J* = 7.2 Hz); 7.55-7.49 (3H, m); 8.01-8.00 (1H, d, *J* = 7.2 Hz); 8.69-8.68 (1H, d, *J* = 8.4 Hz); 11.52 (1H, s). **^{13}C NMR (CDCl$_3$; 150 MHz)** δ 28.5, 52.5, 60.4, 80.3, 115.5, 120.5, 123.0, 127.5, 128.6, 129.2, 131.0, 134.7, 138.1, 141.1, 155.2, 168.6, 169.3. HRMS (ESI): calculated $[M+H]^+$ 385.1763, found m/z . 385.1774. HPLC: retention time (t_R) = 6.679 min.

Boc-D-Phg-Ant-OMe (4D):

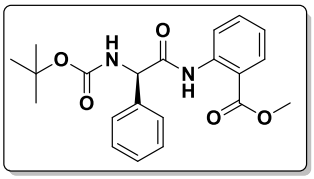

White solid, (286 mg, 62%), **M.P** 95-98°C**, ^{1}H NMR (CDCl$_3$; 400 MHz)** δ 1.44 (9H, s); 3.89 (3H, s); 5.33 (1H, s); 5.82 (1H, s); 7.08-7.05 (1H, t, *J* = 7.6 Hz); 7.33-7.29 (1H, m); 7.39-7.35 (2H, t, *J* = 7.2 Hz); 7.53-7.47 (3H, m,); 7.99-7.97 (1H, d, *J* = 8.0 Hz); 8.67-8.65 (1H, d, *J* = 8.4 Hz); 11.49 (1H, s). **^{13}C NMR (CDCl$_3$; 100 MHz)** δ 28.5, 52.5, 60.5, 80.3, 115.5, 120.5, 123.0, 127.5, 128.6, 129.2, 131.0, 134.7, 138.1, 141.1, 155.2, 168.6, 169.3. HRMS (ESI): calculated $[M+H]^+$ 385.1763, found m/z . 385.1777. HPLC: retention time (t_R) = 6.686 min.

4.13. References

1. Al Toma, R. S.; Brieke, C.; Cryle, M. J.; Süssmuth, R. D. Structural aspects of phenylglycines, their biosynthesis and occurrence in peptide natural products. *Nat. Prod. Rep.* **2015**, *32*, 1207-1235.
2. Salick, D. A.; Kretsinger, J. K.; Pochan, D. J.; Schneider, J. P. Inherent Antibacterial Activity of a Peptide-Based β-Hairpin Hydrogel. *J. Am. Chem. Soc.* **2007**, *129*, 14793-14799.
3. Guha, S.; Chakraborty, T.; Banerjee, A. Water soluble synthetic dieptide-based biodegradable nanoporous materials. *Green Chem.* **2009**, *11*, 1139-1145.
4. Soldatov, D. V.; Moudrakovski, I. L.; Ripmeester, J. A. Dipeptides as microporous materials. *Angew. Chem. Int. Ed.* **2004**, *43*, 6308-6311.
5. Butterfield, D. A.; Hensley, K.; Harris, M.; Mattson, M.; Carney, J. β-Amyloid Peptide Free Radical Fragments Initiate Synaptosomal Lipoperoxidation in a Sequence-Specific Fashion: Implications to Alzheimer′s Disease. *Biochem. Biophys. Res. Commun.* **1994**, *200*, 710-715.
6. Kar, S.; Tai, Y. Marked difference in self-assembly, morphology, and cell viability of positional isomeric dipeptides generated by reversal of sequence. *Soft Matter* **2015**, *11*, 1345-1351.
7. Haldar, D.; Banerjee, A. Intrinsic Amyloidogenic Behavior of Terminally Protected Alzheimer's $A\beta^{17-21}$ Peptide: Self-Aggregation and Amyloid-Like Fibril Formation. *Int. J. Pept. Res. Ther*. **2007**, *13*, 439-446.
8. Dado, G. P.; Gellman, S. H. Intramolecular Hydrogen Bonding in Derivatives of β-Alanine and γ-Amino Butyric Acid: Model Studies for the Folding of Unnatural Polypeptide Backbones. *J. Am. Chem. Soc*. **1994**, *116*, 1054-1062.
9. Palai, B. B.; Sharma, N. K. N-Arylated peptide: troponyl residue influences the structure and conformation of N-troponylated-(di/tri)-peptides. *CrystEngComm* **2021**, *23*,131-139.
10. Dandurand, J.; Samouillan, V.; Lacoste-Ferre, M. H.; Lacabanne, C.; Bochicchio, B.; Pepe, A. Conformational and thermal characterization of a synthetic peptidic fragment inspired from human tropoelastin: Signature of the amyloid fibers. *Pathol. Biol.* **2014**, *62*, 100-107.

4.14. Selected spectra

4.14.1. Spectra of peptide Boc-Ant-L-Phg-OMe (4A):

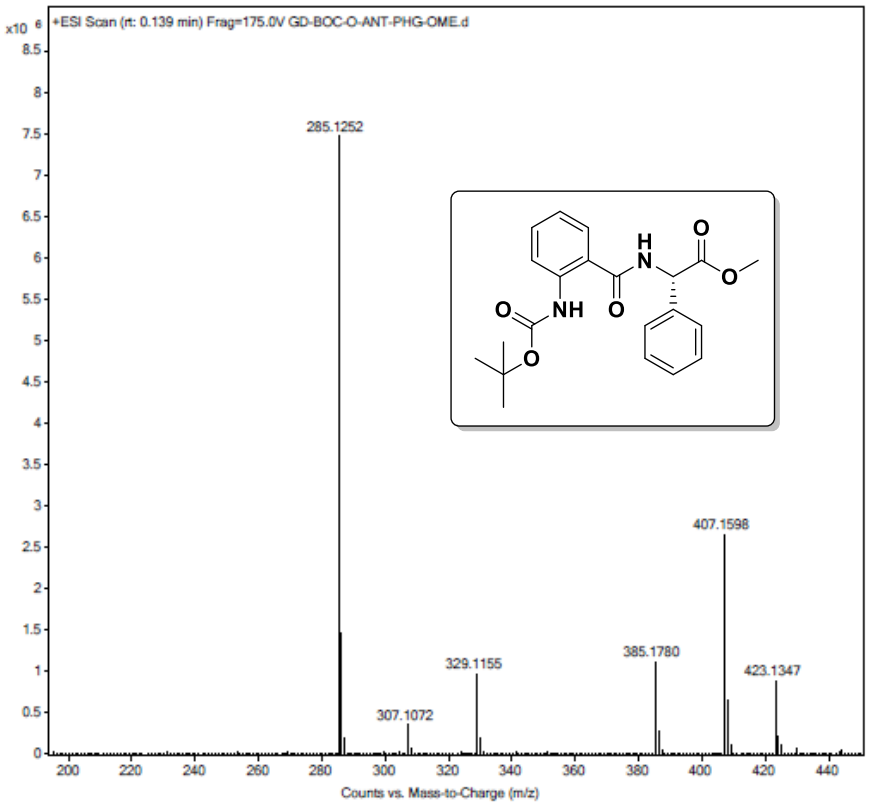

Figure 4.13. *MS spectra of peptide* ***Boc-Ant-L-Phg-OMe (4A)***

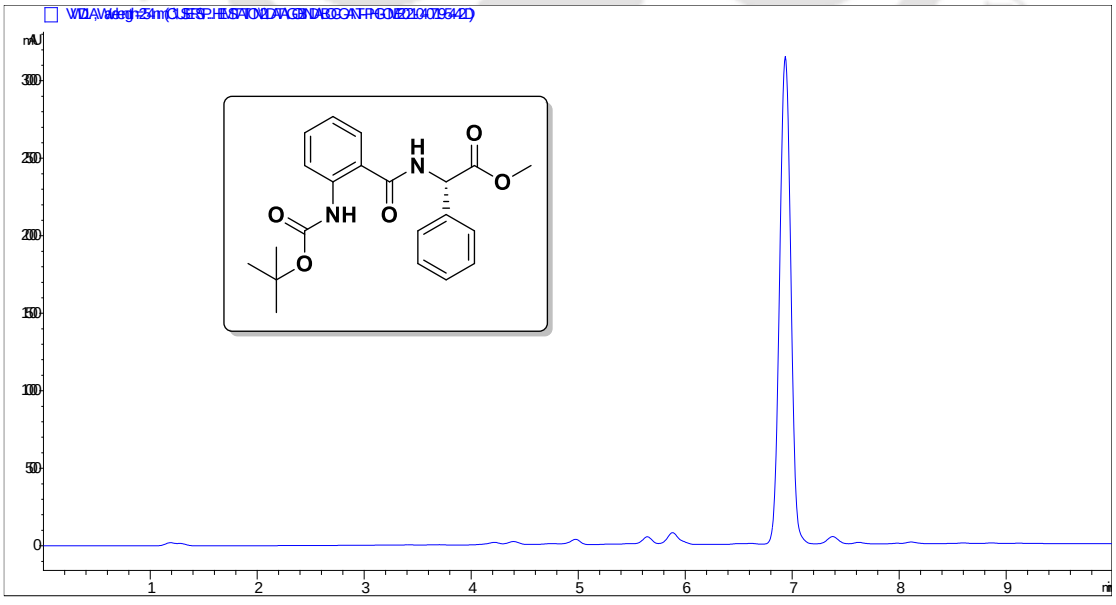

Figure 4.14. *HPLC profile picture of purified peptide* ***Boc-Ant-L-Phg-OMe (4A)***

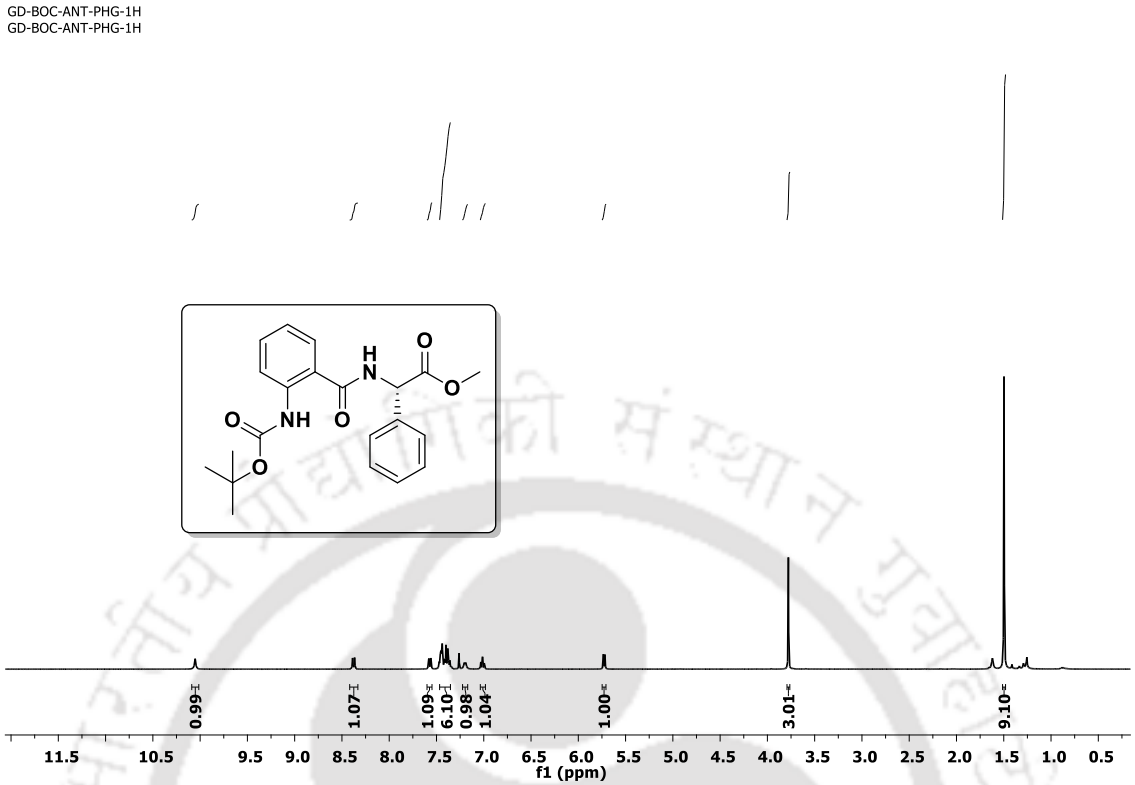

Figure 4.15. *^{1}H NMR spectra of peptide* ***Boc-Ant-L-Phg-OMe (4A)***

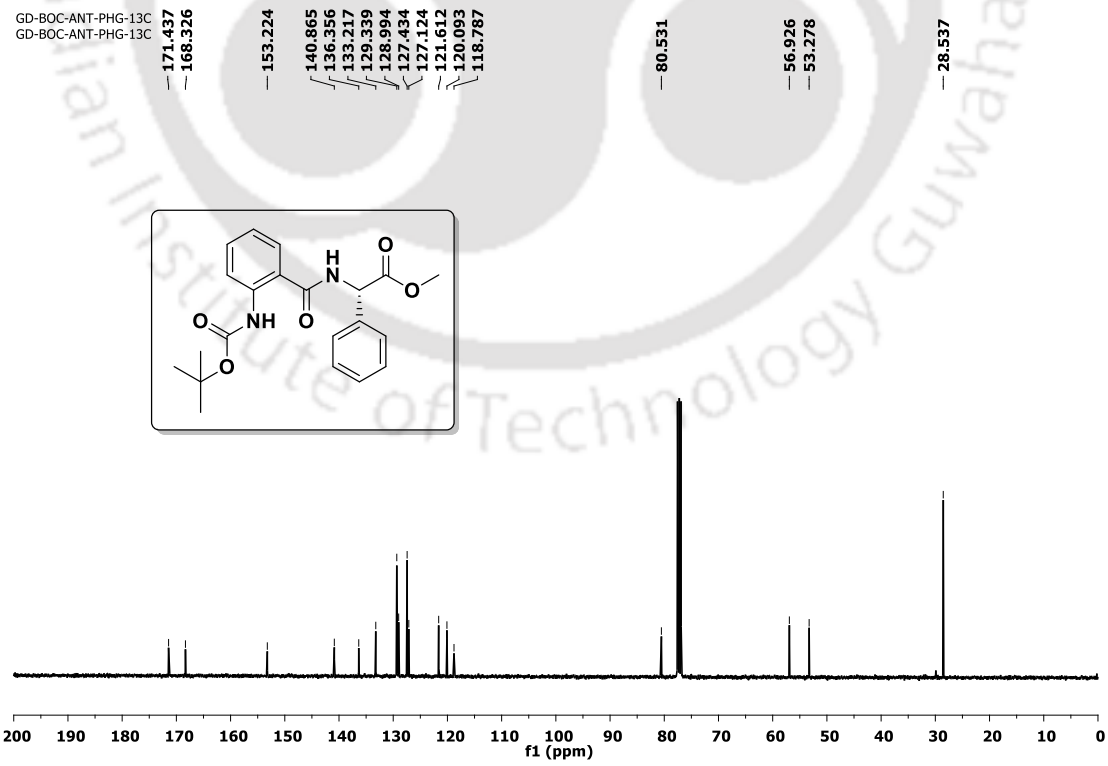

Figure 4.16. *^{13}C NMR spectra of peptide* ***Boc-Ant-L-Phg-OMe (4A)***

4.14.2. Spectra of peptide Boc-Ant-D-Phg-OMe (4B):

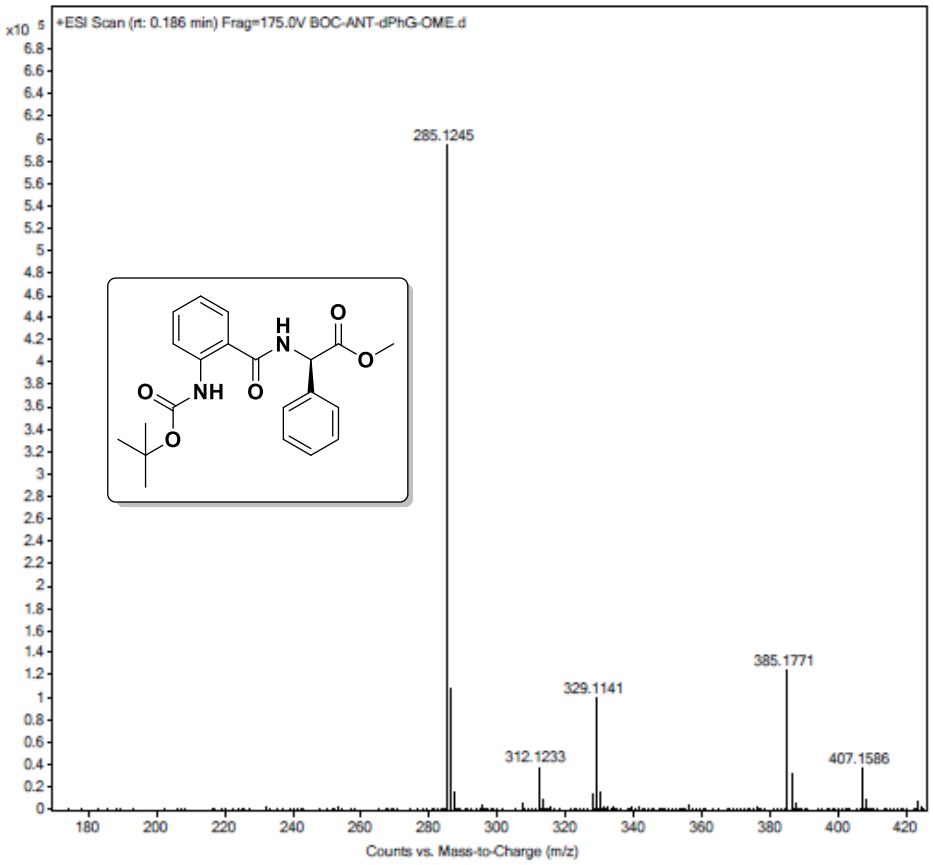

Figure 4.17. *MS spectra of peptide* ***Boc-Ant-D-Phg-OMe (4B)***

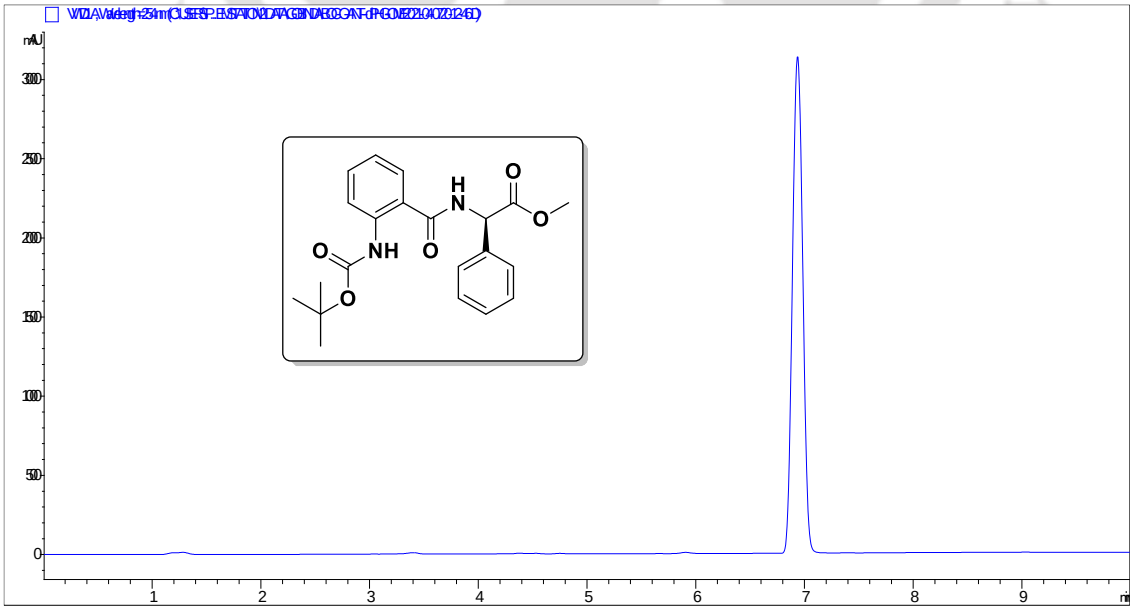

Figure 4.18. *HPLC profile picture of purified peptide* ***Boc-Ant-D-Phg-OMe (4B)***

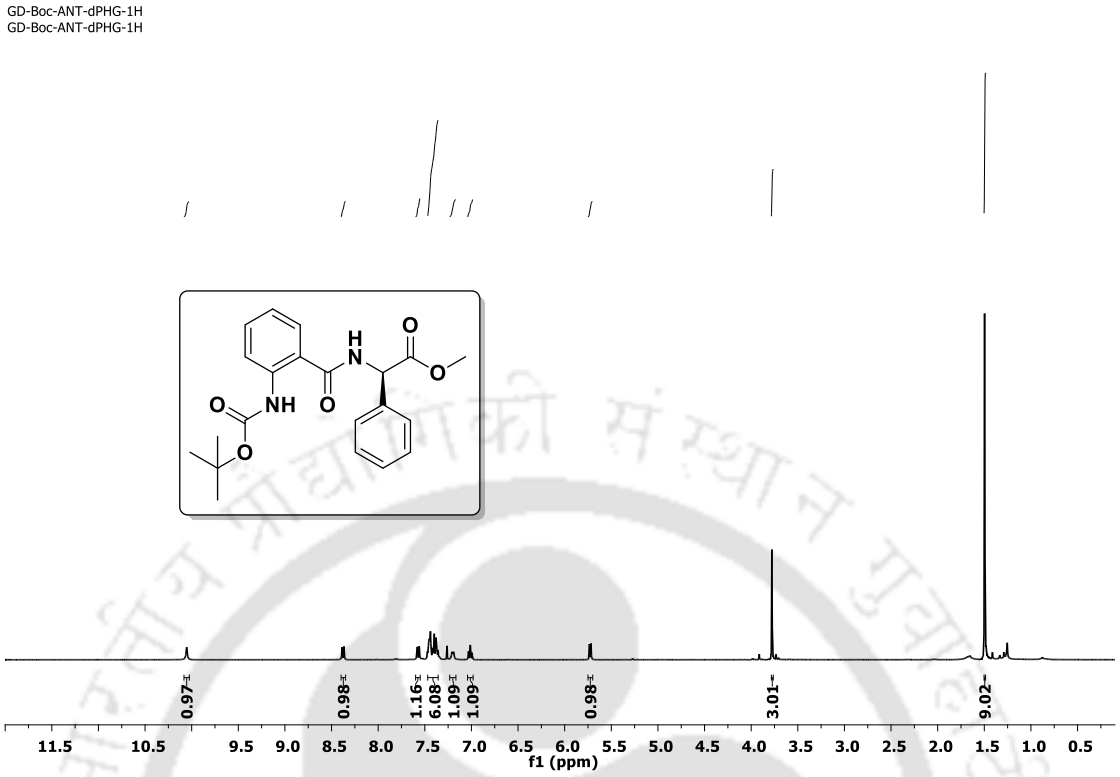

Figure 4.19. *^{1}H NMR spectra of peptide* ***Boc-Ant-D-Phg-OMe (4B)***

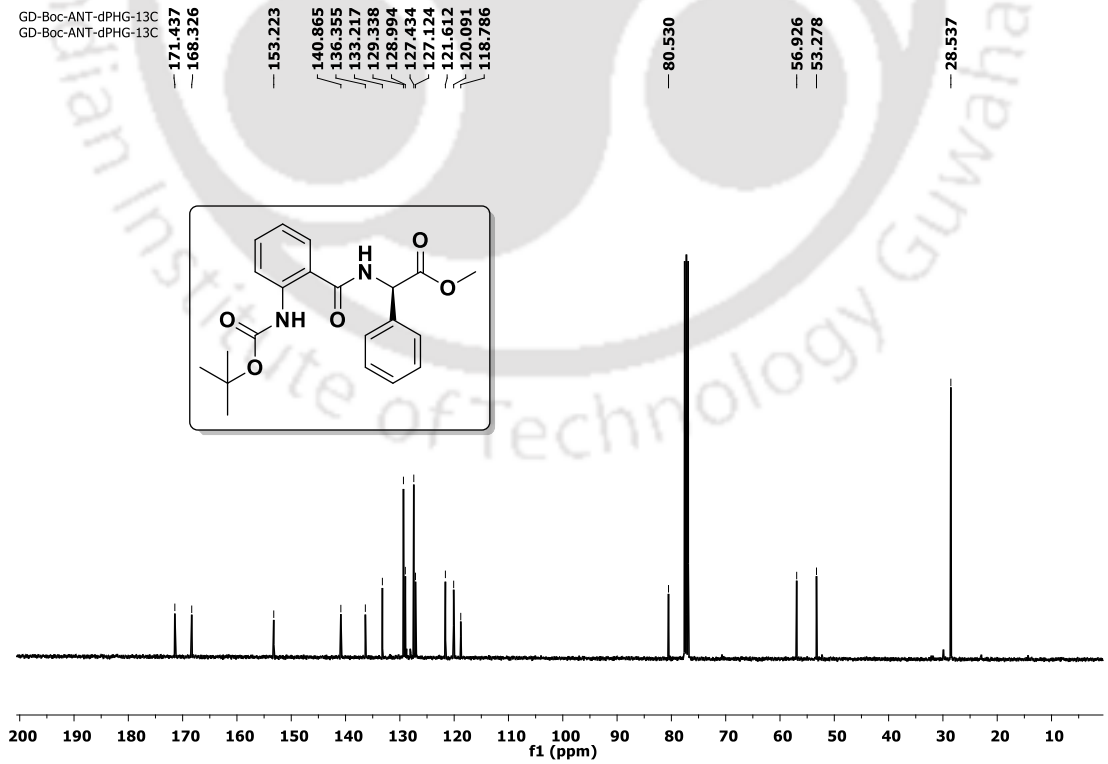

Figure 4.20. *^{13}C NMR spectra of peptide* ***Boc-Ant-D-Phg-OMe (4B)***

4.14.3. Spectra of peptide Boc-L-Phg-Ant-OMe (4C):

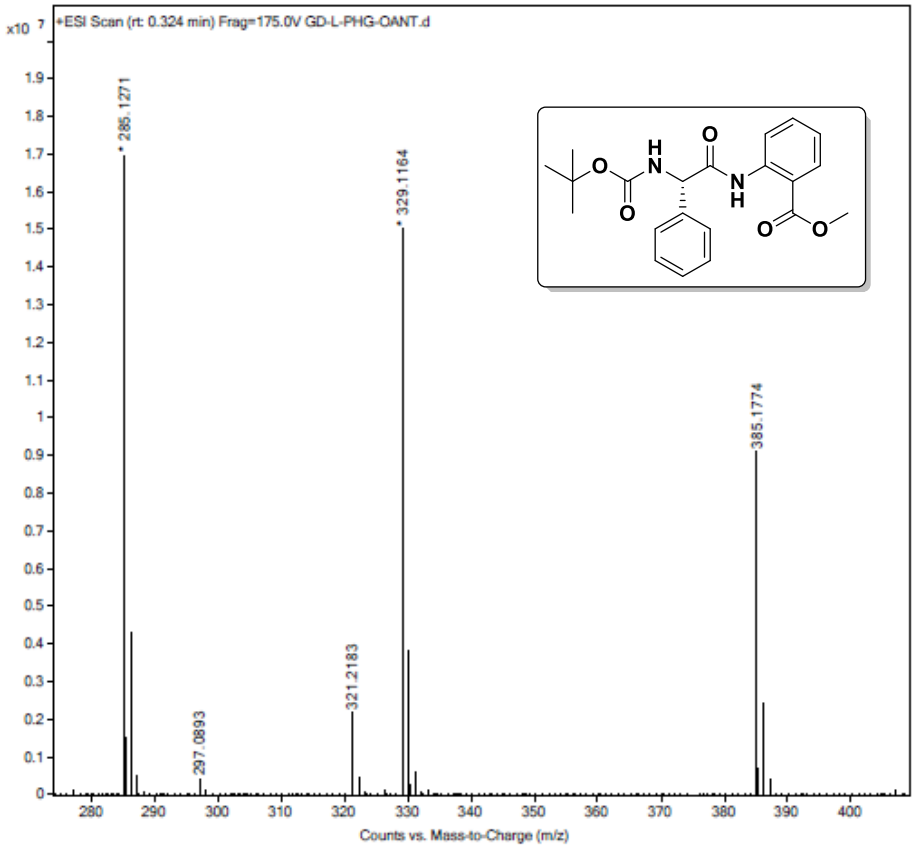

Figure 4.21. *MS spectra of peptide* ***Boc-L-Phg-Ant-OMe (4C)***

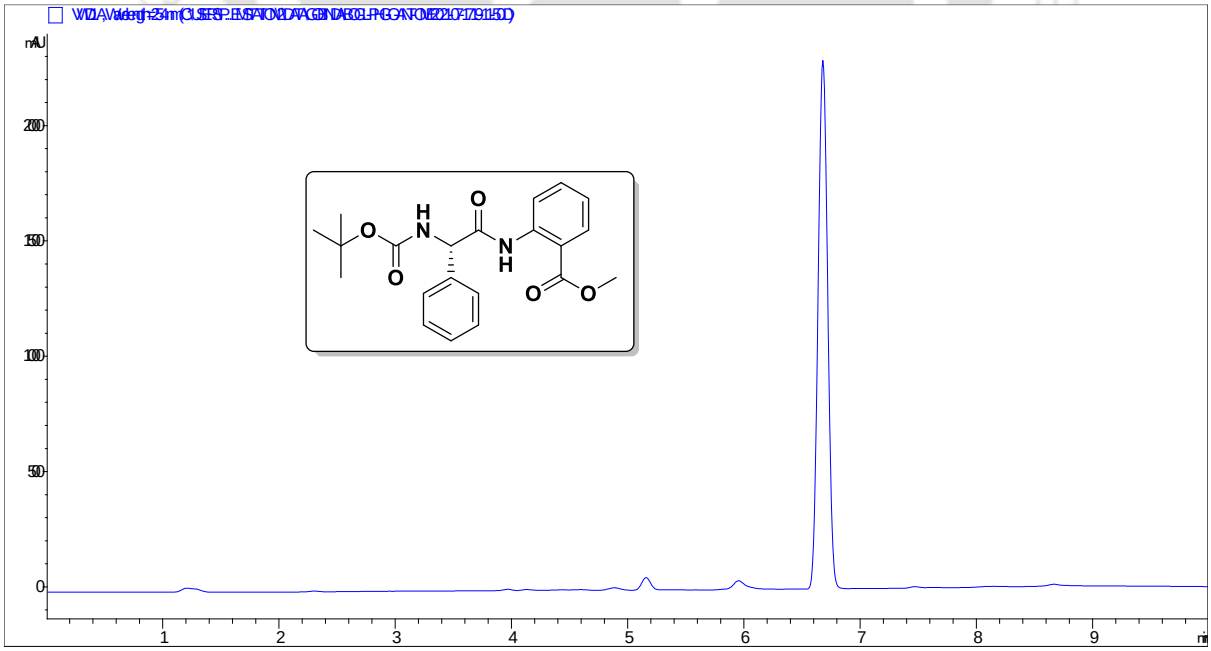

Figure 4.22. *HPLC profile picture of purified peptide* ***Boc-L-Phg-Ant-OMe (4C)***

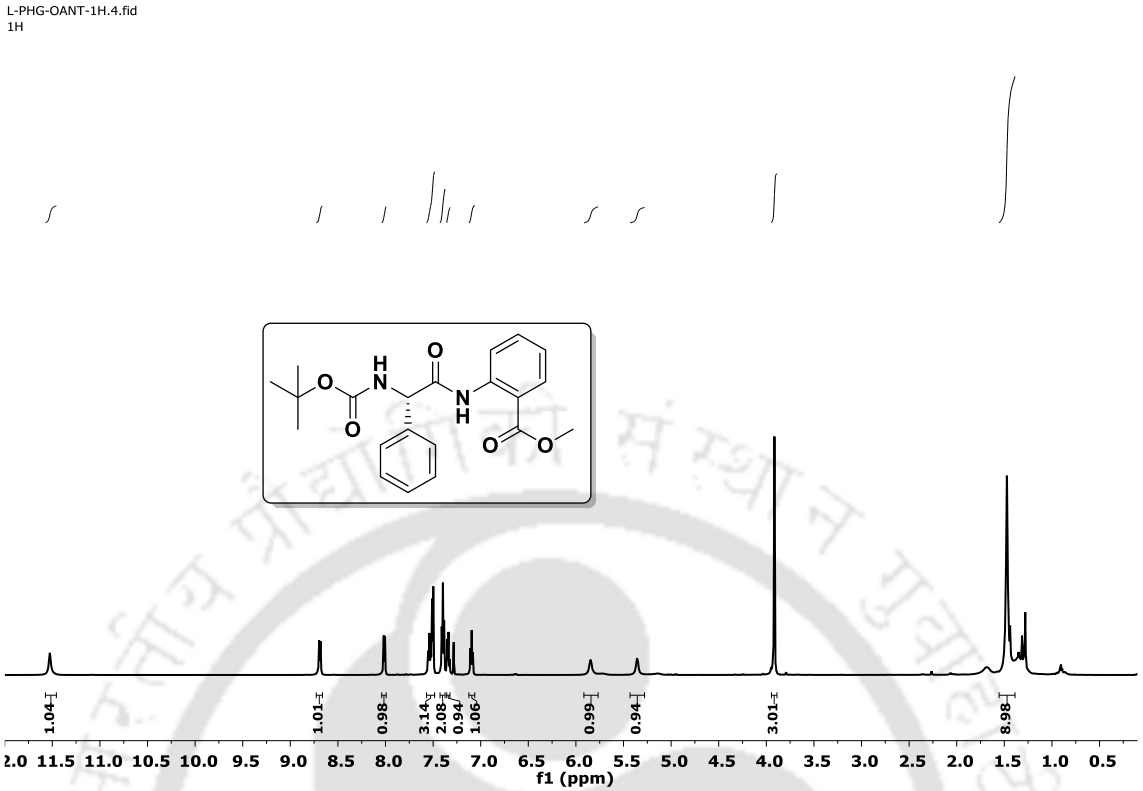

Figure 4.23. *^{1}H NMR spectra of peptide* ***Boc-L-Phg-Ant-OMe (4C)***

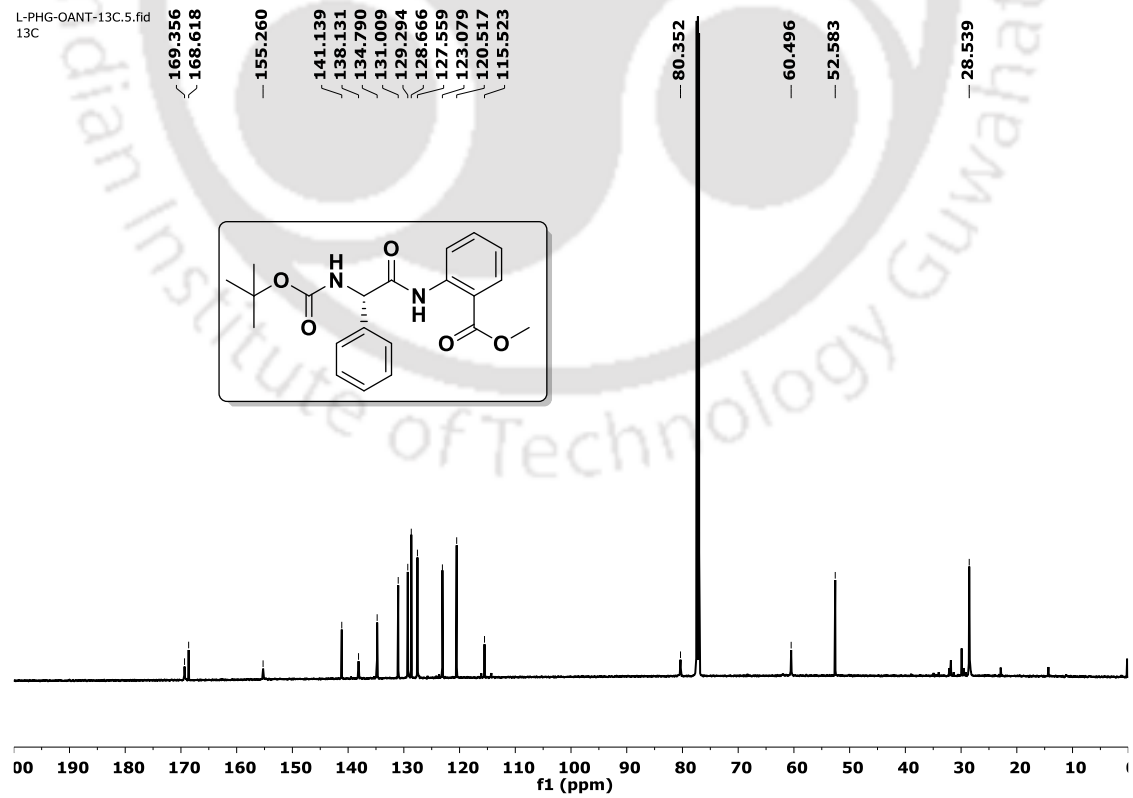

Figure 4.24. *^{13}C NMR spectra of peptide* ***Boc-L-Phg-Ant-OMe (4C)***

4.14.4. Spectra of Peptide Boc-D-Phg-Ant-OMe (4D):

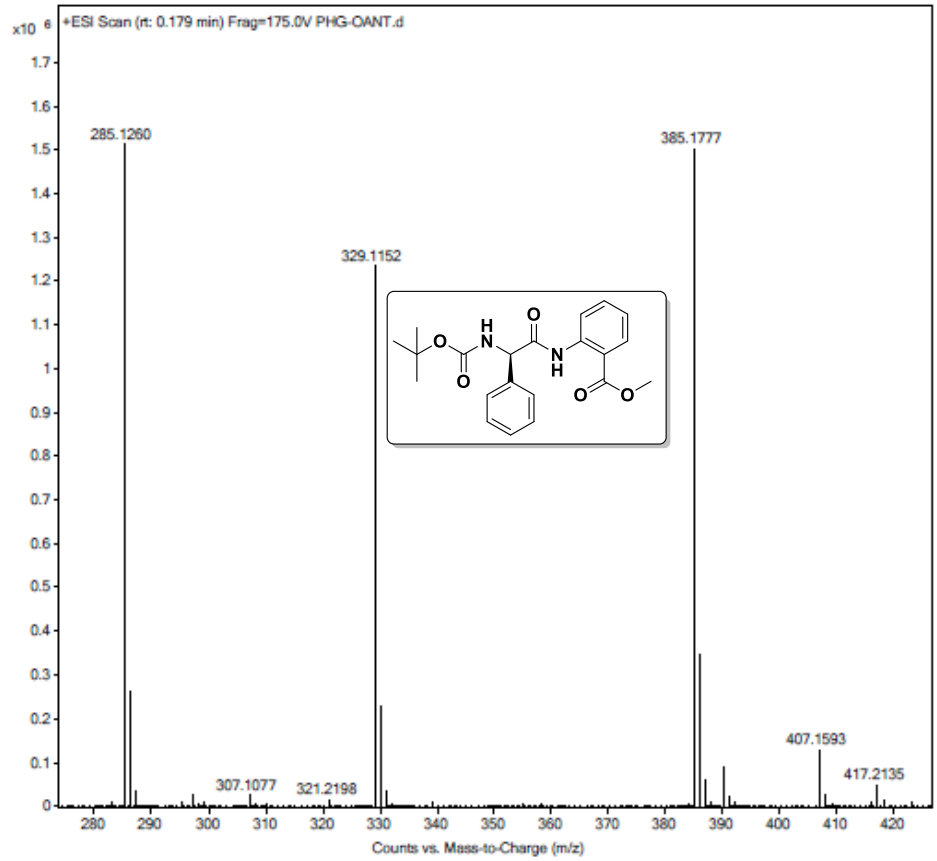

Figure 4.25. *MS spectra of peptide* ***Boc-D-Phg-Ant-OMe (4D)***

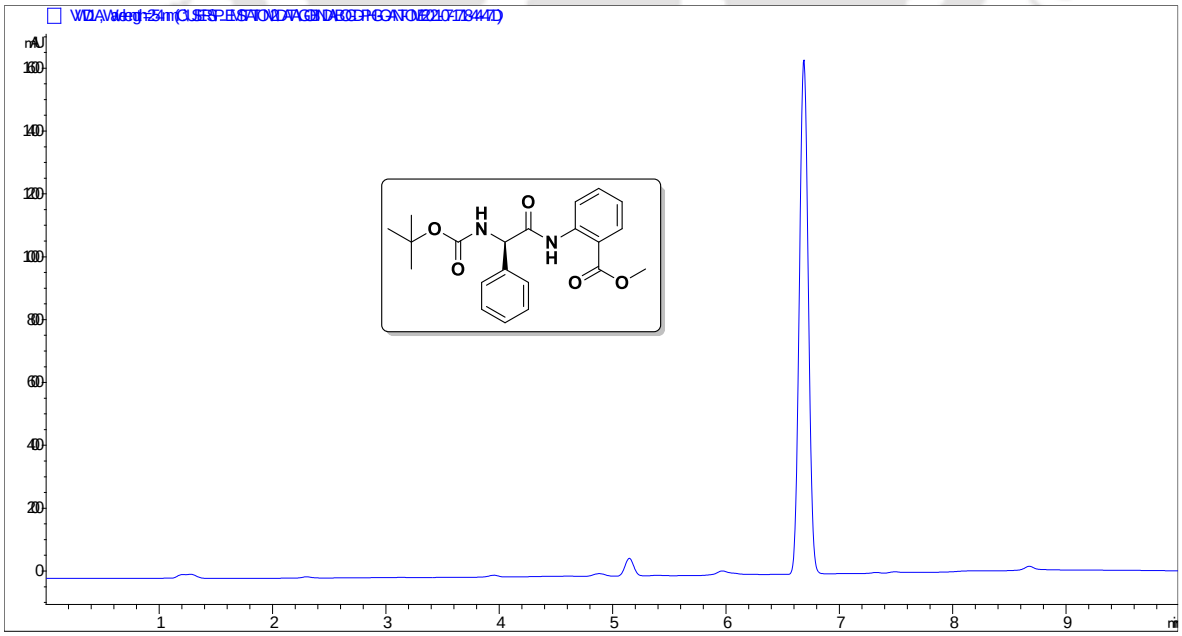

Figure 4.26. *HPLC profile picture of purified peptide* ***Boc-D-Phg-Ant-OMe (4D)***

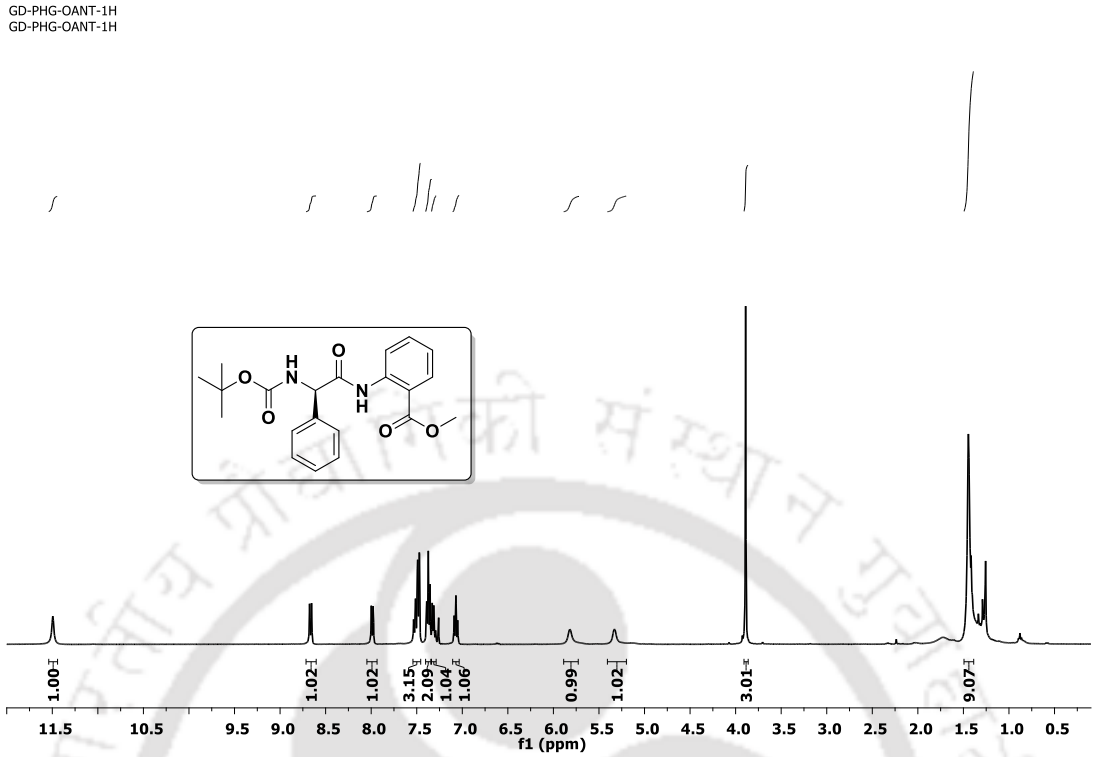

Figure 4.27. *^{1}H NMR spectra of peptide* ***Boc-D-Phg-Ant-OMe (4D)***

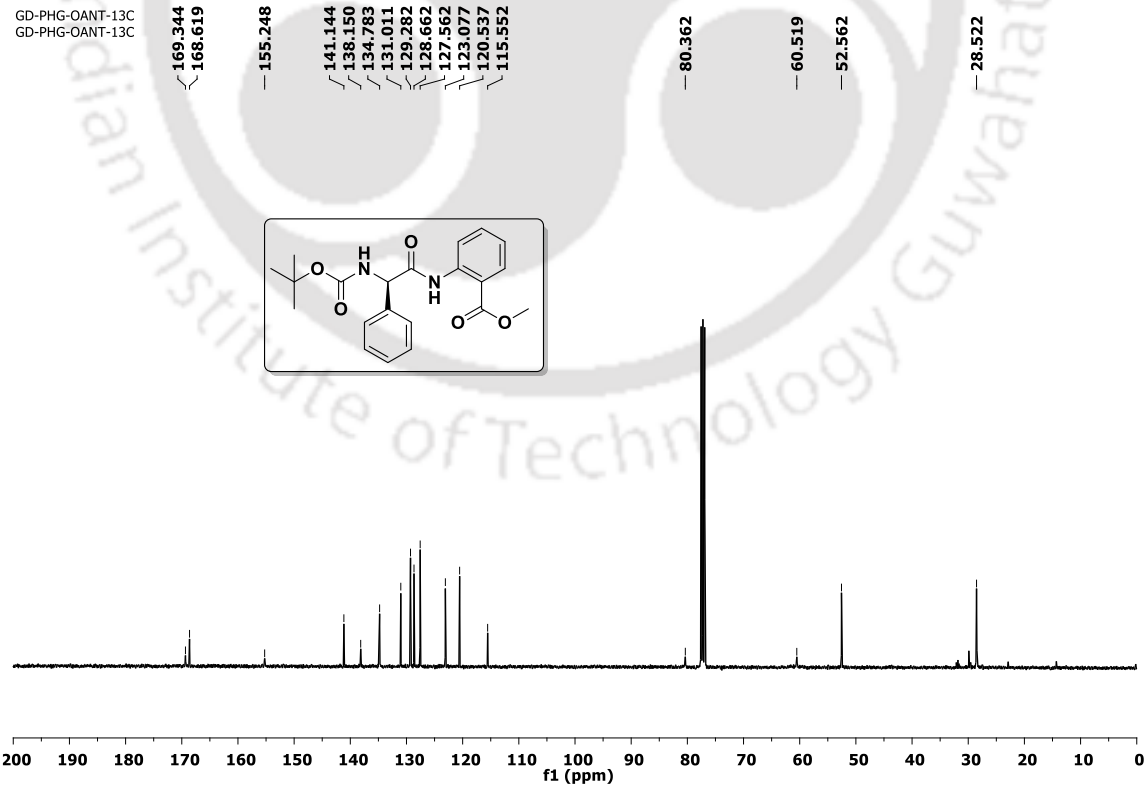

Figure 4.28. *^{13}C NMR spectra of peptide* ***Boc-D-Phg-Ant-OMe (4D)***

Table 4.1. Chemical shift δ (ppm) of hydrogen-bonded protons with the addition of DMSO-d_6

Peptide 1							
DMSO-d_6 (µL)	**0**	**4**	**8**	**12**	**16**	**20**	**24**
NH-Phg	7.189	7.332	7.434	7.580	7.682	7.794	7.873
NH-Ant	10.049	10.053	10.060	10.063	10.072	10.075	10.081
Peptide 2							
NH-Phg	7.183	7.328	7.433	7.611	7.732	7.850	7.934
NH-Ant	10.048	10.055	10.060	10.063	10.071	10.081	10.086
Peptide 3							
NH-Phg	5.814	5.832	5.861	5.883	5.919	5.968	6.005
NH-Ant	11.500	11.507	11.518	11.522	11.526	11.539	11.543
Peptide 4							
NH-Phg	5.813	5.836	5.864	5.879	5.906	5.940	5.962
NH-Ant	11.500	11.510	11.521	11.524	11.529	11.538	11.539

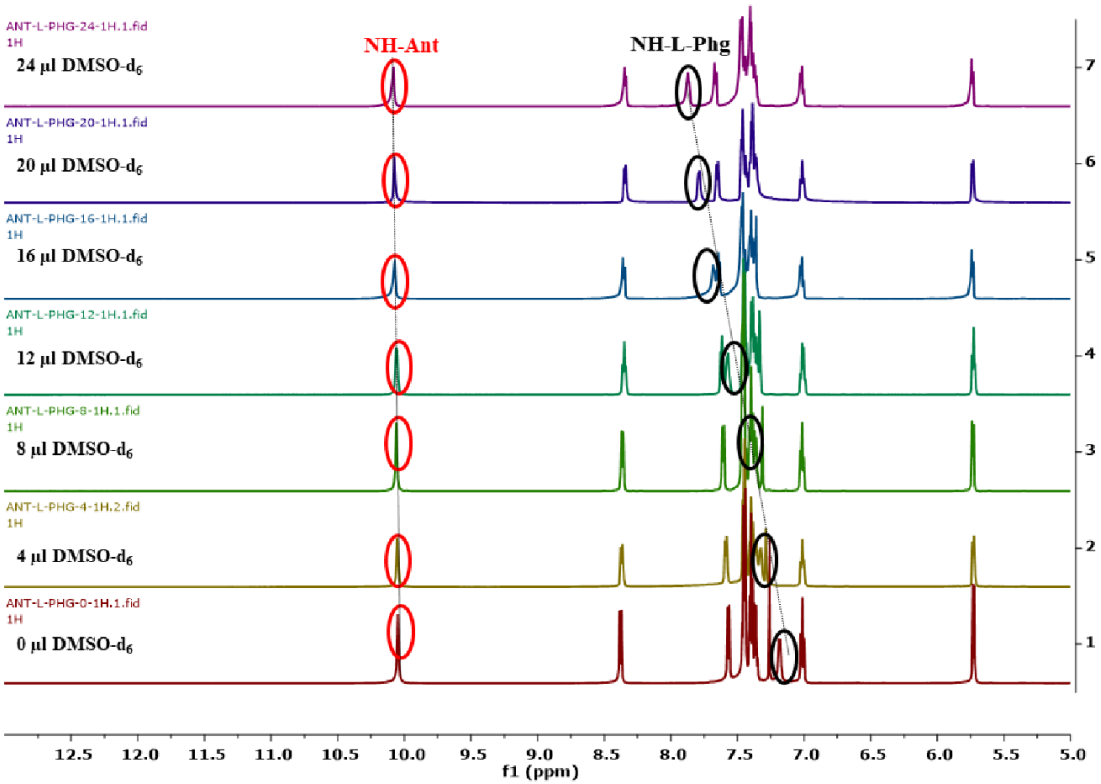

Figure 4.29. *Partial titration spectra of peptide* ***4A*** *in $CDCl_3$ with DMSO-d_6.*

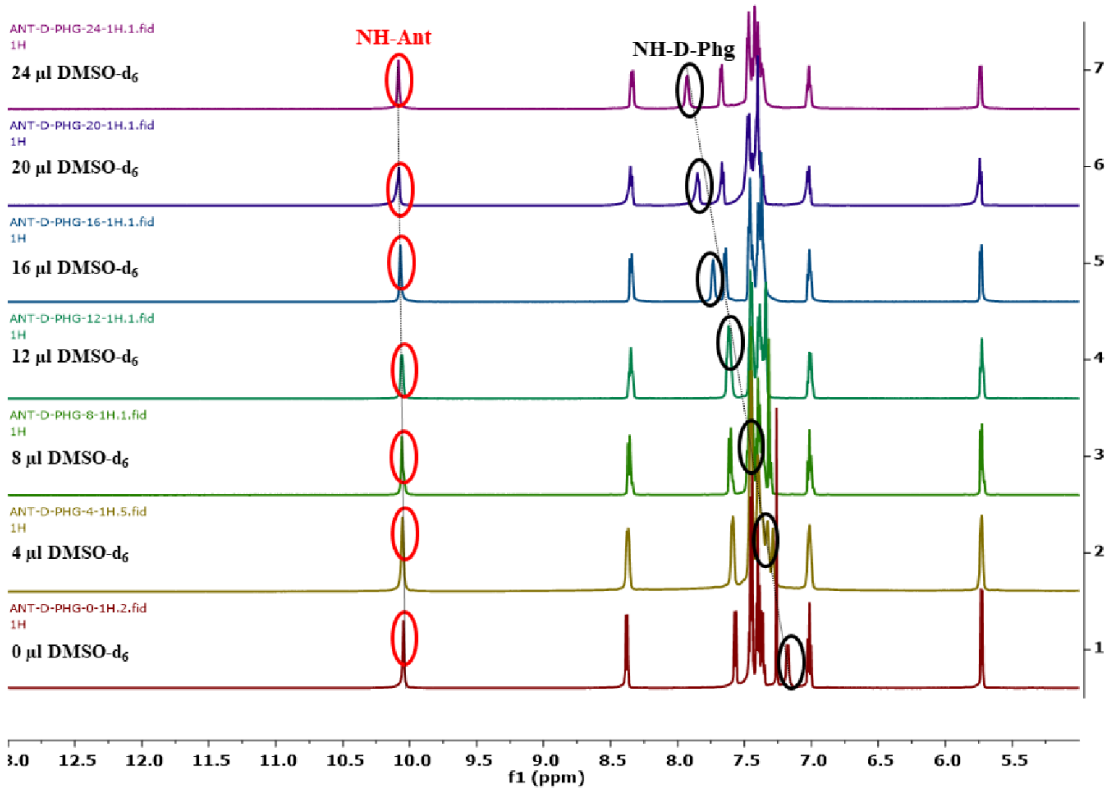

Figure 4.30. *Partial titration spectra of peptide* ***4B*** *in $CDCl_3$ with DMSO-d_6.*

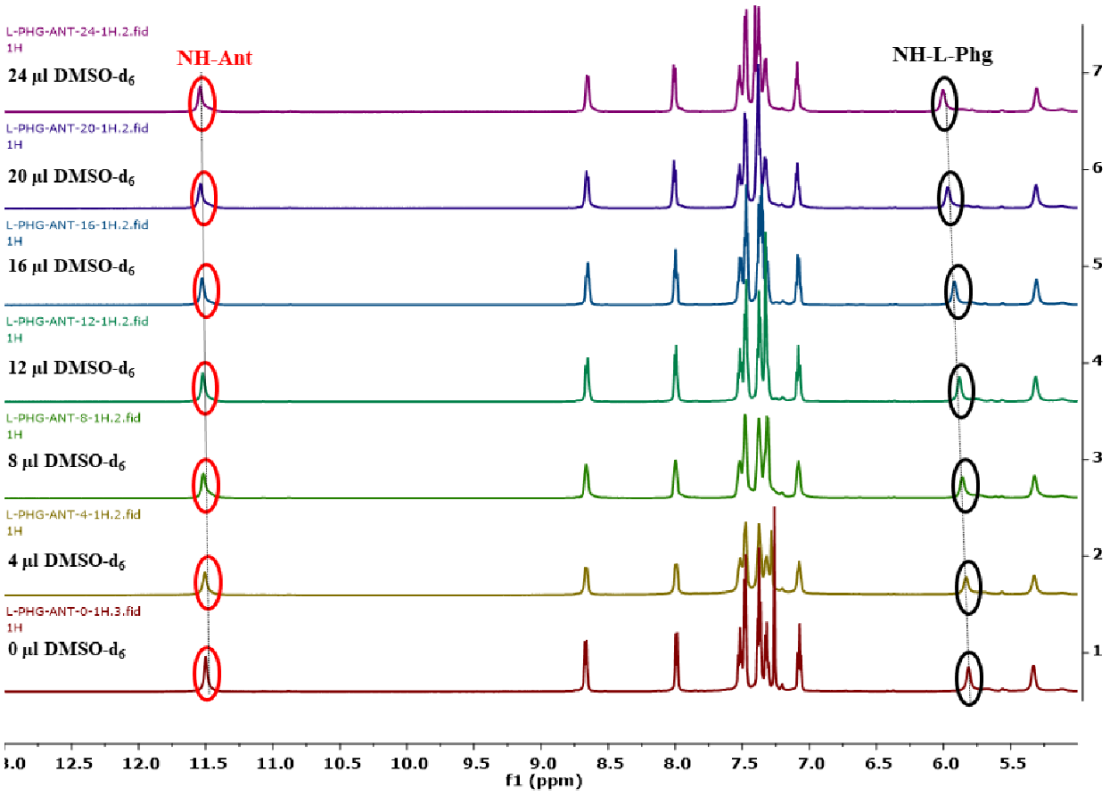

Figure 4.31. *Partial titration spectra of peptide* ***4C*** *in $CDCl_3$ with DMSO-d_6.*

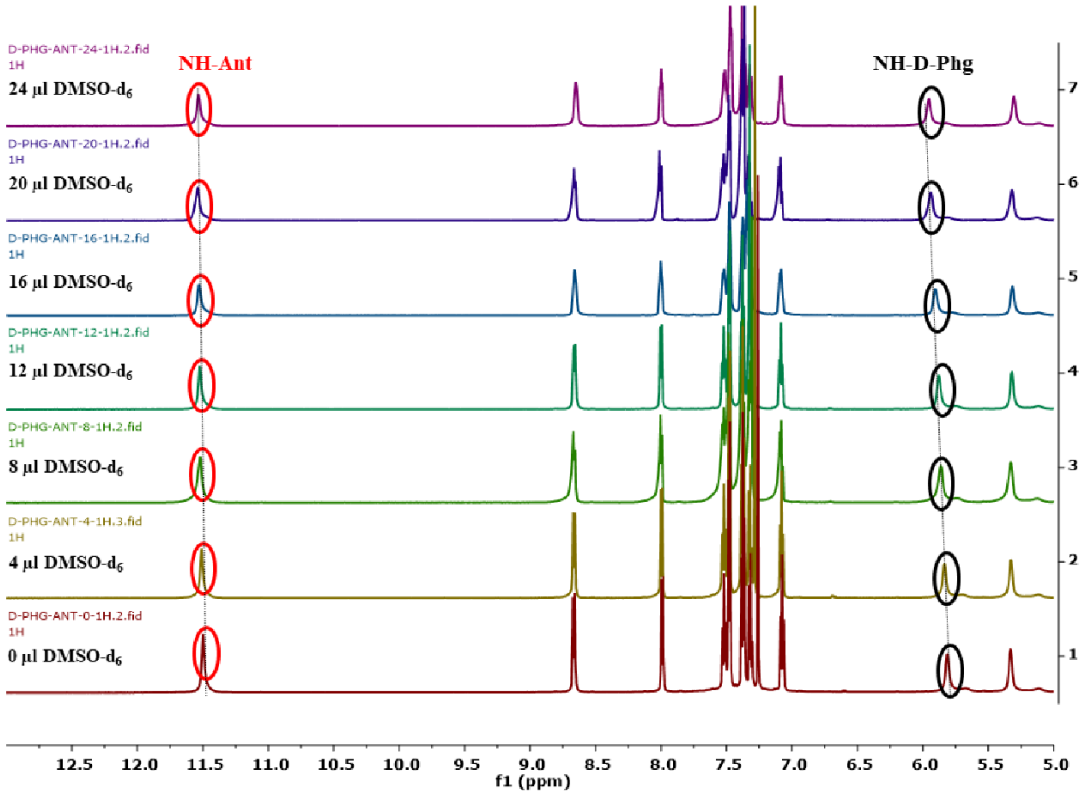

Figure 4.32. *Partial titration spectra of peptide* ***4D*** *in $CDCl_3$ with DMSO-d_6.*

4.15. Crystallographic data

Table 4.2. Selected backbone torsion angles (°) of peptides

peptide		ω_0	ω_1	ϕ_1	ϕ_2	ψ_1	ψ_2	θ_1
Peptide 4A	N1-C5-O1-C2 = -177.0(2)	C6-N1-C5-O1 = 170.5(3)	C13-N2-C12-C11 = 178.3(3)	C11-C6-N1-C5 = -169.0(3)	C20-C13-N2-C12 = -63.9(3)	N2-C12-C11-C6 = -148.9(3)	O5-C20-C13-N2 = 156.2(3)	N1-C6-C11-C12 = -6.7(4)
Peptide 4B	N1-C5-O1-C2 = 177.6(2)	C6-N1-C5-O1 = -170.5(2)	C13-N2-C12-C11 = -178.4(2)	C11-C6-N1-C5 = -169.6(2)	C20-C13-N2-C12 = 63.9(2)	N2-C12-C11-C6 = -148.5(2)	O5-C20-C13-N2 = -156.4(2)	N1-C6-C11-C12 = 6.7(3)
Peptide 4C	N1-C5-O1-C1 = -171.7(3)	C6-N1-C5-O1 = 175.4(3)	C14-N2-C13-C6 = 178.6(3)	C13-C6-N1-C5 = -108.2(3)	C19-C14-N2-C13 = 162.9(3)	N2-C13-C6-N1 = 147.3(3)	O5-C20-C19-C14 = -177.2(3)	N2-C14-C19-C20 = 4.0(5)
Peptide 4D	N1-C5-O1-C1 = 171.8(3)	C6-N1-C5-O1 = -175.4(2)	C14-N2-C13-C6 = -178.6(2)	C13-C6-N1-C5 = 108.4(3)	C19-C14-N2-C13 = -162.9(3)	N2-C13-C6-N1 = -147.4(2)	O5-C20-C19-C14 = 177.0(2)	N2-C14-C19-C20 = -4.0(4)

Table 4.3. Hydrogen bonding parameters of crystal of peptides

Type	H···A(Å)	D···A(Å)	D-H···A(º)
Peptide 4A			
N1-H1···O3	2.00	2.6960(3)	137
N2-H2···O2	2.16	3.0095(3)	169
Peptide 4B			
N1-H1···O3	2.00	2.696(3)	137
N2-H2···O2	2.16	3.010(3)	169
Peptide 4C			
N2-H2···O4	1.98	2.662(4)	135
N1-H1···O3	2.03	2.894(4)	173
Peptide 4D			
N2-H2···O4	1.98	2.661(4)	135
N1-H1···O3	2.03	2.894(4)	173

Table 4.4. Crystallographic refinement details for Peptides

Parameters	**Boc-Ant-L-Phg-OMe (4A)**	**Boc-Ant-D-Phg-OMe (4B)**	**Boc-L-Phg-Ant-OMe (4C)**	**Boc-D-Phg-Ant-OMe (4D)**
Formula	C_{21} H_{24} N_2 O_5	C_{21} H_{24} N_2 O_5	C_{21} H_{24} N_2 O_5	C_{21} H_{24} N_2 O_5
Fw	384.42	384.42	384.42	384.42
Crystal system	Monoclinic	Monoclinic	Triclinic	Triclinic
Space group	*P2(1)*	*P 21*	*P-1*	*P-1*
a/Å	9.9889(9)	9.967(7)	10.5740(6)	10.5787(6)
b/Å	10.8567(12)	10.881(8)	10.9521(7)	10.9535(6)
c/Å	9.9953(10)	9.994(7)	11.4570(8)	11.4597(7)
α/°	90.00	90.00	109.580(2)	109.577(2)
β/°	105.531(3)	105.28(2)	98.665(2)	98.666(2)
γ/°	90.00	90.00	117.163(2)	117.160(2)
V/Å^3	1044.38(18)	1045.5(13)	1036.68(11)	1037.58(10)
Z	2	2	2	2
D_c/g cm^{-3}	1.222	1.221	1.232	1.230
μ Mo K_α/mm^{-1}	0.088	0.088	0.088	0.088
F000	408	408	408.0	408
T/K	296(2)	296(2)	296(2)	296(2)
θ max.	24.99	24.98	25.00	25.00
Total no. of reflections	24291	22462	15191	30304
Independent reflections	3657	3653	3648	3654
Observed reflections	2708	3204	2224	2472
Parameters refined	258	259	257	258
R_1, I > 2σ(I)	0.0468	0.0377	0.0586	0.0541
wR_2, I > 2σ(I)	0.1252	0.1122	0.1659	0.1599
GOF (F^2)	0.869	0.921	1.068	0.970
CCDC No.	2119283	2119284	2119285	2119286

Chapter 5

Significant change in morphology through replacement of Phe by Trp: molecular-level insights

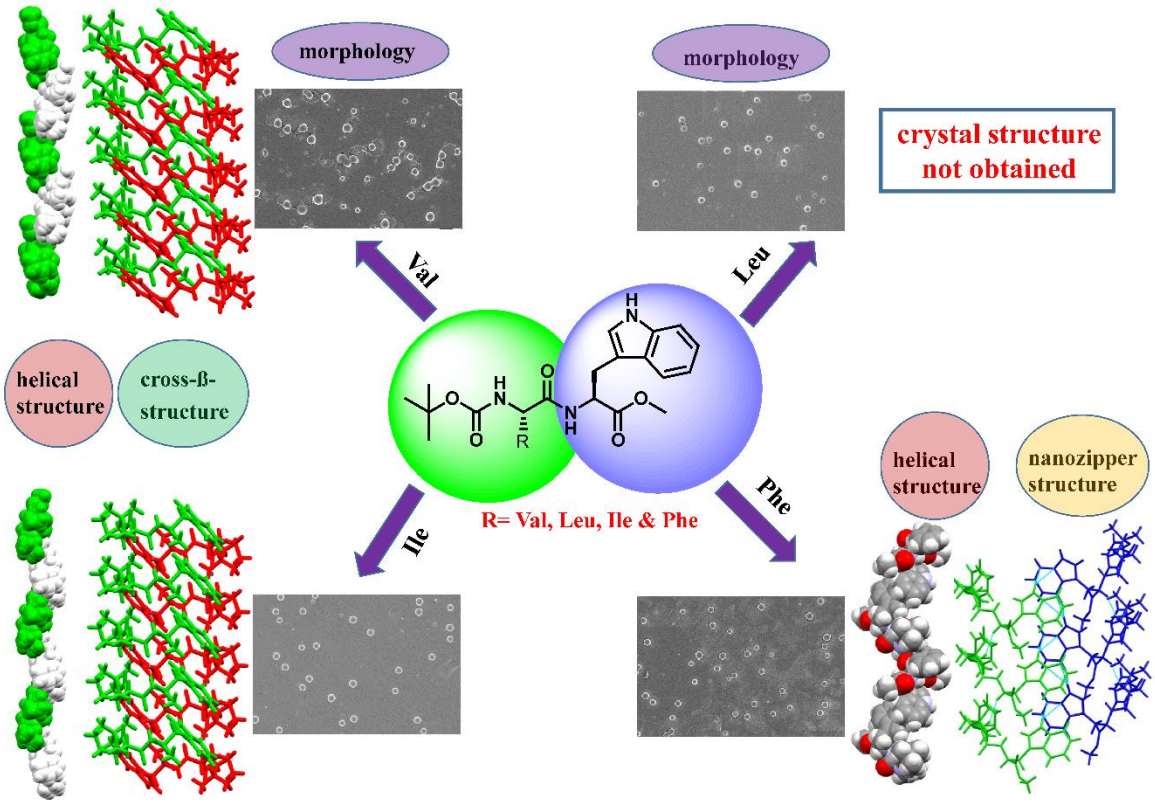

5.1. Background

In chapters 3 and 4, we discussed the conformation, morphology, and self-assembly diversity of terminally protected dipeptides depending on protecting group and alternation of the peptide sequence. Self-aggregation of the central hydrophobic region ($A\beta_{18-20}$) of $A\beta_{42}$ peptide is mainly responsible for fibril formation and causes Alzheimer's disease.[1] Very few works are available for inhibiting fibril formation of short peptides by modification of amyloidogenic sequence.[2,3] Tryptophan residue is involved in forming the novel structural motif and functional materials.[4,5] Moreover, Various Trp-conjugates play function as an inhibitor and anti-aggregating agents for fibril formation.[6,7] By this inspiration, we replaced the Phe residue with Trp in amyloidogenic dipeptide sequences and investigated their conformational and morphological change.

5.2. Design of peptides

At first, we designed four tryptophan-containing terminally protected dipeptides by replacing Phe with Trp of Val-Phe ($A\beta_{18-19}$) and Phe-Phe ($A\beta_{19-20}$) peptide and other two dipeptides. Such as Boc-Val-Trp-OMe (**VW**), Boc-Leu-Trp-OMe (**LW**), Boc-Ile-Trp-OMe (**IW**), Boc-Phe-Trp-OMe (**FW**) (Figure 5.1).

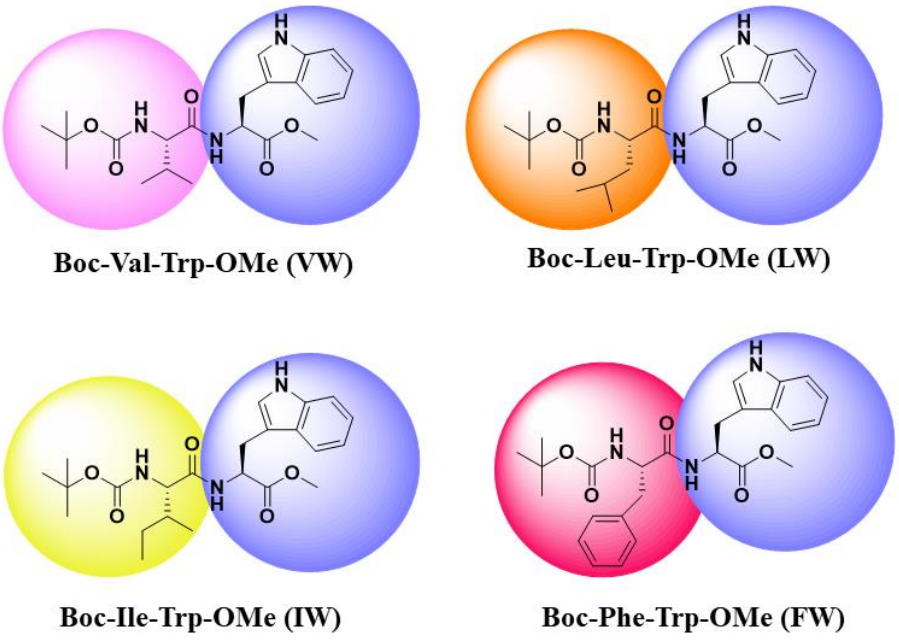

Figure 5.1. *Chemical structures of designed di-peptides*

5.3. Synthesis and characterization of the designed peptides

To perform the experiment, the designed terminally protected dipeptides were initially synthesized in solution using a conventional methodology (Scheme 5.1).[8] We also synthesized corresponding Phe containing dipeptides by a similar methodology. The purified peptides were characterized by 1D ^{1}H and ^{13}C NMR spectroscopy and Mass spectrometry.

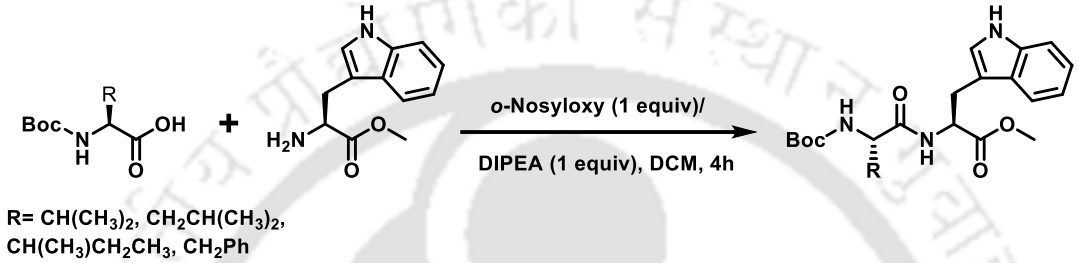

Scheme 5.1. *Schematic representation of the synthesis of dipeptides in solution*

5.4. Morphology analysis

Firstly, the field emission scanning electron microscopy (FESEM) was used to investigate the morphology. For this purpose, each of the peptides was dissolved in a 1:1 acetonitrile-water mixture, each with a concentration of 1.5 mM. The peptide solutions were incubated for four days at 37 °C, and FESEM images were recorded. Interestingly, FESEM images of all designed peptides displayed a similar kind of spherical structure in solution (Figure 5.2a, 5.2c, 5.2e, 5.2g). The diameter of spheres varies from nm to μm range. Although, their peptide backbone contains different aliphatic and aromatic amino acids in each peptide sequence.

Furthermore, we also investigated the morphology of peptides **VF**, **LF**, and **FF** under identical conditions. Interestingly, peptides displayed various fiber structures (Figure 5.2b, 5.2d, 5.2h).[2,9] Our previously reported **IF** peptide also formed a fiber-like structure under an identical condition to this work (Figure 5.2f).[10] Therefore, a morphological transition from fiber to spherical structure occurred just by replacing phenylalanine with tryptophan.

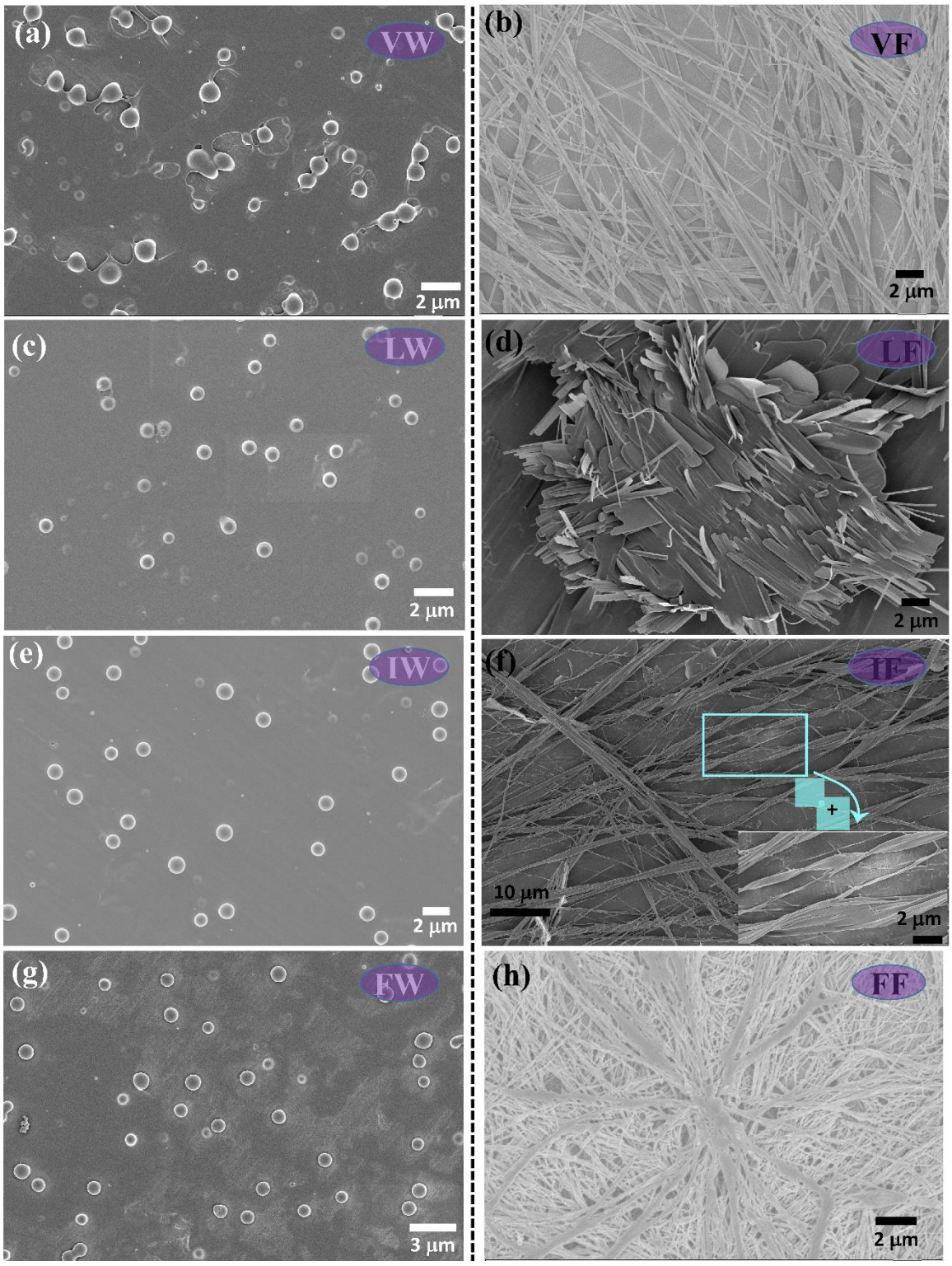

Figure 5.2. *FESEM images (a, c, e, g) displaying spherical morphology of terminally protected peptides* ***VW***, ***LW***, ***IW***, *and* ***FW***, *respectively. (b, d, f, h) displaying various fibrillary morphology of corresponding Phe containing dipeptides such as* ***VF***, ***LF***, ***IF***, *and* ***FF***. *Image (f) taken from J. Mol. Str.* ***2020***, *1221, 128877.*

Next, the morphology of the peptides was also investigated by AFM. To perform this experiment, the above-mentioned peptide solutions of 1.5 mM were diluted to 30 μM solutions after four days of incubation. A small amount of these solutions was placed over the microscopic slide and allowed to dry; AFM analysis was carried out with these dried samples. All the designed peptides formed spherical morphology like FESEM (Figure 5.3a, 5.3c, 5.3e, 5.3g). Reported terminally protecting **VF** and **FF** peptides sample in 2:1 MeOH: H_2O displayed fibrilar morphology in AFM (Figure 5.3b, 5.3h). **LF** and **IF** peptides also displayed different fibrillar morphology (Figure 5.3d, 5.3f). All the microscopic technique reveals that tryptophan-containing four dipeptides displayed spherical morphology, where all corresponding Phe containing dipeptides formed various length fiber structures. So, the total morphological change observed was just an alternation of one aromatic amino acid.

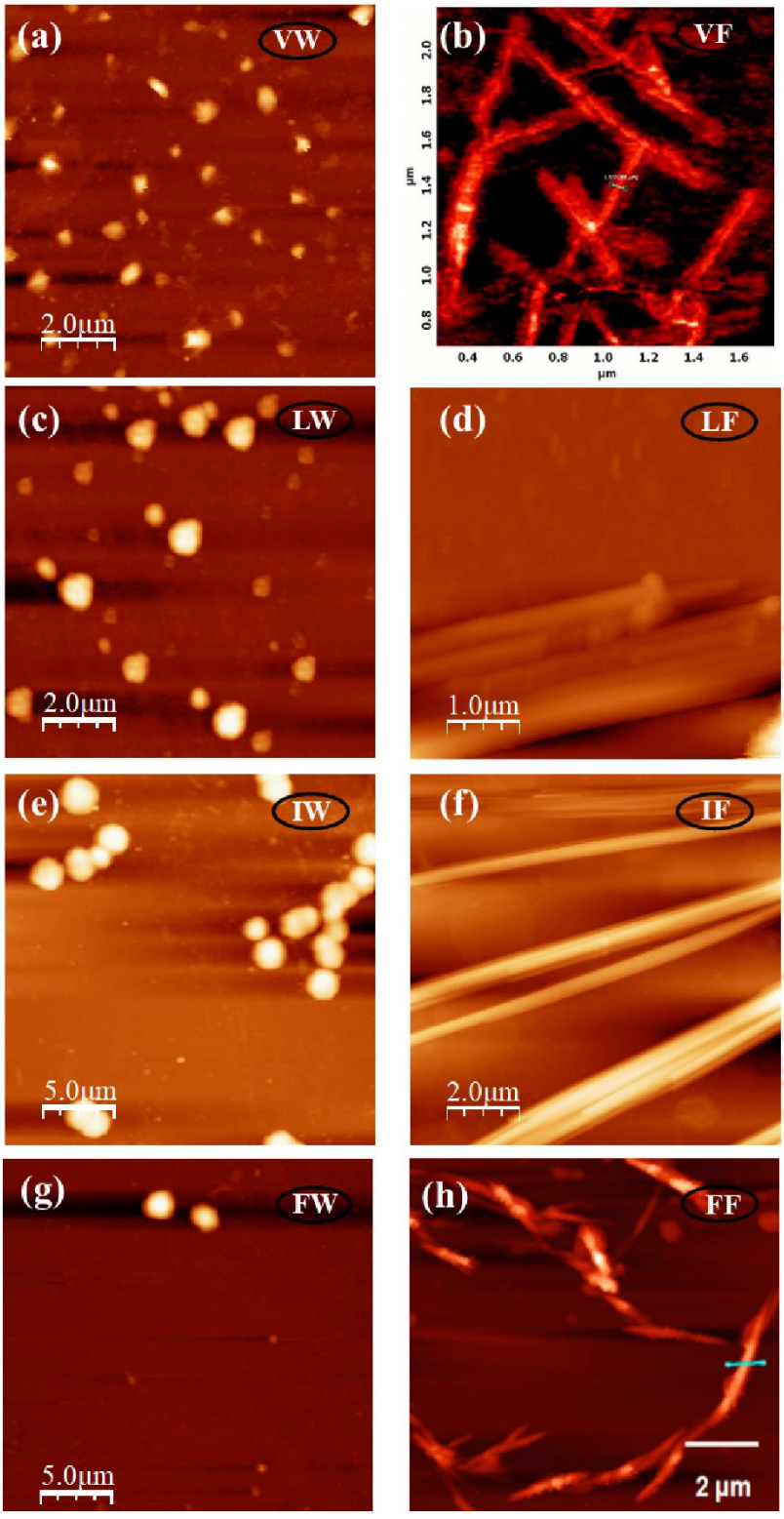

Figure 5.3*. AFM images (a, c, e, g) displaying spherical morphology of terminally protected peptide* ***VW****,* ***LW****,* ***IW****, and* ***FW****, respectively. (b, d, f, h) displaying various fibrillary morphology of corresponding Phe containing dipeptides such as* ***VF****,* ***LF****,* ***IF****, and* ***FF****. Image (b, h) taken from Org. Biomol. Chem.* ***2011****, 9, 3787 and Cryst. Growth Des.* ***2014****, 14, 1032, respectively.*

5.5. Conformation analysis by CD experiment in solution

After that, Circular Dichroism (CD) spectroscopy was carried out to obtain information about the secondary structure conformation of dipeptides. Peptide solutions of 1.5 mM after incubation for four days were diluted to 750 μM solution (to suppress the overvoltage in CD) in 50% acetonitrile-water, and CD analysis was performed. All peptides displayed a strong positive cotton effect near 230 nm due to the presence of tryptophan residue.[11] The three aliphatic-aromatic amino acids containing peptides (**VW**, **LW**, and **IW**) exhibited an almost similar negative band around 195-217 nm, indicating the presence of a mixture of β-sheet and random coil structure (Figure 5.4a, 5.4c, 5.4e). Moreover, aromatic-aromatic amino acid (**FW**) bearing peptides showed different positive bands at 198 nm and negative bands (195 nm and 213 nm), suggesting the existence of a mixture of β-sheet and β-turn structures (Figure 5.4g). The secondary structure conformation determination of those peptides is difficult. This may be due to the coexistence of multiple secondary conformations.

Furthermore, we performed CD experiment of phenylalanine containing dipeptides, and for this, 4-days incubated 1.5 mM peptide solution in 50% acetonitrile-water diluted to 375 μM to prevent high HT voltage. On the contrary, **VF**, **LF**, and **IF** displayed two positive bands at 196 nm and around 217 nm indicating the existence of a mixture of β-sheet and β-turn conformations in solution (Figure 5.4b, 5.4d, 5.4f). Peptide **FF** exhibited two positive cotton effects at 197 nm and 220 nm suggesting the presence of β-strand structure (Figure 5.4h). Therefore, the above observation suggests that protected Trp and Phe containing different dipeptides exhibited significantly different cotton effects in CD spectra.

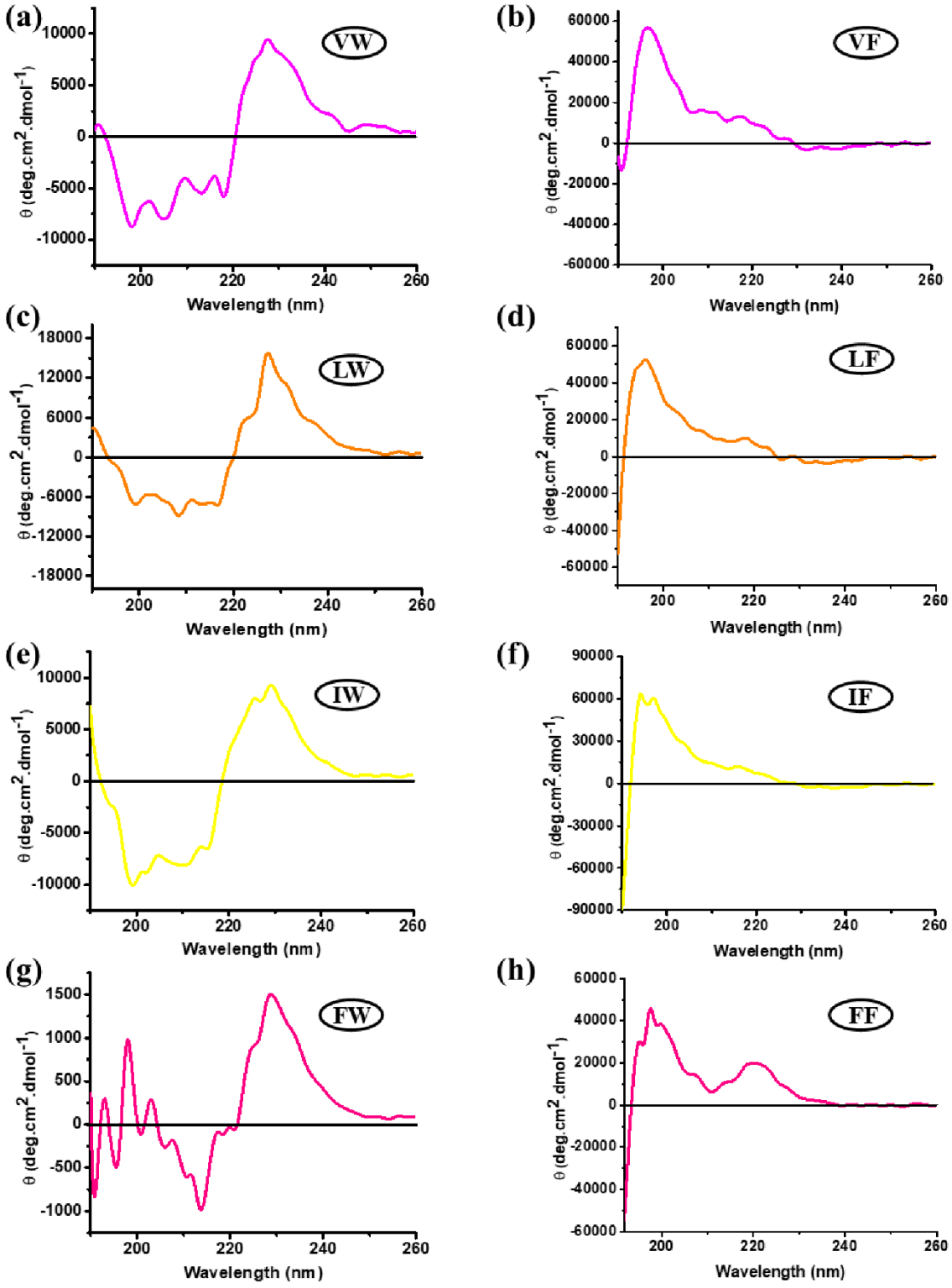

Figure 5.4. *(a, c, e, g) represents CD spectra of 4 days incubated 750 μM peptide solution of* ***VW***, ***LW***, ***IW*** *and* ***FW*** *in 50% ACN/H_2O, respectively. (b, d, f, h) represents CD spectra of 4 days incubated 375 μM peptide solution of* ***VF***, ***LF***, ***IF*** *and* ***FF*** *in 50% ACN/H_2O, respectively.*

5.6. Investigation of secondary structure by FT-IR

Next, solid-state FT-IR of all peptide aggregate mass obtained from ACN/H_2O was performed to investigate the secondary structural conformation. The IR stretching frequency range 3500-3200 cm^{-1} is very significant for the N-H stretching of the peptide. The region 1800-1500 cm^{-1} is an indicative band for the amide I, amide II (bending peak), and urethane groups (hydrogen-bonded). A characteristic peak at around 3322 cm^{-1} (**VW**, **IW**) and 3277 cm^{-1} (**LW**, **FW**) indicate the presence of strongly hydrogen-bonded NH groups. Moreover, the intense peak at around 3382-3410 cm^{-1} was observed, suggesting all NH groups had not been participating in the intermolecular hydrogen bonding of all peptides. The amide I band at 1736, 1689, 1652 $cm^{-1,}$ and amide II bands at 1522 cm^{-1} indicated the presence of a strongly hydrogen-bonded network for **VW**. In the case of **LW**, amide I bands at 1746, 1663 cm^{-1} and amide II band at 1504 cm^{-1} suggested the existence of widely hydrogen-bonded networks. **IW** displayed an almost similar IR stretching band. The obtained IR stretching band of amide I and amide II suggests the presence of a hydrogen-bonded β-sheet structure in solid-state. For **FW**, amide I bands at 1751, 1688 cm^{-1}, and amide II band 1517 cm^{-1} also indicated the availability of the hydrogen-bonded antiparallel network (Figure 5.5). The IR spectra of reported protecting **VF** and **FF** peptides showed little difference in stretching frequency compared to **VW** and **FW**.

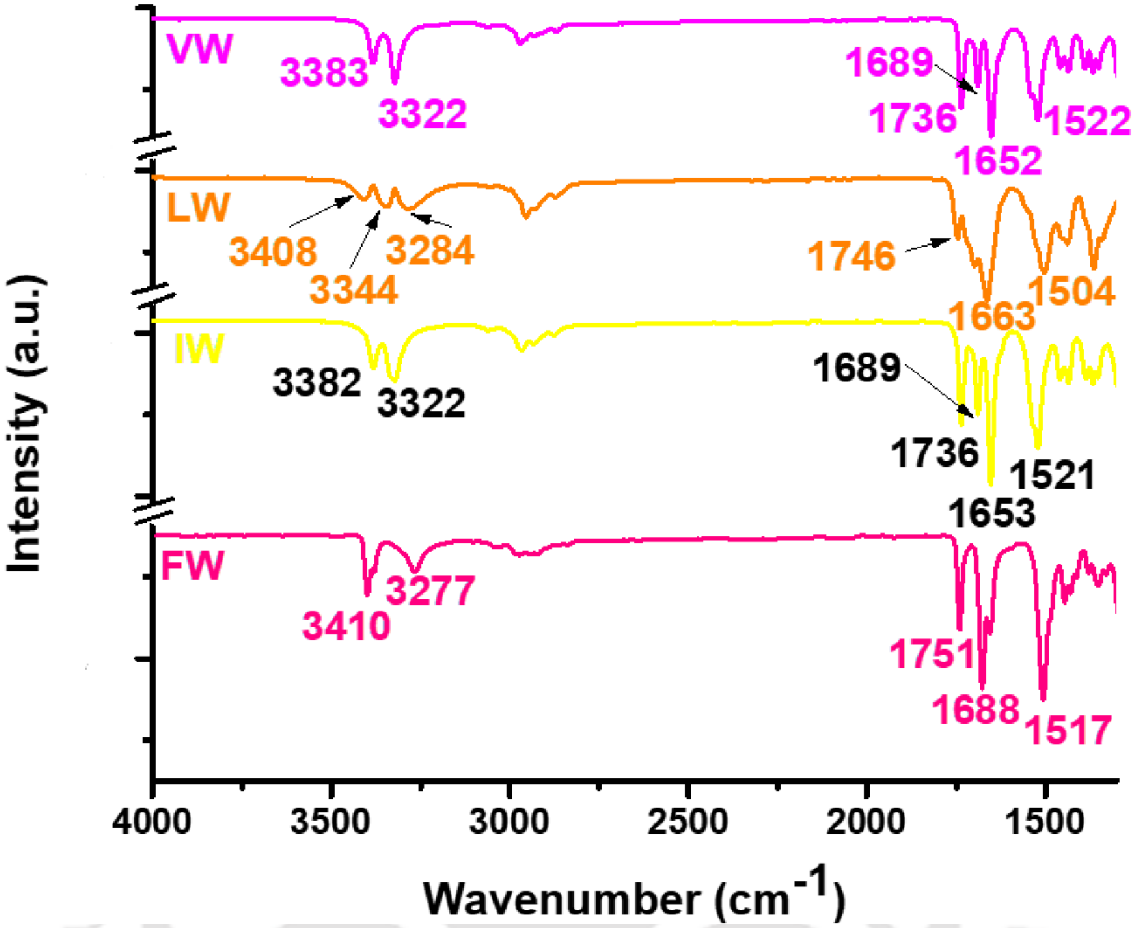

Figure 5.5. *FT-IR spectra of 4 days incubated peptide aggregate of* ***VW****,* ***LW****,* ***IW****, and* ***FW*** *in solid-state, respectively.*

5.7. Investigation of self-assembly process by SC-XRD

Next, to obtain atomic-level structural information and self-assembly in solid-state, single-crystal X-ray diffraction (SC-XRD) was performed. The slow evaporation of acetonitrile-water at room temperature provided a colorless well-ordered single crystal of peptide **VW**, **IW**, and **FW**. However, we did not get a crystal of peptide **LW** under a similar crystalline condition.

The peptide **VW** crystalizes in a Monoclinic crystal system with *P 21* space group and contains one molecule in its asymmetric unit. Two monomeric units are strongly interlinked via two intermolecular hydrogen bonds between i) Boc C=O and Val NH (N1-H1···O2, 2.16 Å, 2.97 Å, 157^{o}), ii) Val C=O and Trp NH (N2-H2···O3, 2.14 Å, 3.00 Å, 176^{o}). Moreover, both subunits can intermolecularly hydrogen-bonded through Trp C=O and Trp (indole group) NH (N3-H3···O4, 2.12 Å, 2.97 Å, 168^{o}). However, the Parallel β-sheet structure was formed via regularly interconnected two backbone containing H-bond interaction along the crystallographic *a*-axis. (Figure 5.6a) In higher-order supramolecular packing, peptide **VW** self-organises to multi-layer cross β-sheet structure with both the meridional 5.0 Å distance (the separation between two backbones within one β-sheet) and the equatorial 9.0 Å distances (the distance between layers) along crystallographic *a*-axis (Figure 5.6b). By using Trp C=O and Trp (indole group) NH hydrogen bond, it formed helical arrangement along *b*-axis (Figure 5.6a, 5.6b). **VW** peptide also formed sheet-like layer structure through various intermolecular hydrogen bonds and weak non-covalent interaction along *b*-axis (Figure 5.7).

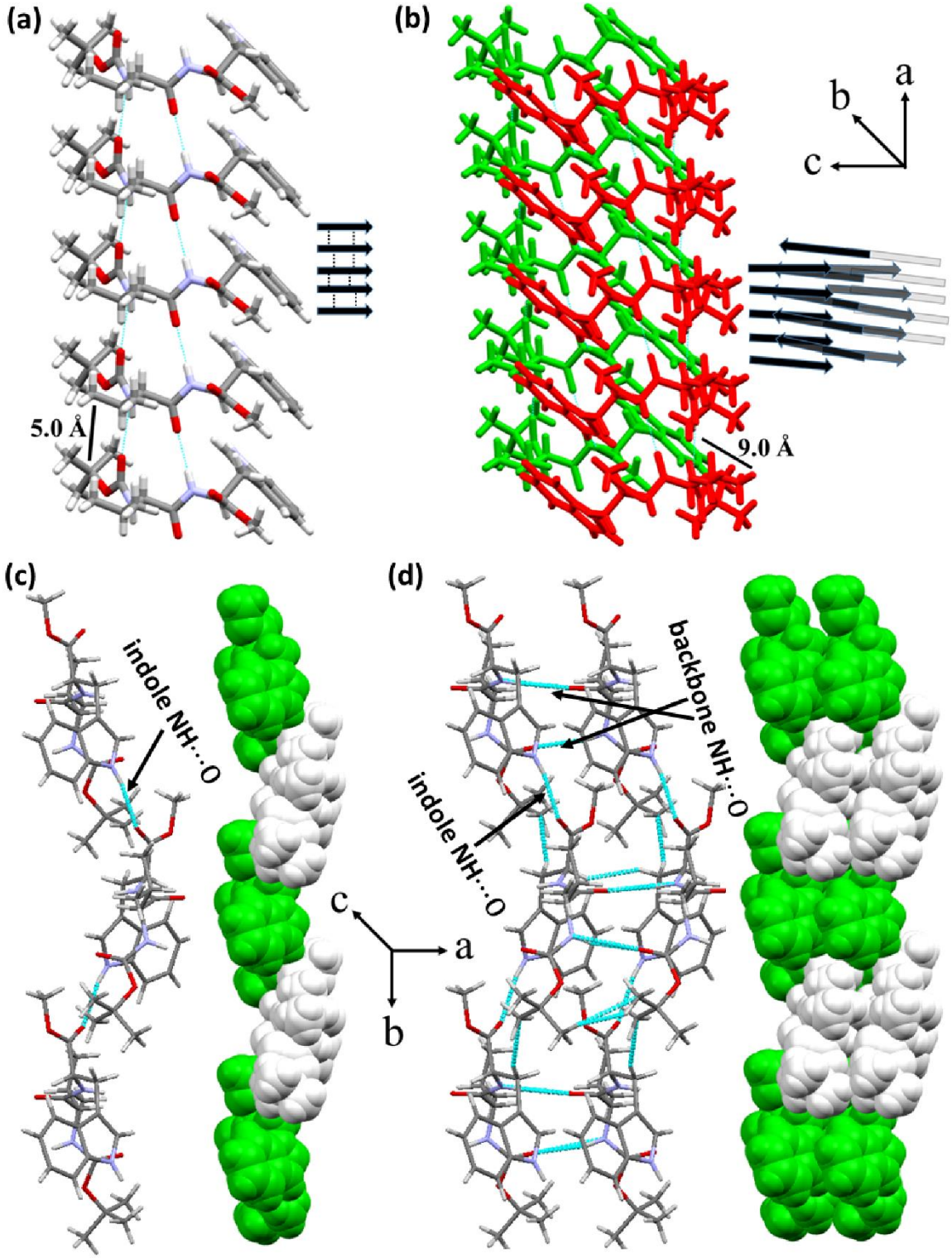

Figure 5.6. *(a) Parallel β-sheet architecture via intermolecular hydrogen bond, (b) Supramolecular cross-β-structure of* ***VW*** *peptide at higher-order molecular packing along a-axis, (c, d) supramolecular helical arrangement via intermolecular hydrogen bond along b-axis of peptide* ***VW****.*

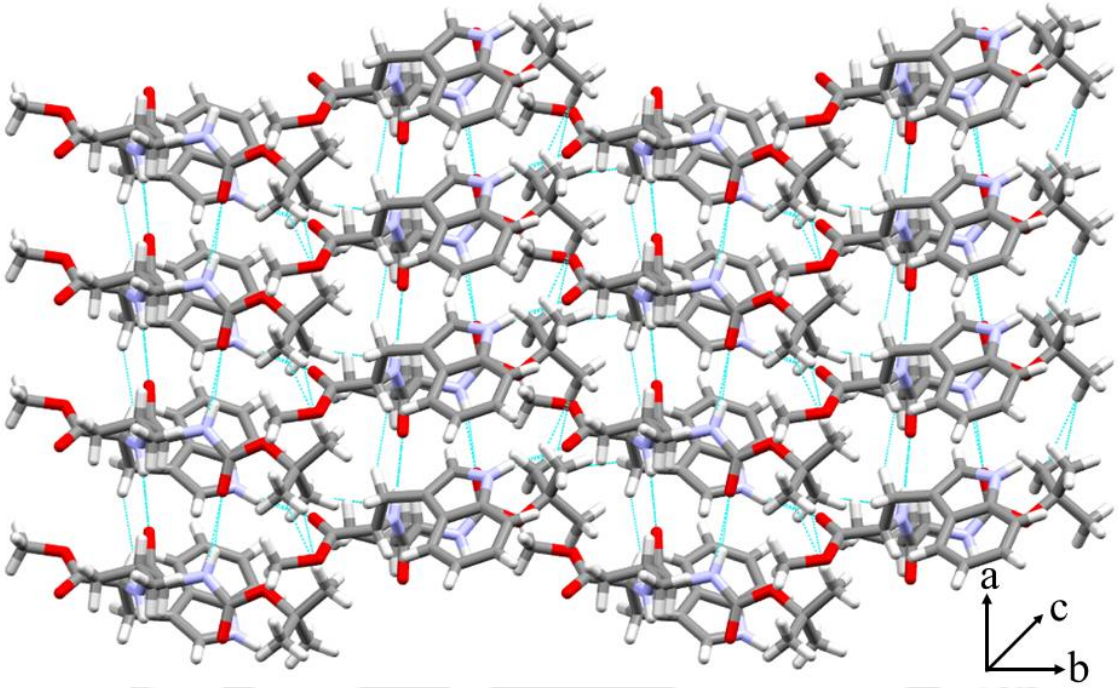

Figure 5.7. *Sheet-like layer structure formation through intermolecular hydrogen bond and various non-covalent interactions at higher-order self-assembly along b-axis of peptide* ***VW****.*

Compared to **VF**[9] peptide, **VW** also formed parallel β-sheet and cross-β-structure structure through two similar kinds of intermolecular H-bonding in the backbone, but two extended contacts (Trp NH and carbonyl 'O') available for another intermolecular H-bonding for **VW** (Figure 5.8a, 5.8b). Which interconnected two tryptophan through intermolecular H-bonding (indole ring NH···O=C) (Figure 5.8c). This extra H-bonding generates various supramolecular arrangements, such as helical and sheet-like layer architecture discussed earlier. Moreover, in higher-order crystal packing, **VW** exhibited a discontinued supramolecular zigzag arrangement which stabilized through indole NH···O (2.122 Å) interaction, and **VF** displayed a different discontinued helical arrangement stabilized through aromatic CH···HC (2.391 Å) interaction (Figure 5.8c, 5.8d). This different kind of molecular arrangement for **VW** than **VF** may be a reasonable driving force for generated spherical rather than fibrous morphology.

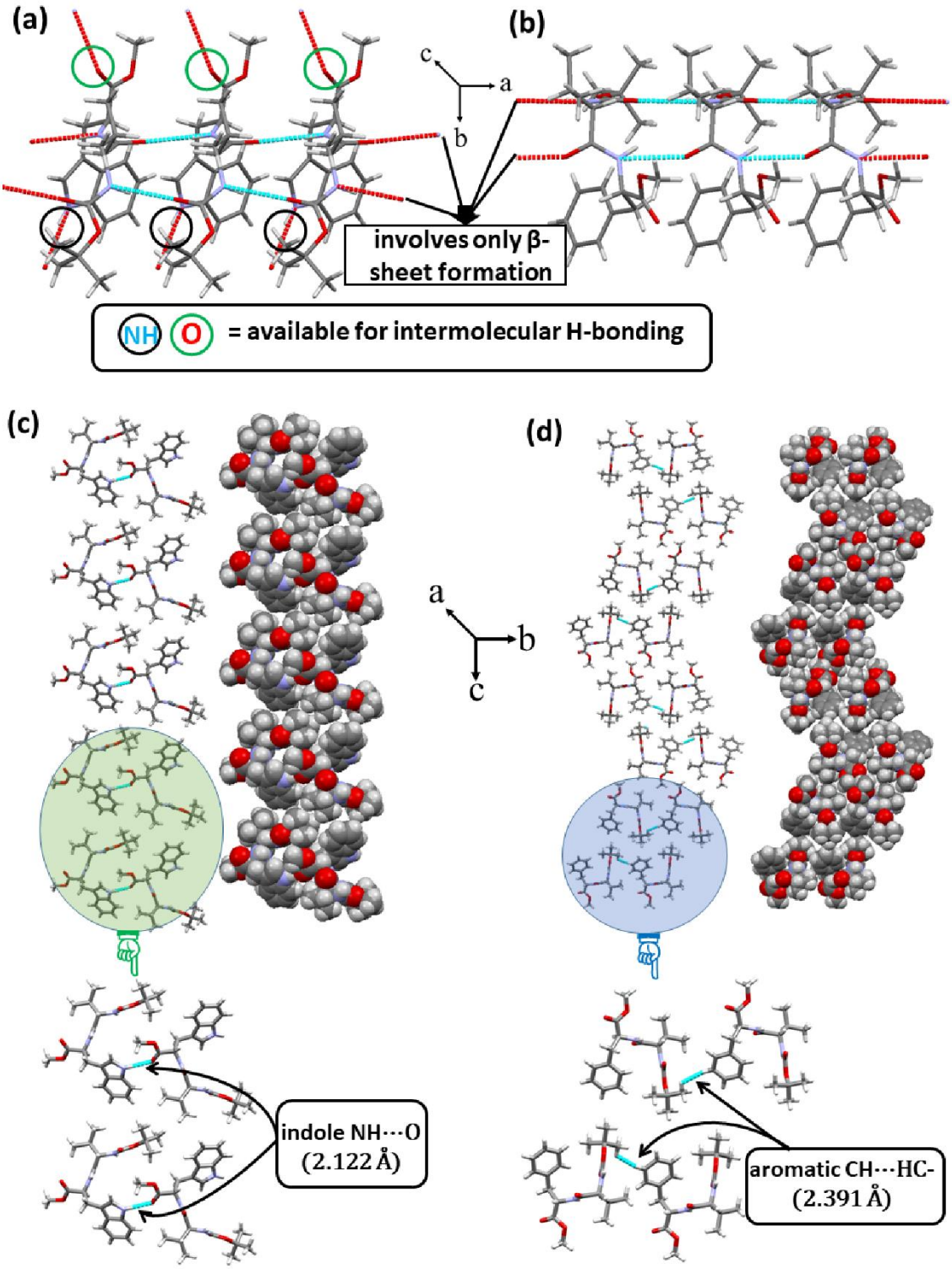

Figure 5.8. *(a, b) represents parallel β-sheet structure of* ***VW*** *and* ***VF****, respectively (c) Supramolecular zigzag arrangement of* ***VW*** *peptide at higher-order molecular packing, (d) supramolecular helical arrangement of* ***VF*** *peptide at higher-order molecular packing. Crystallographic data of* ***VF*** *peptide taken from Org. Biomol. Chem.* ***2011****, 9, 3787. (CCDC No.- 801305).*

The peptide **IW** crystalizes in a Monoclinic crystal system with *P2(1)* space group and contains one molecule in its asymmetric unit. Two monomeric units are strongly interlinked via two intermolecular hydrogen bonds between i) Boc C=O and Val NH (N1-H1···O2, 2.20 Å, 3.00 Å, 155^{o}), ii) Val C=O and Trp NH (N2-H2···O3, 2.15 Å, 3.00 Å, 171^{o}). Moreover, both subunits can intermolecularly hydrogen-bonded through Trp C=O and Trp (indole group) NH (N3-H3···O4, 2.16 Å, 3.00 Å, 167^{o}). However, the Parallel β-sheet structure was formed via regularly interconnected two backbone containing H-bond interaction along the crystallographic *a*-axis (Figure 5.9a). In higher-order supramolecular packing, peptide **IW** self-organizes to multi-layer cross β-sheet structure with both the meridional 5.0 Å distance (the between two backbones within one β-sheet) and the equatorial 9.0 Å distances (the distance between layers) along crystallographic *a*-axis (Figure 5.9b). By using Trp C=O and Trp (indole group) NH hydrogen bond, it formed helical arrangement along *b*-axis (Figure 5.9c, 5.9d). **IW** peptide also formed sheets-like layer structures through various strong intermolecular hydrogen bonds and weak non-covalent interactions along *c*-axis (Figure 5.10).

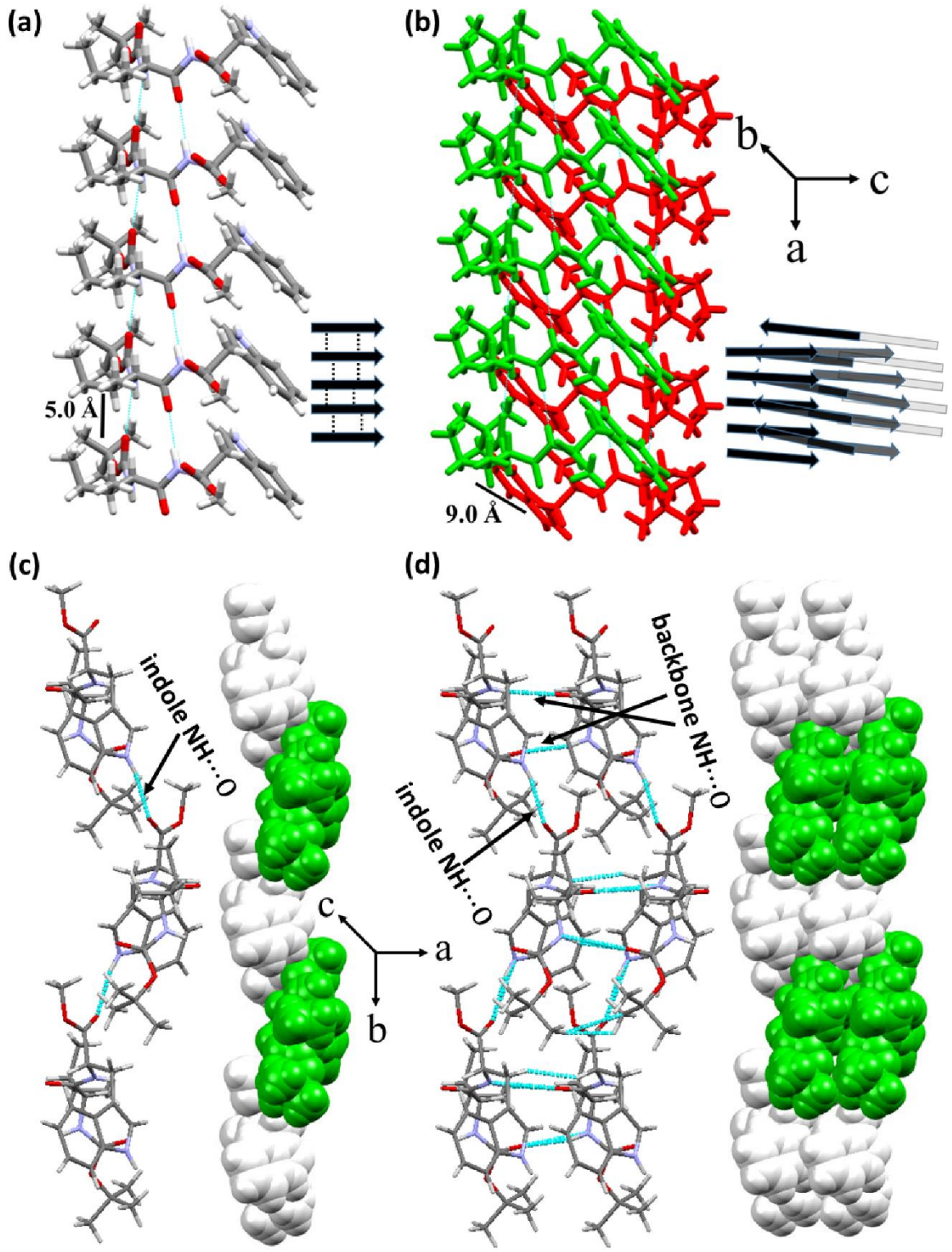

Figure 5.9. *(a) Parallel β-sheet architecture via an intermolecular hydrogen bond, and (b) Supramolecular cross-β-structure of* ***IW*** *peptide at higher-order molecular packing along a-axis, (c, d) supramolecular helical arrangement via intermolecular hydrogen bond along b-axis of peptide* ***IW****.*

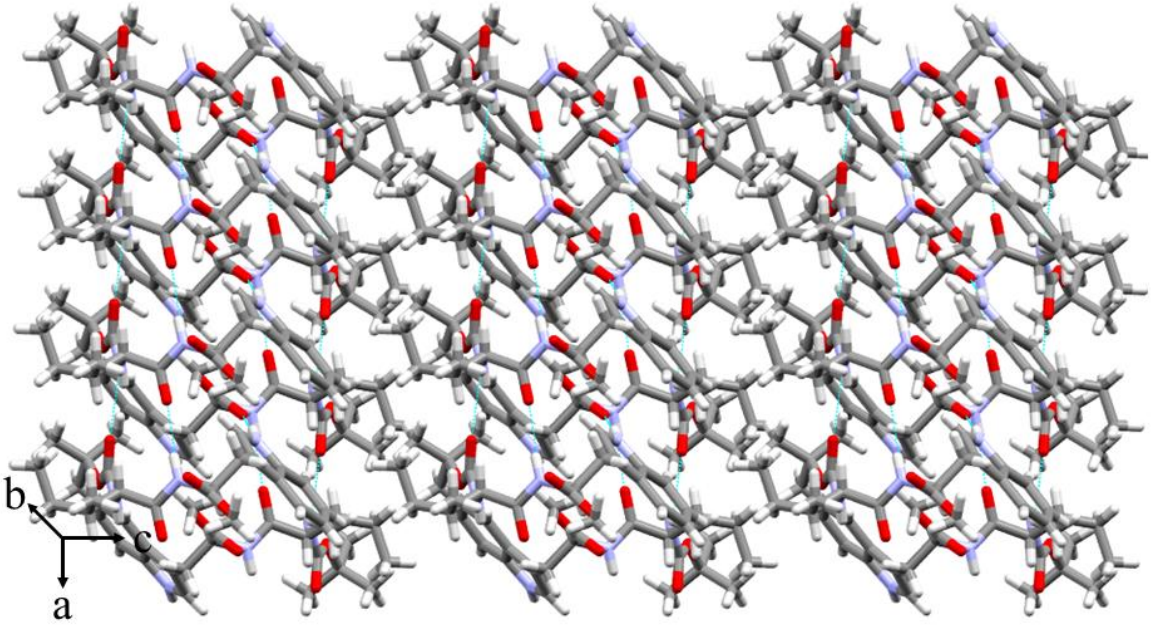

Figure 5.10. *Sheet-like layer structure formation through intermolecular hydrogen bond and various non-covalent interactions at higher-order self-assembly along c-axis of peptide* ***IW****.*

In comparison to **IF**[10] peptide, **IW** also formed parallel β-sheet structure through two similar kinds of intermolecular H-bonding in the backbone, but two extended contacts (Trp NH and carbonyl 'O') available for another intermolecular H-bonding for **IW** (Figure 5.11a, 5.11b), which interconnected two tryptophan through intermolecular H-bonding (indole ring NH···O=C) (Figure 5.11c). This extra H-bonding generates various supramolecular arrangements such as helical and sheet-like layer architecture discussed earlier. Moreover, in higher-order crystal packing, **IW** exhibited discontinued supramolecular zigzag arrangement, which stabilized through indole NH···O (2.158 Å) interaction, and IF displayed different discontinued helical arrangement stabilized through aromatic CH···C (2.885 Å) and CH···O (2.636 Å) interaction (Figure 5.11c, 5.11d). This different molecular arrangement for **IW** than **IF** may be a plausible driving force for generated spherical morphology rather than fibrous morphology.

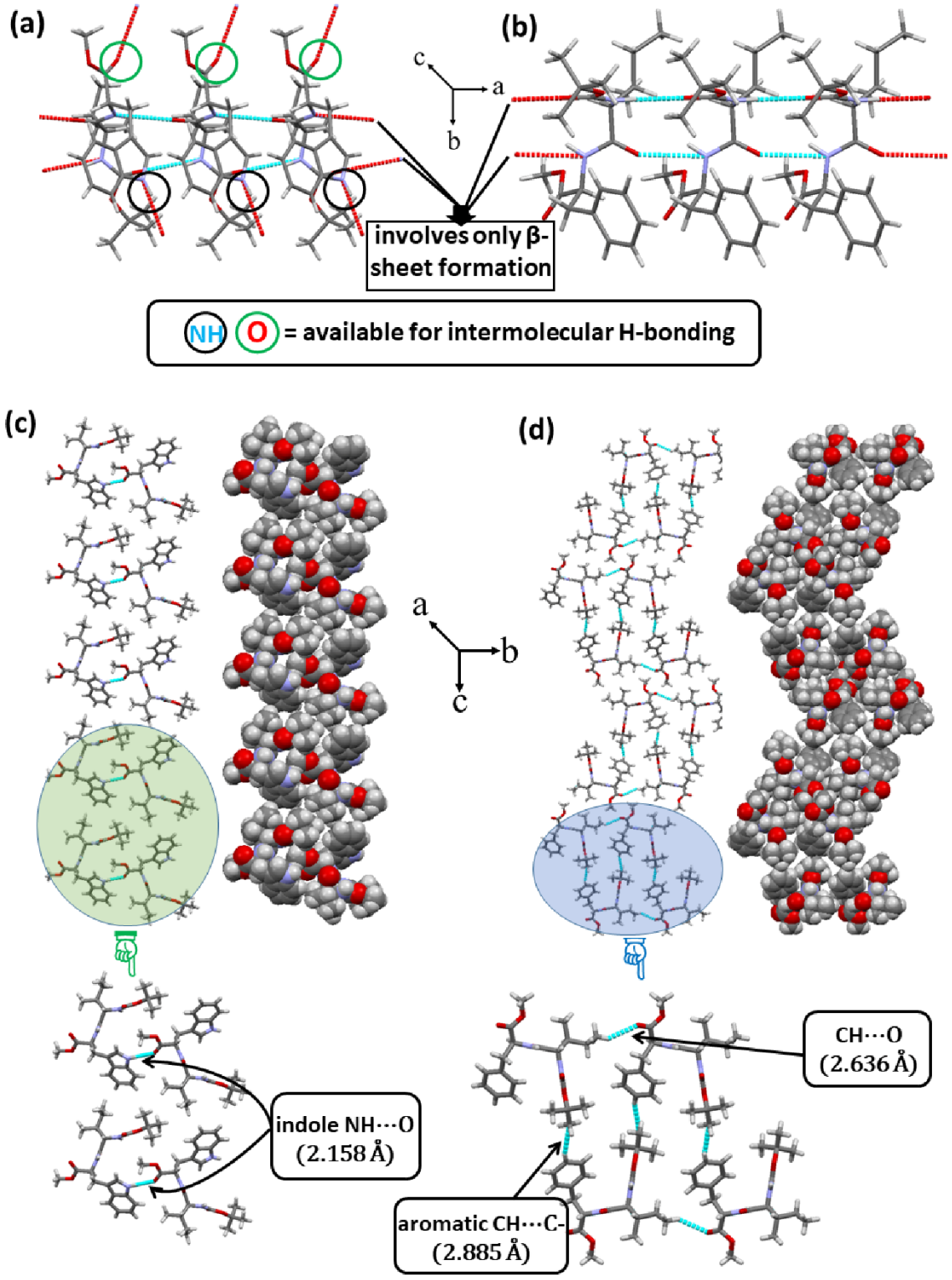

Figure 5.11. *(a, b) represents the parallel β-sheet structure of* ***IW*** *and* ***IF****, respectively (c) Supramolecular zigzag arrangement of* ***IW*** *peptide at higher-order molecular packing, (d) supramolecular helical arrangement of* ***IF*** *peptide at higher-order molecular packing. Crystallographic data of* ***IF*** *peptide is taken from J. Mol. Str.* ***2020****, 1221, 128877(CCDC No.-1973966).*

The peptide **FW** crystalizes in an Orthorhombic crystal system with *p_21_21_21* space group and contains one molecule in its asymmetric unit (Figure 5.12a). Its inverse γ-turn conformation, commonly called the open turn, is recognized by the lack of any intramolecular hydrogen bond (Figure 5.12b). Interestingly, dipeptide **FF** formed inverse γ-turn conformation, which differs in only a slight backbone torsion angle compared to peptide **FW**. Peptide molecule stabilized through one intermolecular hydrogen bond between Phe C=O and NH (N1-H1···O3, 2.42 Å, 2.95 Å, 119°) and tryptophan NH-π interaction (average distance 2.804 Å) and made antiparallel β-sheet structure along crystallographic b axis (Figure 5.12c, 5.12d).

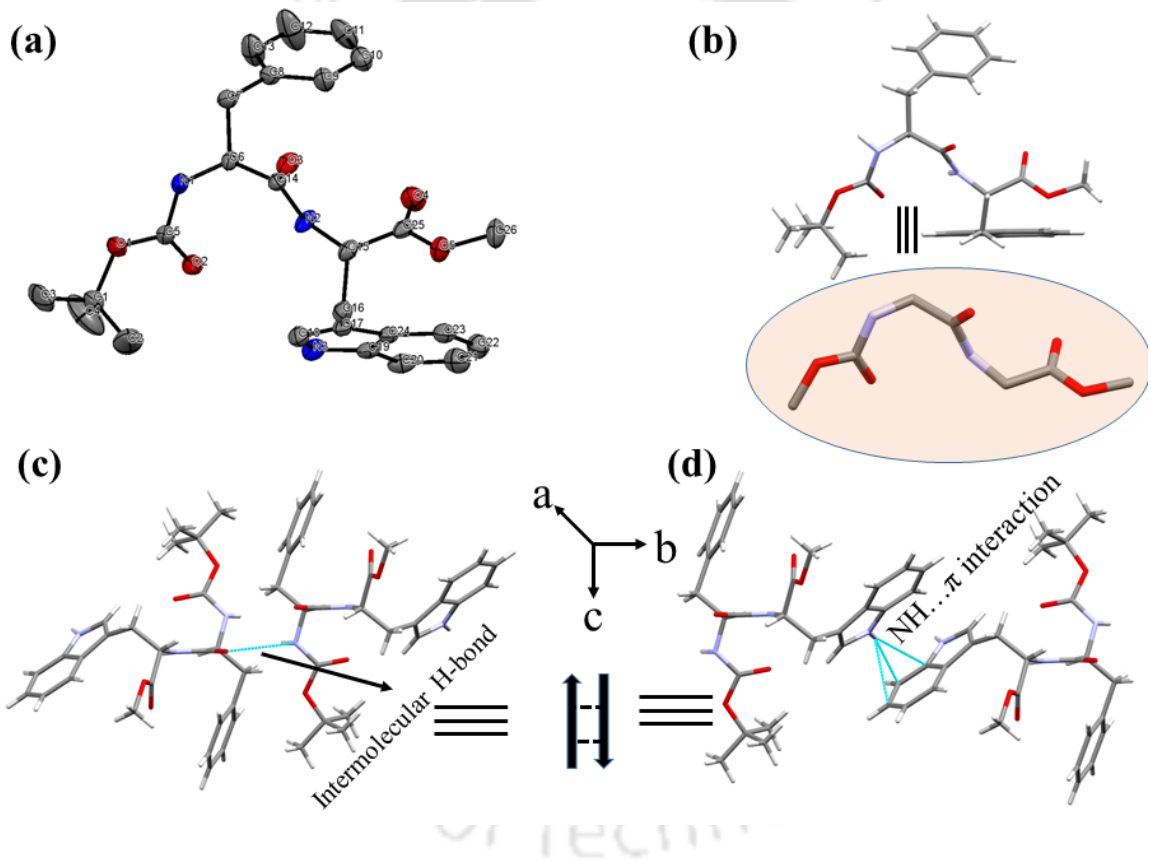

Figure 5.12. *(a) ORTEP profile with 30% ellipsoid probability, (b) open turn conformation (c, d) antiparallel β-sheet arrangement via intermolecular H-bond and NH-π (tryptophan) interaction along crystallographic b-axis of* ***FW*** *peptide.*

Moreover, four molecules interlinked via intermolecular hydrogen bond and NH-π interaction formed a four-membered ring structure along the crystallographic *c*-axis (Figure 5.13a). Higher-order self-assembly also created a columnar structure, stabilized by backbone intermolecular H-bond and side-chain aromatic-aromatic interaction (4.108

Å for tryptophan and 4.019 Å for phenylalanine) along *b*-axis (Figure 5.13b). Peptide subunits interlinked via Van der Walls interaction and NH-π hydrogen bonding interaction to form supramolecular nanozipper structure along crystallographic a-axis. The length of each tooth is 6.02 Å, the internal width is 9.14 Å, and the total width is 15.63 Å of the zipper (Figure 5.13c). So, the indole moiety (tryptophan) of Peptide **FW** plays a principal function in zipper formation and interconnects the two zipper columns. To the best of our knowledge, this is the first report of di-peptides-based supramolecular nanozipper structure formation. Moreover, this peptide's sheet-like layer architecture was also noticed along the crystallographic *c*-axis in higher-order packing (Figure 5.13d). Furthermore, **FW** displayed a helical arrangement via intermolecular hydrogen bond and NH-π interaction along the crystallographic *b*-axis (Figure 5.13e, 5.13f).

In comparison to **FF**[2] peptide (presence intramolecular H-bond), **FW** also formed antiparallel β-sheet structure through one similar kind of intermolecular H-bonding in the backbone, but two extended contacts (Trp–indole NH and aromatic benzene ring) available for another NH-π hydrogen bonding interaction for **FW**. (Figure 5.14a, 5.14b) Which interconnected two tryptophan through intermolecular H-bonding (indole ring NH-π) (Figure 5.14c). Although, **FW** formed a columnar structure (Figure 5.13b) like **FF** through intermolecular H-bonding (2.427 Å for **FW** and 2.118 Å for **FF**) and aromatic-aromatic interaction (4.108 Å, 4.019 Å for **FW** and 4.166 Å, 4.001 Å for **FF**), but extra NH-π (average distance 2.804 Å) interaction provided different continuous columnar arrangement (Figure 5.14c) than **FF** (Figure 5.14d). This extra H-bonding generates various supramolecular arrangements such as nanozipper structure, and helical and sheet-like layer architecture discussed earlier. This different molecular arrangement for **FW** than **FF** may be a plausible driving force for generating spherical morphology rather than fibrous morphology.

Hydrogen bonding parameters, Backbone torsion angles (deg), and crystallographic refinement details of peptide **VW**, **IW**, and **FW** have been listed in Table 5.2, Table 5.3, and Table 5.4, respectively. (Section 5.15)

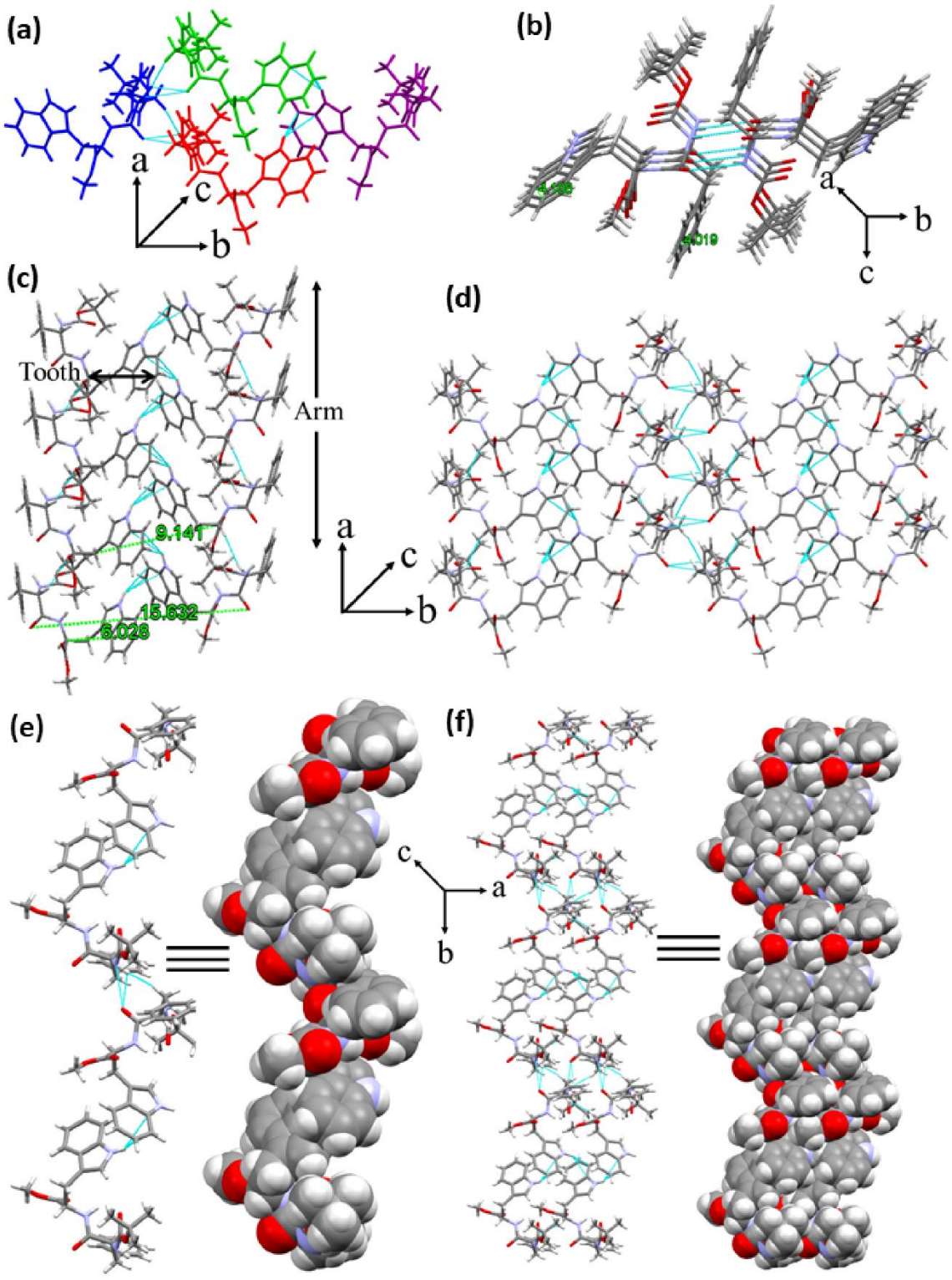

Figure 5.13. *(a) Tetrameric structure via intermolecular H-bonding and NH-π interaction along c-axis, (b) Columnar structure through intermolecular H-bonding and aromatic interaction along a-axis, (c) Supramolecular nanozipper structure along crystallographic a-axis, (d) Sheet like layer structure along the crystallographic c axis, (e, f) Represents helical like arrangement in the supramolecular assembly along b axis of* ***FW*** *peptide.*

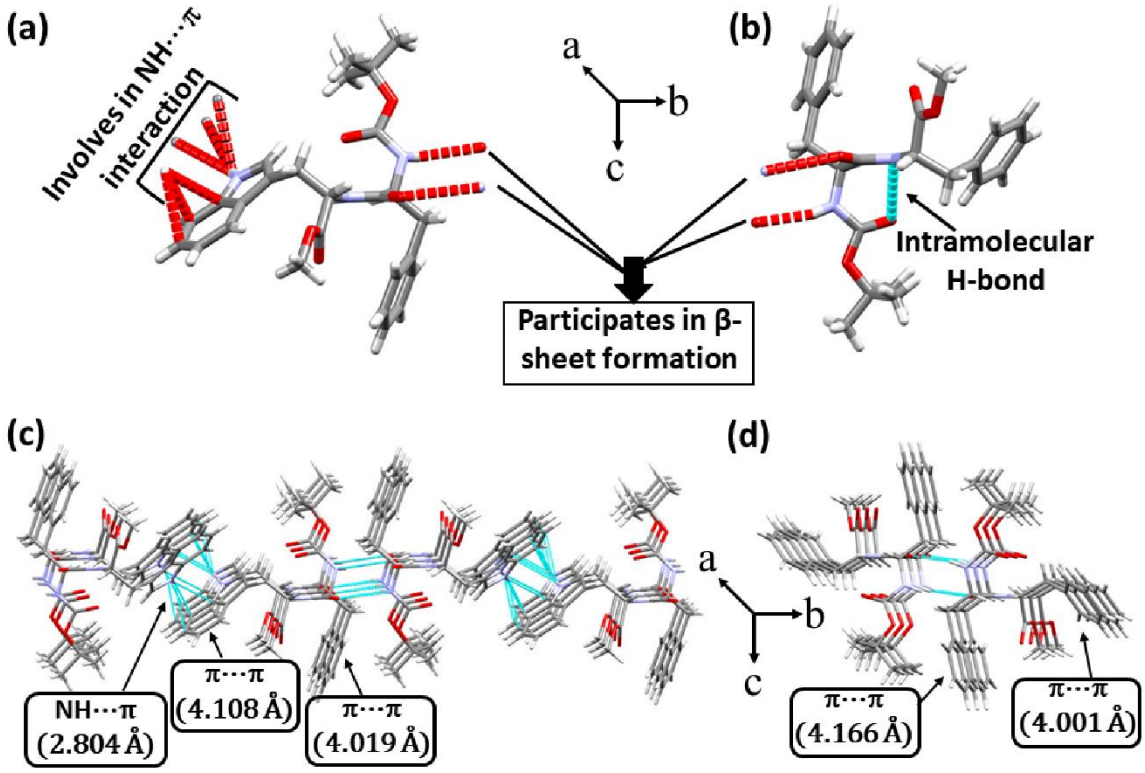

Figure 5.14. *(a, b) Represents different interaction pathways of* ***FW*** *and* ***FF****, respectively (c) Supramolecular continuous columnar structure of* ***FW*** *peptide at higher-order molecular packing, (d) Supramolecular columnar structure of* ***FF*** *peptide in higher-order molecular packing. Crystallographic data of* ***FF*** *peptide taken from Cryst. Growth Des.* ***2014****, 14, 1032 (CCDC No.- 948376).*

Therefore, overall crystallographic insights of Trp and Phe containing protected di-peptides revealed that the indole NH group plays a crucial role in morphology determination. A comparison Table 5.1 was listed for Trp and Phe containing various protected di-peptides to understand the morphological and structural heterogeneity better.

Table 1: Morphological and structural heterogeneity of terminally protected dipeptides.

Peptide	Morphology	SC-XRD	Peptide	Morphology	SC-XRD
VW	Spherical structures were obtained by FESEM and AFM.	parallel β-sheet (*a*-direction) and helical arrangement (*b*-direction), in higher-order molecular packing - cross-β-structure (*a*-direction), and **sheet-like layer architecture (*b*-direction) and Supramolecular zigzag arrangement (*c*-direction).** **Interactions:** Intermolecular backbone NH···O=C, **indole NH···O=C interaction.**	**VF**	amyloid-like fibril structure obtained by AFM.	parallel β-sheet (*a*-direction) and in higher-order molecular packing - cross-β-structure (a-direction) and **supramolecular helical arrangement (*c*-direction).**[9] **Interactions:** Intermolecular backbone NH···O=C, aromatic **CH···HC(CH_3) interaction.**
LW		-	**LF**	Rod-like fiber structure obtained by FESEM.	-
IW		parallel β-sheet (*a*-direction) and helical arrangement (b-direction), in higher order molecular packing - cross-β-structure (*a*-direction), and **sheet-like layer architecture (*c*-direction) and Supramolecular zigzag arrangement (*c*-direction).** **Interactions:** Intermolecular backbone NH···O=C, **indole NH···O=C interaction.**	**IF**	ribbon-like fiber structure obtained by FESEM.	parallel β-sheet (*a*-direction) and in higher-order molecular packing - cross-β-structure (*a*-direction) **and supramolecular helical arrangement (*c*-direction).**[10] **Interactions:** Intermolecular backbone NH···O=C, **aromatic CH···C(CH_3), (CH_3) CH···O=C interaction**.
FW		Open turn conformation, anti-parallel β-sheet structure (*b*-direction), in higher order molecular packing- columnar structure (*a*-direction)., **nanozipper structure (a-direction)., helical and sheet-like layer architecture (*b*-direction).** **Interactions:** Intermolecular backbone NH···O=C, π-π, and **NH-π interaction**.	**FF**	twisted fibrillar morphology obtained by FESEM and AFM.	γ-turn conformation, anti-parallel β-sheet structure (*b*-direction), in higher-order molecular packing- columnar structure (*a*-direction).[2] **Interactions:** Intermolecular backbone NH···O=C, π-π, intramolecular **NH···O=C interaction.**

5.8. Thermal stability of peptide nanostructures

Next, to examine the thermal stability of all designed peptides, we performed TGA analysis of aggregated mass acquired after incubation. In general, weight loss of peptides was observed in two thermal stages in TGA plot. The temperature range 25-200 °C is known for weight loss due to the release of absorbed water molecules and 200-500 °C for weight loss due to breaking the peptide bond. Mass loss of all peptides started above 200 °C, suggesting significant thermal stability because of forming a stable supramolecular structure. Moreover, no weight loss was detected in the region 25-200 °C, showing no absorbed water or solvent molecules were present (Figure 5.15).

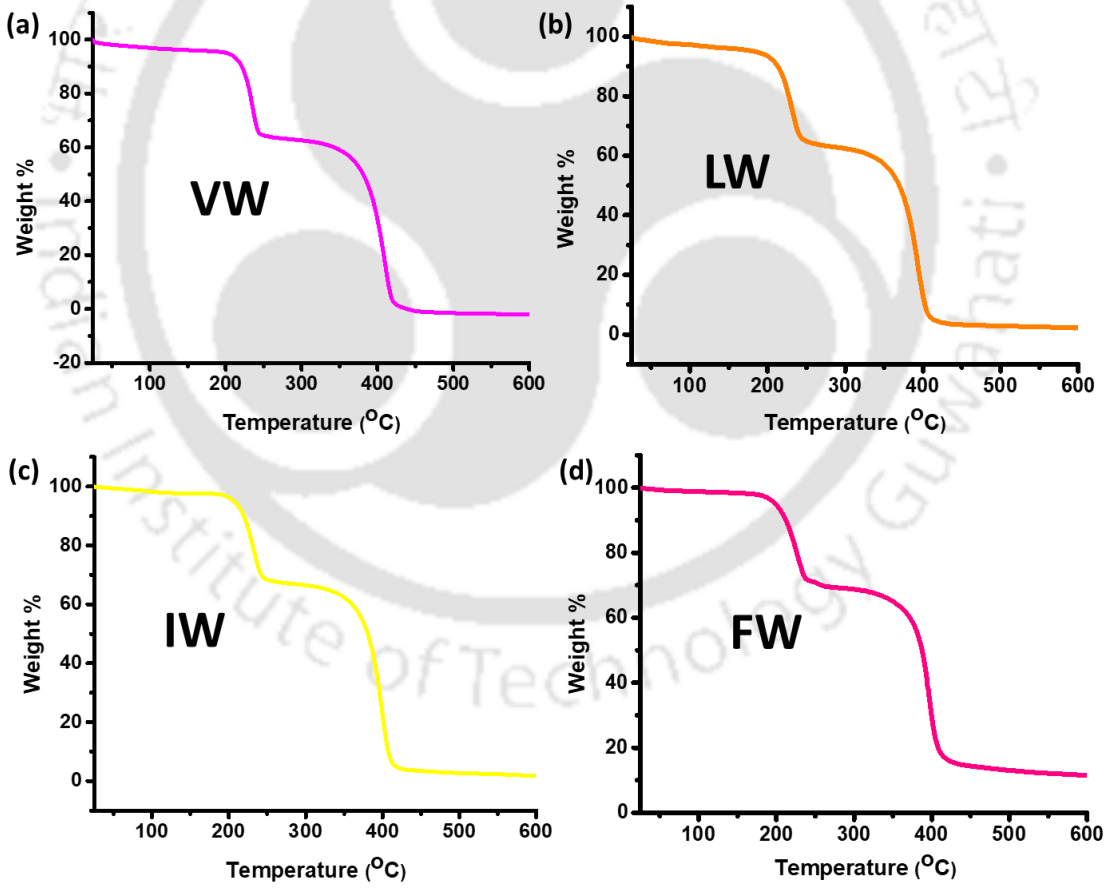

Figure 5.15. *(a, b, c, d) represents TGA profile of aggregated mass of peptide* ***VW***, ***LW***, ***IW***, *and* ***FW***, *respectively.*

5.9. Conclusion

In summary, we have exposed the supramolecular self-assembly, morphology, and atomic-level molecular arrangement of terminally protected four dipeptides such as Boc-Val-Trp-OMe (**VW**), Boc-Leu-Trp-OMe (**LW**), Boc-Ile-Trp-OMe (**IW**), and Boc-Phe-Trp-OMe (**FW**). The peptide contains a tryptophan analog of biologically important Val-Phe and Phe-Phe peptides. The morphology analysis by FESEM and AFM suggested that all peptides formed spherical structures in solution. Interestingly, single-crystal X-ray diffraction (SC-XRD) revealed that peptide **VW** and **IW** displayed parallel β-sheet structure, cross-β-structure (the separation between antiparallel layers), and sheet-like layer structure, and helical arrangement via different intermolecular H-bond and non-covalent interaction in solid-state. Furthermore, peptide **FW** exhibited open turn conformation, antiparallel β-sheet arrangement, columnar structure, supramolecular nanozipper structure, sheet-like layer arrangement, and helical architecture through intermolecular H-bond, NH-π interaction, and aromatic-aromatic interaction in solid-state. This may be the first example of dipeptide (**FW**) based open turn conformation and nanozipper structure.

Interestingly, the entire morphological transition from fiber to spherical structure was observed by just replacing one Phe with Trp. Therefore, -NH group of indole rings plays a significant role in structural determination. These results further may help to design novel nanostructures with small peptides.

5.10. Experimental section

5.10.1. Materials and instrumentations

As described in chapter 7

5.10.2. Representative procedure for the synthesis of dipeptides

The solution containing Boc-Val-OH (400 mg, 1.84 mmol), *o*-NosylOXY (601 mg, 1.84 mmol), and DIPEA (237 mg, 1.84 mmol) were mixed in DCM and was stirred for 15 min at room temperature. After pre-activation, the neutralized H_2N-Trp-OMe (479 mg, 2.20 mmol) solution and the reaction mixture were mixed, and the stirring continued for 4h. The completion of the coupling reaction was checked by TLC observation. After that, the diluted reaction mixture in 50 ml DCM was allowed to work up by 20 ml 10% citric acid, 10% $NaHCO_3$ solution (every 3 times), and brine solution, respectively. The organic layer was collected and dried over $CaCl_2$ and concentrated using a rotary evaporator. The crude reaction mixture obtained was purified by column chromatography. 1D ^{1}H and ^{13}C NMR spectroscopy and Mass spectrometry were employed to characterize the peptide.

5.10.3. Sample preparation

1.5 mM of peptides solution in 50% acetonitrile-water were incubated for four days at 37 °C.

After incubation, we performed FESEM, AFM, and CD analysis.

5.11. Characterization data

Boc-Val-Trp-OMe (VW):

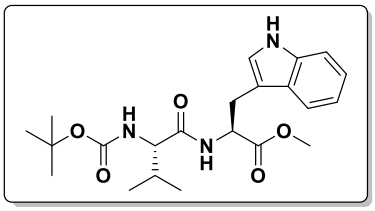

White solid, (630 mg, 82%), **M.P** 146-148°C, **^{1}H NMR ($CDCl_3$; 600 MHz)** δ 0.86-0.85 (3H, d, *J* = 6.6 Hz); 0.93-0.92 (3H, d, *J* = 6.6 Hz); 1.44 (9H, s); 2.09-2.06 (1H, m); 3.34-3.26 (2H, m); 3.65 (3H, s); 4.01 (1H, s); 4.93-4.92 (1H, d, *J* = 6.6 Hz); 5.18 (1H, s); 6.59 (1H, s); 6.99 (1H, s); 7.13-7.11 (1H, t, *J* = 7.2 Hz); 7.19-7.17 (1H, t, *J* = 7.2 Hz); 7.35-7.34 (1H, d, *J* = 7.8 Hz); 7.54-7.52 (1H, d, *J* = 8.4 Hz);

8.50 (1H, s); **^{13}C NMR ($CDCl_3$; 150 MHz)** δ 17.7, 19.2, 27.7, 28.4, 31.2, 52.5, 52.9, 59.8, 80.0, 109.6, 111.5, 118.5, 119.7, 122.2, 123.3, 127.5, 136.3, 156.0, 171.6, 172.2. HRMS (ESI): calculated $[M+H]^+$ 418.2342, found m/z . 418.2340. HPLC: retention time (t_R) = 5.477 min.

Boc-Leu-Trp-OMe (LW):

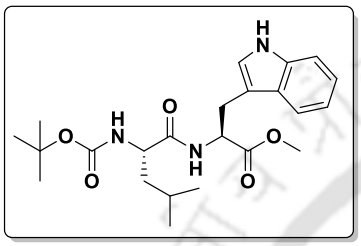

White solid, (605 mg, 81%), **M.P** -58-63°C, **^{1}H NMR ($CDCl_3$; 400 MHz)** δ 0.87-0.86 (6H, d, *J* = 4.0 Hz); 1.29-1.25 (1H, m); 1.40 (9H, s); 1.63-1.56 (2H, m); 3.29-3.28 (2H, d, *J* = 4.8 Hz); 3.62 (3H, s); 4.13-3.97 (1H, m); 5.13-4.87 (2H, m,); 6.71 (1H, s); 6.98 (1H, s); 7.10-7.06 (1H, t, *J* = 7.6 Hz); 7.16-7.13 (1H, t, *J* = 6.8 Hz); 7.32-7.25 (1H, m); 7.51-7.49 (1H, d, *J* = 8.0 Hz); 8.50 (1H, s); **^{13}C NMR ($CDCl_3$; 100 MHz)** δ 21.9, 23.0, 24.8, 27.7, 28.4, 41.4, 52.4,53.1, 53.3, 80.1, 109.6, 111.5, 118.6, 119.6, 122.2, 123.3 127.6, 136.2, 155.7, 172.2, 172.6. HRMS (ESI)**:** calculated $[M+H]^+$ 432.2498, found m/z . 432.2514. HPLC: retention time (t_R) = 5.804 min.

Boc-Ile-Trp-OMe (IW):

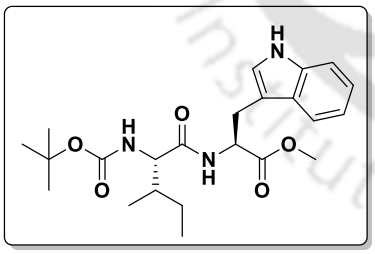

White solid, (598 mg, 80%), **M.P** 137-140°C, **^{1}H NMR ($CDCl_3$; 600 MHz)** δ 0.90-0.85 (6H, m); 1.05 (1H, s); 1.45 (9H, s); 1.81-1.78 (2H, m); 3.37-3.28 (2H, m); 3.67 (3H, s); 3.98 (1H, s); 4.94 (1H, s); 5.11 (1H, s); 6.46 (1H, s); 7.05 (1H, s); 7.15-7.12 (1H, t, *J* = 7.2 Hz); 7.21-7.18 (1H, t, *J* = 7.2 Hz); 7.37-7.35 (1H, d, *J* = 7.8 Hz); 7.55-7.54 (1H, d, *J* = 7.8 Hz); 8.29 (1H, s); **^{13}C NMR ($CDCl_3$; 150 MHz)** δ 11.6, 15.5, 24.7, 27.8, 28.5, 37.6, 52.5, 52.9, 59.3, 80.0, 109.8, 111.4, 118.6, 119.8, 122.4, 123.2, 127.6, 136.3, 155.9, 171.4, 172.2. HRMS (ESI): calculated $[M+H]^+$ 432.2498, found m/z . 432.2503. HPLC: retention time (t_R) = 5.800 min.

Boc-Phe-Trp-OMe (FW):

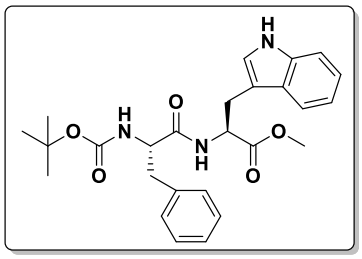

White solid, (550 mg, 78%), **M.P** 169-171°C, **^{1}H NMR (CDCl$_3$; 600 MHz)** δ 1.28 (9H, s); 2.97-2.91 (2H, m); 3.20-3.13 (2H, m); 3.54 (3H, s); 4.28 (1H, s); 4.79 (1H, s); 4.88 (1H, s); 6.33 (1H, s); 6.79 (1H, s); 6.99-6.97 (1H, t, *J* = 7.2 Hz); 7.10-7.08 (3H, t, *J* = 7.2 Hz); 7.15-7.12 (1H, t, *J* = 7.2 Hz); 7.19-7.17 (2H, m); 7.25-7.24 (1H, d, *J* = 8.4 Hz); 7.29-7.28 (1H, d, *J* = 6.6 Hz); 8.13 (1H, s); **^{13}C NMR (CDCl$_3$; 150 MHz)** δ 27.8, 28.3, 38.4, 52.5, 53.1, 55.8, 80.2, 109.8, 111.5, 118.6, 119.8, 122.3, 123.1, 127.1, 127.6, 128.7, 129.5, 136.2, 136.7, 155.4, 171.0, 171.9. HRMS (ESI): calculated $[M+H]^+$ 466.2342, found m/z . 466.2352. HPLC: retention time (t_R) = 5.802 min.

Boc-Val-Phe-OMe (VF):

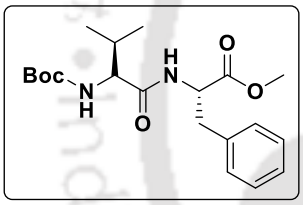

White solid, (591 mg, 84%), **^{1}H NMR (CDCl$_3$; 600 MHz)** δ 0.88-0.87 (3H, m); 0.93-0.91 (3H, d, *J* = 6.6 Hz); 1.45 (9H, s); 2.08-2.07 (1H, m); 3.15-3.07 (2H, m); 3.70 (3H, s); 3.93 (1H, s); 4.89-4.85 (1H, m); 5.12 (1H, s); 6.53 (1H, s); 7.12-7.11 (2H, d, *J* = 6.6 Hz); 7.24-7.22 (1H, m); 7.29-7.27 (2H, m); **^{13}C NMR (CDCl$_3$; 150 MHz)** δ 17.8, 19.2, 28.4, 31.0, 38.0, 52.4, 53.2, 60.0, 79.9, 127.2, 128.7, 129.3, 135.8, 155.8, 171.5, 171.8. HRMS (ESI): calculated $[M+H]^+$ 379.2233, found m/z . 379.2240.

Boc-Leu-Phe-OMe (LF):

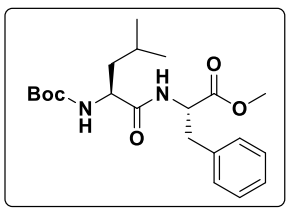

White solid, (492 mg, 72%), **^{1}H NMR (CDCl$_3$; 600 MHz)** δ 0.94-0.90 (6H, m); 1.35-1.30 (1H, m); 1.45 (9H, s); 1.69-1.65 (2H, m); 3.19-3.08 (2H, m); 3.73 (3H, s); 4.10 (1H, s); 4.88-4.83 (2H, m); 6.52-6.51 (1H, d, *J* = 7.2 Hz); 7.13-7.12 (2H, d, *J* = 7.2 Hz); 7.31-7.24 (3H, m); **^{13}C NMR (CDCl$_3$; 150 MHz)** δ 23.0, 24.8, 28.4, 29.9, 38.1, 41.4, 52.5, 53.3, 80.2, 127.3, 128.7, 129.5, 135.9, 155.7, 171.8, 172.3. MALDI-TOF mass: calculated $[M+K]^+$ 431.194, found m/z . 431.157.

Boc-Ile-Phe-OMe (IF):

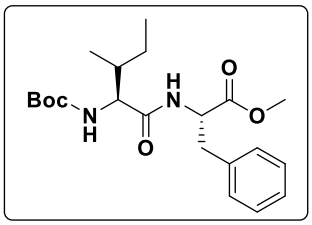

White solid, (548 mg, 80%), **^{1}H NMR (CDCl$_3$; 600 MHz)** δ 0.88-0.87 (6H, m); 1.07 (1H, s); 1.44 (9H, s); 1.82-1.72 (2H, m); 3.15-3.07 (2H, m); 3.70 (3H, s); 3.93 (1H, s); 4.89-4.85 (2H, m); 5.00 (1H, s); 6.33 (1H, s); 7.11-7.10 (2H, m); 7.28-7.24 (3H, m); **^{13}C NMR (CDCl$_3$; 150 MHz)** δ 11.6, 15.6, 24.8, 28.5, 37.4, 38.1, 52.5, 53.2, 59.4, 80.0, 127.3, 128.8, 129.4, 135.8, 155.8, 171.4, 171.8.

Boc-Phe-Phe-OMe (FF):

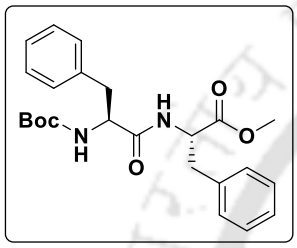

White solid, (511 mg, 79%), **^{1}H NMR (CDCl$_3$; 600 MHz)** δ 1.41 (9H, s); 3.10-3.02 (4H, m); 3.68 (3H, s); 4.36 (1H, s); 4.80 (1H, s); 5.03 (1H, s); 6.40 (1H, s); 7.01-7.00 (2H, d, *J* = 6.6 Hz); 7.21-7.20 (2H, d, *J* = 6.6 Hz); 7.26-7.23 (4H, m); 7.31-7.28 (2H, m); **^{13}C NMR (CDCl$_3$; 150 MHz)** δ 28.4, 38.1, 38.4, 52.4, 53.4, 55.8, 80.3, 127.1, 127.2, 128.6, 128.7, 129.3, 129.5, 135.8, 136.6, 155.4, 170.9, 171.5. HRMS (ESI): calculated $[M+H]^+$ 427.2233, found m/z . 427.2225.

5.12. References

1. Taubes, G. Misfolding the Way to Disease: Amyloid diseases such as Alzheimer's may result when proteins fold up incorrectly, causing them to aggregate and deposit abnormally in or around cells. *Science* **1996**, *271*, 1493-1495.
2. Bera, S.; Jana, P.; Maity, S. K.; Haldar, D. Inhibition of Fibril Formation by Tyrosine Modification of Diphenylalanine: Crystallographic Insights. *Cryst. Growth Des.* **2014**, *14*, 1032-1038.
3. Paikar, A.; Debnath, M.; Podder, D.; Sasmal, S.; Haldar, D. Synthesis and structural investigation of 2-aminomethyl-3-(4-methoxy-phenyl)-propionic acid containing a peptide analogue of the amyloidogenic AS(6–7) sequence: inhibition of fibril formation. *Org. Biomol. Chem.* **2017**, *15*, 4218-4225.
4. Ray, S.; Drew, M. G. B.; Das, A. K.; Haldar D.; Banerjee, A. Nanozipper formation in the solid state from a self-assembling tripeptide with a single tryptophan residue. *Tetrahedron Lett.* **2006**, *47*, 2771-2774.
5. Bera, S.; Xue, B.; Rehak, P.; Jacoby, G.; Ji, W.; Shimon, L. J. W.; Beck, R.; Král, P.; Cao, Y.; Gazit, E. Self-Assembly of Aromatic Amino Acid Enantiomers into Supramolecular Materials of High Rigidity. *ACS Nano* **2020**, *14*, 1694-1706.
6. Paul, A.; Li, W. H.; Viswanathan, G. K.; Arad, E.; Mohapatra, S.; Li, G.; Jelinek, R.; Gazit, E.; Li, Y. M.; Segal, D. Tryptophan-glucosamine conjugates modulate tau-derived PHF6 aggregation at low concentrations. *Chem. Commun.*, **2019**, *55*, 14621-14624.
7. Paul, A.; Pinter, M. F.; Alvarez, D. E.; Milordini, G.; Gazit, E.; Zacco, E.; Segal, D. Tryptophan-galactosylamine conjugates inhibit and disaggregate amyloid fibrils of Aβ42 and hIAPP peptides while reducing their toxicity. *Commun Biol* **2020**, *3*, 484.
8. Dev, D.; Palakurthy, N. B.; Thalluri, K.; Chandra, J.; Mandal, B. Ethyl 2-Cyano-2-(2-nitrobenzenesulfonyloxyimino)acetate (*o*-NosylOXY): A Recyclable Coupling Reagent for Racemization-Free Synthesis of Peptide, Amide, Hydroxamate, and Ester. *J. Org. Chem.* **2014**, *79*, 5420-5431.
9. Maity, S.; Kumar, P.; Haldar, D. An amyloid-like fibril-forming supramolecular cross-β-structure of a model peptide: a crystallographic insight. *Org. Biomol. Chem.* **2011**, *9*, 3787.
10. Roy, S.; Giri, R. S.; Dolai, G.; Mandal, B. Role of side-chain and chirality of the amino acids on the supramolecular assemblies of dipeptides. *J. Mol. Str.* **2020**, *1221*, 128877.
11. Myer, Y. P.; MacDonald, L. H. The Circular Dichroism of L-Tryptophan by an Improved Dichrograph. *J. Am. Chem. Soc.* **1967**, *89*, 7142-7144.

5.13. Selected spectra

5.13.1. Spectra of peptide Boc-Val-Trp-OMe (VW):

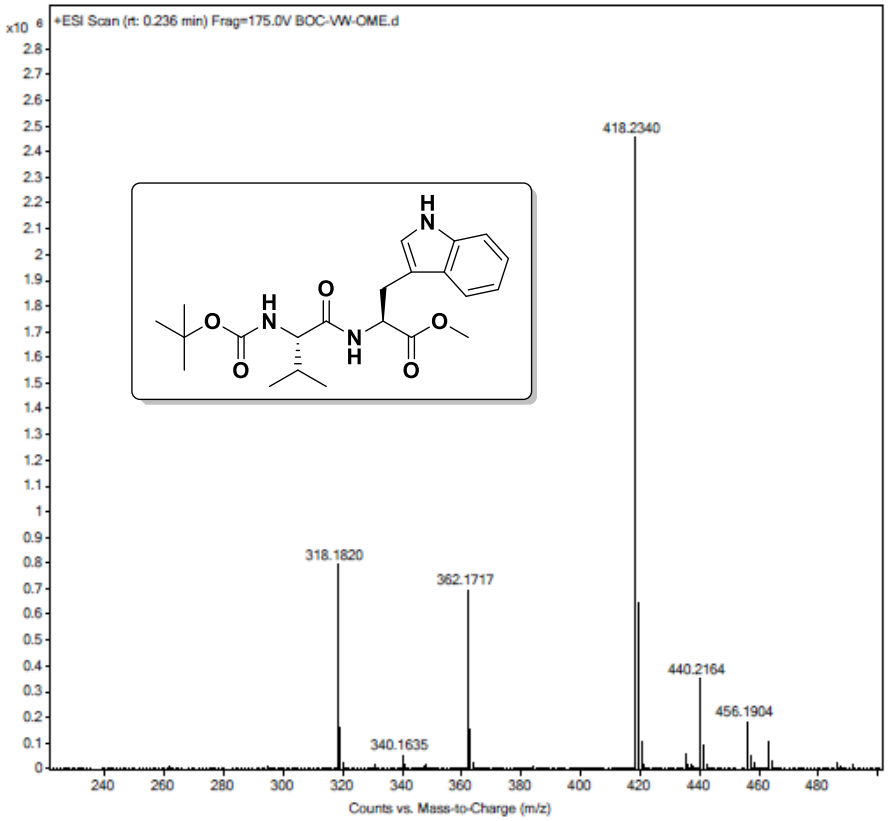

Figure 5.16. *MS spectra of peptide* ***Boc-Val-Trp-OMe (VW)***

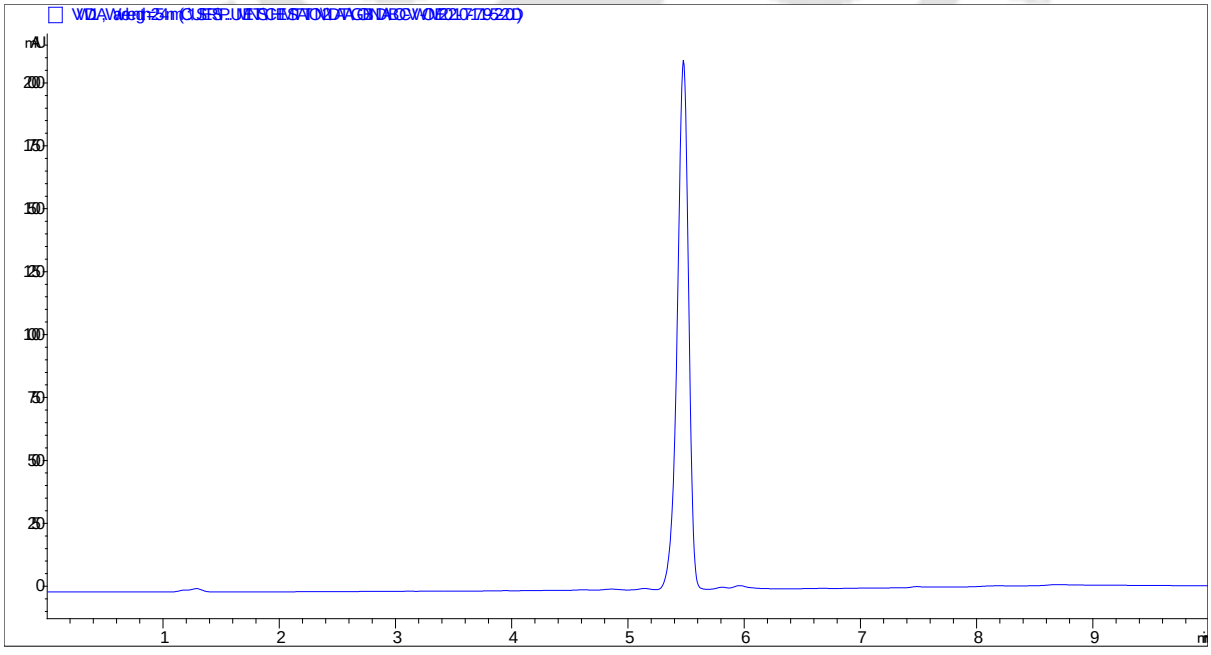

Figure 5.17. *HPLC profile picture of purified peptide* ***Boc-Val-Trp-OMe (VW)***

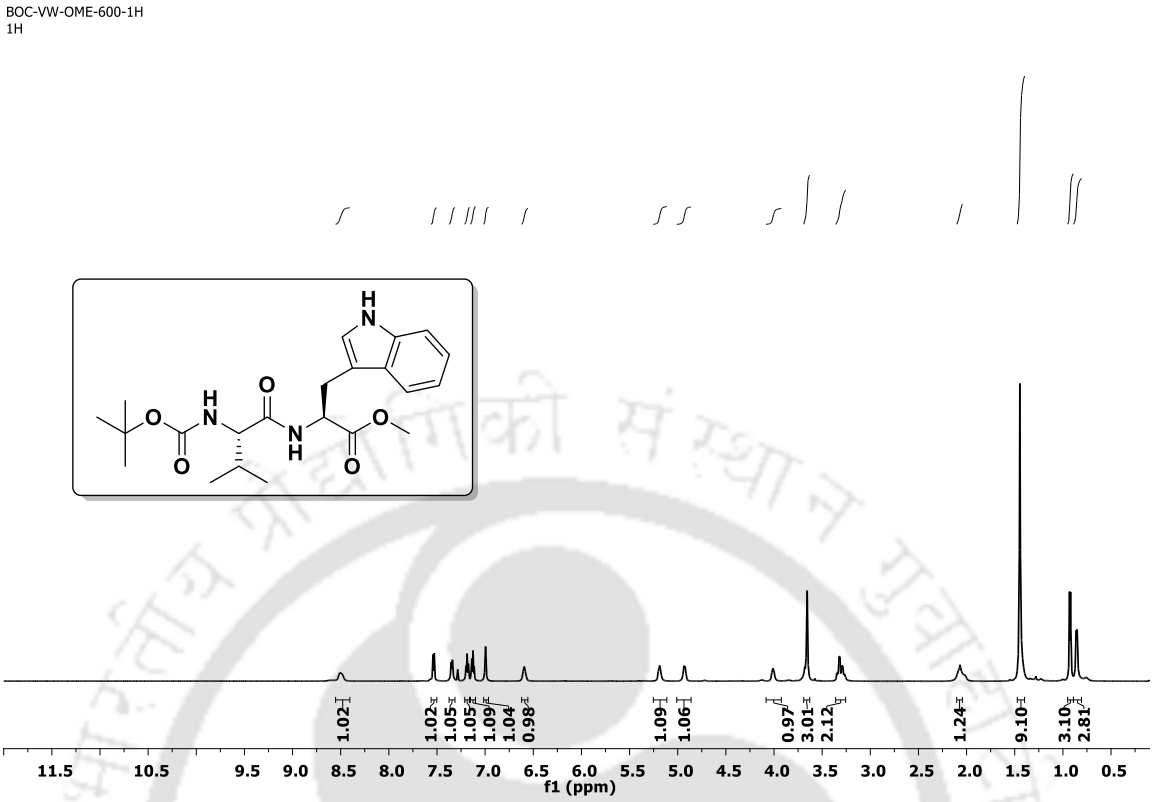

Figure 5.18. *^{1}H NMR spectra of peptide* ***Boc-Val-Trp-OMe (VW)***

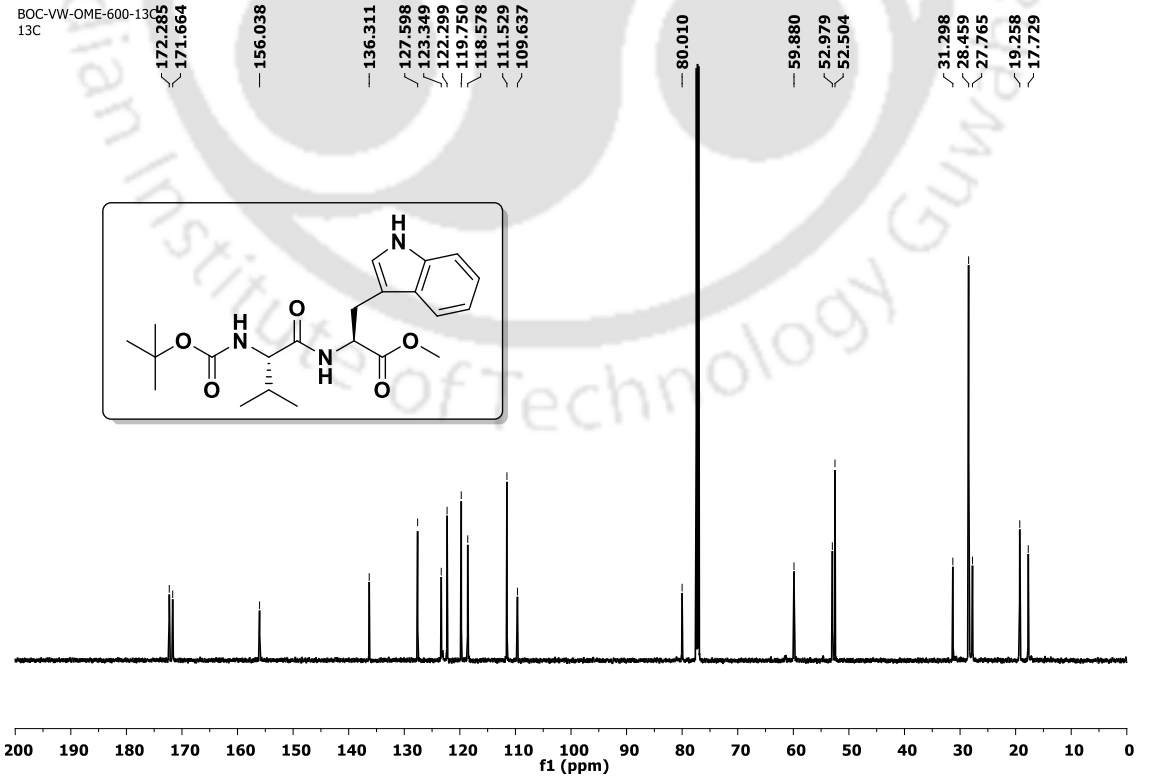

Figure 5.19. ^{13}C NMR spectra of peptide **Boc-Val-Trp-OMe (VW)**

5.13.2. Spectra of peptide Boc-Leu-Trp-OMe (LW)

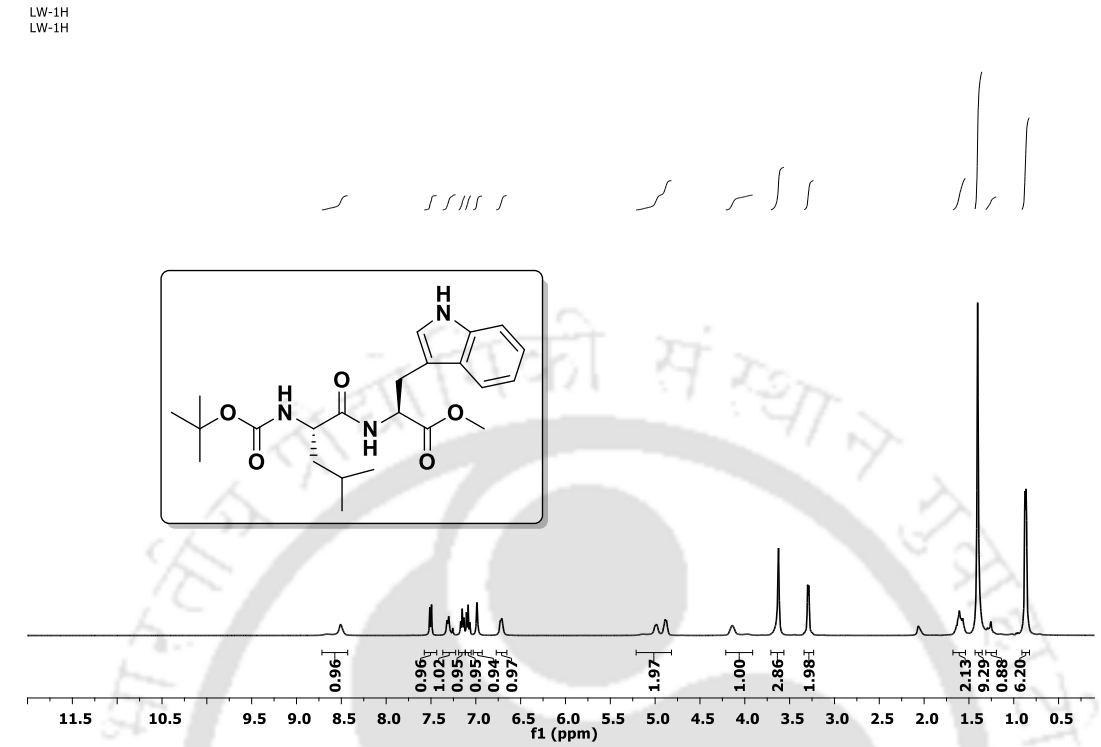

Figure 5.20. *^{1}H NMR spectra of peptide* ***Boc-Leu-Trp-OMe (LW)***

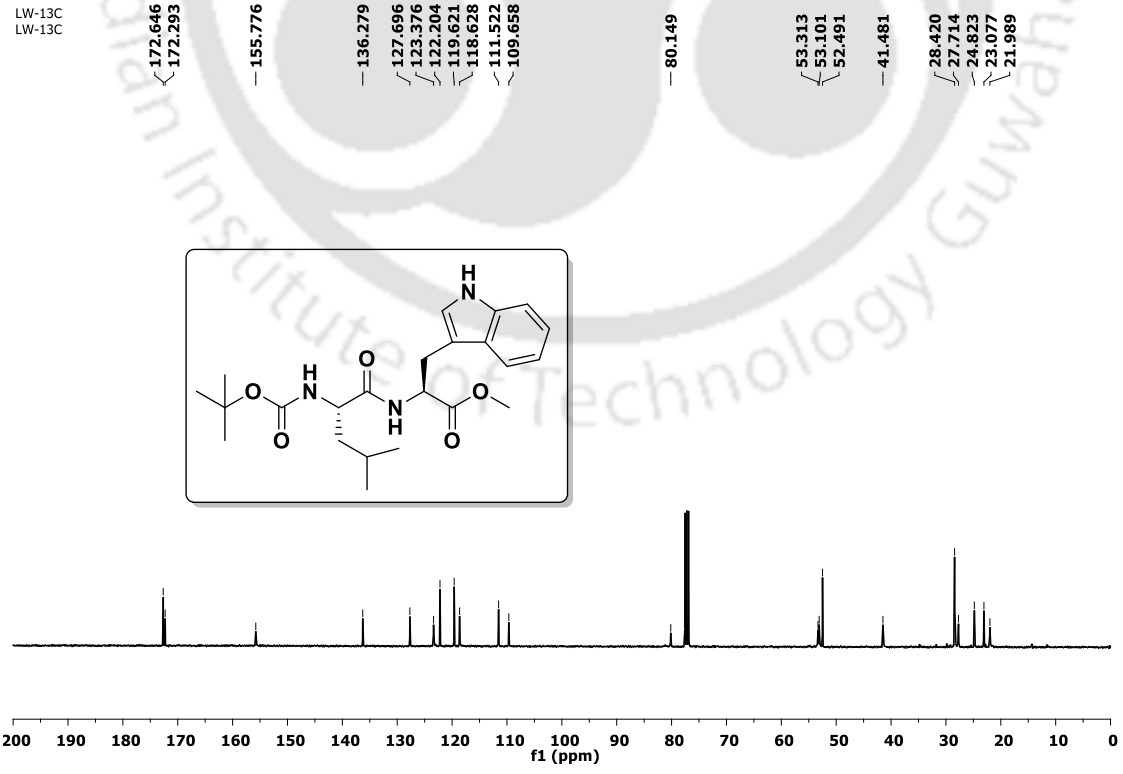

Figure 5.21. *^{13}C NMR spectra of peptide* ***Boc-Leu-Trp-OMe (LW)***

5.13.3. Spectra of peptide Boc-Ile-Trp-OMe (IW):

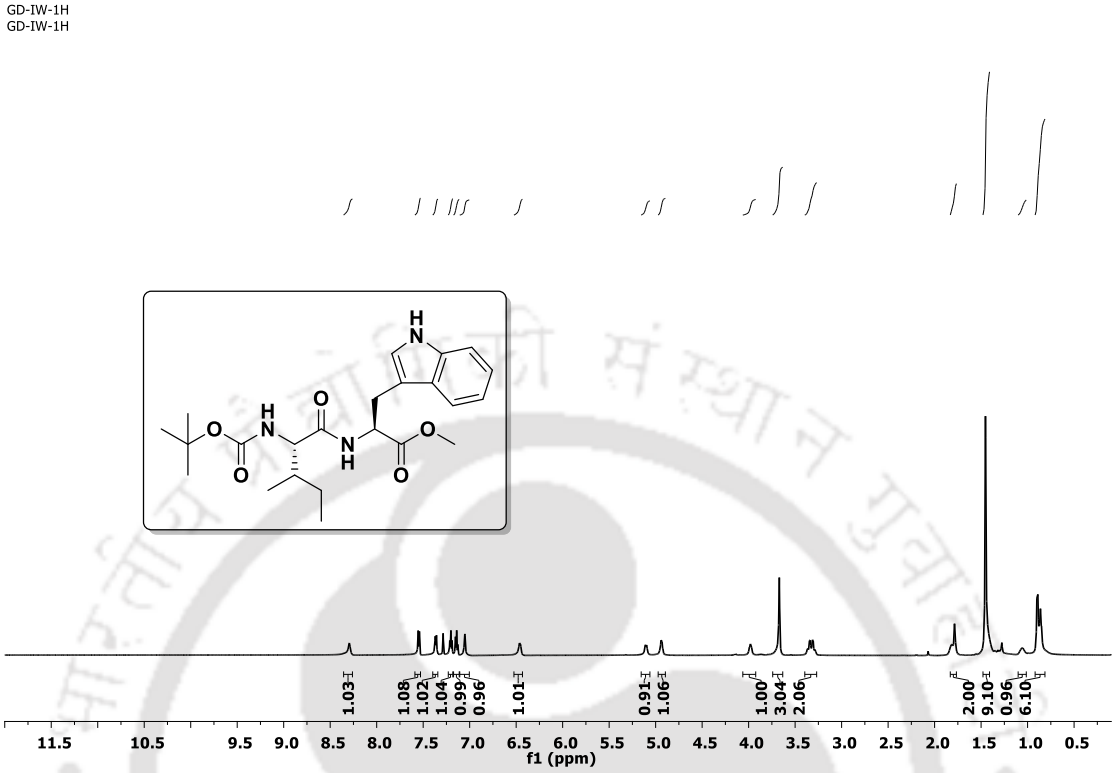

Figure 5.22. *^{1}H NMR spectra of peptide* ***Boc-Ile-Trp-OMe (IW)***

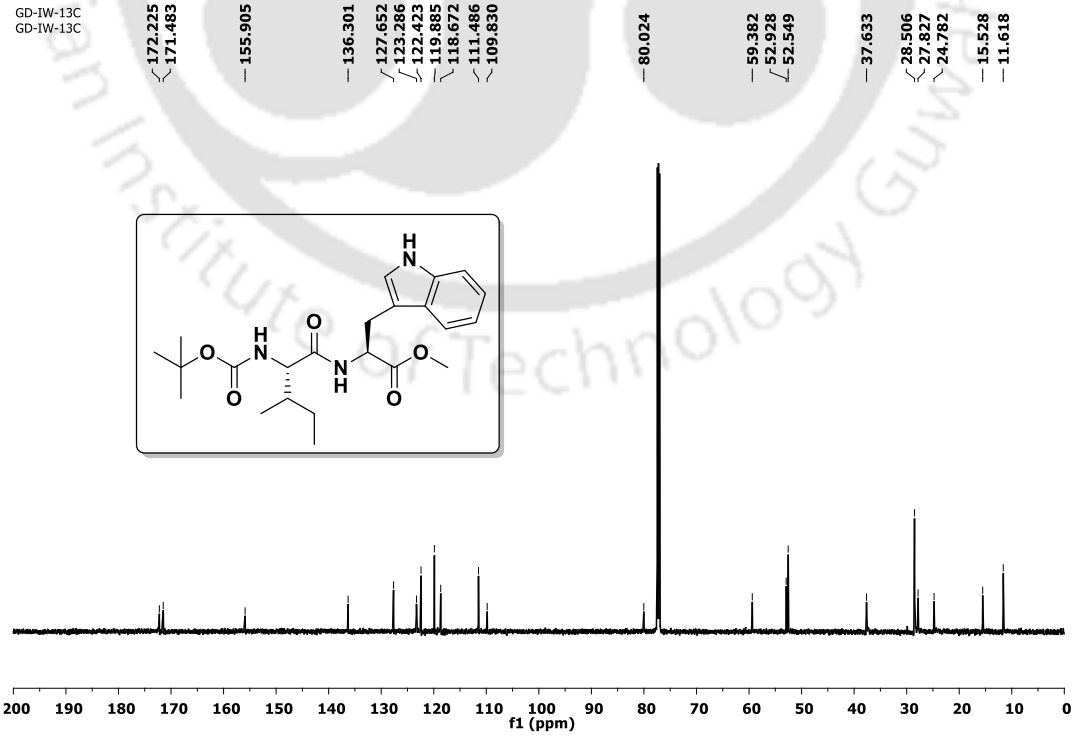

Figure 5.23. *^{13}C NMR spectra of peptide* ***Boc-Ile-Trp-OMe (IW)***

5.13.4. Spectra of peptide Boc-Phe-Trp-OMe (FW)

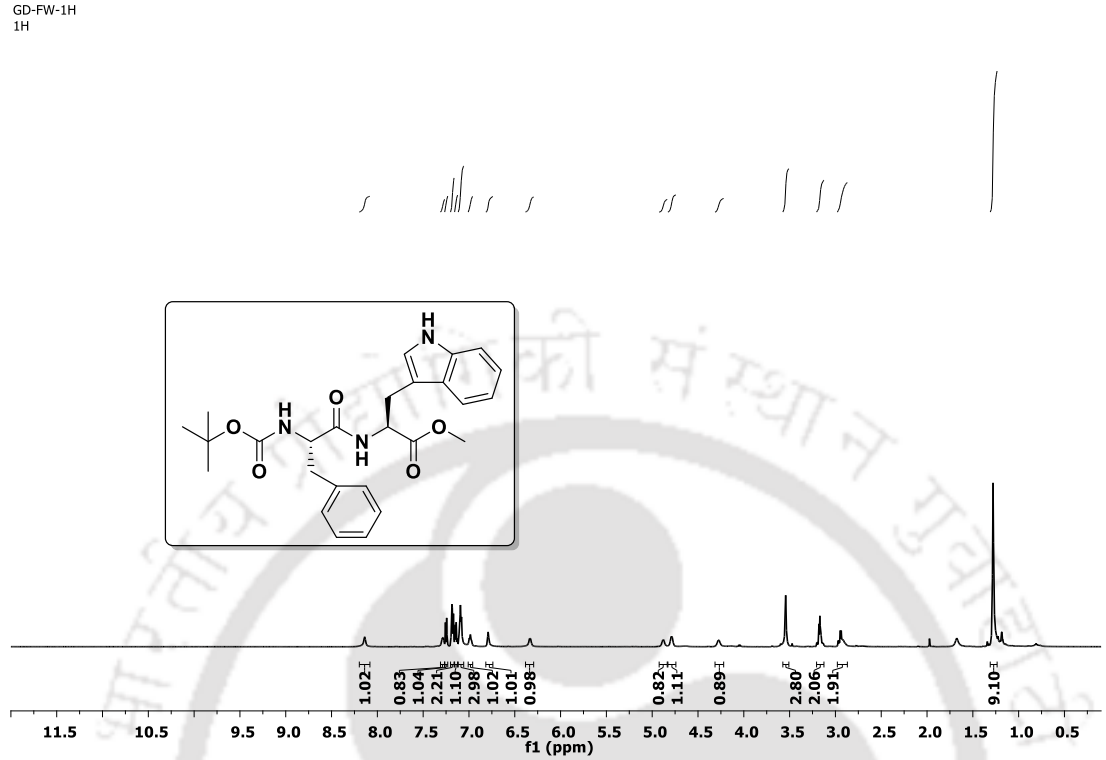

Figure 5.24. *^{1}H NMR spectra of peptide* ***Boc-Phe-Trp-OMe (FW)***

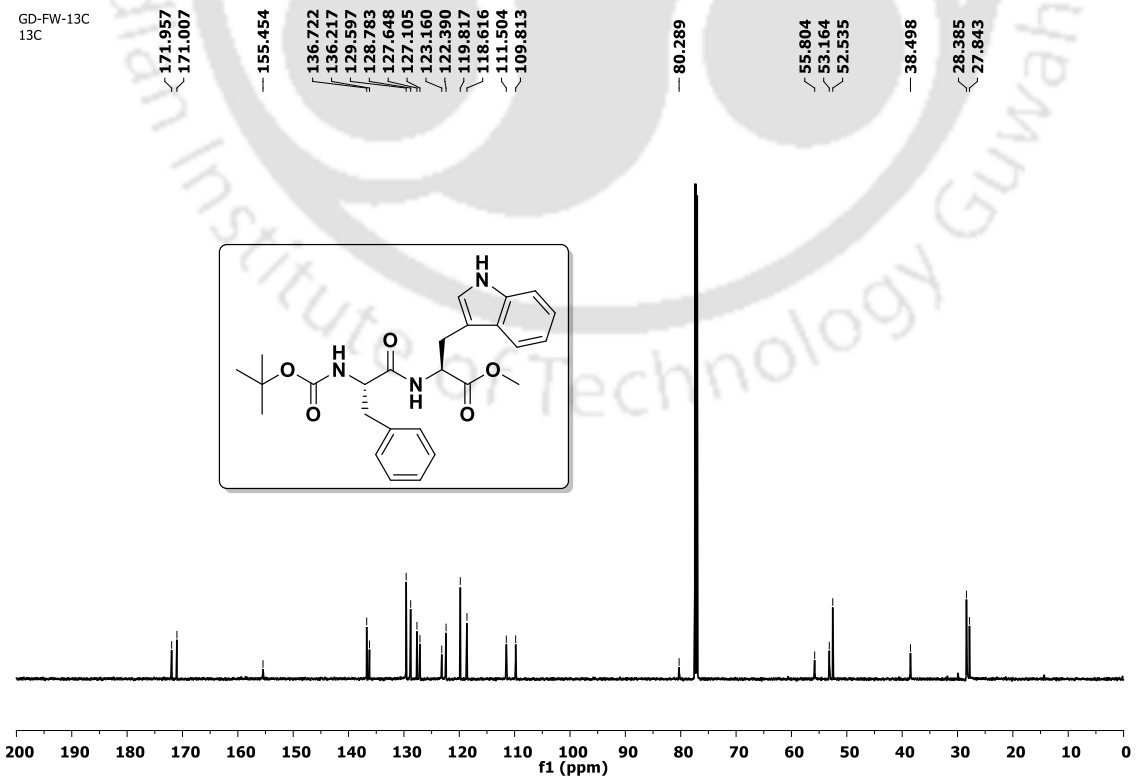

Figure 5.25. *^{13}C NMR spectra of peptide* ***Boc-Phe-Trp-OMe (FW)***

5.14. Crystallographic data

Table 5.2. Torsion angles (deg) of dipeptides **VW**, **IW**, and **FW**

peptides	*ω1*	*ω2*	*ϕ1*	*ϕ2*	*ψ1*	*ψ2*
VW	O1-C5-N1-C6 = -167.7(3)	C6-C10-N2-C11 = 174.0(3)	C5-N1-C6-C10 = -129.0(3)	C10-N2-C11-C21 = -84.7(4)	N1-C6-C10-N2 = 114.4(3)	N2-C11-C21-O5 = 154.2(3)
IW	O1-C5-N1-C6 = -166.5(2)	C6-C11-N2-C12 = 174.2 (2)	C5-N1-C6-C11 = -124.9(3)	C11-N2-C12-C22 = -84.8(3)	N1-C6-C11-N2 = 108.9(3)	N2-C12-C22-O5 = 150.9(3)
FW	O1-C5-N1-C6 = -175.8(3)	C6-C14-N2-C15 = -173.1 (3)	C5-N1-C6-C14 = -80.2(5)	C14-N2-C15-C25 = -98.9(5)	N1-C6-C14-N2 = 102.0(4)	N2-C15-C25-O5 = 168.0(3)

Table 5.3. Hydrogen bonding parameters of crystals of peptide VW, IW and FW

Type	H…A(Å)	D...A(Å)	D-H...A(º)
Peptide VW			
N1-H1···O2	2.14	2.958(4)	157
N2-H2···O3	2.13	2.992(4)	177
N3-H3···O4	2.12	2.961(5)	168
Peptide IW			
N1-H1···O2	2.20	3.0055(5)	155
N2-H2···O3	2.15	3.0013(5)	171
N3-H3···O4	2.16	3.0007(5)	167
Peptide 4			
N1-H1···O3	2.42	2.952(5)	119

Table 5.4. Crystallographic refinement details for Peptides VW, IW and FW

Parameters	**VW**	**IW**	**FW**
Formula	C_{22} H_{31} N_3 O_5	C_{23} H_{33} N_3 O_5	C_{26} H_{31} N_3 O_5
Fw	417.50	431.52	465.54
Crystal system	Monoclinic	Monoclinic	Orthorhombic
Space group	*P 21*	*P2(1)*	*p_21_21_21*
a/Å	5.0318(18)	5.0877(7)	6.2164(11)
b/Å	17.410(5)	17.693(3)	18.140(3)
c/Å	13.519(4)	13.504(2)	21.874(5)
α/°	90.00	90.00	90.00
β/°	91.388(12)	91.924(6)	90.00
γ/°	90.00	90.00	90.00
V/Å^3	1184.0(6)	1214.9(3)	2466.6(8)
Z	2	2	4
D_c/g cm^{-3}	1.171	1.180	1.251
μ Mo K_α/mm^{-1}	0.083	0.083	0.087
F000	448	464	988
T/K	296(2)	296(2)	296(2)
θ max.	24.99	25.00	25.00
Total no. of reflections	33372	14200	22499
Independent reflections	4128	4238	4345
Observed reflections	3650	3238	2027
Parameters refined	279	287	312
R_1, I > 2σ(I)	0.0863	0.0512	0.0621
wR_2, I > 2σ(I)	0.2122	0.1336	0.1294
GOF (F^2)	1.199	0.733	0.773
CCDC No.	2144259	2144261	2144263

Chapter 6

Supramolecular insights of hetero-chiral tripeptides ($A\beta_{18-20}$) in solid and solution state

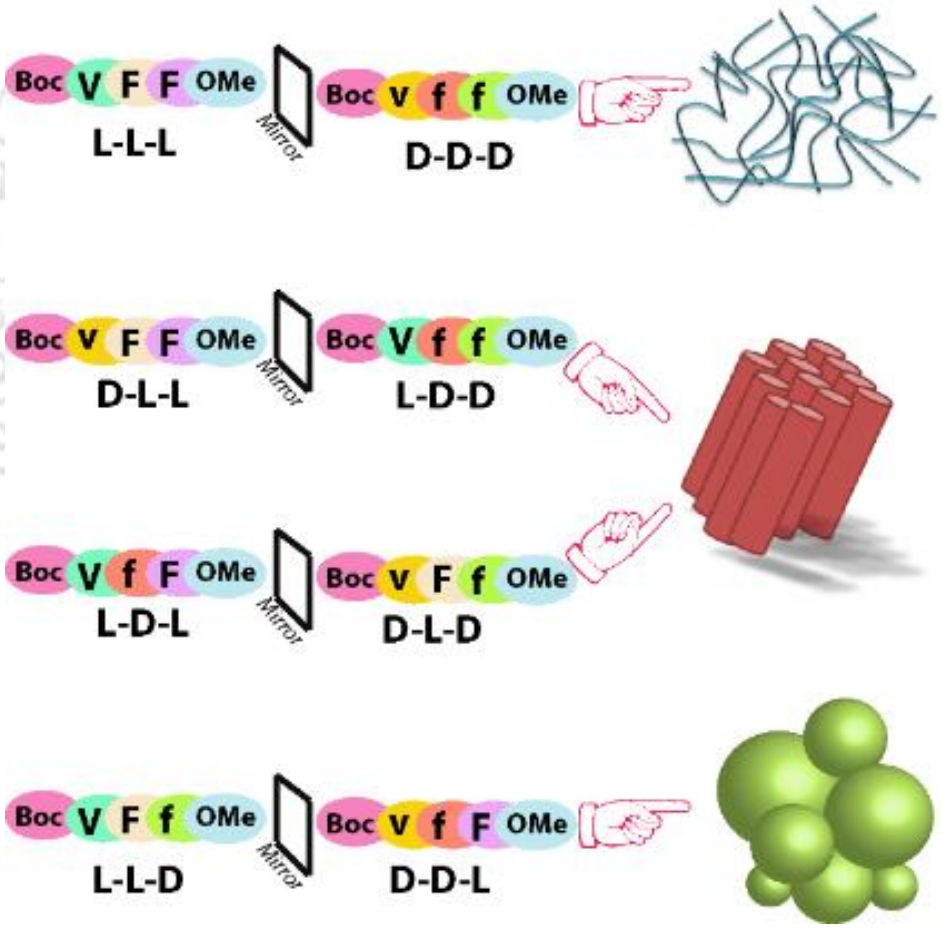

6.1. Background

In the past three-chapter, we discussed natural and unnatural amino acid-containing di-peptides' morphology, conformation, and self-assembly study. Alzheimer's disease (AD) mainly causes the accumulation of Amyloid-beta ($A\beta_{42}$) fibrils in the human brain.[1] It is not clear the structural properties of the full chain of the $A\beta_{42}$ sequence till now. Scientists developed structural features of various short peptide fragments of $A\beta_{42}$ sequence via various instrumental techniques.[2-6] Although various gelation properties of VFF ($A\beta_{18-20}$) peptides were investigated by varying chirality of amino acids and solvent polarity, their structural features remain unknown.[7,8] Herein, we designed eight stereoisomers of protected VFF ($A\beta_{18-20}$) peptide and studied their structural, self-assembly and morphological properties.

6.2. Design of peptides

The N and C-terminal protected tripeptide Boc-Val-Phe-Phe-OMe, having sequence equality with the central hydrophobic core of amyloid-beta ($A\beta_{18-20}$) peptide, which plays a crucial role in fibril formation in Alzheimer's disease. To investigate the chirality effect on self-assembly properties of tripeptide of Boc-Val-Phe-Phe-OMe, eight tripeptides with all possible combinations of D, L amino acids were designed such as Boc-L-Val-L-Phe-L-Phe-OMe (**VFF**) and Boc-D-Val-D-Phe-D-Phe-OMe (**vff**); Boc-D-Val-LPhe-L-Phe-OMe (**vFF**) and Boc-L-Val-D-Phe-D-Phe-OMe (**Vff**); Boc-LVal-D-Phe-L-Phe-OMe (**VfF**) and Boc-D-Val-L-Phe-D-Phe-OMe (**vFf**); and Boc-L-Val-L-Phe-D-Phe-OMe (**VFf**) and Boc-D-Val-D-Phe-L-Phe-OMe (**vfF**) (Figure 6.1).

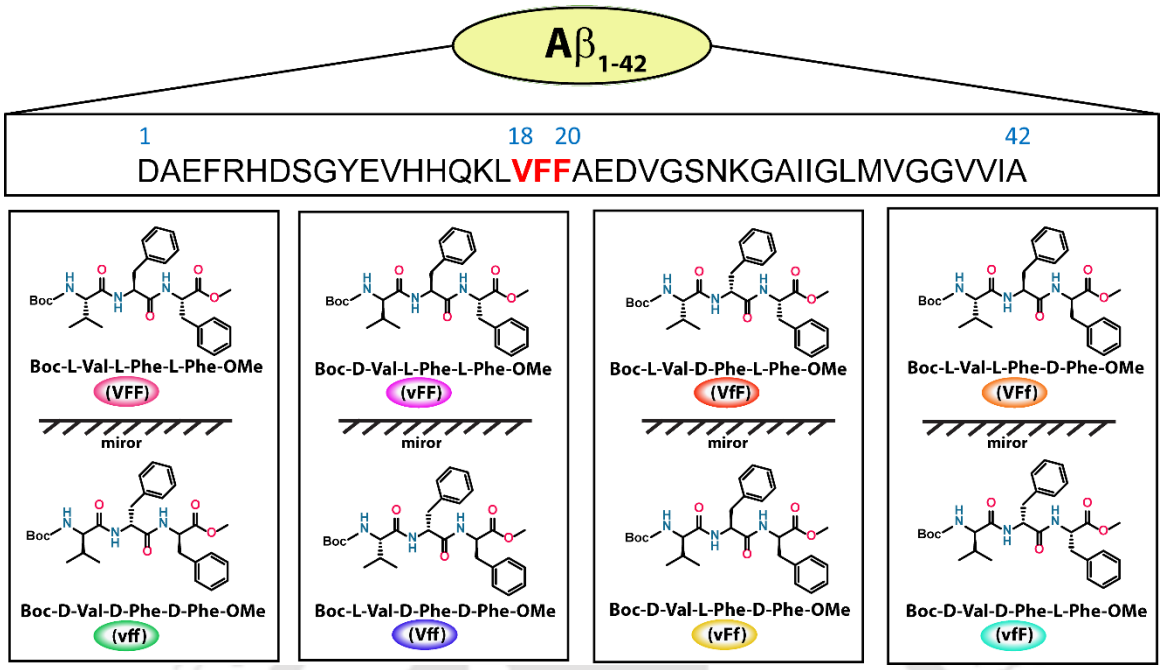

Figure 6.1. *Amyloid β ($A\beta_{1-42}$) peptide sequence and the chemical structures of heterochiral enantiomeric tripeptides.*

6.3. Synthesis and characterization of the designed peptides

All tri-peptides were synthesized by conventional peptide coupling methods in the solution phase using o-NosylOXY as a coupling reagent (Scheme 6.1). After synthesis the peptides were purified by silica gel column chromatography and characterized by mass spectrometry as well as 1D (^{1}H, ^{13}C) NMR spectroscopy, and purity was checked by reverse-phase HPLC.

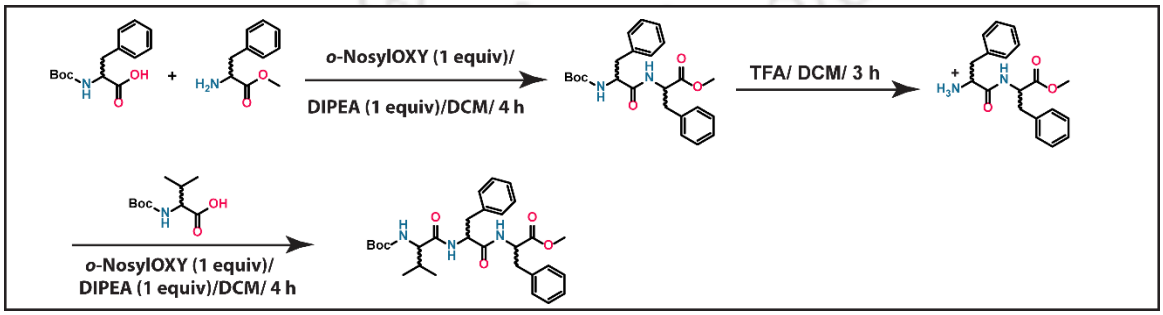

Scheme 6.1. *Schematic representation of tri-peptide synthesis in solution.*

6.4. Morphology of designed peptides

To understand the morphological variety of self-assembled tripeptides, we prepared a 1.5 mM solution for all of these peptides in acetonitrile-water (1: 1) and incubated for four days at 37 °C. After that, 10 µL solutions of each peptide were drop cast on the microscopic slide for optical microscopic images and glass containing Al-foil for FESEM. After drying the samples, we collected optical microscope and FESEM images. Optical microscopic and FESEM images revealed that **VFF** and **vff** displayed various micrometers long entangled fibrils network. **vFF** and **Vff** showed rod-like structures with diameters ~3 µm and ~2 µm, respectively. **VfF** and **vFf** also formed rod-like morphology with a diameter of ~0.1 µm for both peptides. Interestingly, **VFf** exhibited two morphologies: rod-like structure (~2 µm diameter) and spherical structure (~0.32 µm diameter). The remaining **vfF** showed only spherical morphology with ~1 µm diameter. (Figure 6.2) Overall morphology analysis revealed that different hetero-chiral peptides showed different morphology, but the enantiomer of corresponding peptides showed almost the same morphology.

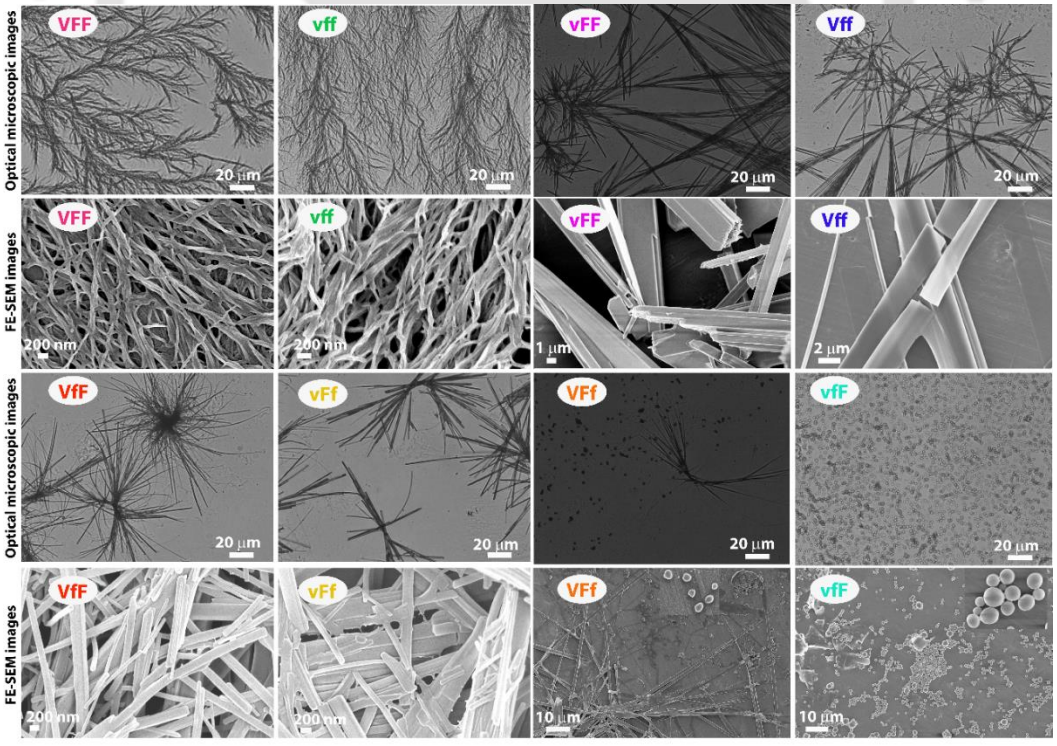

Figure 6.2. *Optical microscopic and FESEM images of self-aggregated enantiomeric peptides in 50% acetonitrile-water solution using a concentration of 1.5 mM.*

6.5. Conformation analysis by CD experiment in solution

Circular dichroism is essential for adequately determining the secondary structure conformation of self-assembled peptides. One characteristic feature of CD is that all enantiomers of relative peptides are shown mirror images from the baseline. Each 1.5 mM four days incubated peptide solution in 50% acetonitrile-water was diluted to 750 µM to overcome high HT voltage and carried out CD analysis. The enantiomeric pair of all tri-peptides displayed opposite CD signals with respect to baseline. Interestingly, four peptides such as (**VFF**, **vff**) and (**vFF**, **Vff**) exhibited either one positive maximum or one minimum negative band around 225-230 nm region. The remaining four peptides, such as (**VfF**, **vFf**) and (**VFf**, **vfF**), did not display any characteristic CD signal in this region (Figure 6.3). All enantiomeric tri-peptides displayed another characteristic: positive maximum or negative minimum bands. The obtained data indicated peptides formed a mixture of beta-sheet and random coil structure is in solution.

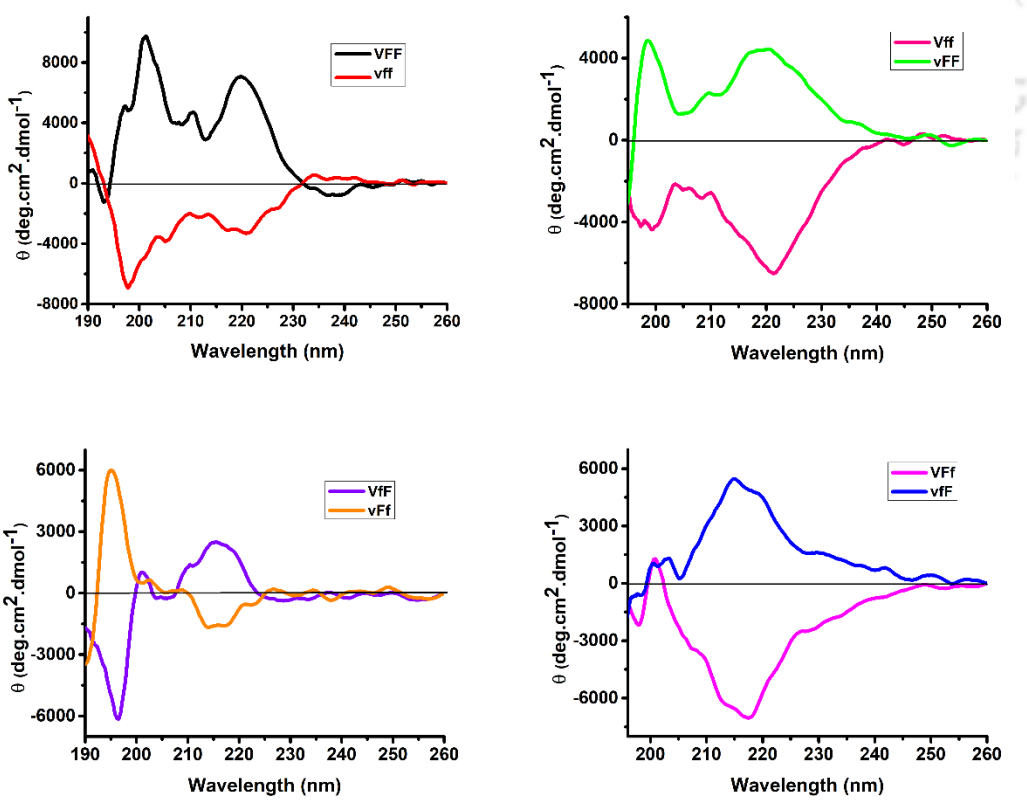

Figure 6.3. *CD spectra of all enantiomeric tripeptide in 50% acetonitrile-water using concentration 750 µM.*

6.6. Investigation of secondary structure by FT-IR

After that, to understand the secondary structure conformation, we performed FT-IR of 4 days incubated peptides sample in acetonitrile-water (1:1) at 37 °C. Amide II and I bands are important for determining secondary structure. The amide I band (1600-1700 cm^{-1}) is related to the C=O stretching frequency and backbone conformation. Amide II band is mainly associated with N-H bending and C-N stretching frequency. The obtained FT-IR spectra displayed a remarkable amide I band nearly at 1645 cm^{-1}, indicating peptides self-assembled in a beta-sheet structure in solution (Figure 6.4).

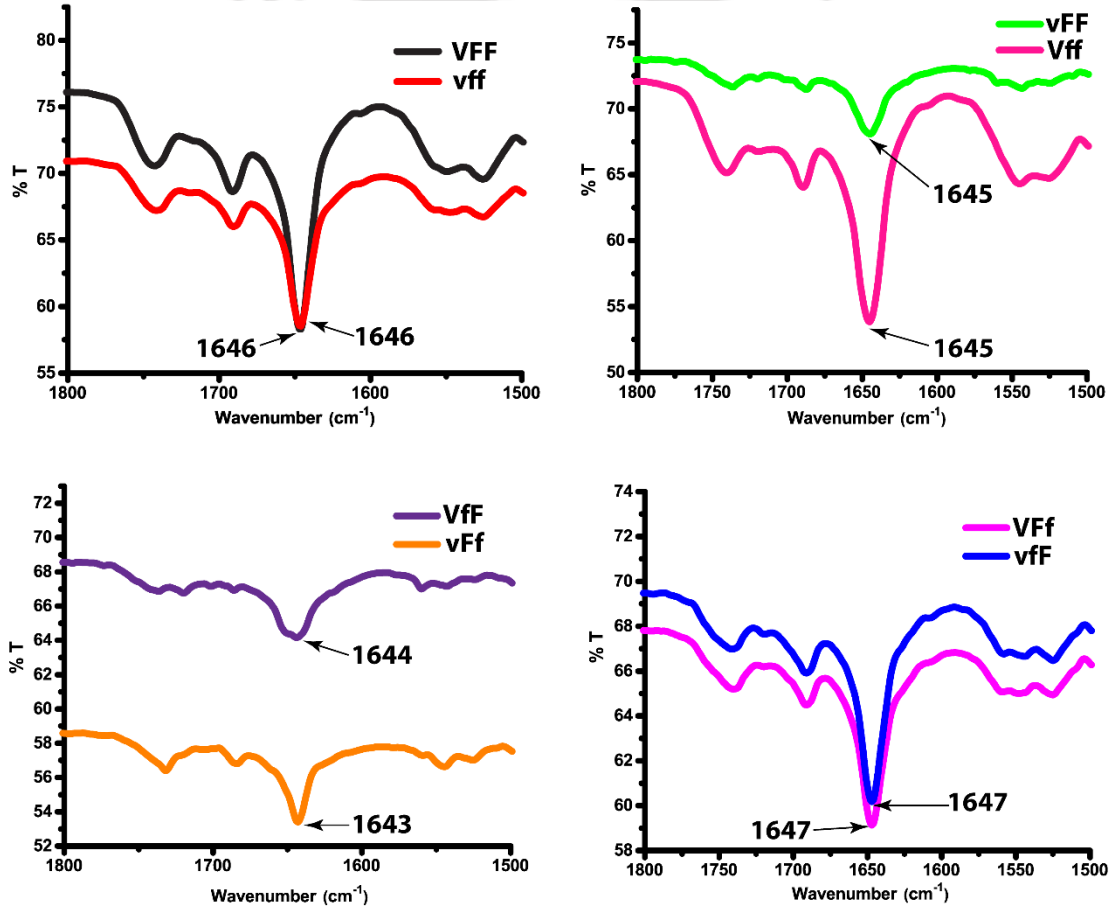

Figure 6.4. *FT-IR spectra of amide I band of all tripeptides.*

6.7. Supramolecular assembly of tri-peptides by SC-XRD

After that, to get molecular-level information, we carried out SC-XRD experiments of heterochiral tripeptides in the crystalline state. The single crystals were obtained by slow evaporation ACN-H_2O solvent at room temperature. The crystal of **VFF** and **vff** were not obtained may be due to their poor crystalline properties. Although we got the crystal of **vFF** and **Vff**, but we could not analyze the structure of **vFF** because of poor crystal quality. Peptide **Vff** crystallized in the monoclinic (*P 21*) system and displayed one molecule in the asymmetric unit in solid-state (Figure 6.5a). In the crystalline state, the peptide stabilized via an intermolecular hydrogen bond and formed a parallel β-sheet structure along the *b*-axis (Figure 6.5b). Two kinds of intermolecular H-bonding interactions are present in peptide crystal structure such as (i) NH group (L-Val) of one subunit interlinked to O=C (urethane) of the next subunit and (ii) NH group (D-Phe) of one subunit interlinked to O=C (L-Val) of another subunit. In higher-order packing, each subunit is further self-organized to form a supramolecular sheet-like structure through various non-covalent interactions along the crystallographic *b*-axis (Figure 6.5c).

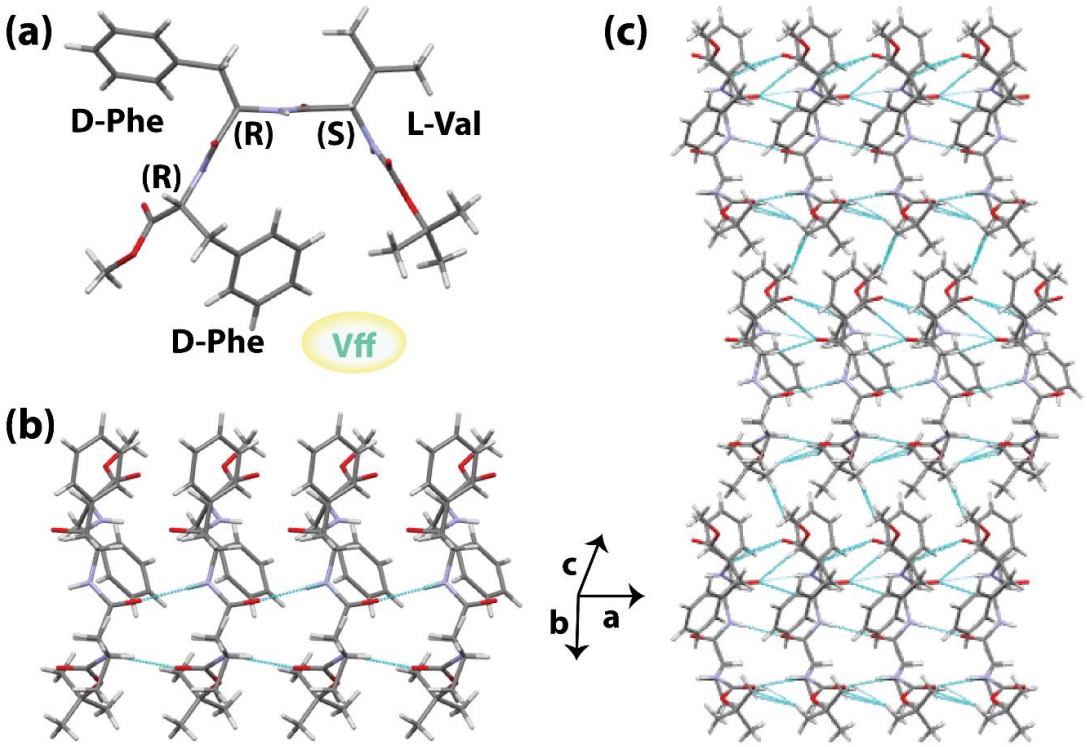

Figure 6.5. *(a) Crystal structure, (b) parallel-β-sheet structure, and (c) sheet-like supramolecular structure in the higher-order assembly of peptide Boc L-Val-D-Phe-D-Phe-OMe (**Vff**)*

Two enantiomeric peptides **VfF** and **vFf** crystallized in the triclinic (*P 1*) system and exhibited one molecule in the asymmetric unit (Figure 6.6a). In the crystalline state, both peptides stabilized via intermolecular hydrogen bonds and formed parallel β-sheet structures along the *a*-axis (Figure 6.6b). Three kinds of intermolecular H-bonding interactions are present in peptide crystal structure such as (i) NH group (Val) of one subunit interlinked to O=C (urethane) of the next subunit, (ii) NH group (Phe) of one subunit interconnected to O=C (Val) of another subunit, and NH group (Phe) of one subunit interlinked to O=C (Phe) of another subunit. Moreover, in higher-order molecular packing, both peptides further self-organized to form supramolecular sheet-like structures through various non-covalent interactions along the crystallographic *c*-axis (Figure 6.6c).

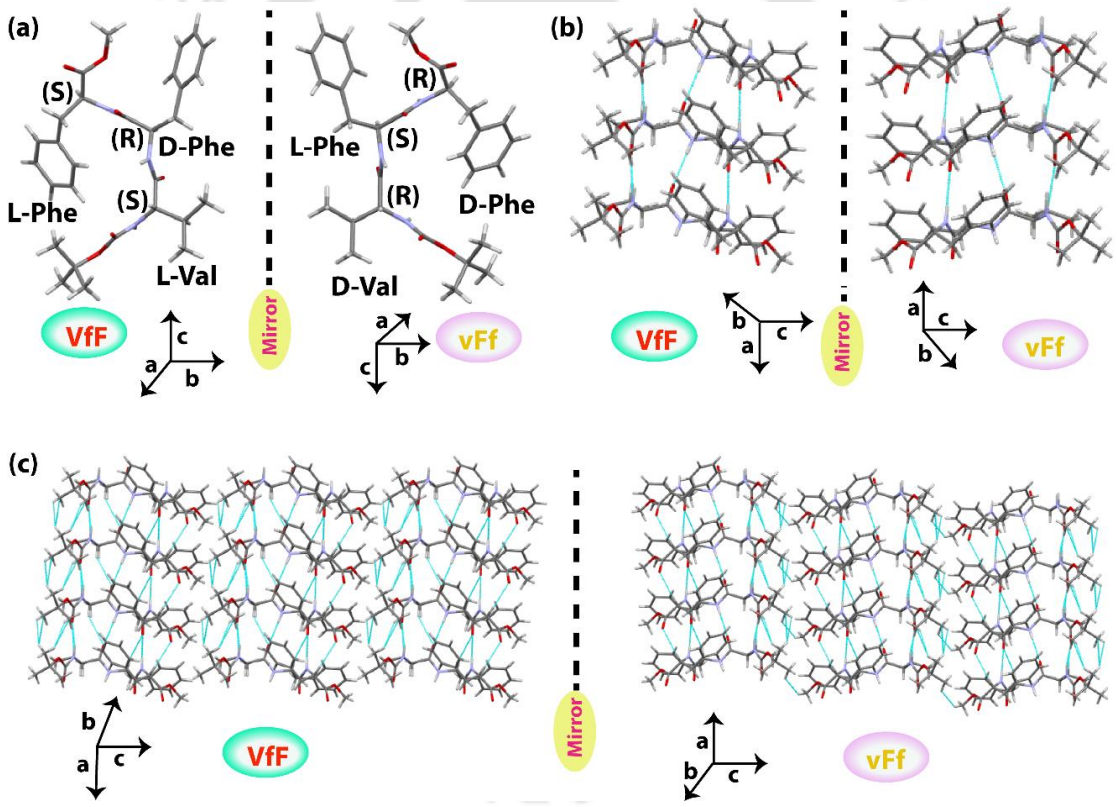

Figure 6.6. *Enantiomeric (a) crystal structure, (b) parallel β-sheet structure, and (c) supramolecular sheet-like structure in higher-order packing of peptide Boc-L-Val-D-Phe-L-Phe-OMe (**VfF**) and Boc-D-Val-L-Phe-D-Phe-OMe (**vFf**)*

Another two enantiomeric peptides **VFf** and **vfF** crystallized in an orthorhombic (*P 21 21 21*) system and displayed one molecule in the asymmetric unit (Figure 6.7a). In the crystalline state, both peptides stabilized via intermolecular hydrogen bond and formed

parallel β-sheet structures along the *a*-axis (Figure 6.7b). Three kinds of intermolecular H-bonding interactions are present in peptide crystal structure such as (i) NH group (Val) of one subunit interlinked to O=C (urethane) of the next subunit, (ii) NH group (Phe) of one subunit interconnected to O=C (Val) of another subunit, and NH group (Phe) of one subunit interlinked to O=C (Phe) of another subunit. Moreover, in higher-order molecular packing, both peptides further self-organized to form a helical sheet-like structure through various non-covalent interactions along the crystallographic *c*-axis (Figure 6.7c). Furthermore, a spacefill representation of both peptides exhibited mirror image helical architecture along *c*-axis (Figure 6.7d). The measured backbone torsion angles, intermolecular H-bonding, and crystallographic refinement data are listed in Tables 6.2, 6.3, and 6.4 (Section 6.14).

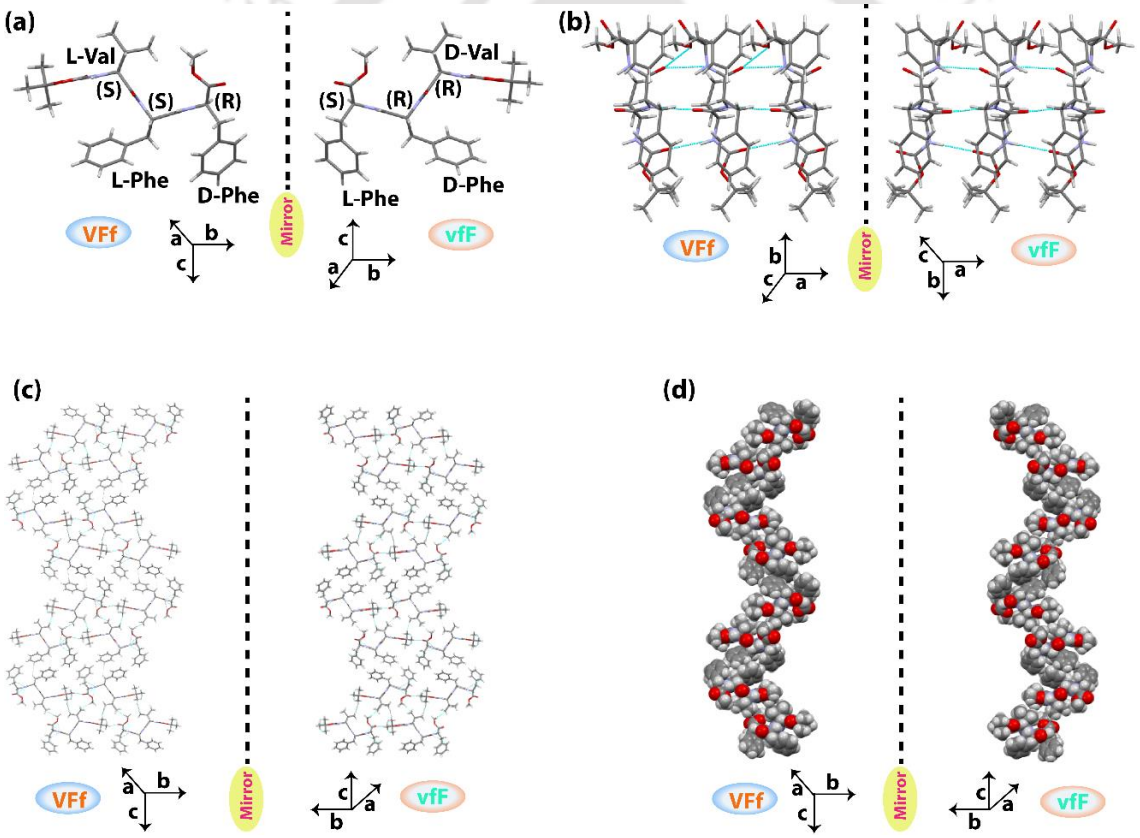

Figure 6.7. *Enantiomeric (a) crystal structure, (b) parallel β-sheet arrangement, (c) helical sheet-like structure, and (d) helical spacefill representation in higher-order packing, of peptides Boc-L-Val-L-Phe-D-Phe-OMe (**VFf**) and Boc-D-Val-D-Phe-L-Phe-OMe (**vfF**)*

Therefore, overall SC-XRD analysis revealed that five peptides with different chirality created parallel β-sheet arrangements via intermolecular H-bonding. Moreover, further

self-association of **Vff**, **VfF**, and **vFf** exhibited sheet-like architecture, and peptides **VFf** and **vfF** exhibited helical sheet-like arrangement. A mirror image relationship was noticed for enantiomeric peptides in the crystallographic arrangement. So, chirality plays a significant role in different crystallographic arrangements.

6.8. ThT dye-binding affinity of peptides by fluorescence microscope

After that, we performed fluorescence microscopy to check the amyloidogenic nature of self-assembled peptides. For this purpose, each peptide solution mixed with ThT dye, used to identify amyloid fibrils. We noticed that all tri-peptides displed several fiber networks in the ThT test and its corresponding bright-field analysis (Figure 6.8). Therefore, all peptides can bind with ThT dye, which suggests all self-aggregated tri-peptides formed supramolecular β-sheet structures, which was also confirmed by CD, FT-IR, and SC-XRD techniques. ThT dye-binding affinity suggests close relationships between these peptides with various amyloidogenic diseases, such as Parkinson's and Alzheimer's disease. In this context, our group also discussed the ThT dye-binding affinity of three di-peptides $A\beta_{39\text{-}40}$, $A\beta_{40\text{-}41}$, and $A\beta_{41\text{-}42}$.

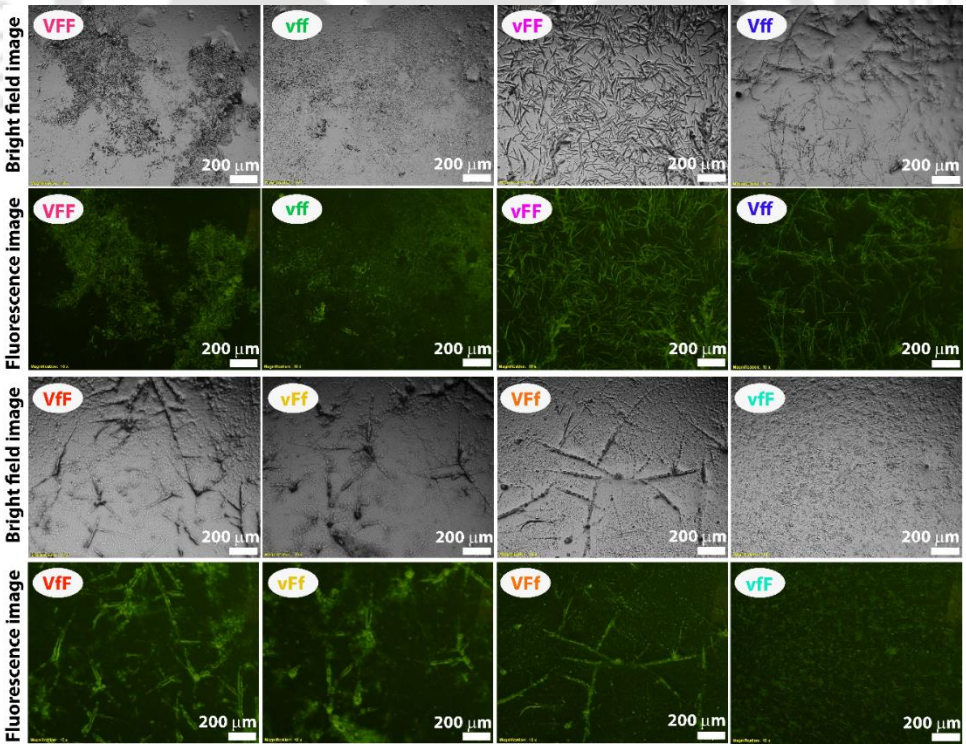

Figure 6.8. *Bright-field and corresponding fluorescence images of peptides stained with ThT.*

A Table 6.1 is listed to compare our results with previously reported ones.

Table 6.1. Noted structural variation of protected and unprotected **VFF** tripeptide stereoisomers (**VFF** represents L-amino acids and vff represents D-isomers).

	peptides		FESEM	CD	FT-IR	SC-XRD	ThT Experiment
Previous works	**Protected**	VFF	entangled nanofiber networks.[7]	significant conformational change after and before sonication.[7]		-	-
	Unprotected	vFF, Vff	-	β-sheet structure. [8]	anti-parallel beta-sheet.[8]	-	uninterrupted fiber networks.[8]
		VfF, vFf	-			-	isolated amyloid structures.[8]
		vFF, fFV	-	β-sheet structure. [9]	anti-parallel beta-sheet for fFV.[9]	-	tangled networks.[9]
		VFF, FFV	-	no predominant secondary structure.[9]	mixture of secondary structure predominantly anti-parallel aggregate for VFF and random coil for FFV.[9]	-	-
		fFV, Ffv	-	β-sheet structure.[10]	anti-parallel beta-sheet.[10]	-	complicated fiber networks.[10]
		FfV, fFv and FFv, ffV	-	no predominant secondary structure.[10]		-	isolated amyloid structures.[10]
Present work	**Protected**	VFF, vff	entangled networks of fibrils	mixture of β-sheet and random coil	parallel beta-sheet	-	fiber networks
		vFF, Vff	rod-like structures	mixture of β-sheet and random coil	parallel beta-sheet	parallel-β-sheet structure, sheet-like supramolecular structure (Vff)	fiber networks
		VfF, vFf	rod-like structures	mixture of β-sheet and random coil	parallel beta-sheet	parallel-β-sheet structure, sheet-like supramolecular structure	fiber networks
		VFf	rod-like and spherical structure	mixture of β-sheet and random coil	parallel beta-sheet	parallel-β-sheet structure, helical sheet-like structure	fiber networks
		vfF	spherical structure				

6.9. Conclusion

In summary, we discussed the morphology, conformation, and supramolecular self-assembly of terminally protected Boc-L-Val-L-Phe-L-Phe-OMe (**VFF**), having structural similarity with $A\beta_{18-20}$ and its stereoisomers. Morphology analysis by FESEM suggested that **VFF** and **vff** formed a ribbon-like fiber network. Peptides **vFF**, **Vff**, **VfF** and **vFf** displayed various diameter rod-like structures. Peptide **VFf** created a mixture (rod-like and spherical structure) of morphology, and **vfF** generated spherical morphology. SC-XRD analysis revealed that the five heterochiral stereoisomers (**Vff**, **VfF**, **vFf**, **VFf** and **vfF**) displayed parallel β-sheet structure in solid-state and in higher-order self-assembly, they further self-organized to create supramolecular sheet-like (for **Vff**, **VfF**, and **vFf**), and helical sheet-like arrangement (for **VFf** and **vfF**). Moreover, CD and FT-IR analysis indicated that all self-assembled peptides created the β-sheet structure in solution. Interestingly, enantiomeric peptides exhibited a mirror image relationship as expected. Moreover, all self-aggregated peptides can bind with amyloid binding ThT dye. Therefore, the chirality of amino acids plays a vital role in supramolecular diversity. In some cases, our protected tri-peptides also exhibited similar properties as unprotected tri-peptides (Table 6.1). The obtained results may help design peptide-based materials with excellent properties.

6.10. Experimental section

6.10.1. Materials and instrumentations

As described in chapter 7

6.10.2. General procedure for the synthesis of tripeptides

o-NosylOXY (1 equiv) and DIPEA (1 equiv) were added to Boc-protected amino acid (1 equiv) dissolved in DCM, and the reaction mixture was then continuously stirred for 5 minutes. 1.2 equiv methyl ester of amino acid dissolved in DCM was first neutralized by DIPEA, then slowly poured into the reaction mixture and stirred at room temperature for another 4-5 h. After the first coupling, the whole solution was diluted with 50 mL DCM solvent and worked up separately with a 10% citric acid solution and saturated $NaHCO_3$ solution (3 times each). The organic portion was dried over the anhydrous $CaCl_2$ and concentrated under reduced pressure. The obtained terminally protected dipeptide was directly treated with TFA:DCM (90:10) for Boc-group cleavage and volatiles were removed by passing N_2 over the reaction mixture. Finally, neutralized N-terminus free dipeptide was reacted with another Boc-protected amino acid by following the above technique, and the crude tripeptide was obtained. Purification was done by column chromatography over silica gel (60-120 mesh) using EtOAc/Hexane as a mobile phase.

6.10.3. Synthesis of peptide Boc-L-Val-L-Phe-L-Phe-OMe (VFF)

A representative protocol: 265 mg (1.0 mmol) Boc-L-Phe-OH was dissolved in DCM (25 mL). 129 mg (1.0 mmol) DIPEA and 327 mg (1.0 mmol) *o*-NosylOXY were added to that solution and stirred for 5 min for activation. Then, 214 mg (1.2 mmol) of neutralized H_2N-L-Phe-OMe was slowly mixed to the reaction mixture and uniformly stirred for four more hours at room temperature to complete the coupling process. The reaction mixture was diluted with 50 mL DCM and worked up with a 10% citric acid solution and saturated $NaHCO_3$ solution separately (three times each). The organic layer was kept under reduced pressure to get crude terminally protected dipeptide Boc-L-Phe-L-Phe-OMe. To get amine-free dipeptide, Boc-group was cleaved by TFA. After that, neutralized H_2N-L-Phe-L-Phe-OMe was coupled with Boc-L-Val-OH to get the desired tripeptide. Finally, the crude solid product was purified by silica gel column chromatography using EtOAc/Hexane as a

mobile phase. The purity of the synthesized tripeptide was examined by reversed-phase analytical HPLC. The peptide was characterized by 1D (^{1}H and ^{13}C) NMR spectroscopy and mass spectrometry.

6.10.4. Sample preparation

1.5 mM each peptide solution was prepared using a 50% acetonitrile-water solvent. The prepared peptides solutions were incubated for four days at 37 °C. After that, incubated stock solutions were used for CD, FESEM, Fluorescence images, Optical microscopic images, and IR sample preparation.

6.11. Characterization data

Boc-L-Val-L-Phe-L-Phe-OMe (VFF).

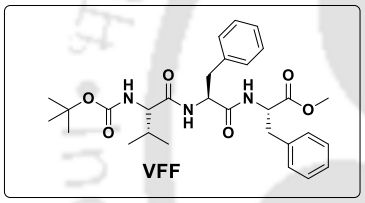

White solid, **^{1}H NMR (600 MHz, $CDCl_3$)** δ 0.79-0.78 (3H, d, J = 6 Hz); 0.87-0.86 (3H, d, J = 7.2 Hz); 1.43 (9H, s); 2.08-2.03 (1H, m); 3.10-2.96 (4H, m); 3.65 (3H, s); 3.92-3.90 (1H, t, J = 6.6 Hz); 4.67-4.64 (1H, dd, J = 6.6 Hz); 4.74-4.71 (1H, dd, J = 6 Hz); 5.01 (1H, s); 6.33 (1H, s); 6.64 (1H, s); 6.96-6.95 (2H, d, J = 6.6 Hz); 7.28-7.18 (8H, m). **^{13}C NMR (150 MHz, $CDCl_3$)** δ 17.6, 19.4, 28.4, 30.9, 38.0, 38.3, 52.3, 53.6, 54.4, 60.1, 80.2, 127.2, 127.3, 128.7, 128.8, 129.3, 129.5, 135.8, 136.4, 156.0, 170.3, 171.4, 171.6. ESI-MS: calculated $[M+H]^+$ 526.2917, obtained m/z 526.2921. HPLC: retention time (t_R) = 5.83 min. The purified tripeptide 390 mg (Yield = 74% w.r.t. initial substrate Boc-L-Phe-OH)

Boc-D-Val-D-Phe-D-Phe-OMe (vff)

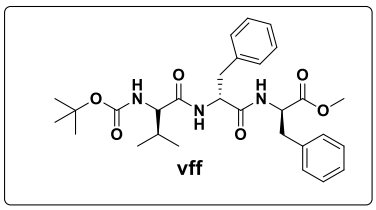

White solid, **^{1}H NMR (600 MHz, $CDCl_3$)** δ 0.73-0.71 (3H, d, J = 6.6 Hz); 0.79-0.78 (3H, d, J = 6.6 Hz); 1.36 (9H, s); 1.99-1.95 (1H, m); 2.98-2.89 (4H, m); 3.56 (3H, s); 3.88-3.85 (1H, t, J = 7.8 Hz); 4.67-4.62 (2H, m); 5.06 (1H, s); 6.45 (1H, s); 6.72 (1H, s); 6.90-6.89 (2H, d, J = 6.6 Hz); 7.19-7.10 (8H, m). **^{13}C NMR (150 MHz, $CDCl_3$)** δ 17.6, 19.3, 28.4, 30.8, 38.0, 38.3, 52.4, 53.6, 54.2, 60.1, 80.1, 127.1, 127.2,

128.7, 128.7, 129.3, 129.5, 135.7, 136.4, 156.0, 170.4, 171.3, 171.7. ESI-MS: calculated $[M+H]^+$ 526.2917, obtained m/z 526.2919. HPLC: retention time (t_R) = 5.83 min. The purified tripeptide 380 mg (Yield = 72% w.r.t. initial substrate Boc-D-Phe-OH).

Boc-D-Val-L-Phe-L-Phe-OMe (vFF)

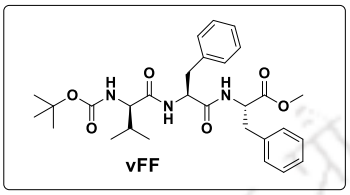

White solid, **^{1}H NMR (600 MHz, $CDCl_3$)** δ 0.73-0.72 (3H, d, *J* = 6.6 Hz); 0.77-0.76 (3H, d, *J* = 6 Hz); 1.45 (9H, s); 1.96-1.95 (1H, m); 3.08-2.99 (4H, m); 3.67 (3H, s); 3.87-3.85 (1H, t, *J* = 6.6 Hz); 4.78-4.75 (2H, m); 5.20 (1H, s); 6.74 (1H, s); 6.79 (1H, s); 7.03-7.02 (2H, d, *J* = 6 Hz); 7.18-7.17 (2H, d, *J* = 6.6 Hz); 7.28-7.20 (6H, m). **^{13}C NMR (150 MHz, $CDCl_3$)** δ 18.1, 19.2, 28.4, 31.0, 37.8, 37.8, 52.4, 53.7, 54.2, 60.2, 80.2, 127.1, 127.2, 128.7, 128.8, 129.3, 129.4, 136.0, 136.5, 156.1, 170.7, 171.5, 171.9. ESI-MS: calculated $[M+H]^+$ 526.2917, obtained m/z 526.2915. HPLC: retention time (t_R) = 5.88 min. The purified tripeptide 376 mg (Yield = 71% w.r.to initial substrate Boc-L-Phe-OH).

Boc-L-Val-D-Phe-D-Phe-OMe (Vff)

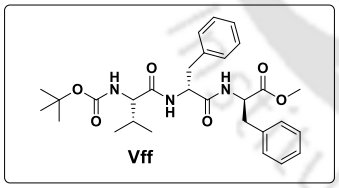

White solid, **^{1}H NMR (400 MHz, $CDCl_3$)** δ 0.74-0.72 (3H, d, *J* = 6.8 Hz); 0.78-0.77 (3H, d, *J* = 6.4 Hz); 1.44 (9H, s); 2.00-2.19 (1H, m); 3.07-2.96 (4H, m); 3.66 (3H, s); 3.82-3.79 (1H, t, *J* = 7.6 Hz); 4.71-4.65 (1H, dd, *J* = 7.2 Hz); 4.77-4.72 (1H, dd, *J* = 6.8 Hz); 4.99-4.97 (1H, d, *J* = 7.2 Hz); 6.38-6.36 (1H, d, *J* = 6.4 Hz), 6.50-6.48 (1H, d, *J* = 6.4 Hz); 7.00-6.99 (2H, d, *J* = 5.2 Hz), 7.17-7.16 (2H, d, *J* = 6.8 Hz), 7.26-7.21 (6H, m). **^{13}C NMR (100 MHz, $CDCl_3$)** δ 17.7, 19.2, 28.5, 30.8, 37.8, 37.9, 52.4, 53.6, 54.2, 60.4, 80.3, 127.2, 128.7, 128.9, 129.4, 129.5, 136.1, 136.5, 156.1, 170.0, 171.5, 171.7. ESI-MS: calculated $[M+H]^+$ 526.2917, obtained m/z 526.2925. HPLC: retention time (t_R) = 5.89 min. The purified tripeptide 365 mg (Yield = 69% w.r.t. initial substrate Boc-D-Phe-OH).

Boc-L-Val-D-Phe-L-Phe-OMe (VfF)

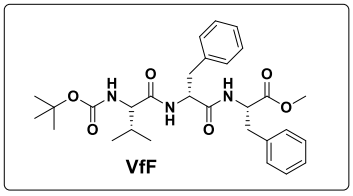

White solid, **^{1}H NMR (600 MHz, $CDCl_3$)** δ 0.74-0.72 (3H, d, J = 6.6 Hz); 0.77-0.76 (3H, d, J = 5.4 Hz); 1.42 (9H, s); 1.98-1.94 (1H, m); 3.09-2.97 (4H, m); 3.63 (3H, s); 3.86-3.84 (1H, t, J = 6 Hz); 4.81-4.74 (2H, m); 5.16 (1H, s); 6.77 (1H, s); 6.85 (1H, s); 6.97-6.96 (2H, d, J = 6 Hz); 7.14-7.13 (2H, d, J = 6.6 Hz); 7.26-7.21 (6H, m). **^{13}C NMR (150 MHz, $CDCl_3$)** δ 17.7, 19.2, 28.4, 31.0, 38.0, 38.1, 52.4, 53.5, 54.3, 60.1, 80.1, 127.1, 127.2, 128.7, 128.8, 129.3, 129.5, 135.9, 136.6, 156.0, 170.6, 171.8, 171.8. ESI-MS: calculated $[M+H]^+$ 526.2917, obtained m/z 526.2929. HPLC: retention time (t_R) = 5.89 min. The purified tripeptide 395 mg (Yield = 75% w.r.t. initial substrate Boc-D-Phe-OH).

Boc-D-Val-L-Phe-D-Phe-OMe (vFf)

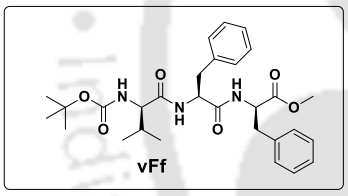

White solid, **^{1}H NMR (600 MHz, $CDCl_3$)** δ 0.76-0.75 (3H, d, J = 6.6 Hz); 0.79-0.78 (3H, d, J = 6 Hz); 1.43 (9H, s); 1.99-1.96 (1H, m); 3.00-2.99 (4H, m); 3.66 (3H, s); 3.86-3.85 (1H, t, J = 6 Hz); 4.82-4.72 (2H, m); 5.11-5.10 (1H, d, J = 7.8 Hz); 6.68 (1H, s); 6.78 (1H, s); 6.98-6.97 (2H, d, J = 6.6 Hz); 7.16-7.15 (2H, d, J = 7.2 Hz); 7.28-7.23 (6H, m). **^{13}C NMR (150 MHz, $CDCl_3$)** δ 17.7, 19.2, 28.4, 30.9, 38.0, 38.1, 52.4, 53.5, 54.3, 60.2, 80.1, 127.2, 127.3, 128.7, 128.8, 129.3, 129.5, 135.9, 136.6, 156.0, 170.5, 171.8, 171.8. ESI-MS: calculated $[M+H]^+$ 526.2917, obtained m/z 526.2924. HPLC: retention time (t_R) = 5.89 min. The purified tripeptide 385 mg (Yield = 73% w.r.to initial substrate Boc-L-Phe-OH).

Boc-L-Val-L-Phe-D-Phe-OMe (VFf)

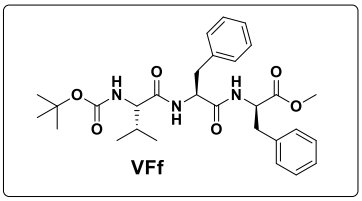

White solid, **^{1}H NMR (600 MHz, $CDCl_3$)** δ 0.74-0.73 (3H, d, *J* = 6.6 Hz); 0.78-0.72 (3H, d, *J* = 6.6 HZ); 1.45 (9H, s); 1.98-1.95 (1H, m); 3.09-2.99 (4H, m); 3.67 (3H, s); 3.86-3.83 (1H, t, *J* = 6.6 Hz); 4.79-4.71 (2H, m); 5.13-5.11 (1H, d, *J* = 8.4 Hz); 6.60-6.59 (1H, d, *J* = 7.8 Hz); 6.69-6.68 (1H, d, *J* = 7.2 Hz); 7.03-7.02 (2H, d, *J* = 6 Hz); 7.18-7.17 (2H, d, *J* = 7.2 Hz); 7.28-7.22 (6H, m). **^{13}C NMR (150 MHz, $CDCl_3$)** δ 17.7, 19.2, 28.4, 30.9, 37.8, 37.8, 52.4, 53.6, 54.2, 60.3, 80.2, 127.1, 127.2, 128.7, 128.8, 129.3, 129.5, 136.0, 136.5, 156.0, 170.6, 171.5, 171.8. ESI-MS: calculated $[M+H]^+$ 526.2917, obtained m/z 526.2918. HPLC: retention time (t_R) = 5.86 min. The purified tripeptide 370 mg (Yield = 70% w.r.to initial substrate Boc-L-Phe-OH).

Boc-D-Val-D-Phe-L-Phe-OMe (vfF)

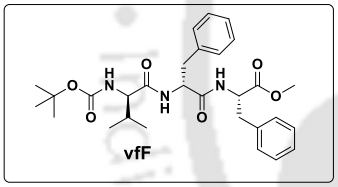

White solid, **^{1}H NMR (600 MHz, $CDCl_3$)** δ 0.79-0.78 (3H, d, *J* = 6 Hz); 0.88-0.87 (3H, d, *J* = 6.6 Hz); 1.43 (9H, s); 2.08-2.07 (1H, m); 3.07-2.98 (4H, m); 3.63 (3H, s); 3.95-3.93 (1H, t, *J* = 6.6 Hz); 4.78-4.72 (2H, m); 5.09 (1H, s); 6.81 (1H, s); 6.98-6.97 (2H, d, *J* = 6 Hz); 7.14-7.13 (2H, d, *J* = 6.6 Hz); 7.29-7.22 (6H, m). **^{13}C NMR (150 MHz, $CDCl_3$)** δ 17.5, 19.3, 28.4, 30.7, 37.8, 38.2, 52.3, 53.7, 54.1, 60.2, 80.2, 127.1, 127.2, 128.6, 128.7, 129.3, 129.5, 136.0, 136.5, 156.1, 170.5, 171.5, 171.7. ESI-MS: calculated $[M+H]^+$ 526.2919, obtained m/z 526.2927. HPLC: retention time (t_R) = 5.87 min. The purified tripeptide 378 mg (Yield = 72% w.r.to initial substrate Boc-D-Phe-OH).

6.12. References

1. Rajasekhar, K.; Chakrabarti, M.; Govindaraju, T. Function and toxicity of amyloid beta and recent therapeutic interventions targeting amyloid beta in Alzheimer's disease. *Chem. Commun.* **2015**, *51*, 13434-13450.
2. Maity, S.; Kumar, P.; Haldar, D. An amyloid-like fibril-forming supramolecular cross-β-structure of a model peptide: a crystallographic insight. *Org. Biomol. Chem.* **2011**, *9*, 3787.
3. Bera, S.; Jana, P.; Maity, S. K.; Haldar, D. Inhibition of Fibril Formation by Tyrosine Modification of Diphenylalanine: Crystallographic Insights. *Cryst. Growth Des.* **2014**, *14*, 1032-1038.
4. Giri, R. S.; Mandal, B. Boc-Val-Val-OMe (Aβ39-40) and Boc-Ile-Ala-OMe (Aβ41-42) crystallize in a parallel β-sheet arrangement but generate a different morphology. *CrystEngComm* **2018**, *20*, 4441-4448.
5. Ray, S.; Das, A. K.; Drew M. G. B.; Banerjee, A. A short water-soluble self-assembling peptide forms amyloid-like fibrils. *Chem. Commun.*, **2006**, 4230-4232.
6. Naskar, J.; Drew, M. G. B.; Deb, I.; Das S.; Banerjee, A. Water-Soluble tripeptide Aβ (9-11) forms amyloid-like fibrils and exhibits neurotoxicity. *Org. Lett.*, **2008**, *10*, 2625-2628.
7. Maity, S.; Kumar, P.; Haldar, D. Sonication-induced instant amyloid-like fibril formation and organogelation by a tripeptide. *Soft Matter* **2011**, *7*, 5239-5245.
8. Marchesan, S.; Styan, K. E.; Easton, C. D.; Waddington, L.; Vargiu, A. V. Higher and lower supramolecular orders for the design of self-assembled heterochiral tripeptide hydrogel biomaterials. *J. Mater. Chem. B* **2015**, *3*, 8123.
9. Marchesan, S.; Easton, C. D.; Kushkaki, F.; Waddington, L.; Hartley, P. G. Tripeptide self-assembled hydrogels: unexpected twists of chirality. *Chem. Commun.* **2012**, *48*, 2195.
10. Marchesan, S.; Easton, C. D.; Styan, K. E.; Waddington, L. J.; Kushkaki, F.; Goodall, L.; McLean, K. M.; Forsythe, J. S.; Hartley, P. G. Chirality effects at each amino acid position on tripeptide self-assembly into hydrogel biomaterials. *Nanoscale* **2014**, *6*, 5172-5180.

6.13. Selected spectra

6.13.1. Spectra of peptide Boc-L-Val-L-Phe-L-Phe-OMe (VFF)

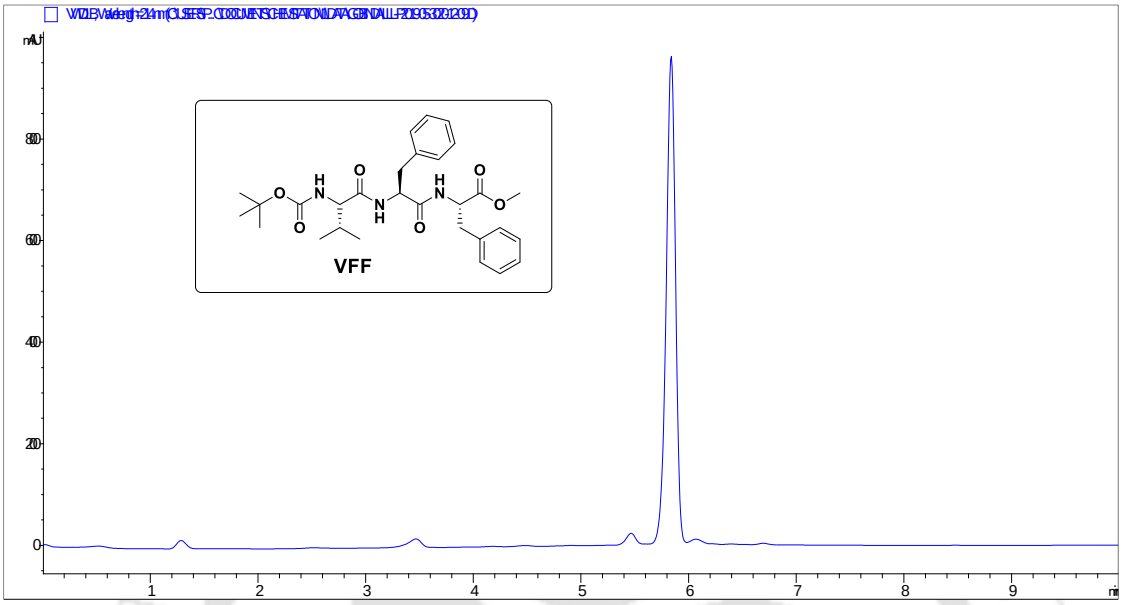

Figure 6.9. *HPLC profile picture of purified peptide* ***VFF***

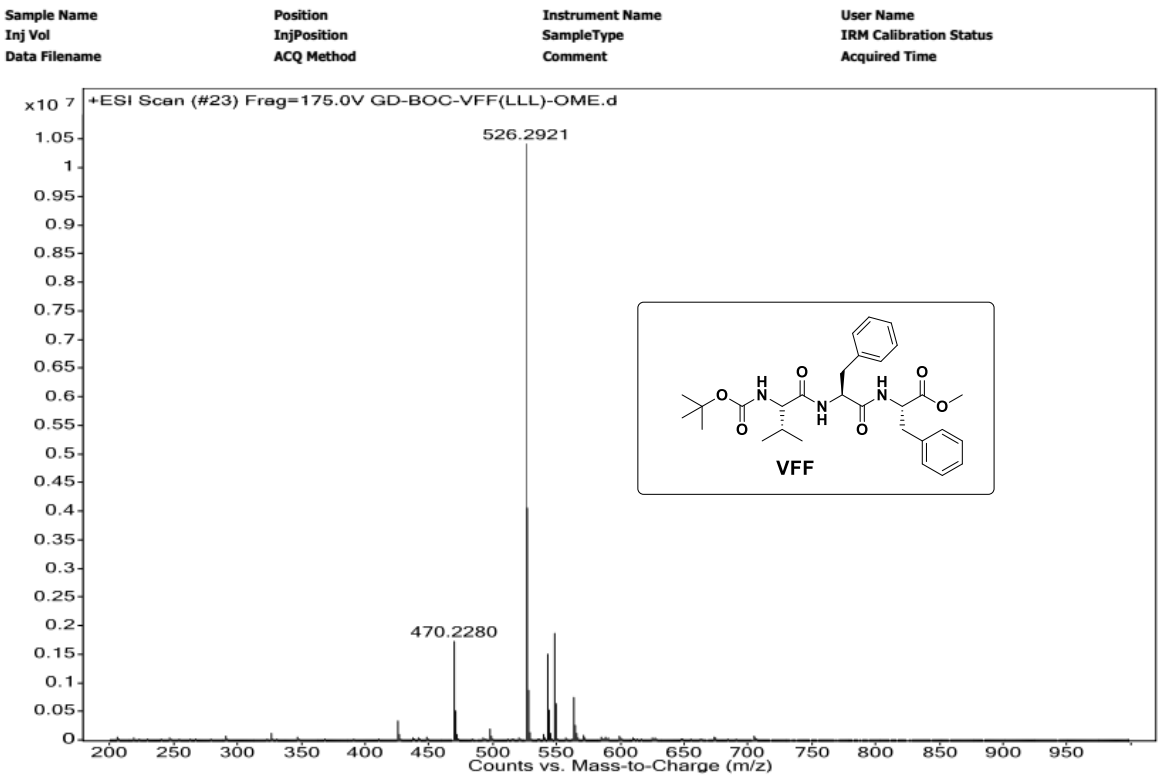

Figure 6.10. *MS spectra of peptide* ***VFF***

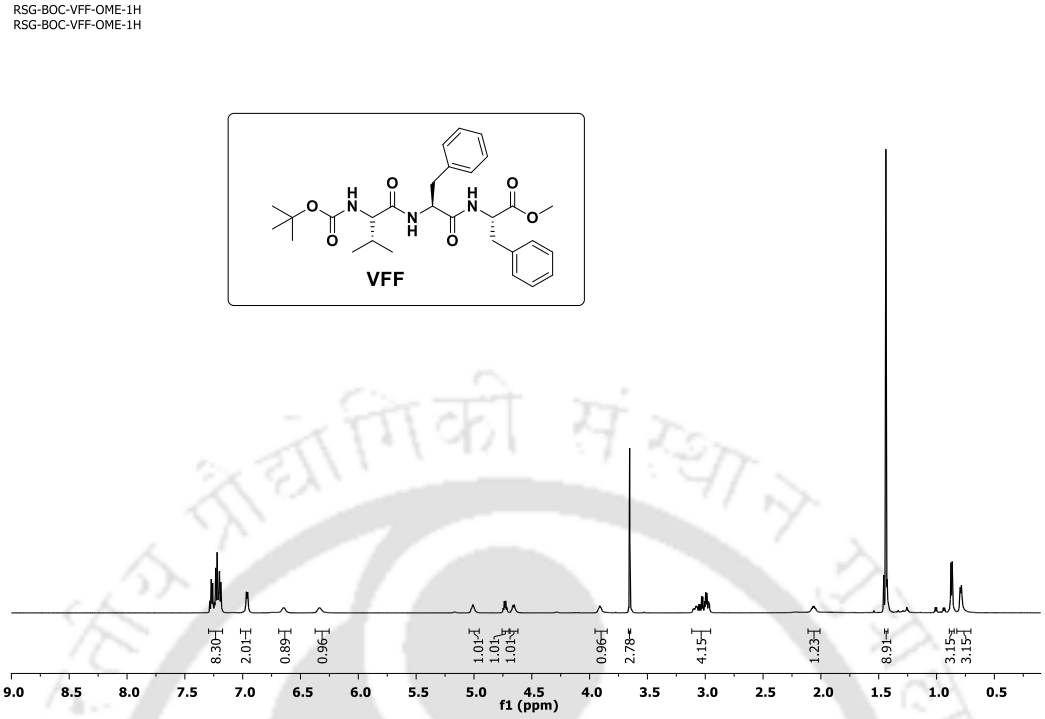

Figure 6.11. *^{1}H NMR spectra of peptide* ***VFF***

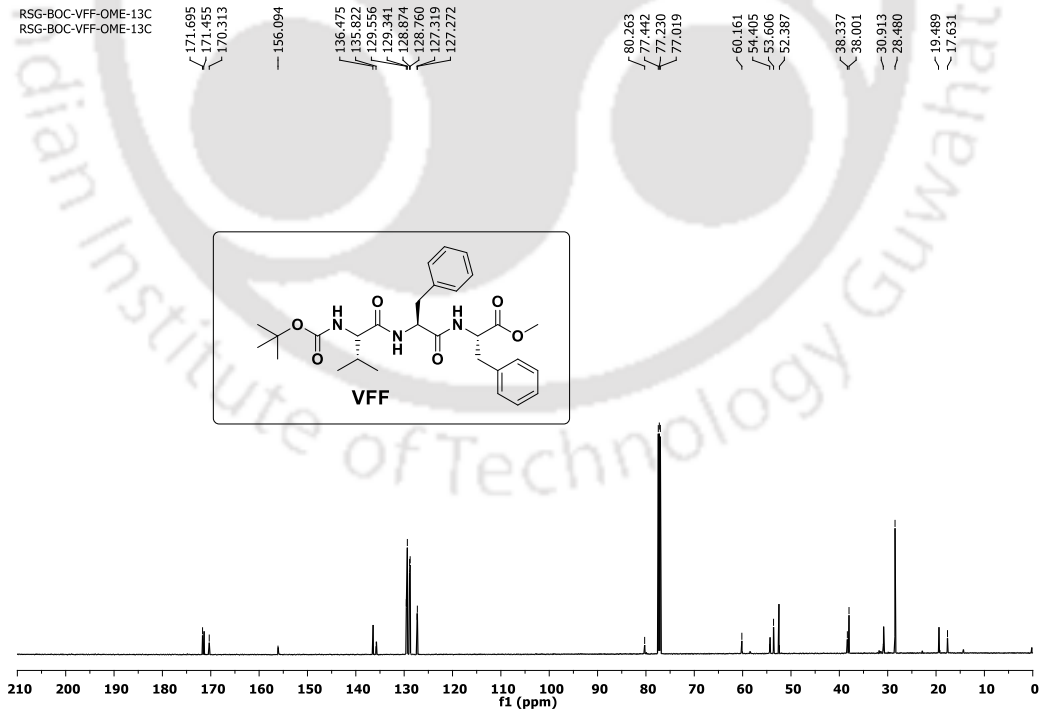

Figure 6.12. *^{13}C NMR spectra of peptide* ***VFF***

6.13.2. Spectra of peptide Boc-D-Val-D-Phe-D-Phe-OMe (vff)

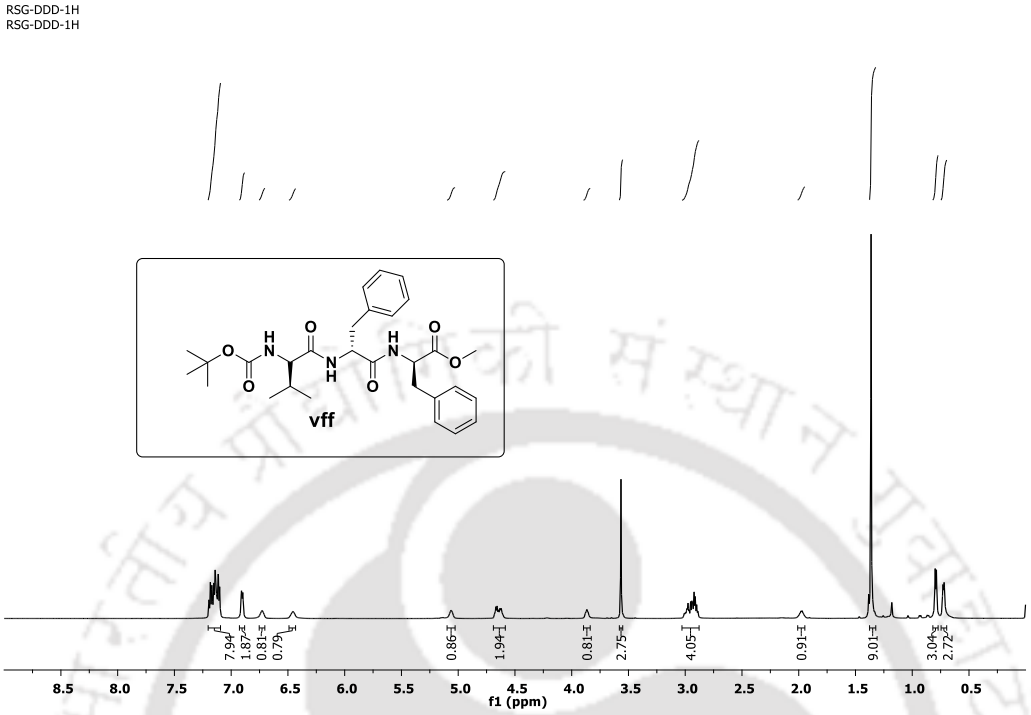

Figure 6.13. *^{1}H NMR spectra of peptide* ***vff***

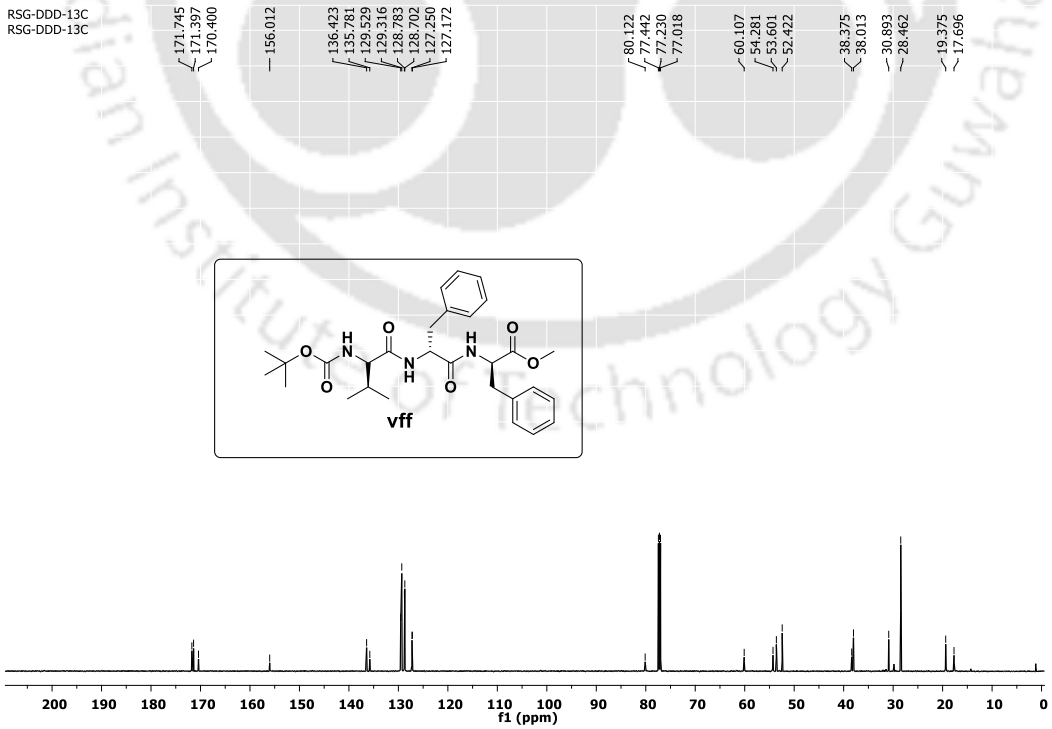

Figure 6.14. *^{13}C NMR spectra of peptide* ***vff***

6.13.3. Spectra of peptide Boc-D-Val-L-Phe-L-Phe-OMe (vFF)

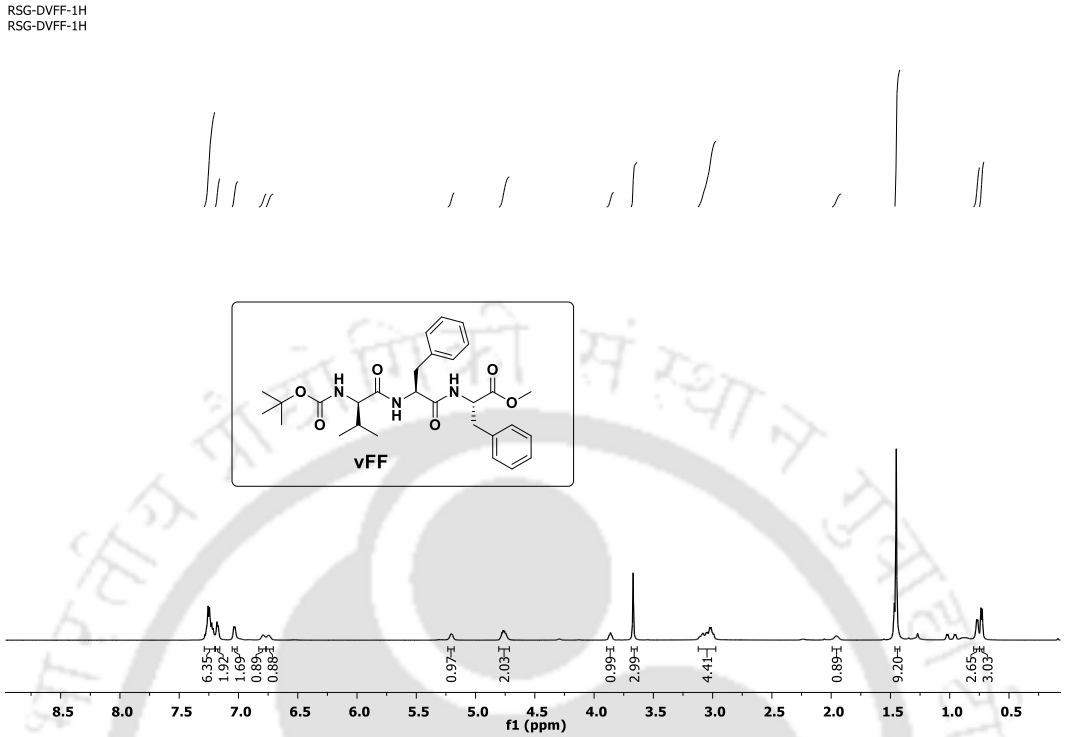

Figure 6.15. *^{1}H NMR spectra of peptide* ***vFF***

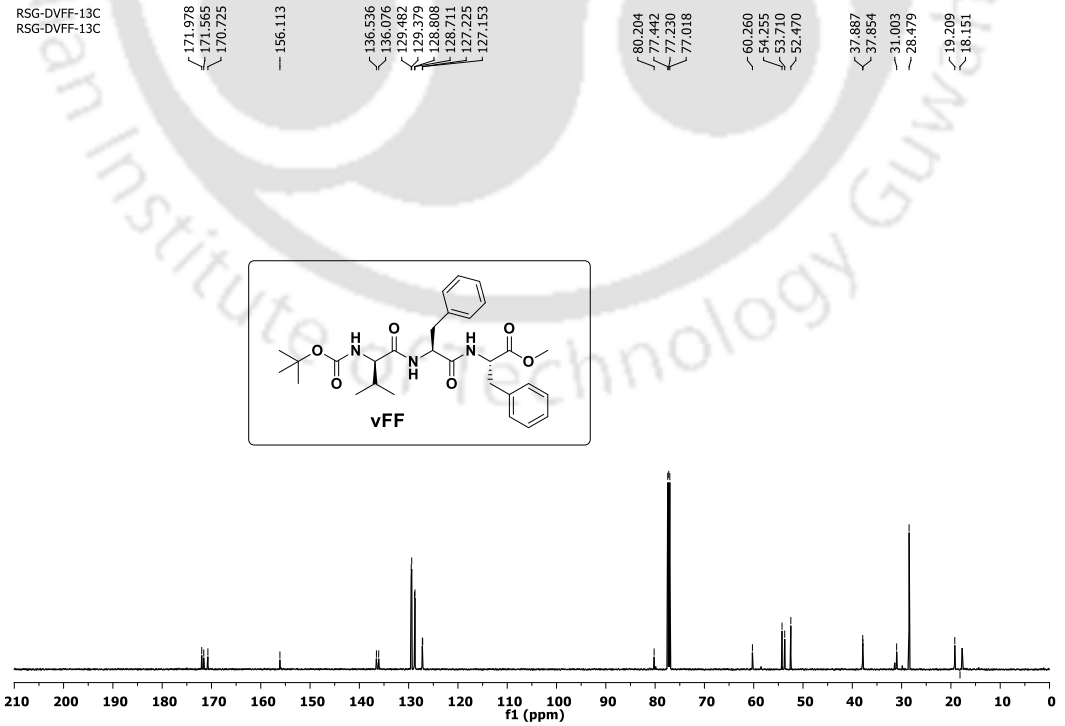

Figure 6.16. *^{13}C NMR spectra of peptide* ***vFF***

6.13.4. Spectra of peptide Boc-L-Val-D-Phe-D-Phe-OMe (Vff)

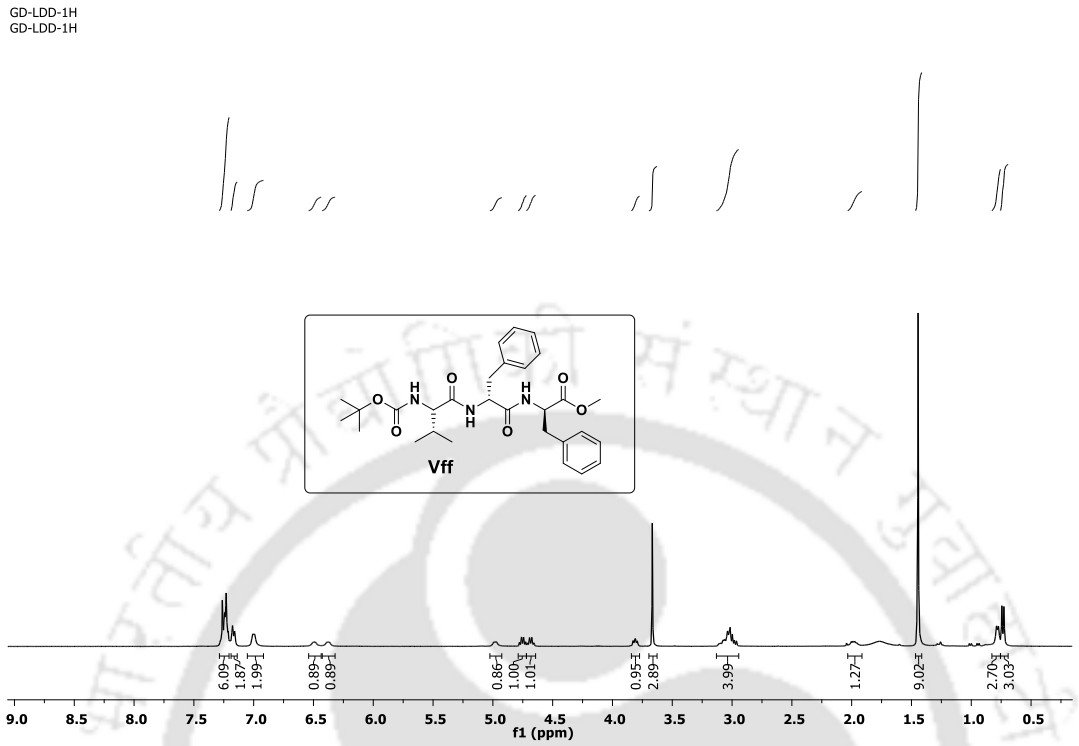

Figure 6.17. *^{1}H NMR spectra of peptide* ***Vff***

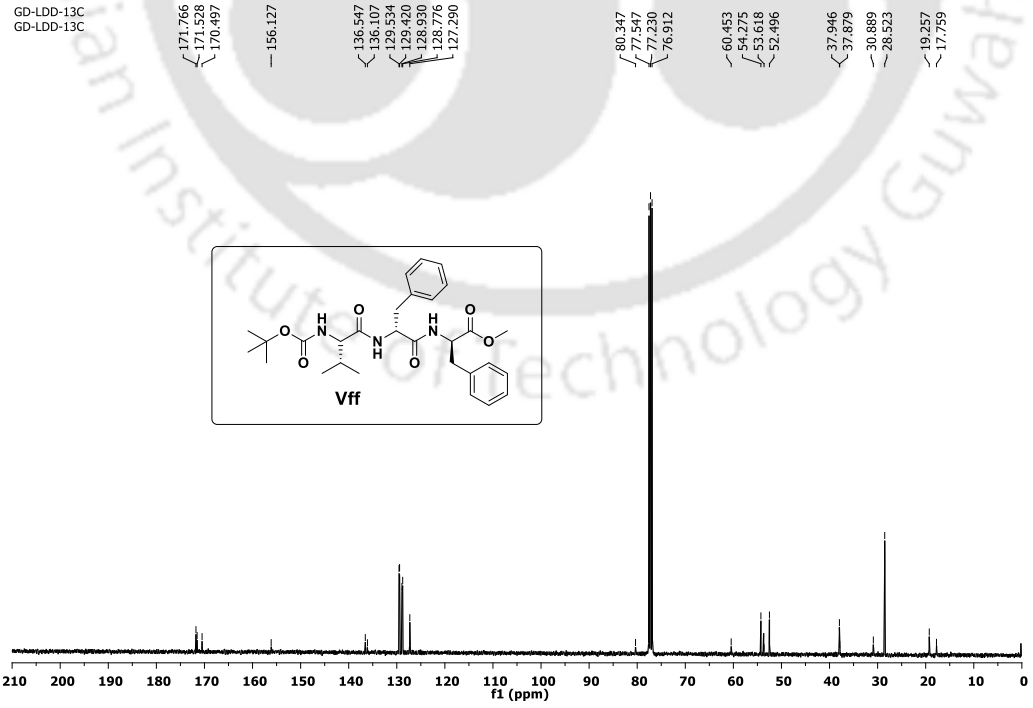

Figure 6.18. *^{13}C NMR spectra of peptide* ***Vff***

6.13.5. Spectra of peptide Boc-L-Val-D-Phe-L-Phe-OMe (VfF)

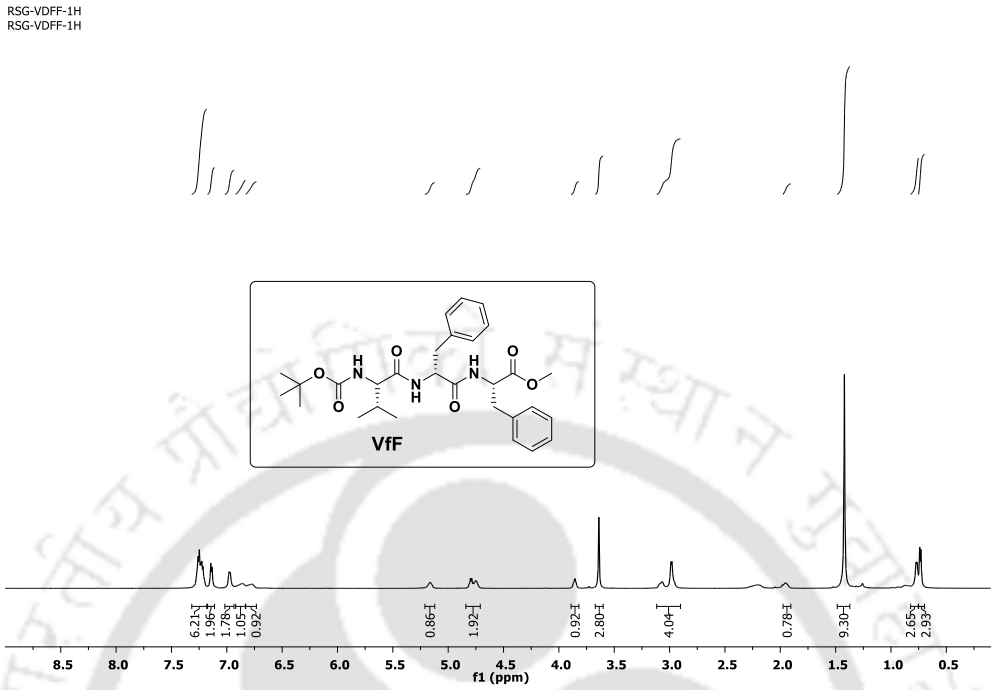

Figure 6.19. *^{1}H NMR spectra of peptide* ***VfF***

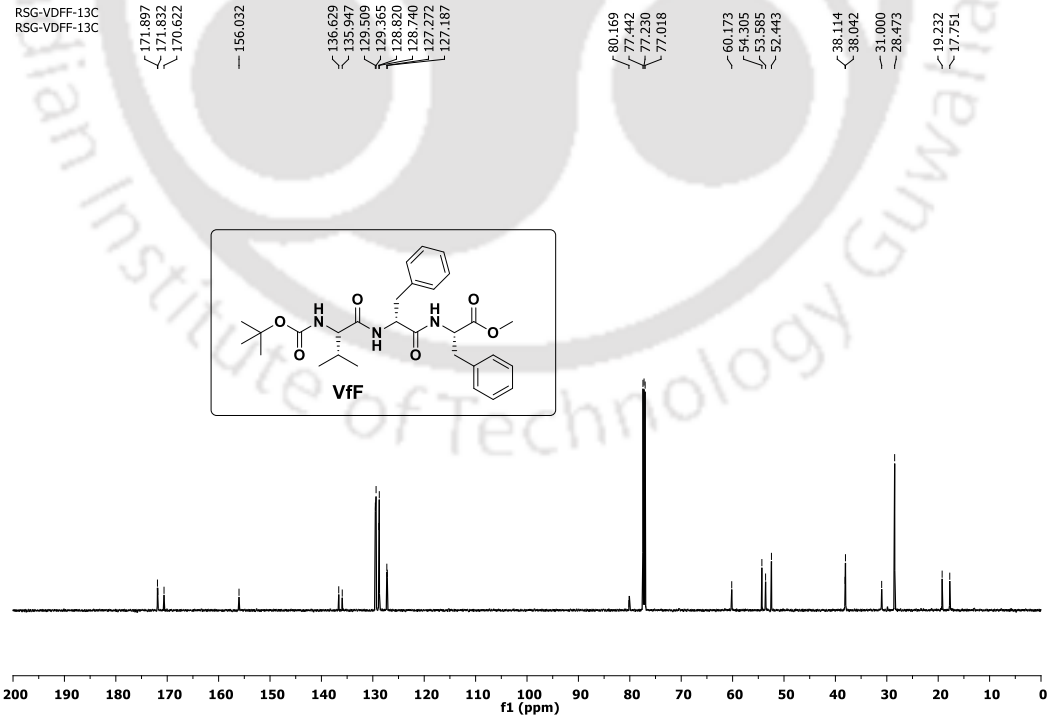

Figure 6.20. *^{13}C NMR spectra of peptide* ***VfF***

6.13.6. Spectra of peptide Boc-D-Val-L-Phe-D-Phe-OMe (vFf)

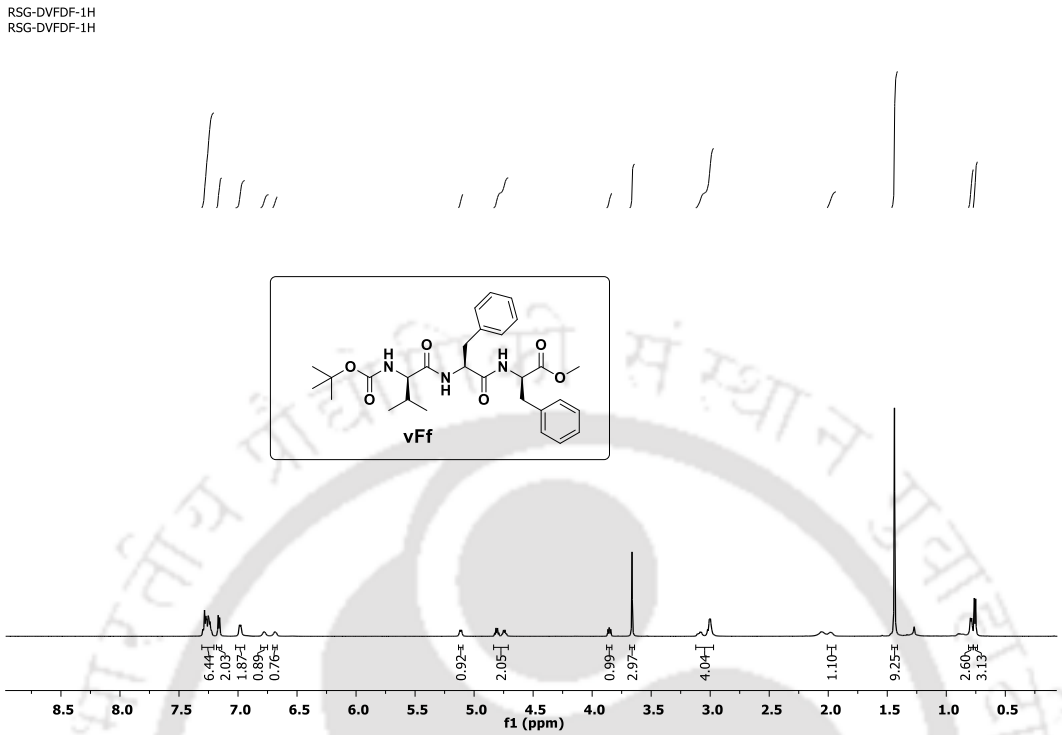

Figure 6.21. *^{1}H NMR spectra of peptide* ***vFf***

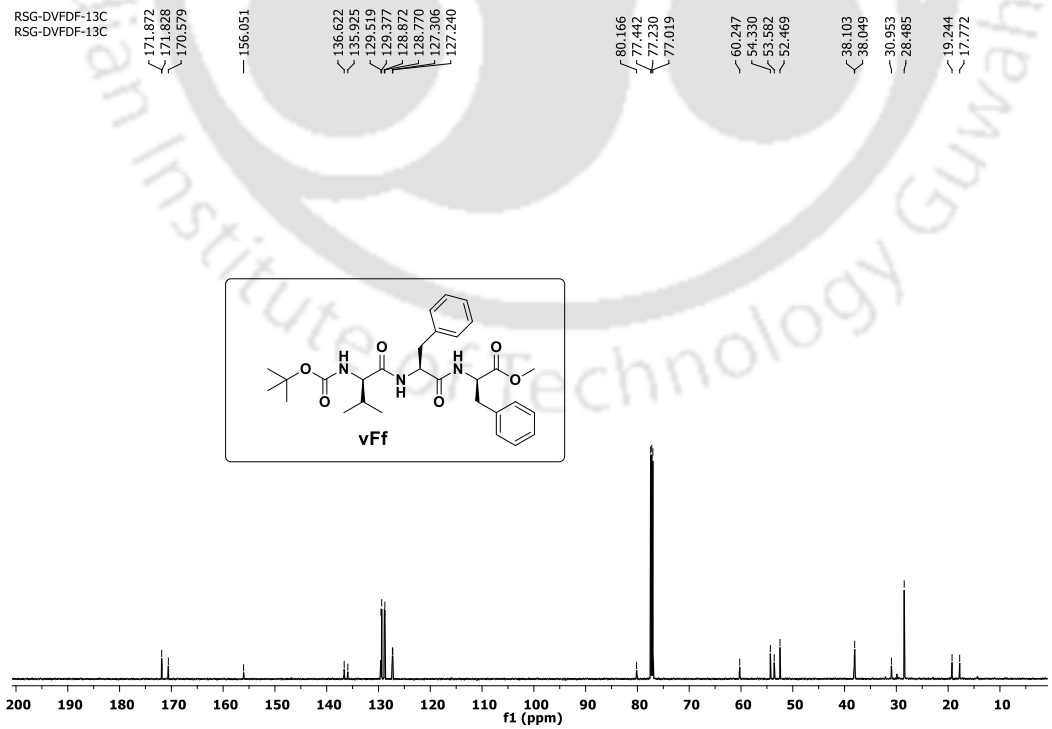

Figure 6.22. *^{13}C NMR spectra of peptide* ***vFf***

6.13.7. Spectra of peptide Boc-L-Val-L-Phe-D-Phe-OMe (VFf)

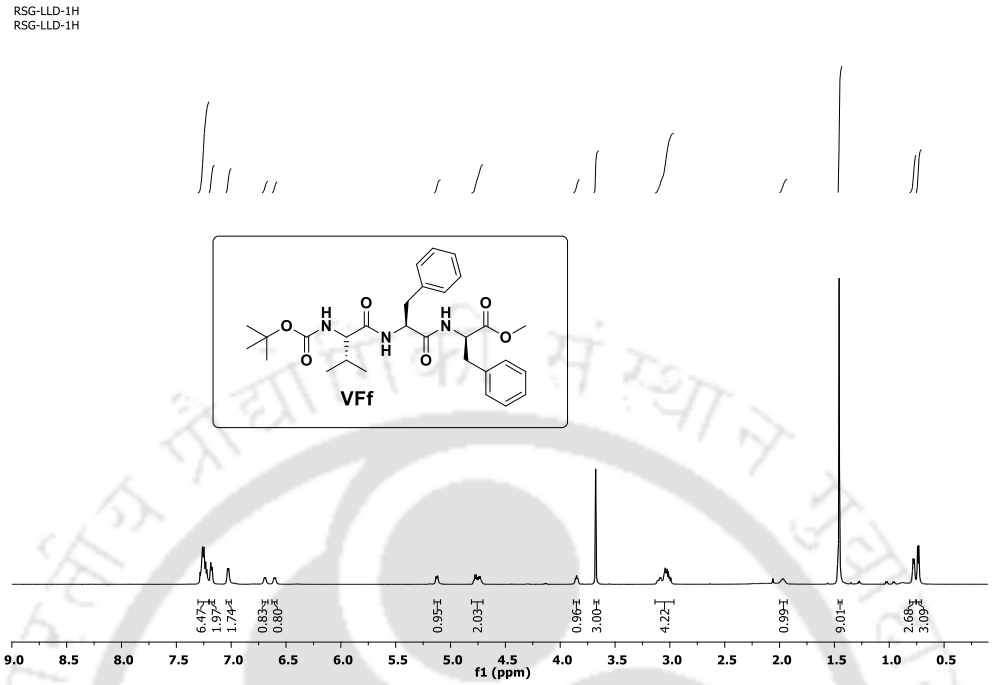

Figure 6.23. *^{1}H NMR spectra of peptide **VFf***

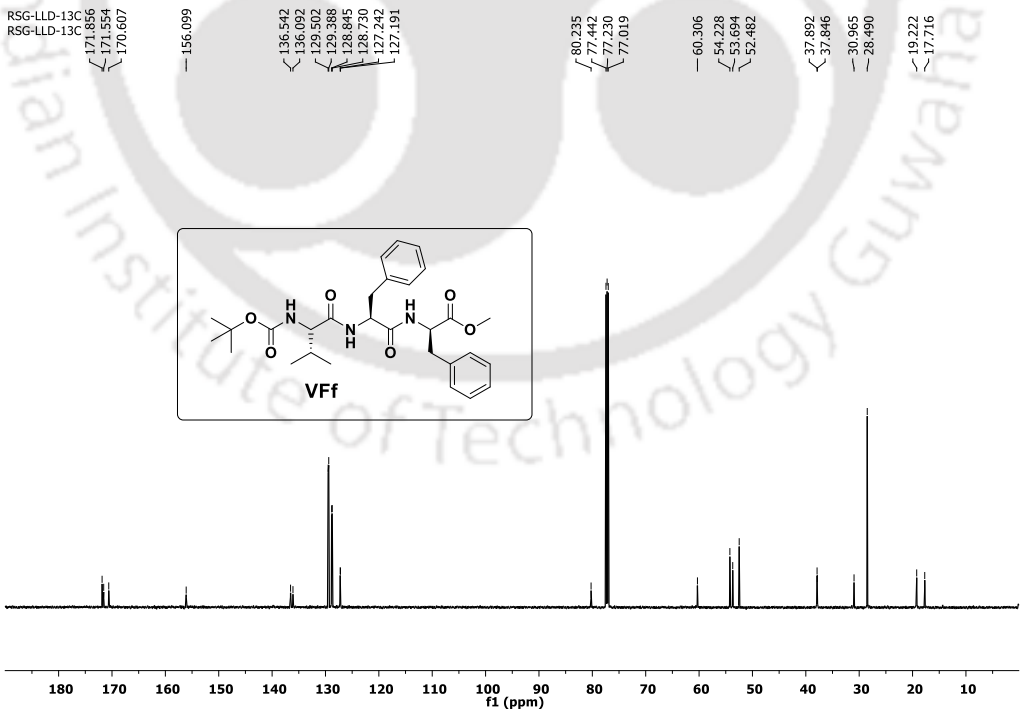

Figure 6.24. *^{13}C NMR spectra of peptide **VFf***

6.13.8. Spectra of peptide Boc-D-Val-D-Phe-L-Phe-OMe (vfF)

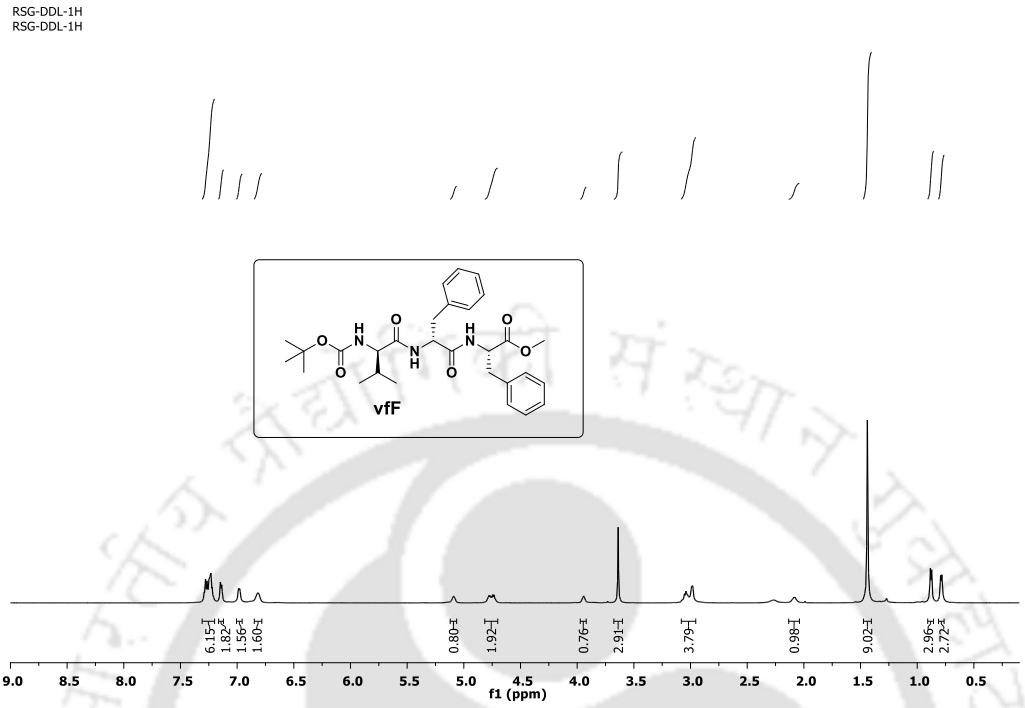

Figure 6.25. *^{1}H NMR spectra of peptide* ***vfF***

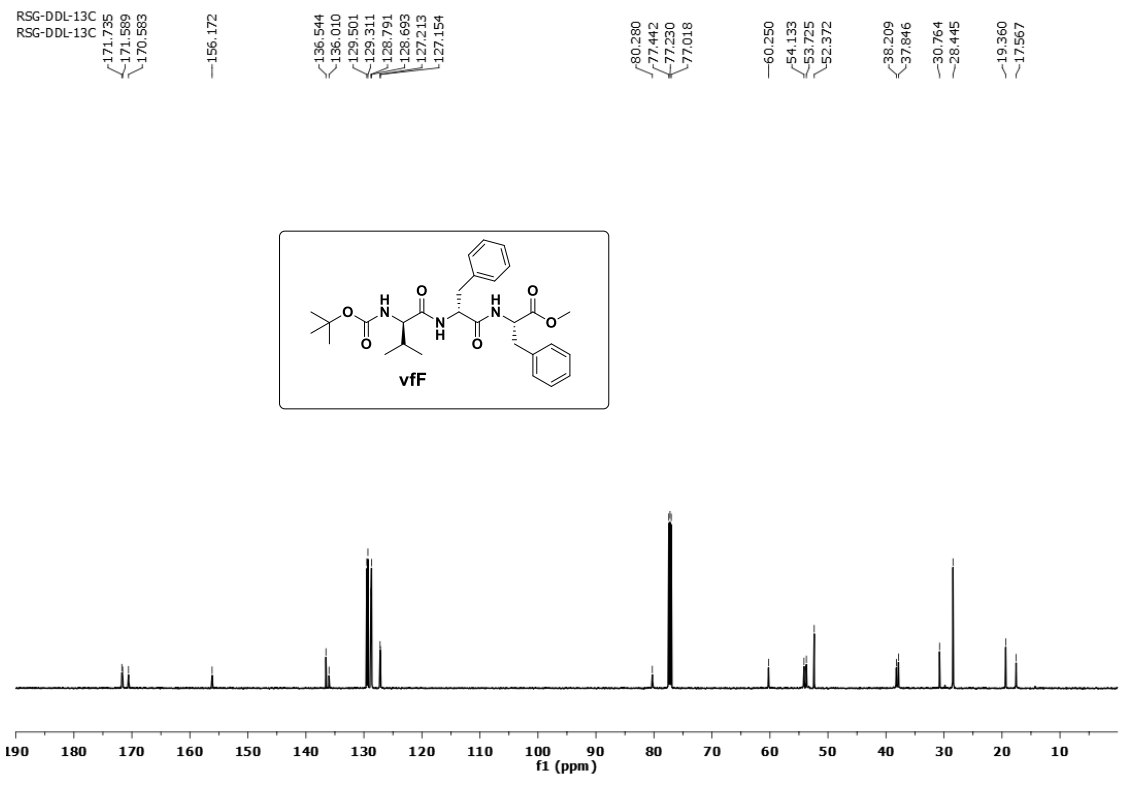

Figure 6.26. *^{13}C NMR spectra of peptide* ***vfF***

6.14. Crystallographic data

Table 6.2. Torsion angles (deg) of tripeptides Vff, VfF, vFf, VFf and vfF

peptides	*ϕ1*	*ϕ2*	*ϕ3*	*ψ1*	*ψ2*	*ψ3*	*ω1*	*ω2*	*ω3*
Vff	C5-N1-C6-C10 = -124.9(6)	C10-N2-C11-C19 = 131.9(5)	C19-N3-C20-C28 = 154.0 (5)	N1-C6-C10-N2 = 112.4(5)	N2-C11-C19-N3 = -113.2(5)	N3-C20-C28-O6 = 176.4(5)	O1-C5-N1-C6 = -176.9(5)	C6-C10-N2-C11 = 174.5 (4)	C11-C19-N3-C20 = 178.9 (5)
VfF	C5-N1-C6-C10 = -125.7(5)	C10-N2-C11-C19 = 129.2(4)	C19-N3-C20-C28 = 52.8(6)	N1-C6-C10-N2 = 116.0(4)	N2-C11-C19-N3 = -107.5(4)	N3-C20-C28-O6 = 40.1(6)	O1-C5-N1-C6 = -176.8(4)	C6-C10-N2-C11 = 170.3 (4)	C11-C19-N3-C20 = 176.2 (4)
vFf	C5-N1-C6-C10 = 124.7(4)	C10-N2-C11-C19 = -128.9(4)	C19-N3-C20-C28 = -52.6 (5)	N1-C6-C10-N2 = -115.1(4)	N2-C11-C19-N3 = 107.5(4)	N3-C20-C28-O6 = -40.8(5)	O1-C5-N1-C6 = 176.9(4)	C6-C10-N2-C11 = -170.2 (3)	C11-C19-N3-C20 = -176.4 (3)
VFf	C5-N1-C6-C10 = -114.5(3)	C10-N2-C11-C19 = -98.3(3)	C19-N3-C20-C28 = 132.5 (3)	N1-C6-C10-N2 = 109.5(3)	N2-C11-C19-N3 = 101.2(3)	N3-C20-C28-O6 = -31.8(4)	O1-C5-N1-C6 = -178.5(3)	C6-C10-N2-C11 = 179.1 (3)	C11-C19-N3-C20 = 176.9(3)
vfF	C5-N1-C6-C10 = 118.8(6)	C10-N2-C11-C19 = 100.8(6)	C19-N3-C20-C28 = -129.4 (6)	N1-C6-C10-N2 = - 110.7(5)	N2-C11-C19-N3 = -103.2(5)	N3-C20-C28-O6 = 31.0(7)	O1-C5-N1-C6 = 174.7(5)	C6-C10-N2-C11 = -179.3 (4)	C11-C19-N3-C20 = -176.9 (5)

Table 6.3. Hydrogen bonding distances (Å) and Bond angles (º) of peptides Vff, VfF, vFf, and VFf

Peptides	D−H···A	*d*(D···H)/Å	*d*(H···A)/Å	*d*(D···A)/Å	<D−H···A/°
Boc-L-Val-D-Phe-D-Phe-OMe (Vff)	N1-H1···O2	0.86	2.15	2.992(5)	167
	N2-H2···O3	0.86	2.15	2.993(5)	168
	N3-H3···O4	0.86	2.33	3.162(5)	163
	C11-H11···O4	0.98	2.46	3.384(6)	157
	C20-H20···O5	0.98	2.30	3.180(7)	148
Boc-L-Val-D-Phe-L-Phe-OMe (VfF)	N1-H1···O2	0.86	2.11	2.957(5)	168
	N2-H2···O3	0.86	2.10	2.937(5)	165
	N3-H3···O4	0.86	2.18	3.028(5)	167
	C11-H11···O4	0.98	2.56	3.447(5)	150
	C20-H20···O5	0.98	2.48	3.352(6)	148
Boc-D-Val-L-Phe-D-Phe-OMe (vFf)	N1-H1···O2	0.86	2.11	2.961(4)	168
	N2-H2···O3	0.86	2.09	2.933(4)	165
	N3-H3···O4	0.86	2.19	3.037(4)	168
	C11-H11···O4	0.98	2.57	3.458(5)	150
	C20-H20···O5	0.98	2.48	3.351(5)	148
Boc-L-Val-L-Phe-D-Phe-OMe (VFf)	N1-H1···O2	0.86	2.10	2.952(4)	169
	N2-H2···O3	0.86	2.08	2.928(4)	168
	N3-H3···O4	0.86	2.11	2.801(4)	137
	C3-H3···O5	0.96	2.54	3.445(4)	157

Table 6.4. Crystallographic data of tripeptides Vff, VfF, vFf, VFf and vfF

Parameters	**Vff**	**VfF**	**vFf**	**VFf**	**vfF**
Formula	C_{29} H_{39} N_3 O_6	C_{29} H_{39} N_3 O_6	C_{29} H_{39} N_3 O_6	C_{29} H_{39} N_3 O_6	C_{29} H_{39} N_3 O_6
Fw	525.63	525.63	525.63	525.63	525.63
Crystal system	monoclinic	triclinic	Triclinic	orthorhombic	orthorhombic
Space group	*P 21*	*P 1*	*P 1*	*P 21 21 21*	*P 21 21 21*
a/Å	5.0081(2)	4.9397(5)	4.9548(4)	5.0710(2)	5.0543(9)
b/Å	26.9990(17)	10.8307(10)	10.8351(12)	15.1956(6)	15.267(3)
c/Å	11.0196(8)	13.6935(13)	13.6908(16)	37.6927(14)	39.355(7)
α/°	90.00	92.411(3)	92.398(9)	90.00	90.00
β/°	92.120(5)	97.809(4)	97.809(8)	90.00	90.00
γ/°	90.00	92.168(4)	92.155(7)	90.00	90.00
V/Å^3	1488.98(15)	724.47(12)	726.85(13)	2904.48(19)	3036.8(10)
Z	2	1	1	4	4
D_c/g cm^{-3}	1.172	1.205	1.201	1.202	1.150
μ Mo K_α/mm^{-1}	0.082	0.084	0.084	0.084	0.081
F000	564.0	282	282	1128	1128
T/K	293(2)	296(2)	293(2)	293(2)	296(2)
θ max.	24.998	27.246	28.887	28.785	24.999
Total no. of reflections	5197	33865	5240	8674	123927
Independent reflections	3574	6425	4205	6013	5313
Observed reflections	2639	3800	2982	5114	3133
Parameters refined	349	349	349	349	364
R_1, I > 2σ(I)	0.0582	0.0592	0.0530	0.0541	0.0689
wR_2, I > 2σ(I)	0.1522	0.1422	0.1158	0.1538	0.1595
GOF (F^2)	0.876	0.849	0.940	0.770	0.876
CCDC No.	2015773	2015774	2015775	2015776	2015777

Chapter 7

Materials and Instrumentations

7.1. Materials

Used unprotected, protected, natural, and unnatural amino acids (except 2-amino benzoic acid), 2-nitrobenzenesulfonyl chloride, and Oxyma were bought from GL Biochem (Shanghai). 2-amino benzoic acid or anthranilic acid was obtained from the Department of Chemistry. DCC, HOBt, and DIPEA were procured from Spectrochem (India). All extra pure grade solvents such as MeOH, Hexane, EtOAc, DMF, DCM, DMSO, THF, and ACN (HPLC grade) and reagents such as citric acid $NaHCO_3$ were purchased from Merck (India). TFA was collected from SRL (India). $CDCl_3$ (for NMR), KBr, and ThT were received from Sigma Aldrich.

7.2. Instrumentations

7.2.1. Chromatographic technique

The progression and completion of the reactions were checked by using silica gel G, silica gel GF254 TLC plate as a stationary phase, and EtOAc/Hexane as a mobile phase. The pure products were separated from the crude reaction mixture by column chromatography using silica gel (60-120 mesh) and EtOAc/Hexane.

7.2.2. High-performance liquid chromatography (HPLC)

The reverse-phase analytical high-performance liquid chromatography (HPLC) was performed on the Agilent 1260 Infinity II system. C18 Agilent column (4.6 × 100 mm, 4 μm) was used for the experiment; 214 and 254 nm dual-wavelength were applied in UV detector. A total run time of 10 minutes, 1 mL/min flow rate, and a linear gradient of 5%-100% acetonitrile with water was applied for analyses.

7.2.3. Solvent evaporation technique

Buchi rotary evaporator was used to remove various solvents under reduced pressure.

7.2.4. Mass spectrometry

The samples for mass spectroscopy were prepared in a sufficient amount of ACN:H_2O mixture. The samples were then filtered, and masses were recorded on Agilent-Q-TOF 6500 instrument using ESI-TOF ("+"ve mode). Analysis of the samples was done using Mass hunter workstation software.

7.2.5. Nuclear magnetic resonance (NMR) spectroscopy

The purified solid peptides were analyzed by ^{1}H and ^{13}C NMR spectra using Bruker Ascend 600, 500, and 400 MHz instruments. Preparation of the NMR samples was done in $CDCl_3$ solvent. Chemical shifts (δ) and coupling constants (J) were recorded in ppm and Hz units, respectively, to reference solvent $CDCl_3$ at δ = 7.26 ppm and δ = 77.23 ppm for ^{1}H NMR and ^{13}C NMR, respectively.

7.2.6. Single-crystal X-ray diffraction (SC-XRD)

The chemical structure of the crystals of peptides was obtained by the single-crystal X-ray diffraction (SC-XRD) technique. A Bruker APEX-II CCD device and an Oxford SuperNova diffractometer (Agilent Technologies), and Mo Kα radiation were used to record the diffraction data at 298K. "Bruker APEX2" and "Bruker SAINT" software were used to analyze the collected data. The crystal structure was solved using SHELXS-97 (Sheldrick 2008) software.

7.2.7. Fourier-transform infrared (FT-IR) spectroscopy

Fourier-transform infrared (FTIR) spectra were obtained from a PerkinElmer Spectrum-One FT-IR spectrophotometer applying KBr pellet and PerkinElmer UATR Two FT-IR spectrometer without KBr pellet. A range of 4000 to 400 cm^{-1} was set for getting solid-state FT-IR spectra at room temperature. The peak analyzer tools of OriginPro 9.0 software was used for IR Spectrum deconvolution.

7.2.8. Melting point

Melting points were recorded on the Buchi melting point apparatus.

7.2.9. Circular dichroism (CD)

The circular dichroism (CD) spectra of all tripeptides were collected by JASCO J-1500 spectropolarimeter. The following parameter, such as 1 mm pathlength, 1 nm bandwidth, 190-260 nm wavelength range, and three accumulations, were used to carry out the experiments. Finally, CD spectra were obtained by plotting molar ellipticity θ (deg. cm^2 $dmol^{-1}$) versus wavelength (nm).

The mean residue molar ellipticity was calculated using the following equation:

θ (deg. cm^2 .$dmol^{-1}$) = Ellipticity (mdeg). 10^6 / Pathlength (mm). [Protein] (μM). N

7.2.10. Thermogravimetric analysis (TGA)

Peptide solution (approximately 5-6 mg/mL) in a different solvent such as ACN/H_2O or Methanol after being kept for incubation (required time) was first dried, and then the obtained solid sample was used for thermogravimetric analysis using a NETZSCH STA 449 F3 thermal analyzer. The following parameters were used for this experiment.

The heating rate of the sample = 10 °C/min in an alumina crucible, and the flow rate of dynamic atmospheric N_2 = 30 cm^3/min.

7.2.11. Optical microscopic images

Optical microscopic images were taken in a Nikon Digital Sight DS-U3 microscope and Olympus BX51 digital microscope. The compatible bright-field images were captured using different magnificence.

7.2.12. Field emission scanning electron microscopy (FESEM)

The morphology of all peptides was investigated using SIGMA-300 (ZEISS) and Gemini-300 (ZEISS) instruments. Samples for the morphological study were prepared by

drop-casting. 10 μL of fresh or incubated peptide solution (1.5 mM or 3 mM) in different solvents was drop cast onto an Aluminum-foil coated glass and was allowed to dry overnight inside a desiccator. FESEM experiment was carried out employing proper parameters.

7.2.13. Field emission transmission electron microscope (FETEM)

To determine the internal morphology of the peptides, FETEM study was carried out. Samples for this study were prepared by drop-casting 10 μL of peptide solution (100 μM or 300 μM) in MeOH or 50% ACN/H_2O (diluted from 1.5 mM stock solution) on a TEM grid and kept for 2 min. After that, staining was done by drop-casting 10 μL of 2% uranyl acetate solution on the same TEM grid and kept for another 2 min. The excess solution was carefully removed using tissue paper and dried in a desiccator. A JEOL 2100F instrument was used to capture the FETEM images.

7.2.14. Atomic force microscopy (AFM)

To check the morphology of the compounds using Atomic force microscopy (AFM), a freshly prepared 30 μM or 60 μM sample solution was prepared via dilution of 1.5 mM solution, which was fresh or incubated for 4-days at 37 °C. After that, 10 μL of the sample solution was drop cast on a clean glass microscopic slide and dried overnight in a desiccator. AFM studies were carried out in an Oxford Cipher instrument, and the obtained data were analyzed using WSxM 5.0 Develop 9.1 software.

7.2.15. Dynamic light scattering (DLS) measurements

Peptide solutions of 1.5 mM prepared in 50% ACN/H_2O were incubated for four days. It was subjected to ultrasonication for 30 minutes before analysis using a Nano-ZS90, Malvern instrument for the dynamic light scattering (DLS) experiment.

7.2.16. N_2 gas adsorption experiment

The N_2 gas adsorption and desorption studies were carried out using Quantachrome Instruments at STP. For this experiment, the peptide samples were initially degassed for 4 h at 40 °C. The Brunauer-Emmett-Teller (BET) equation measured the BET surface areas.

7.2.17. ThT dye interacting image

Sample preparation was carried out by mixing equal volume (5 μL) of incubated peptide samples and ThT (1 mM) in 50 μM PBS (pH 7.4). The resulting mixture was then drop-casted onto a microscopic slide in a controlled manner. An Olympus BX51 digital microscope was used for capturing the brightfield and its correlated fluorescence image. The filter, including excitation range 465-495 nm and emission range 512-558 nm, were applied for this technique.

7.2.18. Fluorescence microscopy and Fluorescence spectroscopy

The characteristics of encapsulation of the vesicular peptides were analyzed using fluorescence experiments against various drug molecules. For the experiment, we prepared a peptide solution of 1.5 mM in 50% ACN/H_2O and 100 μM curcumin, carboxyfluorescein, and rhodamine B, which were incubated separately for two days after ultrasonication for 30 min. Ten microliters of each solution were then dropped cast on the microscopic glass slide, and dried on an incubator at 37 °C. After that, fluorescence microscopy was carried out using an Olympus BX 51 fluorescence microscope with 50x and 100x magnification. To perform the salt-triggered disruption experiment, a 5 mM KCl solution was added to each incubated solution, and the resulting mixture was again incubated for 12 h. Fluorescence microscopy was then carried out to capture the images. In fluorescence emission experiments, the properly incubated 1.5 mM peptide solution and (100 μM) curcumin solution in 50% acetonitrile-water were used to record the spectra (wavelength 450-700 nm) at different time intervals using a Fluoromax spectrofluorometer.

7.2.19. Hirshfeld surface analysis

The CrystalExplorer17 software was used for Hirshfeld surfaces and 2D fingerprint plots analysis.

7.2.20. Computational studies

For the HOMO–LUMO energy calculations, the structure optimization was performed using density functional theory (DFT) analysis. The Gaussian 5.0.9 software and B3LYP/6-31G (d) program were used for it.

Conclusions and Future Directions

Conclusions

The thesis deeply contains supramolecular self-assembly, conformation, and morphology of small important organic molecules and important di-/tri-peptides. The synthesized organic compounds carry promising applications in various fields. The overview of the thesis work has been picturized in scheme1.

In chapter 1, we have discussed the general information about HOBt-based reagents, amino acids, peptides, and the secondary structure of peptides and self-assembly. Moreover, we have also described reported literature related to our work and the drawback of existing work. We planned our objective to address the drawback of previous work.

In chapter 2, we have developed the new modified Yamaguchi Reagent, 1-(2,4,6-trichlorobenzoyloxy)benzotriazole (TCB-OBt), and explored its structural and supramolecular characteristics. We have observed the presence of uncommon O···O interaction in crystal packing. Various microscopic techniques revealed that it formed a well-organized, continuous block-shaped structure. Moreover, this reagent provided significant yield under mild reaction conditions in amidation reactions.

In chapter 3, we have demonstrated the effectiveness of various N-terminal protecting groups such as Boc, Fmoc, *o*-NBS, and *p*-NBS of Ant-Aib dipeptides on self-assembly. Interestingly, we have observed the generation of diverse nanostructures formation depending on N-terminal protecting groups and displayed different supramolecular packing in the solid state. Moreover, formed nano-vesicles have drug encapsulation and releasing properties.

In chapter 4, we have described the self-assembly diversity of enantiomeric and reverse sequences of Ant and Phg containing dipeptides. Interestingly, structural and morphological homogeneity and heterogeneity were observed for enantiomeric and reverse peptide sequences. Moreover, obtained nanostructures have significant thermal stability.

In chapter 5, we have discussed the self-assembly, conformation, and morphology of four Trp-containing dipeptides and their corresponding Phe-bearing dipeptides sequences. Interestingly, the significant morphological transition from various rod-like fiber structures to spherical structures was observed just by replacing Phe with Trp. We have also explained their self-assembly mechanism via SC-XRD.

In chapter 6, we have described the supramolecular insights of hetero-chiral protected tripeptides VFF ($A\beta_{18-20}$) in solid and solution states. Interestingly, we have noticed different kinds of morphology by varying chirality of amino acids. In solid-state, peptides formed various supramolecular architectures. Moreover, all peptides have a ThT binding affinity.

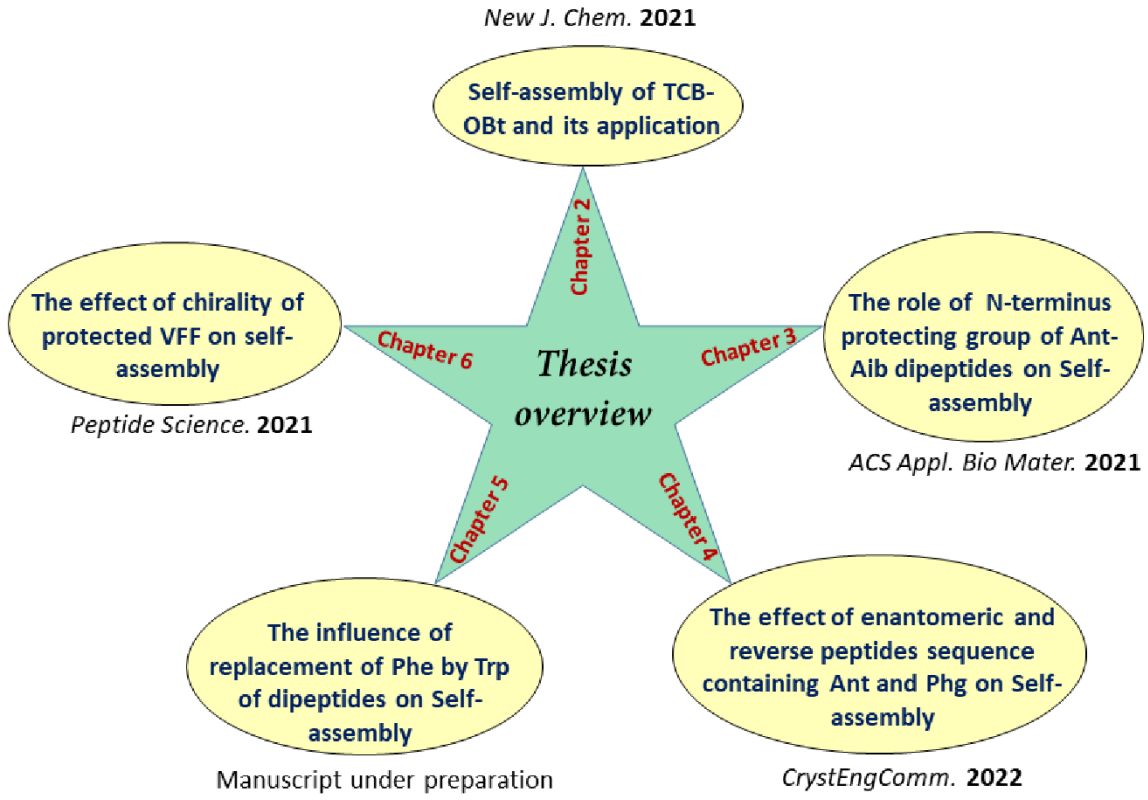

Scheme 1. *Thesis overview*

Future Directions

During my Ph. D. period, I have developed a novel, TCB-OBt, which can be further used in other organic transformations such as esterification, thio-esterification, and some rearrangement reaction like other coupling reagents. Moreover, we have explored some natural/unnatural amino acids containing di-tripeptide-based various nanostructures such vesicles, rods, fiber, etc., and studied their conformational and structural features depending on N-terminal protecting groups, enantiomeric and reverse peptide sequences, incorporating different amino acid in peptides chain and chirality of amino acids. We can synthesize other peptide sequences in this direction and explore their outcome. We can further explore various important di-, tri-, or tetra- peptide-based supramolecular assembly in solution and solid-state. We can also explore the applications of these supramolecular clusters in diverse directions, such as for various gas absorption capabilities or drug delivery.

Index 1: Product Index

Chapter 4			
Chemical structure & Name (mentioned as chapter)	**Page No.**	**Chemical structure & Name (mentioned as chapter)**	**Page No.**
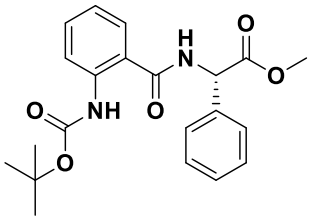 Boc-Ant-L-Phg-OMe (**4A**)	95	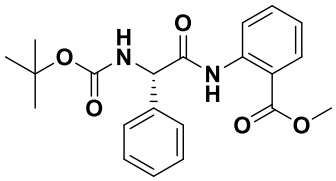 Boc-L-Phg-Ant-OMe (**4C**)	95
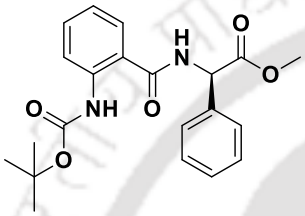 Boc-Ant-D-Phg-OMe (**4B**)	95	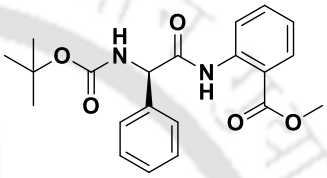 Boc-D-Phg-Ant-OMe (**4D**)	95
Chapter 5			
Chemical structure & Name (mentioned as chapter)	**Page No.**	**Chemical structure & Name (mentioned as chapter)**	**Page No.**
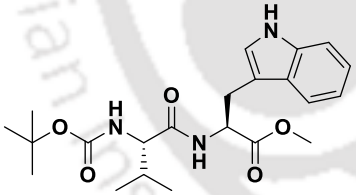 Boc-Val-Trp-OMe (**VW**)	129	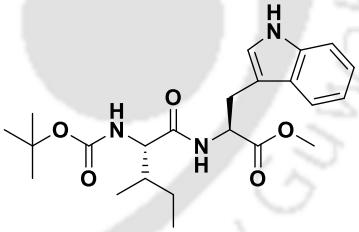 Boc-Ile-Trp-OMe (**IW**)	129
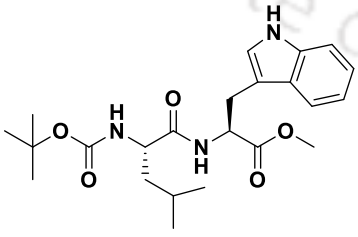 Boc-Leu-Trp-OMe (**LW**)	129	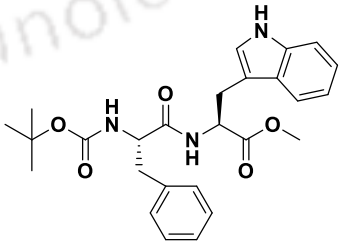 Boc-Phe-Trp-OMe (**FW**)	129

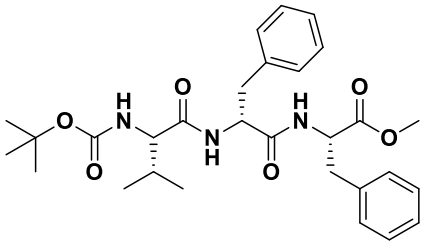 Boc-L-Val-D-Phe-L-Phe-OMe (**VfF**)	166	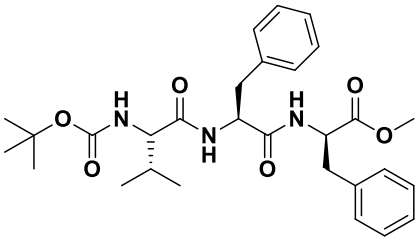 Boc-L-Val-L-Phe-D-Phe-OMe (**VFf**)	166
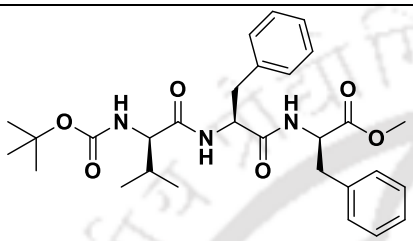 Boc-D-Val-L-Phe-D-Phe-OMe (**vFf**)	166	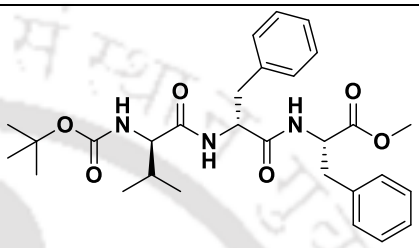 Boc-D-Val-D-Phe-L-Phe-OMe (**vfF**)	166

Index 2: Research Outcome

Publications:

1. **Dolai, G**.; Shill, S.; Roy, S.; Mandal, B. Inhibition of Fibril Formation of Dipeptides by Replacing Phenylalanine with Tryptophan. (**Manuscript under preparation**)
2. **Dolai, G**.; Giri, R. S.; Mandal, B. Versatility in Self-assembly and Morphology of Non-Coded Anthranilic acid and Phenylglycine based Dipeptide Stereoisomers. *CrystEngComm*. **2022**, *24*, 3778-3790.
3. **Dolai, G**.; Giri, R. S.; Mandal, B. Protecting Group-Directed Diversity in the Morphology of Self-Assembled Ant-Aib Dipeptides: Garland-Like Architecture and Nanovesicle Formation. *ACS Appl. Bio Mater*. **2021**, *4*, 8343-8355.
4. **Dolai, G**.; Roy, S.; Sen, S.; Giri, R. S.; Mandal, B. Crystal structure of 1-(2,4,6-trichlorobenzoyloxy) benzotriazole (TCB-OBt): observation of uncommon intermolecular oxygen–oxygen interaction and synthetic application in amidation. *New J. Chem*. **2021**, *45*, 19804-19811.
5. **Dolai, G.;** Giri, R. S.; Roy, S.; Mandal, B. Crystal Structure and Supramolecular Arrangement of Heterochiral Tripeptides. *Peptide Science*. **2021**, *113*, e24229.
6. Roy, S.; Giri, R. S.; **Dolai, G.;** Mandal, B. Role of side-chain and chirality of the amino acids on the supramolecular assemblies of dipeptides. *J. Mol. Struct*. **2020**, *1221*, 128877.
7. Giri, R. S.; Roy, S.; **Dolai, G.**; Manne, S. R.; Pal, S.; Paul, S.; Mandal, B. Nanostructures from protected L/L and D/L amino acid containing dipeptides. *Pept. Sci*. **2020**, *113*, e24176.
8. Giri, R. S.; Roy, S.; **Dolai, G.**; Manne, S. R.; Mandal, B. $FeCl_3$-mediated Boc deprotection: mild facile Boc-chemistry in solution and on resin. *ChemistrySelect* **2020**, *5*, 2050-2056.
9. Giri, R. S.; Manne, S. R.; **Dolai, G.**, Paul, A., Kalita, T., Mandal, B. $FeCl_3$-Mediated side chain modification of aspartic acid- and glutamic acid-containing peptides on a solid support. *ACS Omega***. 2017**, *2*, 6586-6597.

Conferences:

Poster presentation:

1. **Dolai, G.**; Mandal, B. "Unnatural Amino Acids Containing Dipeptides Mediated Diversity in Self-assembly." **North-East Research Conclave (NERC) and Assam Biotech Conclave (ABC) 2022**, 20-22th May 2022, IIT Guwahati, Science Technology and Climate Change Dept. & Dept. of Education, Govt. of Assam.
2. **Dolai, G.**; Mandal, B. "Protecting Group Mediated Diversity in the Self-assembly of Self-Assembled Ant-Aib Dipeptides.**" 28th CRSI National Symposium in Chemistry (CRSI-NSC-28)**, 25-27th March 2022, Department of Chemistry, IIT Guwahati, Page 145 (P-66).
3. **Dolai, G.**; Mandal, B. "Crystal Structure of 1-(2,4,6-Trichlorobenzoyloxy) Benzotriazole (TCB-OBt): Observation of uncommon intermolecular oxygen-oxygen interaction and synthetic application in amidation.**" 20th National Conference on Surfactants, Emulsions and Biocolloids NATCOSEB XX**, 9-11th December 2021, Department of Chemistry, IIT Guwahati, in association with ISSST, Kolkata, Page 57 (P-18).
4. **Dolai, G.**; Mandal, B. "Influence of Chirality on the Molecular Organization of Boc-Val-Phe-Phe-OMe ($A\beta_{18-20}$).**" International Conference on Emerging Trends in Chemical Sciences [ETCS-2020]**, 13-15th February 2020, Guwahati University, Page 189 (P-45).

Workshops:

1. **"Single Crystal X-Ray Diffraction Techniques and its Applications"** organized by North East Centre for Biological Sciences and Healthcare Engineering, Indian Institute of Technology Guwahati, Assam in collaboration with Bruker India Scientific Pvt. Ltd. on 22th - 23th January, 2021.
2. **"Scanning Electron Microscopy: Technique and its Applications"** organized by North East Centre for Biological Sciences and Healthcare Engineering, Indian Institute of Technology Guwahati, Assam in collaboration with Zeiss India, on 15th - 16th June, 2021.

3. **"Nuclear Magnetic Resonance: Technique and its Application"** organized by North East Centre for Biological Sciences and Healthcare Engineering, Indian Institute of Technology Guwahati, Assam in collaboration with Bruker, India, on 23rd - 24th August, 2021.
4. Workshop on procedures and applications of **XRD, XRF and Single Crystal XRD**, 27th July to 1st August, 2018, organized by Sophisticated Analytical Instrument Facility (SAIF), Guwahati, sponsored by Dept, of Science and Technology (DST), govt. of India.

Gobinda Dolai

Personal Information:

Date of Birth: 01st April 1993
Father's Name: Sanatan Dolai
Nationality: Indian
Religion: Hindu
Gender: Male
Tel no. +91-6900899023
Email: gobindadolai66@gmail.com/ gobindadolai@iitg.ac.in

Present Address:

Senior Research Fellow, C/O: Prof. Bhubaneswar Mandal, Laboratory of Peptide & Amyloid Research, Department of Chemistry, IIT Guwahati, Guwahati, Assam, India-781039.

Permanent Address:

Saoraberia Jalpai, Purba Medinipur, West Bengal, India-721652.

Academic Qualifications

07/2016–Present	**Ph.D. in Chemistry (CPI 8.5 out of 10)** Indian Institute of Technology Guwahati, Assam, India-781039 Thesis: **Self-assembly of Small Molecules and Peptides: Relevant Applications** Thesis advisor: Prof. Bhubaneswar Mandal
07/2014–05/2016	**M.Sc. in Chemistry (CPI 8.05 out of 10)** Indian Institute of Technology Guwahati, Assam, India-781039 Thesis: **Synthesis of Cyano Containing Oxa-dienes & Deconjugated enones:- Application in Michael-oxa-Michael Reaction** Thesis advisor: Prof. Subhas Chandra Pan
07/2011–05/2014	**B.Sc. in Chemistry Honours (62.25 %, First Class) with Physics and Mathematics** Midnapore College, Vidyasagar University, West Bengal, India-721101
2009–2011	**Higher Secondary Examination (WBCHSE) (80.4%, First Division, star) with Physics, Chemistry, Mathematics, Biology, English, and Bengali** Dakshin Moyna High School (H. S), West Bengal, India

2009 **Secondary Examination (WBBSE) (78.62%, First Division, Star) with Bengali, English, Mathematics, Physical Science, Life Science, Geography, and History**

Dakshin Moyna High School (H. S), West Bengal, India

Achievements and Awards

- Qualified "Joint Admission Test for M.Sc. (JAM 2014)" examination, India.
- Qualified National Eligibility Test (NET) June-2016 (UGC rank-099), June-2017 (CSIR rank-105), June-2021 (LS rank- 058) in Chemical Science, India.
- Qualified Graduate Aptitude Test (GATE) held in February 2016 (rank-1438), 2022 (rank-468) in Chemistry, organized by the Ministry of Human Resource Development, Government of India.
- Received West Bengal Merit Cum Means Scholarship.
- Received DST-Inspire Fellowship.

Research Experience

- During my Ph.D. studentship, I have worked on developing a new reagent and its synthetic application. I have also investigated molecular self-assembly and secondary structures of small molecules and peptides. Peptides were synthesized using SPPS and in solution, then determined their morphology and explored relevant applications.
- I have expertise in various instrumental techniques, e.g., HPLC, ESI-MS, NMR, CD, FT-IR, Optical-polarizable microscope, *etc.*
- In parallel, I have worked on developing a new method for peptide synthesis in solution and solid support (SPPS) and a new method for side-chain modification of peptides on-resin.

Academic and Professional skills

- **Laboratory and Instrumentation:** Familiar with Synthetic Organic Chemistry, peptide synthesis and their modification (solution phase and solid phase), crystallization of peptides, NMR Spectroscopy, Single-Crystal X-Ray Diffraction (SC-XRD), HPLC, Mass Spectrometry (ESI), FT-IR spectroscopy, FESEM, FETEM, AFM, TGA-DSC, Circular Dichroism (CD), DLS and fluorescence microscopy.

- **Software:** Origin, Adobe Illustrator, MS-Office, ChemDraw, SHELXL, WINGX, Mercury, Mestrenova, and CrystalExplorer17 software.
- **Instrumental Experience**: Selected as an authorized operator for HRMS instrument at 'Department of Chemistry, IIT Guwahati', April 2017-June 2021.
- **Teaching Experience:** Worked as a Teaching Assistant (TA) in B.Tech class at IIT Guwahati, India.
- **Language:** Bengali, English, and Hindi.

Research interests

- Peptide chemistry
- Supramolecular chemistry
- Synthetic organic chemistry